Experiments with Bose-Einstein Condensates in a Double-Well Potential

by

Yong-Il Shin

B.S., Physics (2000)
Seoul National University

Submitted to the Department of Physics
in partial fulfillment of the requirements for the degree of

Doctor of Philosophy

at the

MASSACHUSETTS INSTITUTE OF TECHNOLOGY

February 2006

Author .....
Department of Physics
November 17, 2005

Certified by .....
Wolfgang Ketterle
John D. MacArthur Professor of Physics
Thesis Supervisor

Certified by .....
David E. Pritchard
Cecil and Ida Green Professor of Physics
Thesis Supervisor

Accepted by .....
Thomas J. Greytak
Professor of Physics, Associate Department Head for Education

Experiments with Bose-Einstein Condensates in a Double-Well Potential

by

Yong-Il Shin

Submitted to the Department of Physics
on November 17, 2005, in partial fulfillment of the
requirements for the degree of
Doctor of Philosophy

Abstract

Trapped atom interferometry was demonstrated with Bose-Einstein condensates in an optical double-well trap. Coherent splitting of trapped condensates was performed by deforming an optical single-well potential into a double-well potential, and the relative phase of the two split condensates was shown to be reproducible. Microfabricated atom chips were developed with prospect for chip-based confined-atom interferometry. The same dynamical splitting scheme was implemented in a purely magnetic double-well potential on an atom chip and interference of two split condensates was observed, but not reproducible phase.

Coherent optical coupling between two spatially separated condensates was realized using stimulated light scattering. The relative phase of the two condensates was continuously measured with an optical method, which demonstrated atom interferometry without need for a conventional beam splitter or recombiner. The Josephson-like phase dynamics of the coherent optical coupling was investigated and it was experimentally shown that the induced atomic currents depend on the relative phase of the two condensates and an additional controllable coupling phase.

Condensates in an optical dipole trap were distilled into a second empty dipole trap adjacent to the first one. We showed that the distillation was driven by thermal atoms spilling over the potential barrier separating the two wells and then forming a new condensate. This thermodynamic relaxation process serves as a model system for metastability in condensates and provides a test for quantum kinetic theories of condensate formation.

Doubly quantized vortices were topologically imprinted in spinor condensates and the stability of the vortex state was investigated. The decay of a doubly-quantized vortex core into two singly-quantized vortex cores was observed using a tomographic imaging technique. The characteristic time scale of the splitting process was found to be longer at higher atom density.

Thesis Supervisor: Wolfgang Ketterle
Title: John D. MacAurthur Professor of Physics

Thesis Supervisor: David E. Pritchard
Title: Cecil and Ida Green Professor of Physics

To my parents, Kwang-Bum Shin and Young-Hee Yoon
and my sister Ji-Young

Acknowledgments

My graduate life at MIT was enjoyable. Being a graduate student with oppressive thesis requirements, of course, is generally not an ideal way to be happy, but I can definitely say that my past four and half years in Building 26 was full of challenges and adventures through which I could observe and identify myself. Most of those challenges and adventures resulted from the struggle with super cold sodium atoms, but I know all of these were possible only because there were many people encouraging, supporting and helping me throughout the whole journey.

First of all, I would like to thank Wolfgang Ketterle and Dave Pritchard for providing me with the opportunity to work with them. I was extremely lucky to have Wolfgang and Dave as thesis supervisors not only because they are great physicists but also because they really care about students' independence as researchers. Wolfgang's concise statement and scientific assessment on research projects always provided a clear picture of what we were doing in the lab. His considerate encouragement has been a great source of my 'careless' bravery in experiments. Dave showed me an example of how one can be happy with doing science. His scientific analysis on everything always inspired me. The scientific enthusiasm and the solid work ethic they showed me in the past years have set a standard for me and I believe it will work as a guideline for the rest of my research life.

It has been a great privilege to join the *science chamber* team using MIT's third generation BEC machine. When I joined the team in September 2001, it was eight months after the first BEC with the machine. As a user and janitor of the machine, I am greatly indebted to the builders of the machine. In particular, I thank Ananth Chikkatur and Aaron Leanhardt for teaching me how to drive this wonderful machine for scientific research. Ananth introduced me to the flavor of the BEC experiments at MIT. The patience that he showed me when I worked on my first project, the control system for the translation stage and his leadership in the 'continuous condensate' project really helped me to be integrated in the team.

Aaron laid the solid foundation of our microtrap technique. He initiated the atom chip and the optical double well system, without which the experiments described in this thesis would have never happened. I was always fascinated by his broad knowledge of the machine and his quick evaluation of the feasibility of new experimental ideas. His working style, particularly in the lab, was so strong that sometimes it was quite hard for me to keep following him physically in a literal sense. However, I learned many things from his diligent and thrustful leadership, which essentially helped me to develop my own working style. He was also a selfless leader placing the interest of the whole team before anything. Particularly, I am deeply grateful to him for letting me lead the 'trapped atom interferometer' project when we had to divide our team into two subgroups.

I have been benefited from working with Michele Saba, André Schirotzek, Christian Sanner, Tom Pasquini and Gyu-Boong Jo. Michele was a great labmate who could immediately compensate for the early loss of Aaron. Most of the experiments were carried out with him and his physical insight always brought an interesting spin on our experimental results. He always kindly counseled me on any problem from how to kick a soccer ball better to how to write a research proposal. He has unique and interesting opinions on any issue, so it was great fun to discuss with him, especially in a dark laboratory at around midnight.

Due to the short cycle of the team projects, our team advantageously had excellent diploma students from Germany. André and Christian were diploma students who worked with us for one year. Their enthusiasm and strong motivation helped me to keep myself upright in the mid-period of my graduate life that would have possibly been a slump. André has also been a perfect officemate with agreeable tastes in (heavy-metal) music, (Chinese truck) food, (sweaty) sports, (sleepy) classics, and etc. Having the machine run on Christmas and playing foot-volley ball at early morning with being desperate for the 'recoil momentum' project were small parts of my pleasant memories with him. I am looking forward to working with him in the Li lab soon. Christian was calm and very skillful almost at everything. I have enjoyed talking with him and learning from him. I believe he will make a great scientist. I thank Tom and Gyu-Boong for helping me in the lab and wish them good luck with coming research projects.

Center for Ultracold Atoms was a great place for studying AMO physics. The weekly CUA seminar presented by world-leading speakers was one of the great benefits I have had from the center. Also, the big size of graduate students made it possible to ask diverse helps at various times and to make our own soccer and softball team. I thank Jamil Abo-Shaeer for organizing many unforgettable bond-enhancing gatherings, Claudiu Stan for his professional advises on various technical issues, Kaiwen Xu for discussing theoretical problems and teaching how to make a fiber tip, Deep Gupta for teaching how to change dye, Gretchen Campbell for her considerate caring for group events, Martin Zwierlein for his endless upbeat mood and organizing our soccer team, Micah Boyd for his love of Naboo, and Dave Kielpinski for showing what is the best lab-behavior. I also thank Ellenor Barish, Carol Costa, Maureen Howard, and Maxine Samuels for their administrative help and Fred Cote for his kind advises on machining.

I would like to thank people who supported me outside the lab: Jaehyuk Choi who welcomed me in Cambridge with a McDonald burger for the dinner of the first night, Boguk Kim who shared a dorm apartment with me for one year and evacuated, Daihyun Lim who ruined my precious futon cover with pasting almost digested food, and Kyungjoon Lee who always emphasizes the importance of marriage and brags of his adorable baby. They are all good friends. I am grateful to Prof. Wonho Jhe for introducing atom optics experiments

to me when I had to decide a graduate school. I thank Eunjong Hong and Hyungjoon Cho for their life advises, and the members of the KGSA soccer team for their 'craziness'.

Finally, I thank my family for its unconditional support and love. My parents Kwang-Bum Shin and Young-Hee Yoon have always encouraged me to live with a dream. Without their endless blessing I would not be able to become who I am.

This work was supported by the Army Research Office (ARO), the Defense advanced Research Projects Agency (DARPA), the National Science Foundation (NSF), the National Aeronautics and Space Administration (NASA), and the Office of Naval Research (ONR).

Contents

List of Figures

List of Tables

Chapter 1

Introduction

1.1 Bose-Einstein Condensation in dilute atomic gases

Bose-Einstein Condensation (BEC) is the underlying mechanism for quantum phenomena such as superfluidity and superconductivity. The phenomenon of a macroscopic number of identical particles condensing in a single quantum-mechanical state was predicted in 1924 by Bose and Einstein [12, 13] and has been studied in diverse systems such as He^4 superfluid and superconductors. The history of BEC study in its early stages is reviewed in Ref. [14] and references therein.

In 1995, Bose-Einstein condensation was experimentally realized in a new system: dilute atomic gases [15]. This historic discovery opened a new golden era of BEC study; in contrast to the other systems confronting with the complexity of the particle interaction, the weakly-interacting atomic system provides a unique opportunity for the systematic investigation of Bose-Einstein condensates in a regime where interactions are perturbative and theory-tractable. In the subsequent years, the novel properties of Bose-Einstein condensates such as phase coherence [16], superfluidity, and quantized vortices [17, 18, 19] were experimentally investigated. In recognition of these remarkable achievements, the 2001 Nobel Prize for Physics was awarded to Eric Cornell, Wolfgang Ketterle, and Carl Wieman [20, 21].

Over the last decade, the field of quantum degenerate gases has developed in a dramatic way [22, 23]. The number of species of Bose condensed atoms has grown to two digits[1], and the range of experimental research topics has been extended to spinor condensates [34, 35, 36], condensates in lattice potentials [37, 38], and low-dimensional condensates [39, 40, 41, 42, 43]. This explosive and steady progress in the field was made possible by the constructive interference of technical advances in experimental atomic physics and well-founded condensed matter theory; the current BEC study represents a fascinating

[1] ^{87}Rb [15], ^{23}Na [24], ^{7}Li [25, 26], ^{1}H [27], ^{85}Rb [28], ^{4}He* [29], ^{41}K [30], ^{133}Cs [31], ^{174}Yb [32], and ^{52}Cr [33]

interdisciplinary research area. More surprisingly, quantum degenerate Fermi gases were demonstrated with ^{40}K [44] and ^{6}Li [45] and experimental explorations of the crossover between a BEC and a Bardeen-Cooper-Schrieffer (BCS) superfluid were recently reported, addressing a long-standing problem in condensed matter theory.

My Ph.D. research described in this thesis is mainly concerned with atom optics with Bose-Einstein condensates, which are a gigantic quantum matter wave. Having full control over the phase coherence of matter waves is the ultimate goal of atom optics, which opens the prospects for novel applications such as atom interferometry and quantum information processing. We developed microtraps for condensates, such as magnetic traps with microfabricated atom chips and an optical double-well trap having a tunable well-separation. Most of the experiments in this thesis were designed for investigating technical possibilities to measure and manipulate the relative phase of two separate condensates. As main results, we demonstrated coherent, dynamic splitting of a trapped condensate, optical read-out of the relative phase of two condensates, and optical Josephson-like coupling between two spatially separate condensates.

In this introduction, I present and discuss several crucial concepts for understanding the phenomenon of Bose-Einstein condensation: what determines bosons and fermions, consequences in quantum statistics, a criterion for Bose-Einstein condensation, and an order parameter for the phase transition. A mean-field theory for dilute Bose-Einstein condensates is introduced by deriving the Gross-Pitaevskii equation. In the following discussion on the order parameter of condensates, I address the conceptual question: what is the phase of a Bose-Einstein condensate; is it a real physical quantity or just a convenient field-theoretical tool? There are still theoretical debates on this issue. I simply recapitulate a couple of viewpoints on the controversy and express my preference. This discussion is very relevant to the experiments described in this thesis. In the end, the outline of this thesis is presented.

1.2 Quantum Statistics: Boson vs Fermion

The principle of the indistinguishability of the particles of a same kind requires a fundamental change in the description of a system of identical particles. Even in classical statistical physics, the need for the indistinguishability is indicated in the *Gibbs' paradox*, saying that the fact that identical particles are distinguishable is contradictory to the fact that the entropy is an extensive variable of a system [46]. This can be solved by reducing the configuration space under the principle of indistinguishability, resulting in a topologically different configuration space than the simple Cartesian product of the one-particle spaces [47]. The meaning of the particles being indistinguishable is that the physical situation is unchanged

if the particles are interchanged. In the quantum description, it is expressed as

$$|\psi(P(x_1, \cdots, x_N))|^2 = |\psi(x_1, \cdots, x_N)|^2, \tag{1.1}$$

where ψ is a wave function of the N-particle system, and P is any permutation of the N particle coordinates, $\{x_i\}$. Because any P can decompose into a product of exchanges, χ_{ij}, between two particles, i and j, we have a simple sufficient condition,

$$|\psi(\chi(x_1, \cdots, x_N))|^2 = |\psi(x_1, \cdots, x_N)|^2 \tag{1.2}$$

$$\Leftrightarrow \psi(\chi(x_1, \cdots, x_N)) = e^{i\xi}\psi(x_1, \cdots, x_N). \tag{1.3}$$

Since naturally $\chi^2 = I$, where I is the identical operator[2], $e^{i2\xi} = 1$, i.e., $e^{i\xi} = 1$ or $e^{i\xi} = -1$. According to the exchange property, there are two classes of particles existing in nature: bosons with $e^{i\xi} = 1$ and fermions with $e^{i\xi} = -1$.

The consequences of the restriction deeply affect the quantum statistics which the particles of each class should follow, and the resulting statistics are called Bose-Einstein statistics for bosons and Fermi-Dirac statistics for fermions. For distinguishable particles, the classical statistics is Maxwell-Boltzmann statistics. The most dramatic difference of the two quantum statistics is that many bosons can occupy a same state but fermions are fundamentally prohibited to multiply occupy a state, which is called the *exclusion principle*. Consequently, at zero temperature, i.e, in the true ground state, bosons would be all together in the single-particle ground energy level, and fermions would pile up one particle in each adjacent level from the bottom. One minor remark on the indistinguishability of the particles is that it is a principle, i.e., an axiomatic statement, which has been supported by a myriad of experimental measurements.

What determines particles to be bosons or fermions? There is a *spin-statistics theorem* saying that particles with an integer spin are bosons obeying Bose-Einstein statistics, and particles with a half-odd integer spin are fermions obeying Fermi-Dirac statistics. In the relativistic arguments in context of quantum field theory, the question can be recasted in the following form [49]: what determines the (anti)commutative relations of field operators for particles? The commutative and anti-commutative relation of field operators are associated with bosons and fermions. The basic requirements for a consistent relativistic theory with a given pair of the spin of a particle and the (anti)commutative relations of the field operators are that it should have no negative energy states and that the causality should be preserved, i.e., two observables with a space-like separation should commute each other. Based on

[2]In a higher than three dimensional space, $\chi^2 = I$ is the case. However, in lower dimensions, this requirement is relaxed, resulting in the concept of an anyon [47]. Fractional statistics were experimentally observed in a two-dimensional condensed matter system [48].

these requirements, Pauli [50] showed that particles with integer spin should obey Bose-Einstein statistics due to the causality, and particles with arbitrary half-odd integer spin should obey Fermi-Dirac statistics due to the nonexistence of negative energy states. More rigorous mathematical treatments can be found in Ref. [51].[3]

1.3 Criterion for Bose-Einstein Condensation

Bose-Einstein condensation of particles in a physical system is a macroscopic occupation in a single state of the system; the 'macroscopic' occupation means that the number of particles in the state is a finite fraction of N, i.e., $O(N)$, where N is the total number of particles in the system. In a system of fermionic particles, the occupation number is bounded to be $O(1)$ due to the exclusion principle and thus Bose-Einstein condensation is fundamentally prohibited.

The criterion for Bose-Einstein condensation can be mathematically expressed in a simple form. We have the density matrix, σ, for a given state of the system of identical N boson particles. By definition, the density matrix has all information of the system. We obtain a single-particle density matrix, σ_1, by tracing down σ with respect to particles 2,3,...,N.

$$\sigma_1 \equiv N \ \mathrm{tr}_{2\cdots N}(\sigma), \tag{1.4}$$

where we multiply by N for a physically more intuitive interpretation. Because of the permutation symmetry in the bosonic system, σ_1 has all information about a single particle, i.e., the population distribution and the allowed single-particle states. The eigenfunctions for σ_1, $\{\psi_i\}$, and the corresponding eigenvalues, $\{n_i\}$, represent the single-particle states defined in the given many-body state and the occupation number of each corresponding state, respectively. Therefore, the criterion for Bose-Einstein condensation can be rewritten as

$$\exists n_0 \sim O(N) \Longleftrightarrow \mathrm{BEC}, \tag{1.5}$$

and the associated single-particle wave function, ψ_0 is the state where a macroscopic number of particles stay, and may be called the *wave function of a condensate*. This criterion provides a straightforward evaluation method for the existence of Bose-Einstein condensates, and it can be generally applied to most of systems even in the case including interparticle interactions and not in the true ground state.

Penrose and Onsager generalized the criterion (1.5), and suggested an alternative math-

[3] A non-relativistic geometrical argument was suggested in Ref. [47]. One might find a simple argument with the conjecture that the exchange operator might be expressed as a sum of spin rotation and inversion.

ematical form of the criterion for Bose-Einstein condensation [52]:

$$\lim_{|x-y|\to\infty}\langle\hat{\psi}^{\dagger}(x)\hat{\psi}(y)\rangle = f^{*}(x)f(y) \neq 0, \tag{1.6}$$

and the wave function of the condensate, ψ_0, is one of possible solution for $f(x)$. Yang elaborated on the concept of *off-diagonal long-range order* based on the above criterion, and emphasized that it is a quantum phenomenon not describable in classical mechanical terms [53]. However, the off-diagonal long-range order loses its application to the trapped boson system because the asymptotic behavior is not well defined due to the finite size of the system.

1.4 Phase Transition and Order Parameter

Bose-Einstein condensation, first introduced as a pure population condensing effect, is a quantum phase transition. Thermodynamic calculations of an interacting bose gas show a discontinuity of specific heat at the beginning of condensation, implying that Bose-Einstein condensation is a second-order phase transition[4] [54]. The analogy between the discontinuity in this phase transition and the λ-transition of liquid He^4, at which the specific heat becomes logarithmically infinite, hinted that the underlying principle of the superfluidity of liquid He^4 might be Bose-Einstein condensation [55].

In most of phase transitions, a phase with higher symmetries transforms into a phase with lower symmetries as the temperature comes down through the critical temperature. A liquid changes into a solid, losing translational and rotational symmetries, and a ferromagnet obtains a macroscopic net magnetization in the absence of a magnetic field, losing the symmetry of spin rotation. Accordingly, the ground state of the system at zero temperature might not have the full symmetries residing in the governing Hamilitonian. Many possible but 'non-superposable' ground states would be degenerate and equivalent with respect to the lost symmetry, but one of them should be selected for each real system. In this context, the idea of *spontaneous symmetry breaking* has been introduced to account for the critical phenomena in condensed matter physics and elementary particle physics [56, 49].

In his discussion of a second-order phase transition, Landau pointed that in order to quantitatively describe a phase transition, *an order parameter*, vanishing in one phase and becoming non-zero in the other phase, is necessary to describe the dynamics of the new phase [57]. For example, the order parameter for the solid is the crystal structure and for the ferromagnet is the net magnetization. It is commonly believed that establishing a nonzero order parameter in a phase transition comes with the spontaneous symmetry

[4]Bose-Einstein condensation in an non-interacting bose gas is a first-order transition like a liquid-gas transition.

breaking.

What is the broken symmetry in Bose-Einstein condensation, and what is the corresponding order parameter? This question is quite legitimate because we know that Bose-Einstein condensation is a second-order phase transition, and as investigated in He^4 superfluidity, the macroscopic properties of a Bose-Einstein condensed phase is totally different from a non-condensed phase. The off-diagonal long-range order might be an order parameter for Bose-Einstein condensates, which has been objected due to the physical requirement that the order parameter should be determined by local dynamical variables [54]. The choices of the broken symmetry and the order parameter are not always obvious from the first principles. Generally, people suggest that Bose-Einstein condensation break the gauge symmetry related to the choice of a global phase of creation and annihilation operators and that the order parameter be equal to the wave function of the condensate.

1.5 Macroscopic Matter Wave

A pictorial description on the condensation process [58] provides insight into the wave function of a condensate, elucidating the aforementioned mathematical criterion. In quantum mechanics, the wave nature of a particle delocalizes the particle over its de Broglie wavelength, $\lambda_{dB} = \sqrt{2\pi\hbar^2/mk_BT}$. When the temperature of a gas gets low enough to make λ_{dB} comparable to the interparticle separation $n^{-\frac{1}{3}}$, where n is the density of particles, matter wave packets of the indistinguishable particles start overlapping. When the phase space density $\rho = n\lambda_{dB}^3$ exceeds 1, the phase transition to a single macroscopic matter wave occurs. This is a Bose-Einstein condensate: a gigantic quantum object.

The macroscopic matter wave is embodied by the wave function of the condensate. In following, I summarize a mean-field (Hartree) approach to obtain the *Gross-Pitaevskii equation* which describes BEC dynamics in terms of the wave function of the condensate. Basically, mean-field description deals with how a single particle feels the averaged interaction from the other particles.

The Hamiltonian of a system of N interacting particles is

$$H = \sum_{i=1}^{N}\left[\frac{p_i^2}{2m} + V(x_i)\right] + U_0\sum_{i<j}\delta(x_i - x_j), \tag{1.7}$$

where $V(x)$ is the external potential for particles and the interparticle potential is simplified by defining an effective potential[5] with $U_0 = \frac{4\pi a\hbar^2}{m}$, where a is the s-wave scattering length.[6] The physical justification for the s-wave approximation can be found in Ref. [54].

[5] Fermi first introduced this approach as the 'pseudopotential' method. E. Fermi, *Ricerca Sci.***7**, 13 (1936).
[6] For ^{23}Na, $a = 2.93 \pm 0.06$ nm from Ref. [59], which gives $U_0 = h \times 1.62 \times 10^{-14}$ kHz/cm^3.

The mean-field theory starts with an ansatz for the many-body wave function,

$$\Psi(x_1, x_2, ..., x_N) = \prod_{i=1}^{N} \phi(x_i), \tag{1.8}$$

and the total energy of state, E, will be

$$E = N \int dx \Big[\frac{\hbar^2}{2m} |\nabla \phi(x)|^2 + V(x)|\phi(x)|^2 + \frac{N-1}{2} U_0 |\phi(x)|^4 \Big]. \tag{1.9}$$

Minimization of E subject to the constraint of normalization of $\phi(x)$ and the introduction of the wave function of the condensate, $\psi(x) = \sqrt{N}\phi(x)$, would result in the time-independent Gross-Pitaevskii equation,

$$\Big[-\frac{\hbar^2}{2m}\nabla^2 + V(x) + U_0|\psi(x)|^2 \Big]\psi(x) = \mu\psi(x), \tag{1.10}$$

where $\mu = \partial E/\partial N$ is the chemical potential of the system. The generalized time-dependent Gross-Pitaevskii equation $i\hbar\frac{\partial}{\partial t}\psi(x,t) = \mu\psi(x,t)$ gives a non-linear Schrödinger equation governing the dynamics of the wave function of the condensate.

The mean-field approach has been very successful in accounting for most of the experimental results. Nevertheless, as being one of simplest approaches for many-body systems, the mean-field theory has some theoretical inconsistencies to be improved. Leggett [60] pointed out that the mathematical origin of the limitation is the fact that the trial ansatz (Eq. 1.8) does not allow two-particle correlation and restricts the whole description in a reduced Hilbert space. Since the two-particle interaction would cause some correlation between particles especially in a short range separation, a better ansatz should accommodate the possibility of two-particle correlations, which is the essence of the advanced *Bogoliubov* approach. For theoretical details, please refer to Ref. [61, 62, 60].

From the viewpoint of a macroscopic matter wave, Bose-Einstein condensates open a new era for atom optics; BECs are to atom interferometry what lasers are to optical interferometry, i.e., a coherent, single-mode, and highly brilliant source. Since the remarkable demonstration of the macroscopic interference of two gaseous Bose-Einstein condensates [16], exploiting the laser-like coherence of gaseous Bose-Einstein condensates has been one of hottest topics in atom optics. Furthermore, the nonlinearity due to atom-atom interactions in the governing Hamiltonian allows the study of nonlinear atom optics. Analogies of the phenomena in nonlinear optics, such as matter wave amplification [63], four-wave mixing [64, 65], and soliton formation [66] have been experimentally demonstrated.

1.6 Phase of a Condensate

At first sight, using the wave function of a condensate for describing its dynamics inspires us to believe that this method might be the only natural choice for the order parameter for Bose-Einstein condensation. However, when it comes to symmetry breaking, the situation is in confusion. Theoretically, it is generally believed that Bose-Einstein condensation is a spontaneous breakdown of the gauge symmetry resulting in the well-defined global phase factor of the field operator, $\hat{\psi}$, for particles.

$$\langle\hat{\psi}(x)\rangle_{\mathrm{BEC}} = \phi(x) \neq 0, \tag{1.11}$$

which means that in the presence of a Bose-Einstein condensate, the expectation value of the field operator has a non-vanishing value, i.e., a coherent state of matter. The function $\phi(x)$ is equivalent to the wave function of the condensate, possessing a well-defined phase, i.e, $\phi(x) = \sqrt{n(x)}e^{i\theta(x)}$, where n is the particle density of the condensate and θ is the phase of the condensate. Anderson [67] argued that the observation of Josephson effects demonstrated the existence of the phase of a condensate, emphasizing that every part of condensates should have a definite phase value. Furthermore, some people argue that Eq. (1.11) is even the only legitimate definition of the order parameter. Most of established theoretical works were based on the assumption of the gauge symmetry breaking.

However, the non-vanishing expectation value of the field operator $\hat{\psi}$ for *massive* particles is not an easy idea to accept. In quantum mechanics, field operators for particles are not observables because of their non-hermitian property, and mathematically the field operators couple two Hilbert subspaces with different particle numbers, i.e., $\hat{\psi} : \mathcal{H}_{N+1} \longrightarrow \mathcal{H}_N$, where $\mathcal{H}_N$ represents a Hilbert subspace with N particles. Generally, $\mathcal{H}_N$'s for a massive particle are distinguishable under the super-selection rules.[7] Therefore, the idea of the non-vanishing expectation value of the field operator, allowing the superposition of states with different particle number, seems to be a theoretically artificial tool.

The necessity of the phase of a Bose-Einstein condensate is controversial. Javanainen and Yoo [68] demonstrated that quantum measurements entangling two condensates generate a relative phase of the two condensates. Mølmer [69] criticized that the phase concept in quantum system is overall fictitious, pointing out that observable phenomena do not depend on whether an absolute phase exists or not. Leggett [60] showed his strong opinion that coherent states of matters violating the super-selection rule are physically impossible. Furthermore, a theoretical formalism without assuming the gauge symmetry breaking was developed [70, 71, 72]. On the other hand, Dunningham and Burnett [73] tried to justify the definition of coherent states by introducing a reference condensate as a phase standard.

[7] All observables commute with the atom number operator $\hat{N}$.

Lieb et al. [74] and Sütő [75] showed that the gauge symmetry breaking is asymptotically equivalent to Bose-Einstein condensation in a thermodynamic limit.

I support the opinion that Bose-Einstein condensation does not necessarily imply spontaneous symmetry breaking. First of all, the global phase of a condensate is not measurable. I believe that everything in nature should be understood in its simplest form. Therefore we could abolish the concept of a definite global phase of condensates if only a consistent theory explains the whole phenomena without the concept. The absolute value of a quantum dynamic phase is physically meaningless, and only comparing quantum phases, i.e., measuring relative phases is experimentally allowed via phase sensitive dynamics or interference effects. Even in a single condensate, it is the relative phase of two points of the condensate that is physically relevant. This viewpoint might be similar to Landau's philosophy for hydrodynamic equations, where he mentioned that only important quantities are density and flow rate. In an aesthetic viewpoint, assigning a definite phase to a condensate might look more beautiful from the standpoint of symmetry breaking and second-order phase transitions. In a practical viewpoint, assuming coherent states might be justified to be more efficient for calculations. However, it should be noted that a definite global phase is *not necessary* for describing BEC dynamics.

1.7 Relative Phase of Two Condensates

I emphasized that the relative phase of two condensates is a measurable quantity and does not have a conceptual problem with respect to symmetry breaking. In the following, I illustrate the relative phase, using a two-mode system where only two orthogonal states, are allowed for particles. The two states are designated by ψ_A and ψ_B, and the corresponding field operators are $\hat{a}_A^\dagger$ and $\hat{a}_B^\dagger$, respectively. Two many-body states are considered: a coherent state and a number (Fock) state.

$$\begin{aligned} |\psi_{coh}\rangle &= \frac{1}{\sqrt{2^N N!}}(\hat{a}_A^\dagger + e^{i\phi_r}\hat{a}_B^\dagger)^N|0\rangle \\ &= \frac{1}{\sqrt{2^N N!}}\sum_{n=0}^{N}\binom{N}{n}e^{in\phi_r}\hat{a}_A^{\dagger N-n}\hat{a}_B^{\dagger n}|0\rangle, \qquad (1.12) \\ |\psi_{num}\rangle &= \frac{1}{(N/2)!}\hat{a}_A^{\dagger N/2}\hat{a}_B^{\dagger N/2}|0\rangle, \qquad (1.13) \end{aligned}$$

where $|0\rangle$ is a particle vacuum state. In the coherent state, all particles stay in the same single-particle state, $\frac{1}{\sqrt{2}}(\psi_A + e^{i\phi_r}\psi_B)$, and we say that two condensates represented by ψ_A and ψ_B have a well-defined relative phase ϕ_r. Even though for the two states the average particle numbers in each single-particle state are equal to $N/2$, the coherent state is a superposition of a number of number states with regular phase relations. Number states are

states with fixed particle number in each single-particle state. Therefore, two condensates having a well-defined relative phase means that there is corresponding uncertainty in particle numbers of the two condensates with strong correlation among number states.

The above consideration may be extended to the case of a single condensate. Indeed, in the case of the coherent state, we can call the two condensates as a *single* condensate because one single-particle wave function describes the whole system. If we rephrase this statement, we can claim that the relative phase of any two points in a single condensate is well-defined and consequently there are corresponding density fluctuations in a single condensate. This picture focus just on the internal phase relation in a condensate, not irritating our intuition by breaking particle number conservation. The definition of the long range order parameter shows this intrinsic property of a condensate, even though it can not be rigorously applied to a finite-size sample.

1.8 Outline of the Thesis

This thesis is organized as follows. Chapter 2 briefly describes experimental procedures in our BEC apparatus and introduces the microtraps which we used for the experiments presented in this thesis, such as an optical double-well trap and a magnetic microtrap on an atom chip. Chapter 3 focuses on 'coherent splitting' experiments, where we tried to split a condensate into two parts with a well-defined relative phase. Splitting was performed by deforming a single-well potential into a double-well potential, and this scheme was implemented in an optical trap and a magnetic trap. Chapter 4 describes dynamics of two optically coupled condensates. Two spatially separate condensates were optically coupled via Bragg scattering, and phase-sensitive atomic currents were established between the two condensates. The relative phase was optically read out and the coupling dynamics were experimentally investigated. Chapter 5 and 6 deal with somewhat different topics. Chapter 5 reports thermal relaxation processes in a double-well potential. With a condensate in one well, a metastable state was prepared by making the other well deeper than the well having the condensate. A new condensates formed up in the lower well and the distillation process was studied. Chapter 6 describes vortex experiments with an atom chip. A doubly quantized vortex state were topologically imprinted by adiabatic spin rotation, and a doubly-quantized vortex core was observed to split into two singly-quantized vortex cores. In Chapter 7, some concluding remarks and prospective are included.

Publications directly related to this thesis are added in Appendices B-H. Most of the contents of this thesis are based on what *we* discussed in the publications. Although I tried to put an original spin on discussing our work, large portions of the text reproduce the published work, especially when technical discussions were already optimized for publication.

Chapter 2

BEC Machine and Microtraps

Experimental techniques for producing Bose-Einstein condensates of gaseous atoms have been developed rapidly since the first realization in 1995 [15, 24] with pioneering breakthroughs such as a dark spontaneous force optical trap (dark-SPOT) [76] and a time-averaged orbiting (TOP) trap [77]. Now, the technical recipe for making Bose-Einstein condensates is well established. Moreover, Bose-Einstein condensates were created with all optical methods [78] as well as in a miniaturized magnetic trap [79, 80].

All of the experiments described in this thesis were carried out with BEC-III machine in MIT. The first BEC with the machine was produced in early 2001. A comprehensive description of the machine design and performance is provided in Ref. [81]. In this chapter, I overview the experimental procedures in our apparatus with some maintenance information for next users, and describe the microtraps used for the experiments, such as an optical double-well trap and a magnetic microtrap on an atom chip. The development of atom chips in MIT is outlined at the end of this chapter.

2.1 BEC Experiments in 'Science' Chamber

The BEC-III machine features itself for an auxiliary vacuum chamber - the 'science' chamber (SC).[1] The purpose of the science chamber is to physically separate BEC experiment space from BEC production space. In a conventional BEC apparatus, mechanical and optical accesses to condensates are restricted due to the presence of large magnetic coils and the optics for laser cooling which are indispensable to BEC production. Adding new components on the apparatus without disturbing the pre-existing production setup sometimes requires serious compromises in designing a new experiment. Thus having separate experiment space would give great flexibility to accommodate further complicated experiments and allow a rapid cycle of various experiments as well. The high productivity of the BEC-III machine

[1] Some people prefer the nomenclature of 'experiment' chamber rather than 'science' chamber.

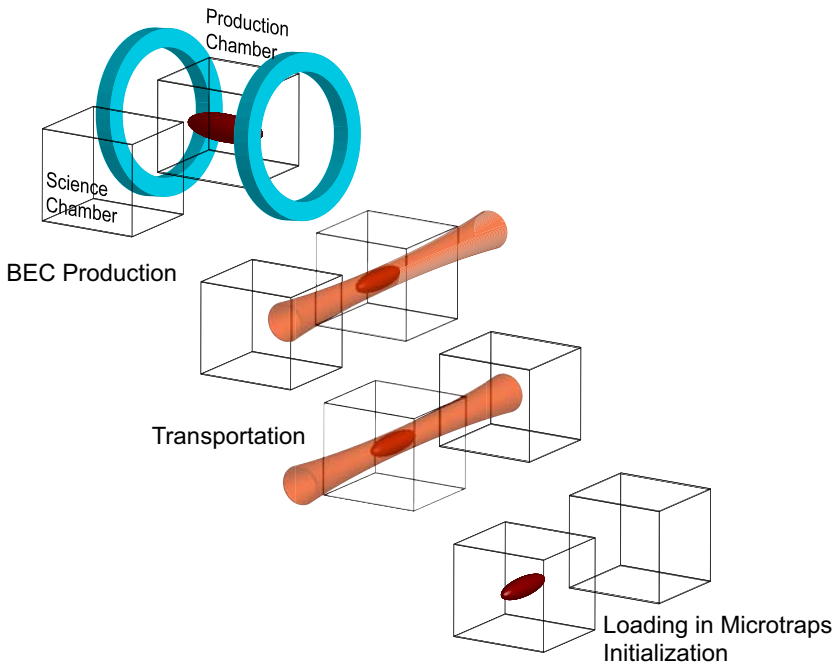

Figure 2-1: Experimental procedures with BEC-III machine. (a) A Bose-Einstein condensate of ^{23}Na atoms is generated in the production chamber after radio-frequency (rf) evaporation cooling in a Ioffe-Pritchard type magnetic trap. (b) The condensate is loaded into optical tweezers and (c) transported into the science chamber by moving the focal spot of the optical tweezers. (d) The condensate is loaded into a microtrap and initialized for further designed experiments.

over the past four years with a very diverse range of experiments definitely proves this advantage. In Figure 2-1, the general experimental procedures with BEC-III machine are illustrated. A Bose-Einstein condensate is produced in the production chamber, and then the condensate is transported to the science chamber by using optical tweezers. Once the condensate is located in the science chamber, it is initialized for a designated experiment; *ready to go for the BEC study.*

2.1.1 Basic Operations

BEC experiments generally consist of three steps: 1) preparing condensates, 2) perturbing and manipulating the condensates, and 3) observing or measuring the condensates' responses. In this secion, I present a very brief overview of the basic operations: production, manipulation, and imaging. For a more comprehensive review and detailed description of hardware and experimental parameters, please refer to Ref. [58, 82, 81].

Production

Bose-Einstein condensates with ^{23}Na atoms in the $|F = 1, m_F = -1\rangle$ state are created in a static Ioffe-Pritchard magnetic trap. A slow thermal atomic beam out of a spin-flip Zeeman slower is continuously loaded into a dark-SPOT [76] type magnetic-optical trap (MOT) [83]. The Zeeman slower has a zero-field point along the axis to increase the capture velocity of the slower. The slow thermal atomic beam has a mean velocity ~ 30 m/s and atomic flux $\sim 10^{11}$ atoms/s. After turning off the atomic beam, atoms are additionally cooled down by applying a dark polarization-gradient cooling (PGC).[2] For the PGC, the frequency of the MOT beams is shifted further to the red and repumping sidebands are added by an electro-optic modulator (EOM). Reviews on laser cooling techniques can be found in Ref. [84, 85, 86, 87]. Atoms in the $|F = 1, m_F = -1\rangle$ state are captured in a Ioffe-Pritchard (IP), cloverleaf magnetic trap. In a dark-SPOT MOT, most of atoms in the center region are in the $|F = 1\rangle$ state. However, we found that a small fraction of atoms are optically pumped into the $|F = 2\rangle$ state by the strong slowing beam passing through the MOT cloud. This might be the reason why a stronger slowing beam results in smaller condensates. After catching the atom cloud in a magnetic trap, forced evaporative cooling is applied using a radio frequency (rf) transition from the $|F = 1, m_F = -1\rangle$ state to the $|F = 1, m_F = 0, +1\rangle$ states. Typical condensates contain over 1.5×10^7 atoms.

Procedure	Duration	Atom number	(density)	Temperature
Atomic oven			(10^{14} cm^{-3})	530 K
Slowing and MOT loading	2 s			~ 1 mK
Dark PGC	5 ms			100 μK
Catching in a IP trap	1 s	10^{10}	(10^{11} cm^{-3})	
rf-evaporation to BEC	~ 25 s	$\sim 1.5 \times 10^7$	(10^{14} cm^{-3})	~ 500 nK
Decompression	2 s			
Loading in Tweezers	0.5 s	$\sim 5 \times 10^6$		
Transporting in the SC	2 s	$1 - 2 \times 10^6$		

Table 2.1: Production procedures. Atoms are loaded in a MOT, cooled down to BEC, and transferred to the science chamber. The duration of each procedure and the approximate atom number, density and temperature after accomplishing each procedure are presented.

Laser system

When BEC-III machine was built, we shared a laser system with the BEC-I machine. Because of high demand, we decided to build a new laser system for BEC-III machine, and in February 2003, BEC-III machine was equipped with its own laser system. The basic

[2] It is called a 'dark' PGC because the most of atoms are in the dark state, $|F = 1\rangle$. As far as I know, the real mechanism of this dark PGC has never been investigated systematically.

design of the new laser system is identical to that of the old laser system. A 589 nm yellow laser light is generated from a dye laser pumped by a 532 nm green laser. The laser frequency is locked to a Fabry-Perot cavity, and the reference for the cavity is an external saturation-absorption spectroscopy (SAS) [88] lock-in scheme. One technically interesting aspect is a 500-600 MHz high frequency acousto-optic modulator (AOM). The diffraction efficiency of the AOM is as high as $\sim 60\%$, but the output mode is not good enough to make the fiber-coupling efficiency over 60%. A schematic diagram of the laser system is in Appendix A.

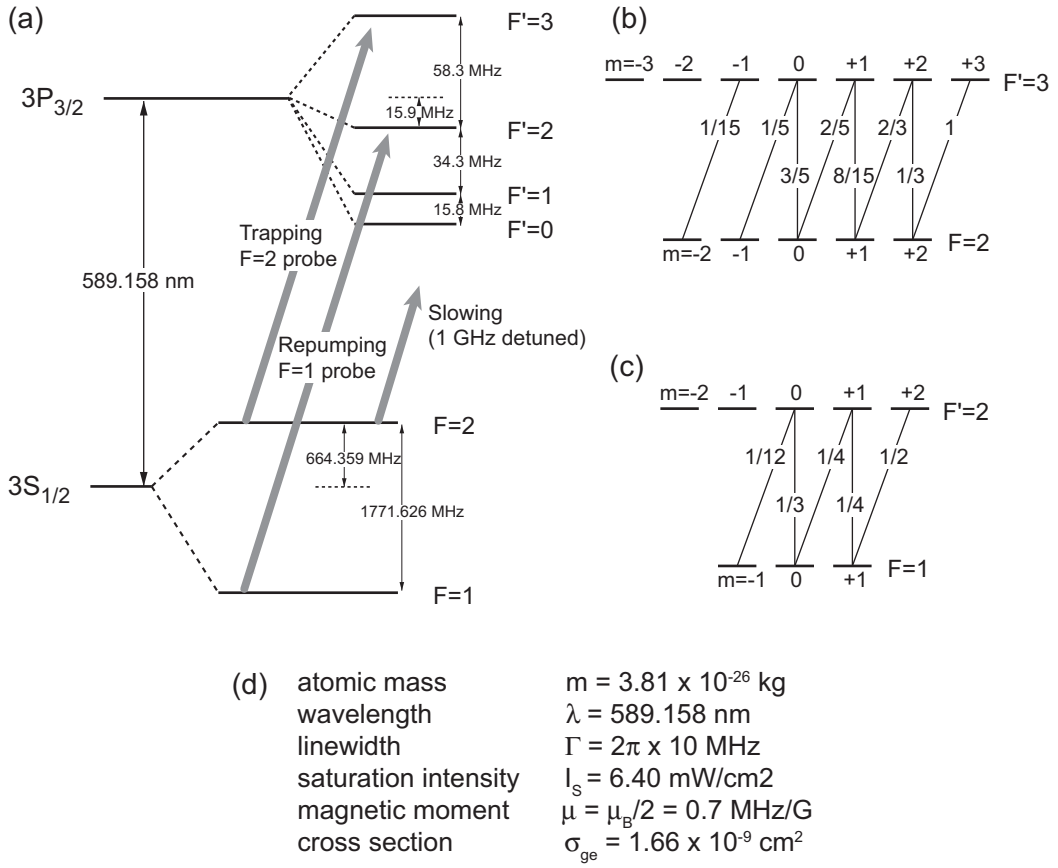

(d)

atomic mass	$m = 3.81 \times 10^{-26}$ kg
wavelength	$\lambda = 589.158$ nm
linewidth	$\Gamma = 2\pi \times 10$ MHz
saturation intensity	$I_s = 6.40$ mW/cm2
magnetic moment	$\mu = \mu_B/2 = 0.7$ MHz/G
cross section	$\sigma_{ge} = 1.66 \times 10^{-9}$ cm^2

Figure 2-2: Sodium ^{23}Na energy levels and the relevant atomic transitions. (a) Laser cooling and optical imaging use the D2 line. Relative strength of the (b) $|F = 2\rangle \rightarrow |F' = 3\rangle$ and (c) $|F = 1\rangle \rightarrow |F' = 2\rangle$ electric dipole transitions [87]. Only σ^+ and half of π transitions are indicated for simplicity. (d) Sodium atomic parameters.

Manipulation Tools

Manipulation of condensates can be categorized into three groups according to the atomic properties effected: 1) center-of-mass motion, 2) atomic transition, and 3) atomic collision.

• *Center-of-mass motion* - Magnetic force and optical dipole force are included in this category, which affect the external motion of atoms in condensates. These forces are based on the magnetic and electric dipole moments of atoms. Potentials with desired configurations can be formed by tailoring the spatial pattern of external fields such as magnetic field and laser beam intensity. All BEC experiments use a trapping potential to isolate atoms from hot and decoherencing environment. The optical dipole potential relies on dipole transitions between excited states and the ground state, i.e., ac Stark shifts, and it can confine atoms in any magnetic state, allowing the study of spinor condensates, which is impossible in an magnetic trap confining atoms only in weak-field seeking states. Furthermore, the laser frequency dependence of optical potential [89] and the interference effects of laser beams provide much wider applications such spin-dependent optical lattice potential [90]. In the experiments described in Chapter 3, condensates wave functions were dynamically deformed by changing the geometry of trapping potentials.

• *Atomic transition* - Atomic optical transition and magnetic transition are used to prepare condensates in target states. This category contains, for examples, Bragg transitions between different external momentum states and Raman transitions between different atomic internal states. Bragg scattering provides a robust probing method for the dynamical structure factor of condensates [91, 92]. In the experiments described in Chapter 4, Bragg scattering was used for detecting the relative phase of two condensates [11] and optically coupling two separate condensates [5].

• *Atomic collision* - BEC dynamics is strongly affected by atom-atom interactions which make atomic condensates an interesting system for many-body physics and nonlinear atom optics. The effective atom-atom interactions are determined by the scattering properties of atoms. The scattering properties are adjustable with external magnetic field. Since an atom has a magnetic moment and consequently the energy levels of the molecular states of two colliding atoms depend on a magnetic field, a scattering resonance happens when the energy of the bound molecular state crosses zero. At this moment the effective scattering length diverges. This is called *Feshbach resonance* [93], which gives a substantial freedom to atomic systems with quantum degenerate gases: an experimental knob for tuning atom-atom interactions. This method allows the study of BEC-BCS crossover.

Transport and Optical Tweezers

The optical tweezers is our method to transport condensates from the main (production) chamber to the Science chamber. The idea is straightforward: loading condensates in an optical dipole trap and moving the center of the optical trap, i.e., the focal spot of the laser beam to the target position in the Science chamber. A schematic setup for the optical tweezers for transportation is provided in Figure 2-3. The early developing story of the

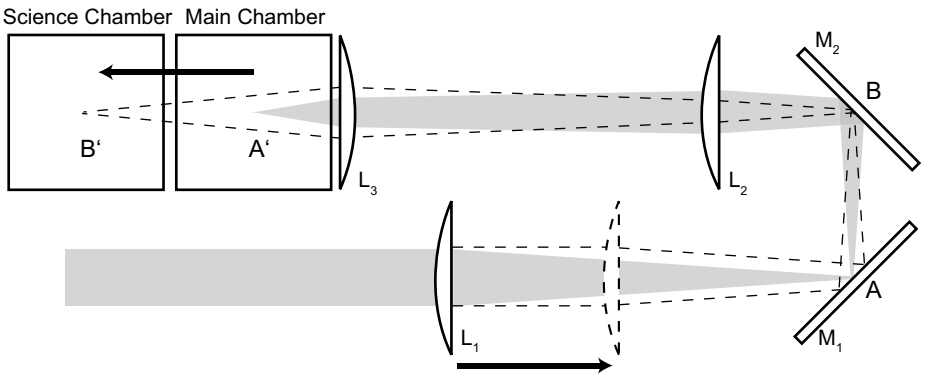

Figure 2-3: Experimental setup for optical tweezers. The collimated infrared (IR) beam is focused by the tweezers lens L_1 and the focal point of the tweezers lens is transferred by the one-to-one telescope (L_2 and L_3), forming optical tweezers in the vacuum chambers. By moving the tweezers lens in the longitudinal propagation direction, the optical tweezers correspondingly move between the production chamber and the science chamber. When the optical tweezers are located in the center of the production chamber (A'), the focal point of the tweezers lens is placed on the first mirror M_1 so that the position A' is adjusted by the second mirror M_2. On the other hand, when the optical tweezers are located in the center of the science chamber (B'), the focal point of the tweezers lens is placed on the second mirror M_2 so that the position B' is adjusted by the first mirror M_1.

optical tweezers is described in Ref. [81]. The first lens is mounted on a linear air-bearing translation stage.[3] The trajectory of the translation stage has a trapezoidal acceleration profile where the acceleration linearly increases and decreases to ensure the total travel time for a given distance. The power of the optical tweezers is roughly proportional to the traveling velocity.[4]

The trajectory of the optical tweezers should pass two points in the chambers. One is the initial position of condensates in the main chamber and the other one is the center of a microtrap in the science chamber. In order to facilitate the two-point alignment of the optical tweezers, two mirrors are placed in the beam path before the one-to-one telescope and the axial positions of two mirrors were selected to make them correspond to the focal positions in the main chamber and the science chamber. This configuration allows, ideally, to move independently the tweezers position in the main chamber and in the science chamber by adjusting one of the mirror at time. Please see Figure 2-3 for details. The positions of the focal spot in the main chamber and the science chamber can be adjusted independently to some extent. This design is extremely helpful when we have two different experiment setups in the science chamber and change the final position of the optical tweezers every other day.

[3] Aerotech ABL20040

[4] The first intuition suggests that the power should be proportional to the acceleration. The power profile was empirically adjusted.

Optical Imaging

Most of the data presented in this thesis was acquired by taking destructive, absorption images. Two atomic transitions were used for this purpose: the $|F = 1, m_F = -1\rangle \rightarrow |F' = 2, m'_F = -2\rangle$ transition ($F = 1$ image) and the $|F = 2, m_F = -2\rangle \rightarrow |F' = 3, m'_F = -3\rangle$ cycling transition ($F = 2$ image). For $F = 2$ images, condensates in the $F = 1$ hyperfine level were optically pumped into the $F = 2$ hyperfine level, and then imaged by the resonant probe beam. The images are focused on a CCD camera. An absorption image of atoms in a trap directly provides the spatial distribution of the trapped atoms. An absorption image after ballistic expansion by releasing atoms out of the trap provides the momentum distribution of the atoms.[5]

Absorption images provide the column density of atomic clouds integrated along the probe beam direction. The total number of atoms, N, in the absorption images taken along z-direction is given

$$N = \int dxdy \frac{-\ln(t(x,y))}{\sigma_0} = \frac{A}{\sigma_0} \sum_{pixels} -\ln(\bar{t}(x,y)), \tag{2.1}$$

where σ_0 is the resonant cross-section, A is the pixel area in the image. t is the transmission, and $\bar{t}$ is the coarse averaged transmission over the pixel area. For $F = 2$ images, $\sigma_0 = 3\lambda^2/2\pi$, and for $F = 1$ images, $\sigma_0 = 3\lambda^2/4\pi$, where λ is the resonance wavelength of the optical transition.

Other image techniques such as absorption imaging, phase-contrast imaging [94], and fluorescent imaging may be used according to the purpose of experiments. Detailed description on the quantitative analysis of absorption images is provided in Ref. [58].

2.1.2 Machine Maintenance

BEC-III machine has been operated about for five years without major problems, which reflects that the machine was designed out of valuable experiences with the previous generation BEC machines. In the following, several maintenance notes are presented.

• *Sodium oven* - The sodium oven is one of the main parts requiring periodic maintenance. We have to open the oven for regular oven cleaning and sodium refill. We added a 45° elbow in front of the half-nipple sodium cup to prevent spilling-over and accommodate more sodium. With 25 g sodium, the operation lifetime showed over 2000 hr which corresponds to the duration of six-month intensive operation. The oven ion pump seems to be degrading. When the oven was designed, an elbow and a Chevron baffle were connected to prevent the ion pump from being seriously poisoned by alkalis, but five-year exposure

[5] During expansion, the mean-field energy of condensates is converted to kinetic energy, giving faster expansion in the more tightly confining direction.

to the running condition may be too much for the ion pump. When the oven was vented and re-pumped out, baking-out of the ion pump turns out to be necessary for achieving the typical pressure $\sim 5 \times 10^{-}8$ torr at the running condition.

• *Science chamber pumping body* - The pumping body for the science chamber was replaced to improve the vacuum in the chamber. In the new pumping body, the ion pump are placed farther away from the science chamber in order to reduce the effect of fields from the ion pump magnet on the experiments. For future reference, the design of the pumping body is included in Appendix. A.

• *Replacing experiment setups in the science chamber* - Experiment setups in the science chamber have been replaced almost every six months. Because the safe region in the science chamber for the optical tweezers to deliver condensates without any serious problem is horizontally $\sim 1''$, the large $6''$-cube science chamber can support a couple of different experiment setups if they do not conflict over optical accesses for probing. Setup replacement takes less than two weeks: venting the chamber, installing new setups, attaining ultra-high vacuum (UHV), and making condensates. Typically, new experiment setups are pre-baked in a test chamber, which helps to get UHV back in the science chamber. In the case of a well-prepared setup, four-day baking at ~ 150 °C is enough to reach the typical vacuum of $\sim 1 \times 10^{-10}$ torr.

2.2 Optical Double-Well Trap

Figure 2-4 shows a schematic diagram of the optical setup for an optical double-well potential which is used for the experiments described in Chapters 3, 4, 5. The separation of two traps is dynamically controlled by the frequency difference of the driving rf signals and the depths of the optical traps were stabilized by giving a negative feedback to the power of the rf signals. It is helpful to select a frequency range where the diffraction efficiency of the AOM is almost uniform. The total power of the laser beam was monitored, and using a pinhole, the power of one of the two diffracted beam was preferentially monitored, too. This double monitoring allows stabilizing the trap depths individually. The optical traps were turned off by switching off the rf signals with additional help of a fast LCD shutter to get rid of leakage lights.

Since the separation of two traps is determined by the frequency difference of the driving rf signals, the trap position fluctuations due to mechanical vibrations of in-transit mirrors is common to both traps. This common-mode rejection feature is crucial to experiments requiring a precise double-well potential. Another advantage of using an AOM is that two optical traps are automatically co-planar, which is important to observe the matter wave interference of two condensates. We tried to generate an optical double-well potential with

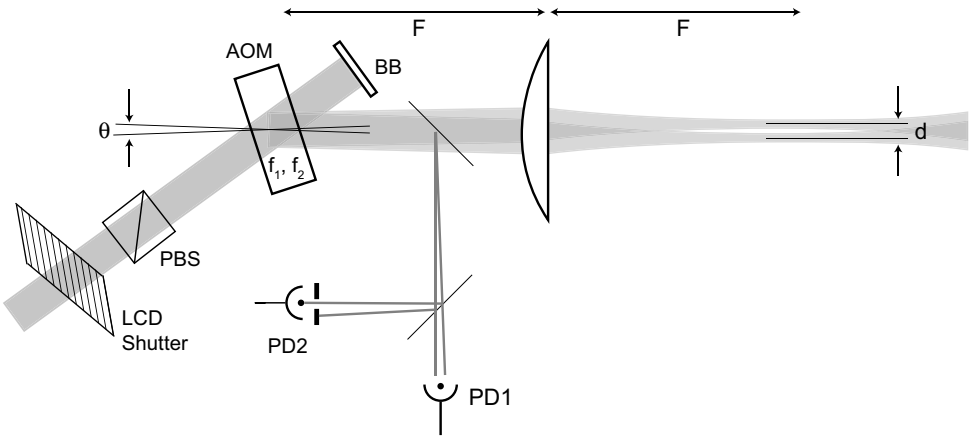

Figure 2-4: Schematic diagram of the optical setup for an optical double-well trap. An acousto-optic modulator (AOM) is driven simultaneously by two frequencies, f_1 and f_2, and diffracted a collimated infrared (IR) beam into two beams. The AOM is placed in the focal plane of a lens of focal length F so that after the lens, the two diffracted beams propagate parallel to each other forming two optical traps. The radial separation of the two traps, d, is controlled by the frequency difference, $\Delta f = |f_1 - f_2|$, determining the diffraction angle difference, θ. The zeroth order beam is blocked before the lens (BB). The laser beams for the optical traps are sampled out and monitored by photo diodes. Photo diode 2 (PD2) preferentially monitors one of the beams.

two independent optical traps using two polarization beam splitters (PBSs), but we could not observe matter wave interference with them, which we attributed to the possible twist of the axes of the two traps. However, one technical note for using an AOM for generating a muti-well potential is that the beam profile of the diffracted beam seems to be affected by the presence of the other diffracted beam. Extreme care was required.

2.3 Magnetic Microtrap on an Atom Chip

The concept of an *atom chip* was introduced with the idea of integrating atom-optics elements on a microfabricated device [95]. The fabrication technology, which has flourished in the micro-electronics industry, makes this idea conceivable. Miniaturizing and aligning atom-optics elements with sub-micron precision would significantly improve control over atoms. Furthermore, since in the proximity of the potential source the field gradient is higher and the length scale of the potential is smaller, using the proximity of miniaturized atom-optics elements would allow tighter confinement with small power consumption and more precise positioning of atoms. At first, atom chips were developed based on millimeter-size current-carrying wires. Magnetic wave guides [96, 97], microtraps [98, 99], and beam splitters [100] were experimentally demonstrated with thermal atoms. Recently, Bose-Einstein condensed atoms were added on this atom chip technology [79, 80], opening

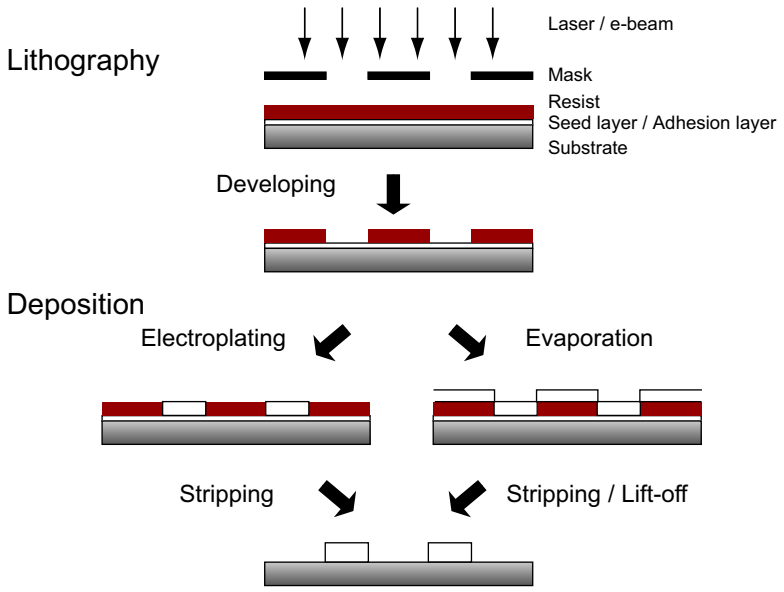

Figure 2-5: Fabrication process for conducting wires on an atom chip. The pattern of wires is defined on a substrate using lithography technique. Conducting wires grow on the substrate with evaporation or (and) electroplating. The final structure is established by chemical processes. For technical information for each fabrication process, refer to Ref. [106].

the prospect for chip-based atom optics with Bose-Einstein condensates as coherent matter wave source [6, 101, 102, 103].

Atom chip technology keeps being developed, including the integration of optical and electric components on a chip as well as magnetic components and extending its format to magnetic films, hard disks, and ferromagnets. Comprehensive reviews on the working principles of microtraps and atom chip fabrication can be found in Ref. [104, 105].

2.3.1 Chip Fabrication

The fabrication procedures for conducting wires on a substrate are illustrated in Figure 2-5. Compared to typical chip devices, an atom chip is a current-based device; the current distribution directly affects the magnetic potential on a chip so that controlling the homogeneous conductivity and the uniform shape of wires determines the performance of the atom chip. Furthermore, the situation becomes more non-trivial because the cross section of the wires should be larger than several ten μm^2 to accommodate an operating current of a few A. The thickness of wires on atom chips will be a few μm, much larger than in thin film (< 1 μm) applications in typical micro-electronics.

Fabricating very uniform conducting wires with a thick metal film is the technical challenge in the atom chip fabrication. Considering the advantage of using the proximity of

wires for tighter confinement, we might suggest to bring atoms closer to the wires in order to reduce the operation current. However, proximity effects put fundamental limits on the closest distance from the wires, which will be described in the next subsection. Practically, fabrication processes and materials should be carefully selected according to the purpose of experiments.

2.3.2 Proximity Effects

Using the proximity of the potential source allows tighter confinement with small power consumption and accurate manipulation of atoms. However, there could be some problems about placing an ultra-cold atom cloud very close to a room-temperature surface. The magnetic field on an atom chip is directly determined by the current distribution in the wires of the atom chip, and thus, if the current distribution is not perfectly controlled, atoms would be affected in an uncontrollable way. Placed closer to the wires, atoms will be more sensitive to imperfections of the current distribution. When an atom in the $|F = 1, m_F = -1\rangle$ state is placed 100 μm away from a straight wire carrying 1 A, the magnetic potential of the atom is 14 MHz, so a small deviation of the current would make a potential variation comparable to condensate's chemical potential which is typically a few kHz.

Proximity effects due to the imperfections of the current distribution can be divided into two groups: static and dynamic. Static effects are about spatial fluctuation of the current distribution. Spatial fragmentation of a condensates near a current-carrying wire was reported in several atom chip experiments [6, 107, 9, 108], and it was found that this fragmentation effect is caused by current path deviations within the conducting wires, i.e., current was not flowing straight so that the magnetic potential along the wire is not uniform [109, 110, 111, 112]. The potential roughness can happen due to imperfect fabrication of wires such as corrugated edges, rough top surface, and inhomogeneous deposition of conducting material. Even for very straight wires, current deviations may arise from other fundamental mechanism such as electromigration [113, 114]. The best uniformity in the geometrical shape of wires was reported in Ref. [115], where electron beam lithography and a lift-off procedure were used for making the atom chip. However, they still observed potential roughness and suggested the role of local fluctuations in wire composition.

On the other hand, dynamic proximity effects are about temporal fluctuations of the current distribution, i.e., noise currents in wires. The current noises are fundamental or technical. At a finite temperature, currents are generated by thermal agitation of electrons in a conductor, which is called *Johnson thermal noise* [116]. In magnetic traps, atoms experience magnetic field fluctuations due to the current noise, which have harmful effects such as spin-flip induced trap loss, heating, and decoherence. The field fluctuations might induce magnetic transitions between Zeeman sublevels. Spin-flipped atoms are repelled

from the magnetic trap. Field fluctuations could also shake the magnetic trap and heat up the atoms into higher vibration modes. Heating and reduced trap lifetime near a current-carrying wire were reported in early atom chip experiments [80, 107, 9]. Direct comparison of experimental results with theoretical predictions requires more careful and systematic controls for clear distinction of the effects of the fundamental noises from those of technical noises [9]. Recent observations [108, 117, 118] showed good agreement with theoretical predictions [119, 120, 121], showing a fundamental limit to the lifetime of condensates near a conducting wire.

The proximity effects restrict atom chip design in a serious way. With regard to coherent manipulation, decoherence due to spatially inhomogeneous field fluctuation [122, 123, 124] is a formidable problem to be solved or might be a failure reason for further application such as atom interferometry and quantum information processing. However, various experimental and theoretical investigations for solving or circumventing these problems are undergoing. Long coherence lifetime for internal states was observed with a high value of magnetic field [125], and interestingly, use of dilute alloys of noble metals was suggested to reduce the magnetic noises at low temperature [126].

2.3.3 Current Capacity

The limiting factor for the current capacity for a wire is the increase of the wire temperature due to ohmic heating. The electric resistivity of the wires will subsequently increase so that the heating effect is exponentially accelerated and ends up blowing the wire off. This is how a fuse works to prevent over-current. Therefore, the solution for improving the current capacity of a chip wire is clear: decreasing the electric resistivity of the wire and increasing the thermal conductance to the substrate.

In terms of bulk electric resistivity (Ag: 1.6 $\mu\Omega$·cm, Cu: 1.7 $\mu\Omega$·cm, Au: 2.2 $\mu\Omega$·cm), Ag can be called the best candidate for the conducting material for wires. However, it was reported that Au shows the best performance when microfabricated in small wires, reaching current densities $\sim 10^8$ A/cm^2 at liquid nitrogen temperature [127] and $> 10^7$ A/cm^2 at room temperature [128]. Current density of 10^7 A/cm^2 means that 1 A can flow in a wire of 1 μm height and 10 μm width. Superconductors are excluded in this consideration because of the fundamental limitation on the maximum current density, such as the critical field and flux pinning. In our atom chip development, the sheet resistance of 2 μm-thick evaporated Au film was measured to less than 0.015 Ω/sq. which corresponds to 75 % of the bulk conductivity.[6]

An ideal substrate for an atom chip should be a good electric insulator for preventing leakage currents and a good thermal conductor for fast heat dissipation. We tested silicon

[6]For Au film deposition, we used an external vendor. (Thinfilms, Inc./www.thinfilmsinc.com)

Property	Unit	Si	Al_2O_3	AlN	Al
Thermal conductivity	W/mK	163	27.2	170-190	237
Heat capacity	J/kg mK	700	419	800-1000	900
Thermal expansion	$10^{-6}/°C$	4.2	5.6/5.0	4.6	
Density	g/cm^3	2.3	3.97	3.3	2.7
Electric resistivity	Ω·cm		$> 10^{14}$	$> 10^{14}$	

Table 2.2: Relevant properties of substrate materials. Al_2O_3 has different thermal expansion rates depending on the expanding axis. The data for Al is for comparison.

(Si) substrates, sapphire (Al_2O_3), and aluminium nitride (AlN). Relevant properties of these material are provided in Table. 2.2. All of them have proper electric and thermal properties and have been reported to be used as a chip substrate. Sapphire is attractive for its high optical transmission allowing more optical accesses to atoms. However, it showed relatively poor performance in our test experiments. When a sapphire substrate experienced extreme local heating of a current-carrying wire, it cracked. The chip failure was caused by substrate cracking, not by wire blowing-up. We attribute this result to its relatively low thermal conductivity and thermal expansion coefficients which have different values for two crystal axes. Sapphire seems to be physically vulnerable to high temperature gradients. AlN has as good thermal conductivity as aluminum and Si and it is perfectly insulating as a ceramic material. One technical problem with AlN is that the surface roughness of commercially polished AlN substrates is > 1 μm, which affects the straightness of the metal wires.[7] We found the best solution for our chip substrate to be Si.

2.3.4 Chip Development at MIT

An atom chip setup consists of an atom chip, supporting structure, and electric connection parts. Figure 2-6(d) shows how the components were assembled. The atom chip was glued on an Al base block for better heat dissipation. A vacuum compatible epoxy with high thermal conductivity[8] was used, which significantly helped improve the current capacity of chip wires. The Al block with the atom chip was secured by four stainless rods welded on a vacuum CF flange with a 25-pin type-D electrical feedthrough.[9] Then, the atom chip was electrically connected with a kapton coated UHV ribbon cable to the feedthrough. For connecting external wires to the atom chip, several methods such as spot-welding, mechanical clamping, and soldering were used.

Since 2001, atom chip experiments have been carried out in BEC-III machine and several

[7] In private communication, Anderson group in JILA claimed that they developed a special polishing technique for AlN substrates.

[8] H77 from epoxy technology (www.epotek.com)

[9] MDC vacuum products corp. (www.mdc-vacuum.com) The feedthrough could handle up to 6 A without any vacuum problem. The toughest test condition was 4 pins having 6 A individually.

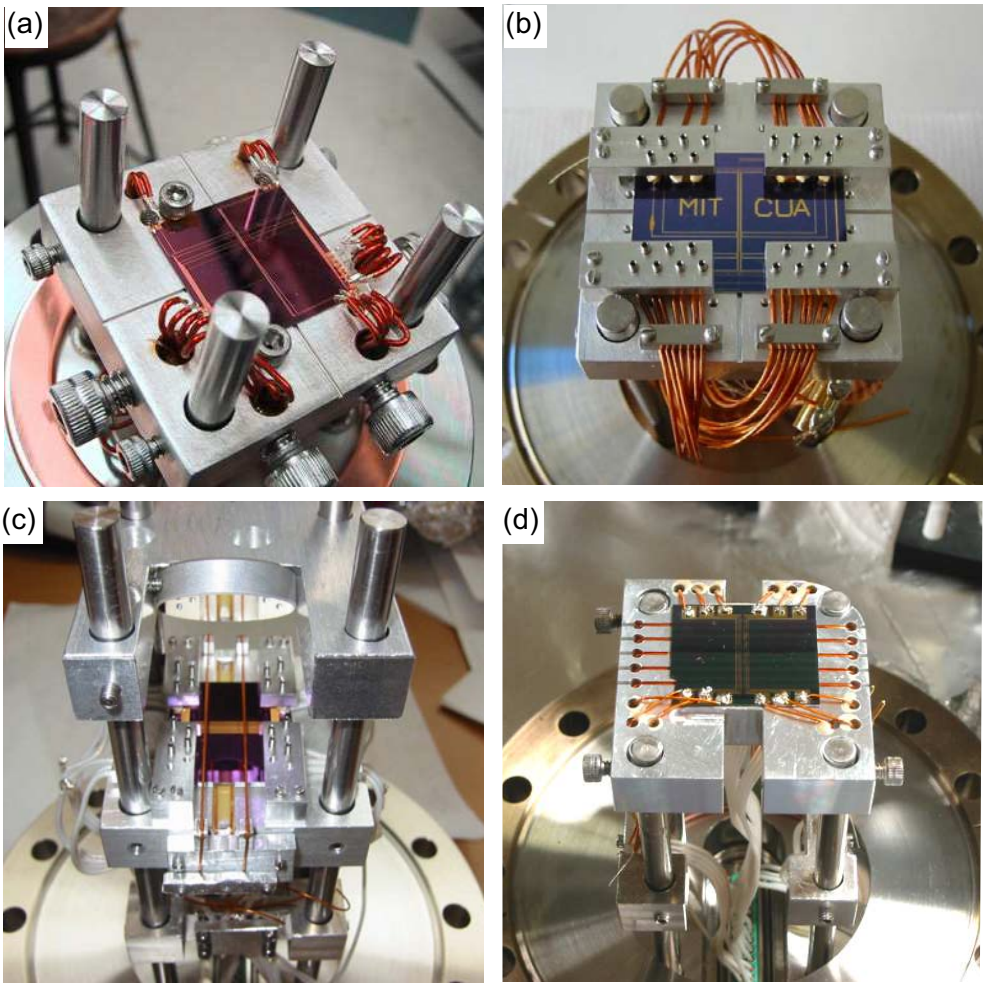

Figure 2-6: Photographs of atom chip sets. (a) Atom chip-I (2001). (b) Atom chip-III (2003). (c) Atom chip-IV (2004). (d) Atom chip-V (2005). The dimension of the aluminum base block in each image is $2'' \times 2'' \times 0.5''$. The features of each atom chip are described in the text.

atom chips were developed. In the following, I describe the features of each atom chip and the technical problems we experienced with each generation. Photo images of the atom chip setups are provided in Figure 2-6.

Atom chip-I (October 2001) featured a Z-wire trap and a straight magnetic wave guide. The atom chip was fabricated by the Microsystems Technology Laboratories in MIT. Copper wires were electroplated to a thickness of 10 μm and the current capacity of a 50 μm-wide wire was less than 1.8 A in a continuous mode. The wire connection was done with spot-welding technique. However, after high temperature baking ($\sim 200^{\circ}$C), 70% of connections fell off so that we could not make full use of all wires on the chip. Excitationless propagation of condensates in a magnetic waveguide [6] and topological formation of vortex states [8] were demonstrated. Furthermore, the spatial fragmentation of condensates near a wire was first reported with this chip [6], and the proximity effects were subsequently studied [9].

From the second generation, we have collaborated with Mukund Vengalattore at Harvard, Prentiss group. We provided him with optical masks and metal-filmed substrates, and he fabricated atom chips for us. Atom chip-II (December 2002) was designed for generating a double-well potential using a two-wire scheme [129]. The chip surface faced sideways in order to open a vertical optical access. Electric connection was done by a mechanical clamping method. A group of several wires were pressed down on the corresponding connection pads by a single ceramic bar. Unfortunately, the chip performance was disastrous after high temperature baking; non-negligible leakage currents run between wires which were supposed to be isolated. We attributed this failure to the breakdown of the insulating layer due to the combination of high pressure from the clamps and high baking temperature. Because several wires were placed under one single clamping bar, to ensure that all wires were connected it was likely to overpressure the external wires on the chip.

With lessons from Atom chip-II, we improved a couple of issues with Atom chip-III (October 2003). To avoid possible overpressure, we individually clamped down external wires on the chip connection pads. A small piece of ceramic was glued on the end of a small screw, and this screw worked as a single clamp secured by a Al holder which provides a spring effect due to its long arm. The structure can be seen in Figure 2-6(b). Also, the other vacuum components except the atom chip were pre-baked in a test chamber at high temperature and the real chip setup was mildly baked in the science chamber at less than 150°C. This individual clamping method was successful. The design of Atom chip-III was similar to that of Atom chip-II, but it has independent endcap wires, which enabled us to study the stability of a doubly quantized vortex state [3].

The goal of Atom chip-IV design (July 2004) was to generate a double-well potential with trapping parameters similar to the optical double-well potential [1] where we demonstrated the feasibility of coherent splitting. To achieve the trapping condition without being

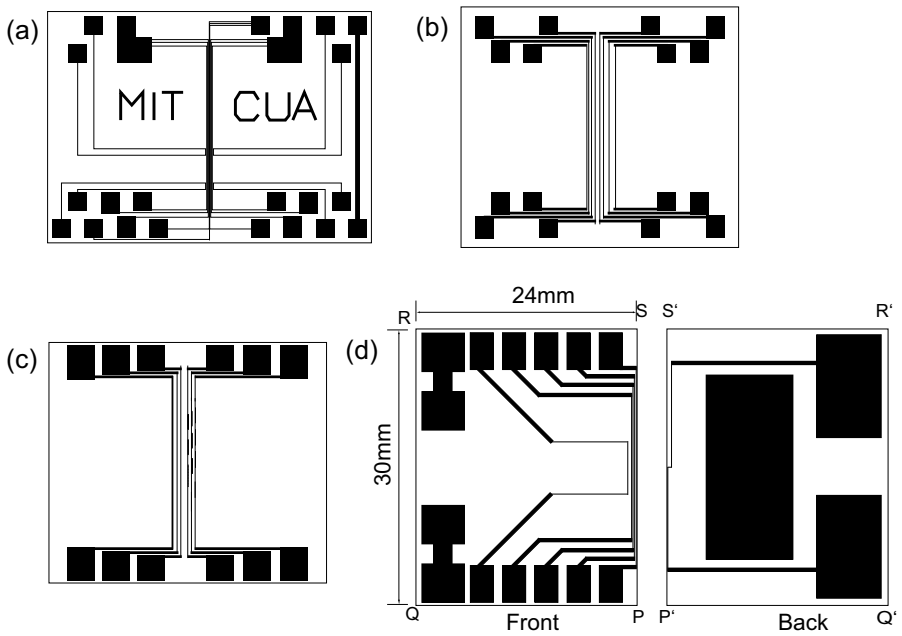

Figure 2-7: Wire patterns of the atom chip. (a) Atom chip-III with four individual endcap wires. A thick line on the right side is a RF antenna. (b) Atom chip-IV. Various spacing between wires for a two-wire scheme. (c) Atom chip-V. Several modulated wires are placed on the right side of the chip. (d) Atom chip-VI. The chip is designed double-sided for implementing the axial splitting.

affected by the proximity effects, we improved the current capacity of chip wires. The chip wires of 12 μm height and 50 μm width were electroplated with Au on a thermally oxidized Si substrate with a 2-μm-thick Au evaporated film. With this hybrid deposition, we could increas the current capacity to 6 A in a continuous mode. Chapter 3 has a detailed description of the chip setup.

Atom chip-V (June 2005) was prepared for the experiment of guiding atoms inside a hollow core photonic crystal fiber. Such a fiber is based on an omnidirectional Bragg reflector formed by a regular array of holes and is able to guide the light inside a hollow core. The atoms can be guided by the light inside the fiber and hopefully trapped and transported efficiently to distant location. The motivation of the experiment is using an atom chip as a precise positioning tool for atoms which may solve the atom-injection problems. Instead of using clamps, external wires were soldered on the chip in order to have open space for integrating a hollow fiber on the atom chip. Silver solder with a high melting point[10] was used for baking and vacuum properties. Technical details for soldering were taken care of by Gyuboong Jo. At the moment when I write this thesis, Atom chip-VI for atom interferometry is in preparation.

[10] Amtech solder products, Inc. (www.amtechinc.com)

Chapter 3

Coherent Splitting of a Condensate in a Double-Well Potential

This chapter describes experimental efforts to demonstrate a coherent beam splitter for developing a chip-based confined-atom interferometer. The results were reported in the following publications:

- Y. Shin, M. Saba, T. A. Pasquini, W. Ketterle, D. E. Pritchard, and A. E. Leanhardt, *Atom Interferometry with Bose-Einstein Condensates in a Double-Well Potential*, Physical Review Letters **92**, 050405 (2004). Included in Appendix B.
- Y. Shin, C. Sanner, G.-B. Jo, T. A. Pasquini, M. Saba, W. Ketterle, D. E. Pritchard, M. Vengalattore and M. Prentiss, *Interference of Bose-Einstein Condensates split with an Atom Chip*, Physical Review A **72**, 021604(R) (2005). Included in Appendix C.

An interferometer is a measurement device based on the wave nature of probe particles. The working principle of the interferometers is that the probe particles are coherently split into two or more paths and then recombined to read out the phase difference among the paths. Thanks to the intrinsic sensitivity of atoms to the environment, atom interferometers have been used to sense accelerations [130, 37] and rotations [131, 132], monitor quantum decoherence [133], characterize atomic and molecular properties [134], and measure fundamental constants [130, 135], showing comparable or even better performances than the optical counterparts. It had been anticipated that exploiting Bose-Einstein condensed atoms would upgrade the conventional thermal-atom interferometers: Bose-Einstein condensates having a uniform quantum phase are to matter wave interferometry what lasers are to optical interferometry, *i.e.* a coherent, single-mode, and highly brilliant source. Moreover, atom interferometry with confined particles has the prospects of improving flexibility and capability in analogy with optical interferometry using fiber-optic devices.

Diverse atom optical elements such as mirrors, beam splitters, gratings and waveguides were introduced, and have been developed for the coherent manipulation of matter waves.

An atom chip, as described in Section 2.3, integrates these elements on a microfabricated device allowing for precise and stable alignment [96, 97, 99]. Recently, this atom chip technology has been combined with Bose-Einstein condensed atoms [79, 80], and opened the prospect for chip-based confined-atom interferometers with Bose-Einstein condensates.

Current proposals for confined-atom interferometers rely on a dynamic method: Splitting an atomic wave packet by deforming a single potential well into two potential wells and recombining the atomic wave packets by the reverse process [129, 136, 137]. This chapter deals with our experimental efforts to implement this scheme with Bose-Einstein condensates in optical and magnetic microtraps. In Section 3.1, I depict the dynamics of a Bose-Einstein condensates in a double-well potential and outline relevant physics for coherent dynamic splitting. In the next two section, I describe the experimental study on dynamic splitting of Bose-Einstein condensates in a double-well potential.

There are two sets of experiments. The first set of the experiments (Section 3.2) used an optical double-well that was introduced in Section 2.2. We demonstrated coherent splitting of Bose-Einstein condensates and performed a trapped atom interferometer with the optical double-well system [1]. These results are remarkable in that the experimental feasibility of the scheme for confined-atom interferometers based on dynamic splitting is confirmed. In addition to technical challenges related to adiabatic manipulation of matter waves, it has not been even theoretically clear if the two condensates generated after macroscopic large splitting end up in a phase-coherent state or a number-squeezed state [138, 139, 140, 141]. A central prerequisite for confined-atom interferometers was demonstrated: A condensate can be *coherently* split into two halves with a determined relative phase and the two halves can be separated by an arbitrary distance, much larger than the dimension of the original condensate.

In the second set of the experiments (Section 3.3), we studied the dynamical splitting of condensates in a purely magnetic double-well potential on an atom chip. Inspired by the observation of coherent dynamic splitting with an optical double-well potential in the previous experiments, we developed an atom chip capable of duplicating the previous experimental conditions such as trap confinement and trapping geometry, which is a quite reasonable strategy for developing a chip-based atom interferometer. Matter wave interference of two split condensates was observed, from which the coherence of the splitting process was investigated. It was found that the stability of the magnetic double-well potential needs to be improved for coherent splitting. I propose several alternative schemes.

3.1 Dynamic Splitting of Condensates

Coherent splitting of matter waves is dividing the matter waves into two different wave packets with a well-defined relative phase, which is a prerequisite for further applications such as atom interferometry and quantum information processing. The methods envisioned for coherent splitting can be divided in two classes. One is splitting in momentum space and subsequently generating a spatial separation, using scattering of atoms from a periodic optical potential [142, 102]. The other is dynamic splitting by directly deforming a single wave packet into two spatially separate wave packets, which can be considered as cutting off the weak link between two wave packets, i.e., stopping tunneling through the barrier separating two wave packets. Splitting in momentum space has led to remarkably clean interferometric measurements and this method was generally used in atom interferometers using thermal atoms in free space. However, it has been pointed out that momentum splitting is not always accompanied by full spatial separation of the two wave packets so that spatially dependent phase shifts induced by atom-atom interactions during separation are problematic [102, 143]. Dynamic splitting in real space instead is perfectly compatible with keeping atoms confined, a feature beneficial to the versatility of interferometers.

3.1.1 BEC in a Double-Well Potential

Dynamic splitting of a Bose-Einstein condensate has been theoretically studied in the context of two coupled condensates in a double-well potential, which is one of the simplest extensions of the study of a single condensate. Since a Bose-Einstein condensate is described by a macroscopic wave function with an arbitrary but fixed phase, the double-well system has quantum tunneling through a potential barrier separating two condensates. Moreover, atom-atom interactions in condensates add to the simple single-particle quantum tunneling system richer physics such as Josephson effects [144] which are direct manifestation of the phase of a macroscopic quantum system.

The governing Hamiltonian in the double-well system can be represented by nonlinear time-dependent many-body Schrödinger equations, which are, however, generally known to be difficult to solve. Most of theoretical investigations were based on the two-mode approximation [145, 146, 141], where the state space of the system is restricted to a smaller space spanned by only two single-particle states. Usually, the two states are the motional ground states for each well or equivalently, the left state ϕ_L and the right state ϕ_R, are simply constructed from the single-particle ground state ϕ_g and the first excited state ϕ_e of the double well potential. $\phi_L \equiv \frac{1}{\sqrt{2}}(\phi_g + \phi_e)$ and $\phi_R \equiv \frac{1}{\sqrt{2}}(\phi_g - \phi_e)$ are localized in the left well and the right well, respectively. $\phi_L(t)$ and $\phi_R(t)$ may be functions of time especially when the double-well potential transforms in dynamic splitting process. There

might be another recipe for the two states: constructing the two wave functions from the Gross-Pitaevskii equations in each well with a given atom number and updating them with atom numbers in each well changing during evolution. However, this method is not only numerically heavy but also unnecessary for our purpose to obtain insights on the underlying physics.

The simplified Hamiltonian in the restricted state-space is given as

$$H = -g(U_1 - 2U_2)a_L^\dagger a_R^\dagger a_L a_R - J[a_L^\dagger a_R + a_R^\dagger a_L] + \frac{1}{2}gU_2[a_L^{\dagger 2} a_R^2 + a_R^{\dagger 2} a_L^2], \tag{3.1}$$

where $a_L^\dagger$ and $a_R^\dagger$ are the mode creation operators for ϕ_L and ϕ_R, respectively. $U_1 = \int dx|\phi_{L,R}|^4$ represents on-site atom-atom interaction in one well and $U_2 = \int dx|\phi_L|^2|\phi_R|^2$ represents atom-atom interaction between the two wells. The first term is proportional to the product of the atom numbers in each well, $N_L N_R = \langle a_L^\dagger a_L a_R^\dagger a_R \rangle$, the second term represents single-particle hopping with the effective single-particle tunneling strength, J,[1] and the third term represents two-particle hopping which will be ignored in the following description. We assumed that ϕ_L and ϕ_R are symmetric and ignored the term proportional to the total atom number, $N = N_L + N_R = \langle a_L^\dagger a_L + a_R^\dagger a_R \rangle$. The complete derivation can be found in Ref. [141].

What is the many-body ground state for this Hamiltonian? The ground state is determined out of the competition between the on-site interaction energy and the tunneling energy. Two limiting cases help understand the physical effects of the energy terms. When there are no atom-atom interactions, i.e., $g = 0$, the ground state is the one with all atoms in the state $\phi_g = \frac{1}{\sqrt{2}}(\phi_L + \phi_R)$, a coherent state with a definite relative phase. On the other hand, when tunneling is prohibited, i.e., $J = 0$, the minimization of the total energy suggests that the ground state is the one with equal population in each well because $N_L N_R$ has a minimum value at $N_L = N_R$ for fixed N. Therefore, the tunneling-dominated situation has the ground state close to a coherent state having a well-defined relative phase, and the interaction-dominated situation has the ground state close to a Fock state having fixed atom numbers for the two wells. In a periodic potential such as an optical lattice, the superfluid-Mott insulator transition originates from the same physical mechanism.

The dynamics of a Bose-Einstein condensate in a double-well potential has been theoretically investigated by many authors, in particular focusing on nonlinear Josephson oscillations. The physical origin of the phenomena is the nonlinear coupling between the relative phase and the population imbalance of two condensates; the two variables are quantum-mechanically conjugate to each other.[2] Since the population imbalance is not accessible

[1] $J = J_0 - gNU_3$, where J_0 is the ideal single-particle tunneling rate, $N = N_L + N_R$ is the total atom number, and $U_3 = \int dx|\phi_L|^2\phi_L^*\phi_R$.

[2] In a thermodynamical limit, $N \gg 1$.

with superconductor Josephson junctions, the system of two coupled atomic condensates allows the investigations of novel effects such as macroscopic quantum self-trapping [147] and π-phase oscillations [148].

A real situation of Bose-Einstein condensates in a double-well potential may have more complicated and interesting physics originated from additional terms ignored in Eq. (3.1). In the experimental situations described in Chapter 4 and 5, the tunneling term is extremely negligible. Instead, the experiment in Chapter 4 deals with an external, optical coherent coupling between two condensates and the experiment in Chapter 5 deals with incoherent thermal coupling between two condensates at finite temperature.

3.1.2 Requirements for Coherent Dynamic Splitting

Coherent dynamic splitting is equivalent to decreasing the tunneling rate $J \to 0$ resulting in a final coherent state with a well-defined relative phase. This splitting can be physically implemented by increasing the height of the potential barrier between the two wells. However, as explained in the previous subsection, the true ground state with $J = 0$ is a Fock state with a completely random relative phase. When we start with a coherent state with large tunneling and increase the height of the potential barrier, the number fluctuation tends to evolve from Poissonian to sub-Poissonian increasing the uncertainty of the relative phase [146]. Therefore, an extremely slow splitting process satisfying the adiabaticity of the internal phase dynamics over the whole process will never generate a coherent state, which suggests one criterion for the upper bound for the time scale of the splitting process.

Fundamental limits on the phase coherence between isolated condensates arise due to the phase diffusion [149, 138, 139, 140, 141]. A coherent state is a superposition of many number states. Due to atom-atom interaction, the energy of a number state nonlinearly depends on the atom number, which cause the relative phase to naturally diffuse [149, 138]. This phase diffusion gives another consideration for the upper bound: The splitting process is required to be finished before the relative phase diffuses away.

One of the conceivable methods for coherent dynamic splitting might be abruptly removing the tunneling between the two wells. However, the abrupt rise of the potential barrier and the accompanying rapid change in the double well potential would induce collective excitations in the initially stationary condensate. Therefore the splitting process should be slow enough to keep the condensates in the stationary ground states of the resulting individual wells. The time scale for ramping up the potential barrier needs to be larger than the oscillation period which is the inverse of the trap frequency.

In conclusion, coherent dynamic splitting requires to be diabatic with respect to the internal phase dynamics and adiabatic with respect to the external motional dynamics. The detailed analysis on the adiabaticity conditions for coherent dynamic splitting can be

found in Ref. [145, 146, 141].

3.2 Coherent Splitting in an Optical Double-Well Potential

Dynamic splitting of Bose-Einstein condensates was investigated first with an optical double-well potential. Condensates were initially loaded from the tweezers into an optical trap shown in figure 3-1(a). The potential barrier between the two wells was smaller than the peak atomic mean field energy so that the trap was characterized as a single-well containing a single connected condensate with a uniform phase. Starting with the dimpled single-well trap was beneficial to reduce collective excitations accompanying the splitting process, such as radial dipole oscillations. Increasing the barrier height without changing the centers of the two wells might be more ideal in terms of quietness, but in atom interferometry larger separation is preferred. After holding the cloud in this dimpled single-well trap over 10 s to damp excitations which might have been caused during the loading procedure, condensates were almost stationary.

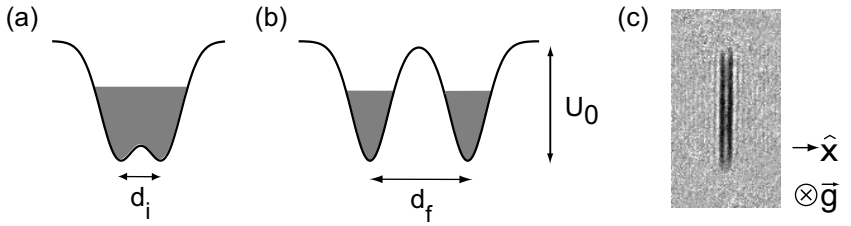

Figure 3-1: Splitting Procedure in an optical double-well potential. A Bose-Einstein condensate was split into two parts by deforming (a) an optical single-well potential into (b) a double-well potential. The experimental setup for the optical double-well potential was described in Section 2.2. The $1/e^2$-intensity radius of the focused beam corresponding to a single-well potential was 5 μm. In the typical experimental condition, the separation of the two well $d_i = 6$ μm for initial single-well trap and $d_f = 13$ μm for final double-well trap. A single, isolated potential well had trap depth of $U_0 = h \times 5$ kHz, which was determined from interferometric measurements described in Section 3.2.2, and radial (axial) trap frequency $f_r = 615$ Hz ($f_z = 30$ Hz). The potential "dimple" in (a) was $< h \times 500$ Hz which was much less than the peak atomic mean field energy of $\sim h \times 3$ kHz allowing the trap to be characterized as a single-well. The potential "barrier" in (b) was $h \times 4.7$ kHz which was larger than the peak atomic mean field energy allowing the resulting split condensates to be characterized as independent. The atom number of condensates was $\sim 10^5$. (c) The absorption image shows two well-separated condensates confined in the double-well potential diagramed in (b). The field of view is 200 μm $\times$ 350 μm. The gravitation, $\vec{g}$, points into the page.

The single-well trap was deformed into the double-well potential shown in figure 3-1(b) by linearly increasing the distance between the two wells to 13 μm in 5 ms. The splitting

time and the final distance between the two wells were experimentally optimized for long coherence time after splitting. The operating principle of the optical double-well potential was described in Section 2.2. The amplitudes of the rf signals were tailored during the splitting process to yield nearly equal population and trap depths for each potential well.

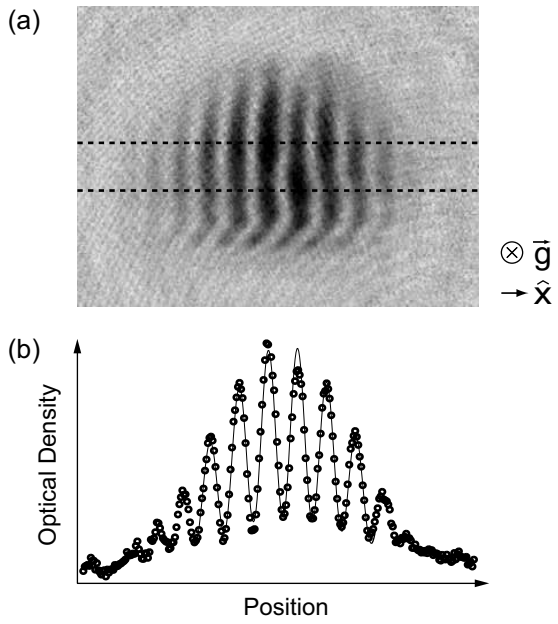

Figure 3-2: Matter wave interference. (a) Absorption image of condensates released from the double-well potential immediately after splitting and allowed to overlap during 30 ms of ballistic expansion. The imaging axis was parallel to the direction of gravitational acceleration, $\vec{g}$. The field of view is 600 μm $\times$ 450 μm. (b) Radial density profiles were obtained by integrating the absorption signal between the dashed lines, and typical images gave $> 60\%$ contrast. The solid line is a fit to a sinusoidally-modulated Gaussian curve from which the spatial phase of the interference pattern was determined (see text for details). This figure presents data acquired in a single realization of the experiment.

The relative phase of the two split condensates was determined by the spatial phase of the matter wave interference pattern formed by releasing the condensates from the double-well potential and letting them ballistically expand and overlap (Figure 3-2). For a ballistic expansion time much larger than the trap oscillation period and neglecting interactions during ballistic expansion, each condensate has a quadratic phase profile [62], $\psi_{\pm}(\vec{r},t) = \sqrt{n_{\pm}(\vec{r},t)}\exp(i\frac{m}{2\hbar t}|\vec{r} \pm \vec{d}/2|^2 + \phi_{\pm})$, where $\pm$ denotes one well or the other, $n_{\pm}$ is the condensate density, m is the atomic mass, $\pm\vec{d}/2$ is the starting position of the ballistic expansion, and $\phi_{\pm}$ is the condensate phase. Thus, the full density profile of the interference pattern takes the form

$$n(\vec{r},t) = (n_+ + n_- + 2\sqrt{n_+ n_-}\cos(\frac{md}{\hbar t}x + \phi_r)), \tag{3.2}$$

where $\phi_r = \phi_+ - \phi_-$ is the relative phase between the two condensates and $\vec{d} = d\hat{x}$. To determine ϕ_r, the integrated cross section shown in Figure 3-2(b) was fit with a sinusoidally-modulated Gaussian curve, $G(x) = A\exp(-(x-x_c)^2/\sigma^2)(1+B\cos(\frac{2\pi}{\lambda}(x-x_0)+\phi_f))$, where ϕ_f is the phase of the interference pattern with respect to a chosen fixed x_0. Ideally, if x_0 is set at the center of the two wells, then $\phi_r = \phi_f$. However, misalignment of the imaging axis with the direction of gravitational acceleration created a constant offset, $\phi_f = \phi_r + \delta\phi$. With $t = 30$ ms the measured fringe period, $\lambda = 41.5$ μm, was within 4% of the point source formula prediction [Eq. (3.2)], $ht/md = 39.8$ μm.

3.2.1 Coherence Time

Each realization of the experiment produced an interference pattern with the same spatial phase. This reproducibility demonstrated that the two condensates in a double-well potential had deterministic relative phase and that deforming the optical potential from a single well into a double well *coherently* split the condensate. This result is remarkable in that it experimentally confirms the feasibility of coherent dynamic splitting of a condensate.

We attribute this success to the favorable feature of the optical setup for a double-well potential: since both wells are derived from a single laser beam passing through an AOM, vibrations and fluctuations of the laser beam are rejected as common modes. Furthermore, an optical trap provides clean releasing of condensates because it can be turned off rapidly. In the past experiment where a double-well potential was created by splitting a magnetically trapped condensate with a blue-detuned laser beam [16], coherent splitting, i.e., a reproducible relative phase between the split condensates could not be observed due to fluctuations in the position and the power of the splitting laser beam and irreproducible turn-off of the high current magnetic trap that initiated ballistic expansion.

The relative phase between the separated condensates was observed to evolve linearly in time (Figure 3-3(a)). This evolution was primarily attributed to a small difference in the well depths. Equal population in each potential well indicates that the well depths of the two wells were equal at the moment of splitting, but due to the frequency-dependent diffraction efficiency of the AOM mentioned before, the well depths could happen to be changed after splitting. Since the two condensates had equal peak atomic mean field energy, the difference of the chemical potentials of the two condensates reflected the difference in the well depths. The rate of relative phase evolution could be tailored by adjusting the relative intensity of the two laser beams generating the wells.

The standard deviation of eight measurements of ϕ_r was < 40 degrees for condensates split then held separated for up to 1 ms and increased to over 90 degrees after 5 ms holding (Figure 3-3(b)). Here, we can ask two relevant questions on coherence after splitting: What determined the initial phase uncertainty and what made the phase uncertainty growing? In

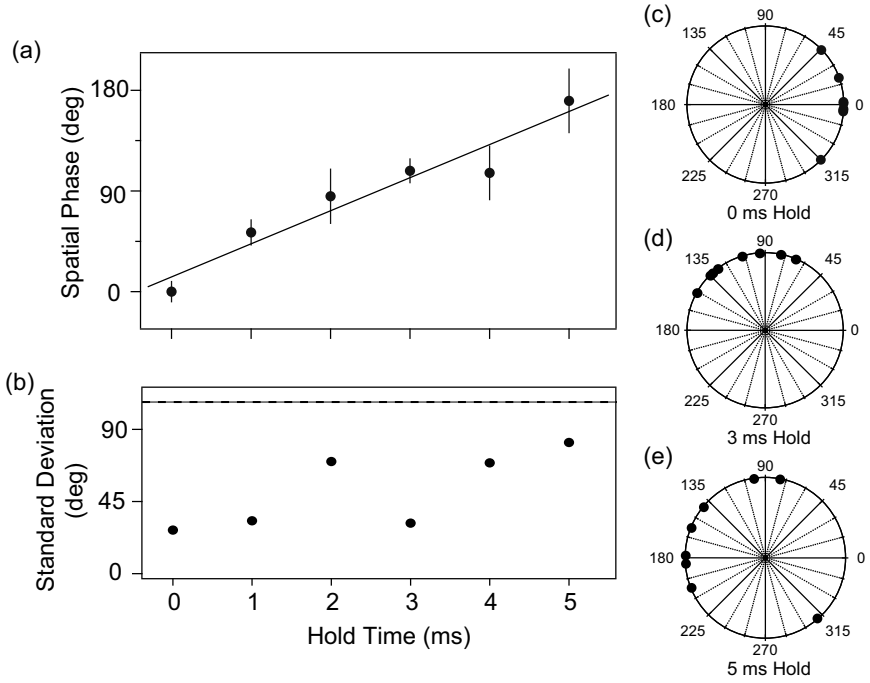

Figure 3-3: Phase coherence of the separated condensates. (a) The spatial phase of the matter wave interference pattern is plotted versus hold time after splitting the condensate. Each point represents the average of eight measurements. The phase evolution was due to unequal trap depths for the two wells, which was determined from the linear fit to be $h \times 70$ Hz or $\sim 1\%$ of the trap depth. (b) Standard deviation of eight measurements of the relative phase. The definition of the standard deviation of phase might not be clear because of the module property of phase. However, considering that a random distribution of phases between -180 and $+180$ degrees would have a standard deviation of ~ 104 degrees (dashed line), the results quantitatively confirm the reproducible nature of the splitting process and the coherent evolution of the separated condensates. Polar plot representation of eight phase measurements for (c) 0 ms holding, (d) 3 ms, and (e) 5 ms.

our experimental condition, we would expect a phase diffusion time $t \sim \frac{\sqrt{N}}{\hbar\ \mu} \approx 250$ ms [149] because of Poissonian number fluctuations in a coherent state. As described in Section 3.1, the localization due to atom-atom interactions may reduce the initial phase coherence of the split condensates but this would also extend the phase diffusion time [138, 139, 140, 150, 141]. Apparently, the coherence time observed in our experiment was almost one order magnitude smaller than this phase diffusion time, so definitely, the coherence time was not limited by these fundamental issues, but some technical issues. For example, we could not certainly determine the spatial phase of fringes at hold times > 5 ms because of axial and breathing-mode excitations created during the splitting process. These excitations are represented as angled and curved fringes, i.e., the relative phase of two condensates along the axial direction is not uniform, meaning relative axial motions of the two condensates. Matter wave interference patterns after 5 ms holding are displayed in Figure 3-4.

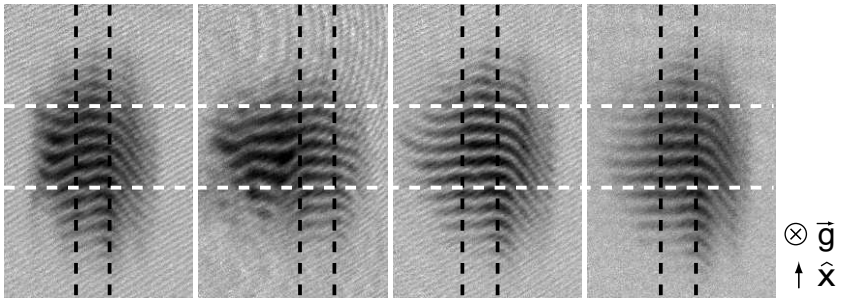

Figure 3-4: Perturbation from splitting process. Matter wave interference patterns after 5 ms holding are displayed. The curvature of the interference fringes increased with hold time limiting the coherence time of the separated condensates to 5 ms. When we determined the relative phase of two condensates from the spatial phase of the interference pattern, we picked up the region where the tangent direction of fringes was parallel to the axial direction, meaning the relative axial motion of the two condensates was at rest. The two black dashed lines in each image indicate the region used for phase measurement and the white dashed lines are guiding lines for phase comparison. The field of view is 450 μm $\times$ 700 μm.

In a perfect symmetric double-well potential, the splitting process can not induce axial relative motions of two split condensates, due to mirror symmetry, and therefore angled fringes would not appear. In principle, slower splitting should result in more straight and parallel fringes, but the straightness of fringe patterns could not be improved with even larger splitting time > 5 ms. Therefore, the observation of angled fringes obviously shows that the two traps are not symmetric. With numerical simulation, Collins *et.al.* [151] pointed that these asymmetric fringe patterns suggest the presence of slight additional geometry variations of the two traps. If the two traps are not parallel, the splitting process would not occur at the same time along the axial direction and the condensates would flow down to the converging direction. If the two traps do not have the same axial position, the splitting

direction would not be normal to the axial direction and induce the relative axial motions. Even though the two optical beams for the two traps have almost same optical paths, they can have different focal positions due to optics aberration and beam profile difference. Unfortunately, there is no easy experimental knob for controlling the relative axial position of the two traps. In the experiment, extreme care for optical alignment was needed.

3.2.2 Trapped Atom Interferometry

As a proof-of-principle experiment, we performed trapped atom interferometry with condensates using the coherent splitter described in the previous section. The phase sensitivity of the trapped-atom interferometer was demonstrated by applying ac Stark phase shifts to either (or both) of the two separated condensates. Phase shifts were applied to individual condensates by pulsing off the optical power generating the corresponding potential well for a duration $\tau_p \ll 1/f_r$. Figure 3-5(a) shows that the spatial phase of the matter wave interference pattern shifted linearly with the pulse duration, as expected. Due to the inhomogeneous optical potential, $U(r)$, the applied ac Stark phase shifts varied across the condensate as $\Delta\phi(r) = -U(r)\tau_p/\hbar$. Averaging this phase shift over the inhomogeneous condensate density, $n(\vec{r})$, we approximate the expected spatial phase shift of the matter wave interference pattern as $\Delta\bar{\phi} = \frac{1}{N}\int d^3\vec{r}\; n(\vec{r})\Delta\phi(\vec{r}) = (U_0 - \frac{2}{7}\mu)\Delta t/\hbar$, where N is the number of atoms, and U_0 is the potential well depth, and μ is the atomic mean field energy.[3] The measured phase shifts yielded $U_0 = h \times 5$ kHz (Figure 3-5(c)), which was consistent with calculations based on the measured trap frequencies.

In a good atom interferometer, the phase evolution of atoms in one arm should be independent of the phase evolution of atoms in the other arm. If there is some interaction between the two arms, i.e., some phase coupling between the two separate condensates, then the relative phase would show nonlinearity such as Josephson oscillations [147, 62], which would make the interpretation of the external effects extremely complicated or practically impossible. Due to the large well separation and mean field energy $h \times 1.7$ kHz below the barrier height, the single-particle tunnelling rate in our system was $\sim 5 \times 10^{-4}$ Hz [62], and the condensates were effectively decoupled. The linear behavior in Figure 3-5(a) of the relative phase of the two condensates indirectly shows the absence of coupling between the two separate condensates.

As a supplementary experiment, we performed an experiment where the time of applying ac Stark phase shifts was controlled. Because the relative phase of the two condensates

[3]This first-order approximation gives rise to an interesting question about its validity. Nonuniform phase shifts physically correspond to forces and cause external motions. In our situation, it is a breathing mode. Phase gradient represents kinetic energy and the subsequent phase evolution would become faster so that the averaging method might underestimte the resulting phase shift. In our experiment, $\tau_p \ll 1/f_r$ to ensure that the phase difference across the condensate is small.

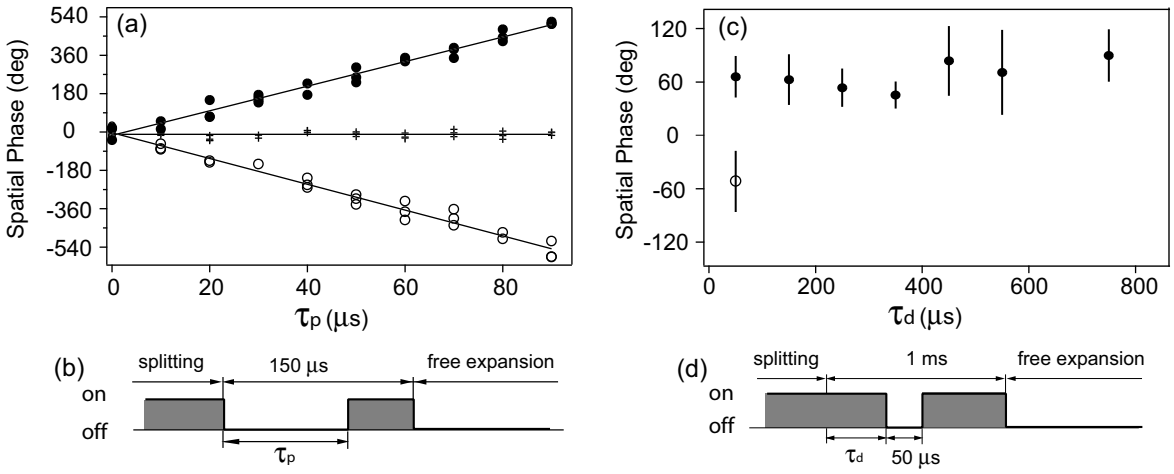

Figure 3-5: Trapped-atom interferometry. (a) ac Stark phase shifts were applied to either well exclusively (solid circles and open circles) or both wells simultaneously (crosses) by turning off the corresponding rf signal(s) driving the AOM for a duration τ_p. The resulting spatial phase of the matter wave interference pattern scaled linearly with τ_p and hence the applied phase shift. Applying the ac Stark shift to the opposite well (solid versus open circles) resulted in an interference pattern phase shift with opposite sign. Applying ac Stark shifts to both wells (crosses) resulted in no phase shift for the interference pattern. This data was taken with a slightly modified experimental setup such that the trap depth of the individual potential wells was $U_0 = h \times 17$ kHz, corresponding to a 270 degree phase shift for a 50 μs pulse. (b) The time sequence of the optical intensity for the well(s) temporarily turned off. (c) Independent evolution of two separate condensates. A 50 μs pulse induced a 70 degree shift independent of the pulse delay, τ_d, showing that there is no phase coupling between the two condensates. The experimental setup was as described in Figure. 3-1 ($U_0 = h \times 5$ kHz). ac Stark phase shifts were applied to either well exclusively in the same way as in (a). (d) The time sequence of the optical intensity for the well temporarily turned off.

was linearly running in time, applying phase shifts at different time means applying it with different relative phases. The measured phase shifts of the matter wave interference depended only on the time-integral of the applied ac Stark phase shifts (Figure 3-5(c)), as expected for uncoupled condensates. The final relative phase, ϕ_r, should be the same on different phase trajectories because the history of phase accumulation does not affect the total amount of accumulated phase. For coupled condensates, a time dependent signal would appear due to nonlinearity.

As a summary of this section, we have performed atom interferometry with Bose-Einstein condensates confined in an optical double-well potential. The large spatial separation between the potential wells guaranteed that each condensate evolved independently and allowed for addressing each condensate individually. The phase readout scheme using matter wave interference after ballistic expansion allowed us to avoid deleterious mean field effects inherent in proposals using in-trap wavepacket recombination [152]. If we propagate the separated condensates along a waveguide prior to phase readout, the atom interferometer would have an enclosed area and become rotation-sensitive. Implementing this idea with chip-based magnetic waveguides [6] is a motivation for the experiment described in the next section.

3.3 Toward Atom Interferometry on an Atom Chip

Encouraged by the successful demonstration of trapped atom interferometry with Bose-Einstein condensates in the previous experiment, we made efforts to realize a chip-based atom interferometer. The reason why we want to do an almost same experiment with an atom chip as what we already did with the optical system is that in the viewpoint of atom interferometry, the magnetic system currently looks more promising to extend to a rotation-sensitive geometry. In addition to the technical advantages of atom chips as discussed in Section 2.3, atom chips based on current-carrying wires can create a magnetic double-guiding potential with adjustable separation.

The primary goal of the following chip experiment is to duplicate the previous optical experiment; achieving coherent splitting of a condensate on an atom chip. Since we demonstrated coherent splitting with the optical double-well potential and identified the experimental parameter window for coherent splitting, generating a magnetic double-well potential having similar trapping parameters would be definitely a reasonable strategy for carrying out the corresponding chip experiment, which suggests that the magnetic double-well potential have trap frequency over 300 Hz and barrier height over 5 kHz with a well-separation less than 30 μm. Although we can fulfill these requirements easily by bringing the atoms very close to the current-carrying wire, deleterious proximity effects such as frag-

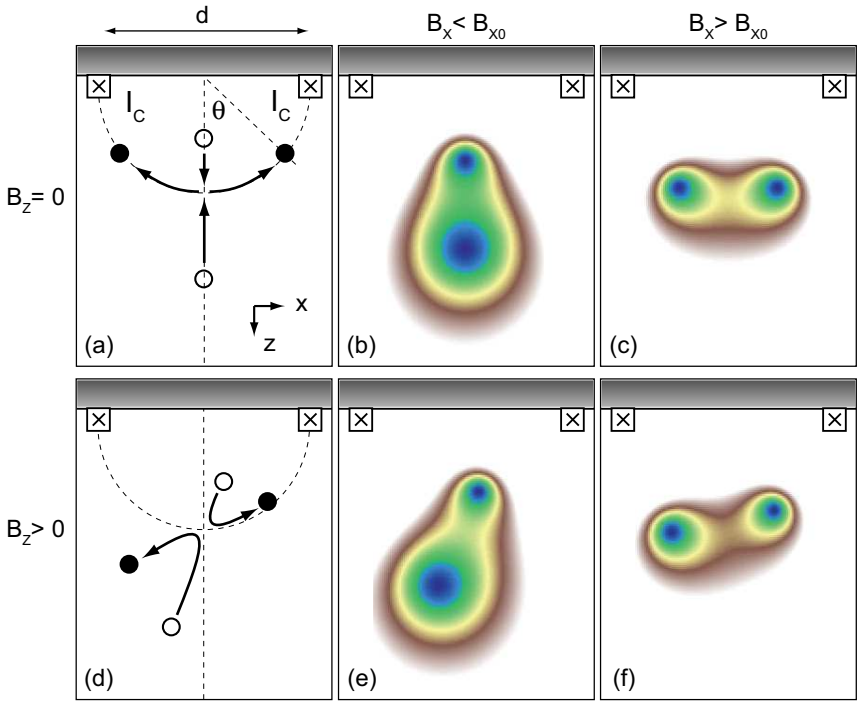

Figure 3-6: Magnetic doube-well potential in a two-wire scheme. An atom chip is set facing $+z$-direction and two straight wires are fabricated on the chip, having currents I_C in $-y$-direction. With an external magnetic field B_x, two local minima in the magnetic field are placed on the same side of the chip. (a) Increasing B_x results in moving the two minima from open circles to solid circles. The dashed line indicate the trajectories which the two minima follow with B_z=0. The center line is perpendicular to the chip surface and in the middle of the two chip wires, and the circle passes the two wire with a diameter of d. At the merge point M, the two minima are coalesced with $B_x = B_{x0}$. Color contour plots of a magnetic field with (b) $B_x < B_{x0}$ and (c) $B_x < B_{x0}$. Corresponding plots for $B_z > 0$ are displayed in (d), (e), and (f). With a non-zero B_z, the two minima can not be completely merged.

mentation and lifetime reduction [6, 107, 9, 108, 111] impose restrictions on the minimum distance between atoms and chip surfaces. With our moderate in-house fabrication quality, the experiment should be performed at least 200 μm away from wires in order to avoid fragmentation [6], meaning that high current capacity is needed for satisfying the above requirements for the trap geometry. Atom chip-IV was developed under this condsideration (Section 2.3).

3.3.1 Magnetic Double-Well Trap

A magnetic double well potential was realized with an atom chip using a two-wire scheme [129]. The basic geometry of an atom chip for a double-well potential is illustrated in figure 3-6. When two chip wires have currents, I_C, in the $-y$ direction and the external magnetic

field, B_x, is applied in the $+x$ direction, two lines of local minima in the magnetic field are generated above the chip surface. Each local minimum has a quadruple field configuration in the xz plane, and with an additional non-zero magnetic field in the axial direction (y-direction), two Ioffe-Pritchard magnetic traps can be formed. The relative magnitude of B_x to the field from I_C determines the direction of separation and the distance of the two traps. The two traps are separated in z-direction with $B_x < B_{x0}$ (Figure 3-6(b)) and in x-direction with $B_x > B_{x0}$ (Figure 3-6(c)). $B_{x0} = \mu_0 I_C/\pi d$ is the critical field magnitude for merging two magnetic harmonic potential to form a single quartic potential, where d is the distance between the two chip wires and μ_0 is the permeability of the vacuum. The merge point is located at the middle of the two wires and $d/2$ away from the chip surface.

When $B_x > B_{x0}$, the two trap centers are located symmetric on the circle which is determined by the two chip wires and the merge point (Figure 3-6(a)), which can be easily understood by observing that the z-component of magnetic field from the two wires is zero on the circle. When the angle of the two trap centers on the circle is 2θ, the corresponding value for B_x is given as

$$B_x = \frac{\mu_0 I_C}{\pi d}\frac{1}{\cos\theta} = \frac{B_{x0}}{\cos\theta}. \tag{3.3}$$

When $\theta \ll 1$, the distance between the two trap centers s is

$$s = d\sin\theta \approx d\sqrt{\frac{2\pi}{\mu_0 I_C}\Delta B_x}, \tag{3.4}$$

where $\Delta B_x = B_x - B_{x0}$.

Experimental procedures are described in Figure 3-7. A condensate is loaded at the bottom well with $B_x < B_{x0}$ and split into two parts by increasing B_x over B_{x0}. The relative phase of the two split condensates is determined by releasing the condensates and recording their interference pattern like in the previous experiment.

3.3.2 Symmetric Axial Confinement

A small magnetic field in the z-direction can break the symmetry between the relative positions of the two traps with respect to the two chip wires, as the two wells have opposite responses to B_z. For example, when $B_x > B_{x0}$ and the two wells are separated in x-direction, positive B_z makes the left well move downward and the right upward (Figure 3-6(f)). Furthermore, with a nonzero B_z, the two wells do not merge completely at any B_x.[4] In order to place the two wells at the same height and split atoms symmetrically, B_z should be kept zero along the axial, y-direction. If B_z changes along the axial direction, the two

[4]This property can be used for asymmetric splitting. In our experiment, $B_z = 0$ was found confirming symmetric splitting with equal populations in each well.

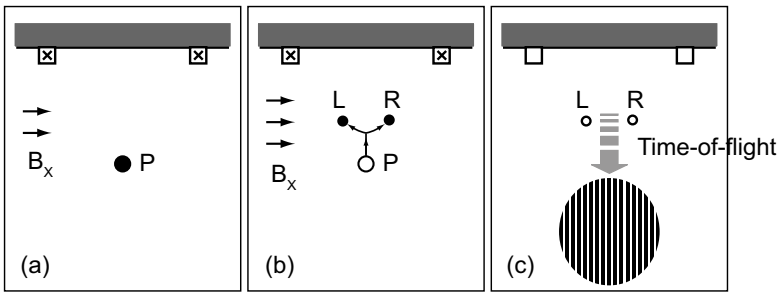

Figure 3-7: Experimental procedures with an atom chip. (a) A condensate is loaded at P. (b) The condensate is split into two parts, L and R, by increasing the external magnetic field B_x. (c) A matter wave interference pattern is formed by releasing the two condensates and letting them overlap during time-of-flight. The relative phase of the two condensate is measured by the spatial phase of the interference pattern.

wells are no longer parallel and the gravitational force would cause an axial displacement of the two split condensates. Therefore, when the axial trapping potential is added to form up Ioffe-Prichard magnetic traps, it should be carefully designed to ensure that condensates split perpendicular to the axial direction and stay in the same axial position. When endcap wires are placed only on the chip surface as in Atom Chip III which was used for vortex experiments in Chapter 6, a non-zero field gradient $\frac{\partial B_z}{\partial y}$ inevitably accompanies a field curvature $\frac{\partial^2 B_y}{\partial y^2}$ for the axial confinement, i.e., B_z changes from positive to negative along the axial direction (Figure 3-8(a)). Actually, we observed that two condensates were axially misaligned after splitting (Figure 3-8(b)), which brought this symmetry issue to our attention.

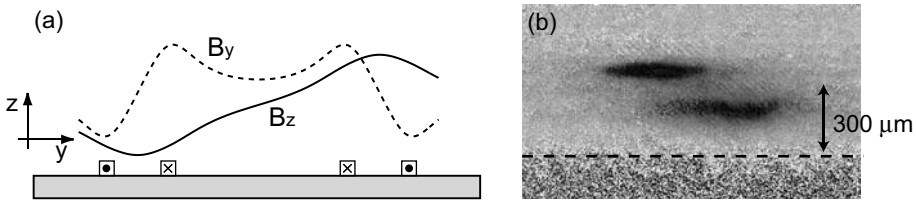

Figure 3-8: (a)Magnetic field from endcap wires for axial confinement. In Atom chip-III, the endcap wires for axial confinement were fabricated on a substrate. The detailed description on the wire pattern can be found in Chapter 6. In addition to the field curvature $\partial^2 B_y/\partial y^2$ for axial confinement, a non-zero field gradient $\partial B_z/\partial y$ is generated from the endcap wires. (b) Absorption image of two split condensates. After splitting, the two split condensates were axially misplaced due to the non-zero field gradient $\partial B_z/\partial y$. The dashed line indicates the chip surface.

The experimental setup of the atom chip is shown in Figure 3-9. The atom chip was set

to face downward and the two traps are horizontally separated when $B_x > B_{x0}$. In order to provide the axial confinement and at the same time minimize $\frac{\partial B_z}{\partial y}$, we placed two pairs of external wires 1.5 mm above and 4 mm below the chip surface. This three-dimensional design of axial confinement was necessary for obtaining the interference signal of two split condensates. Moreover, maintaining the geometric symmetry of two wells will be crucial for longer coherence time after splitting [1].

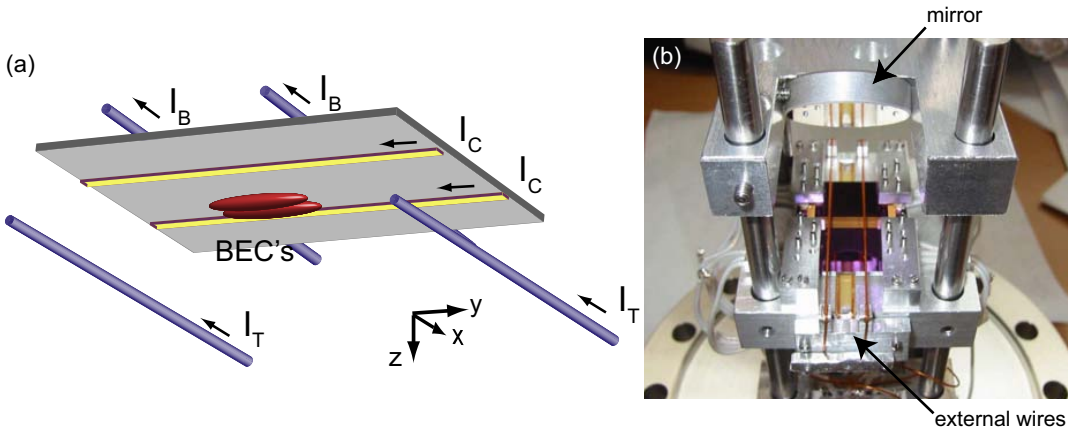

Figure 3-9: (a) Schematic diagram of the atom chip (Atom chip-IV). A magnetic double-well potential is created by two chip wires with a current I_C in conjunction with an external magnetic field. The chip wires of 12 μm height and 50 μm width were electroplated with Au on a thermally oxidized Si substrate with a 2-μm-thick Au evaporated film. The chip was glued on an Al block for heat dissipation and the current capacity was 6 A in a continuous mode. The distance between two wires was 300 μm or 500 μm. A pair of external wires with I_B above the chip surface provided the axial confinement along the y direction, and the other pair of external wires with I_T with the chip surface were used for compensating the anti-symmetry effect from the pair of external wires above the chip surface (for detail, see text). Gravity was in the $+z$ direction. (b) Photo of the atom chip set. Using the chip surface and the mirror, images of atoms can be taken from the direction normal to the chip surface.

3.3.3 Interference of Two Condensates Split with an Atom Chip

Bose-Einstein condensates of $|F = 1, m_F = -1\rangle$ ^{23}Na atoms were loaded in a bottom well with $B_x < B_{x0}$. Experimental parameters were $I_C = 1.8$ A, $B_{x0} = 24$ G, $B_y = 1$ G, $d = 300$ μm, and the axial trap frequency $f_y = 13$ Hz. Condensates were first loaded in the bottom well 500 μm away from the chip surface, brought up to 30 μm below the merge point in 1 s, and held for 2 s in the bottom well to damp out excitations. The whole experiment was carried out with a radio-frequency (rf) shield [58] and before splitting, condensates contained over 8.0×10^5 atoms without discernible thermal components. Splitting was done by ramping $\Delta B_x = B_x - B_{x0}$ linearly from -140 mG to 100 ± 20 mG in 200 ms. The

separation between two condensates was controlled by the final value of B_x. After splitting, two condensates were released from the magnetic trap and the absorption image was taken along the axial direction.

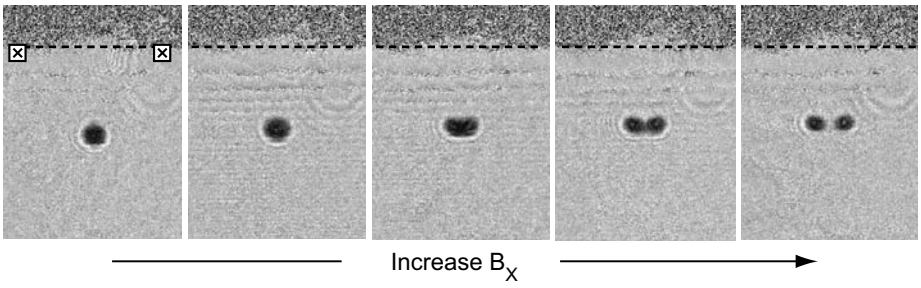

Figure 3-10: Splitting of a condensate on an atom chip. A condensate is split into two parts by increasing the external magnetic field B_x. A series of absorption images of atoms in trap with different B_x are provided.

In order to observe matter wave interference pattern of two split condensates, the two split condensates should spatially overlap during ballistic expansion. It sounds a very simple requirement but extra technical efforts were needed to obtain the first fringe image. First issue was about clean and rapid releasing. In the two wire scheme, the responses of the two wells to an external magnetic field are opposite and thus any kind of uncontrolled residual field in the turn-off process would cause the two condensates to be kicked in opposite directions, preventing a spatial overlap during time-of-flight (Figure 3-11(e)). With high-current fast-switching MOSFETs, the magnetic trap could be turned off within 20 μs much shorter than the inverse of any trap frequency. The external bias field B_x was provided by a pair of macroscopic external coils having currents ~ 28 A.[5]

Second issue was about long-living axial dipole oscillation. In principle, the axial dipole oscillation should not affect the visibility of the interference pattern because the two condensates would oscillate in phase after splitting in a perfectly symmetric double-well potential. Furthermore, this can be used for developing a rotation-sensitive atom interferometer with a guiding potential. However, the axial trap frequencies for two wells were found to be different by 17 % and the two condensates had different axial velocity shortly after splitting, which would result in tilted fringes with respect to the sight line of the absorption image. We attributed this asymmetry to the imperfect fabrication of the chip wires, observing that the fragmentation pattern of clouds near the two wires are different. Furthermore, the centers of the oscillations of the two condensate were axially different. We tried to adjust the currents in the external coils for axial confinement in order to reduce

[5]Another method for clean turn-off might be using the μ-wave transition from the $|1,-1\rangle$ state to $|2,0\rangle$ state [153].

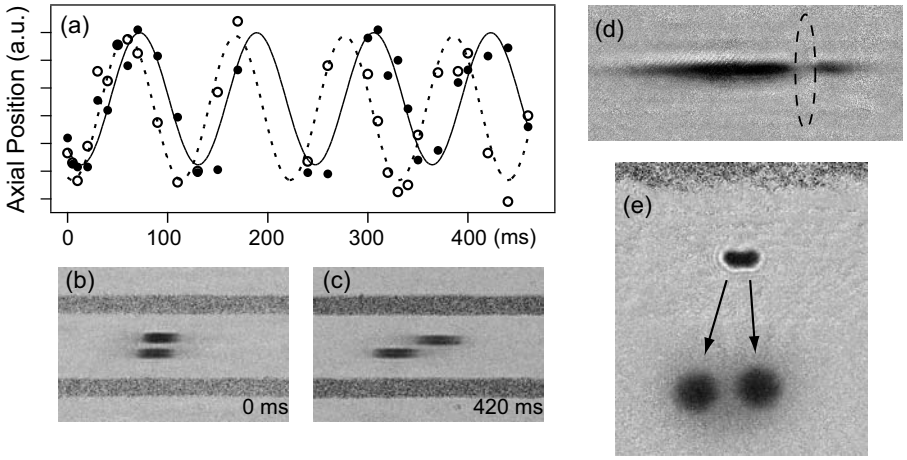

Figure 3-11: Long-living axial motion and unclean releasing. (a) The dipole oscillation in the axial direction had a very long lifetime. After splitting, the two condensates showed different oscillation periods. Bottom absorption images of atoms in traps at (b) 0 ms and (c) 420 ms after splitting. (d) A green light (a repulsive potential) was applied at the end part of condensates in order to damp the long-lived axial dipole oscillation. The dashed region indicates the position of the green light. (e) Non-synchronized slow turn off of the magnetic potential induced mechanical perturbation on two condensates when they were released.

the displacement, and searched for more homogeneous parts of the chip wires. At the end, the long-living axial dipole oscillation was damped by applying a repulsive potential wall at the one end of condensates with a blue-detuned laser beam (532 nm) before splitting.

Finally, matter wave interference fringes were observed after releasing the condensates and letting them expand in time-of-flight (Figure 3-12). High visibility of fringes indicates that the splitting procedure was smooth enough to produce two condensates having uniform phases along their long axis perpendicular to the splitting direction. The relative phase of the two split condensates was determined from the spatial phase of the matter wave interference pattern as in the previous experiment.

The relative phase of two split condensates turned out to be unpredictable when they were fully separated (Figure 3-12). The separation of two condensates was determined from the spacing, λ_s, of the interference fringes, using the formula, $d = ht/m\lambda_s$ The typical fringe spacing was $\lambda \approx 15$ μm with $t = 22$ ms, corresponding to $d \approx 26$ μm. Given the precise knowledge of the fabricated wires, the full trap parameters can be calculated. We assumed that the condensates followed trap centers in the motional ground state. When the separation is less than 20 μm and two condensates are linked, the uncertainty of the spatial phase of fringes was less than 60°, and when the barrier height was over 1.5 kHz, the relative phase started to be random. Since the chemical potential of the condensates, $\mu = 1.4 \pm 0.2$ kHz, was very close to the barrier height, the condensates just started to lose

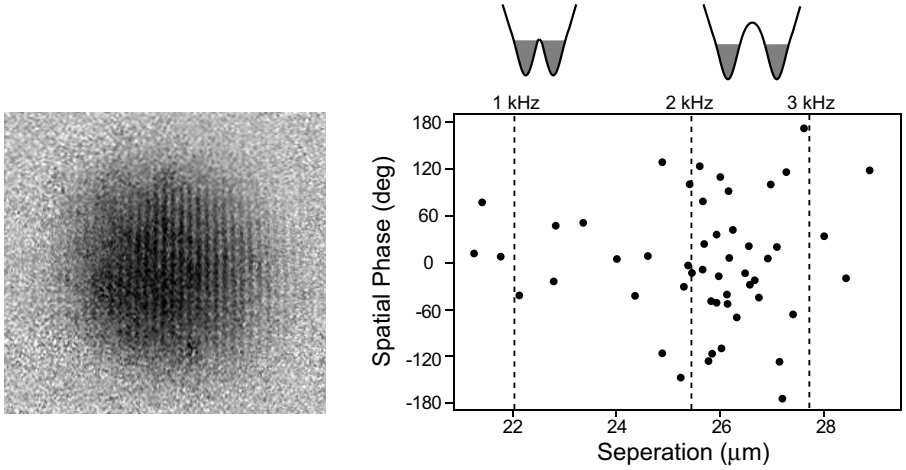

Figure 3-12: Interference of two condensates split with an atom chip. The separation of two condensates was determined from the spacing of interference fringes. Fifty data points for the same experimental conditions are plotted. Three dashed lines indicate the distances of two wells with the barrier height of 1 kHz, 2 kHz, and 3 kHz, respectively. The chemical potential of the condensates $\mu = 1.4 \pm 0.2$ kHz.

their coupling at this point. We tried to reduce the phase uncertainty by optimizing the splitting time, the final separation, and trap frequencies. However, full investigation was limited by short lifetime of condensates near the merge point.

3.3.4 Stability of Trapping Potentials

During the splitting process, condensates experience a dramatic change in the trapping geometry. Figure 3-13 shows how the trapping potential changes during the splitting process. When condensates come closer to the merge point, the bottom well and the top well merge. Generally, the merging of two harmonic conservative potentials creates a quartic potential with zero harmonic trap frequency. Due to gravitation, f_z is always over 200 Hz but f_x vanishes at the merge point. Immediately after the merge point, the trajectory of the trap centers abruptly changes its direction from vertical to horizontal, and the separation of two wells quickly increases to 15 μm with a small magnetic field change of $\delta B_x \approx 10$ mG.

For a single particle in a harmonic potential with trap frequency, f_x, the quantity $\alpha \equiv \frac{1}{f_x^2}\frac{df_x}{dt}$ accounts for the transition probability from the ground state to the first excited state in transforming the potential, and it can parameterize the external adiabaticity of the process. $\alpha \ll 1$ should be maintained to keep the particle staying in the motional ground state. Neglecting the collective excitations of a condensate, we apply this criterion, $\alpha \equiv \frac{1}{f_x^2}\frac{\partial f_x}{\partial B_x}\frac{dB_x}{dt} \ll 1$, to our situation. The harmonic trap frequency, f_x defined at the centers of wells, in the splitting direction vanishes at the merge point. With $\frac{dB_x}{dt} = 1.2$ G/s,

$\alpha < 1$ at $f_x > 150$ Hz, but obviously, α diverges to infinity near the merge point and its definition no longer holds.

Since the energy level spacing becomes smaller, the adiabatic condition in the quartic potential around the merge point becomes more stringent. The abrupt change of trapping potential will induce mechanical perturbations of condensates, particularly inducing quadrupole excitations via coupling between radial modes and axial modes. Subsequent dissipation or coupling into internal excitation modes [101] would make the relative phase of two split condensates unpredictable.

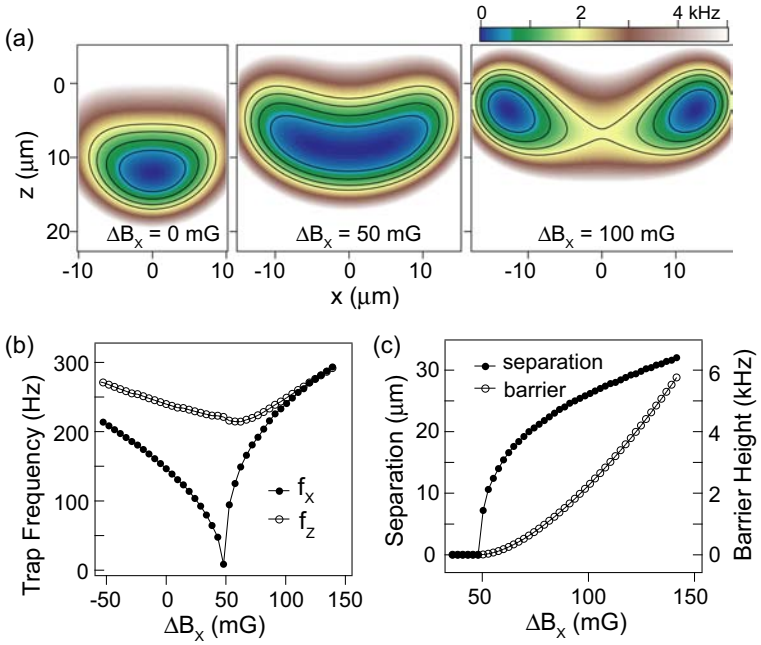

Figure 3-13: Magnetic trapping potential during splitting. (a) Radial cross sections of trapping potential including gravity for ΔB_x=0, 50, 100 mG, where ΔB_x is the field deviation from the critical field magnitude B_{x0} which is the field magnitude for forming a single quartic trap. The origin of coordinates is the merge point without gravity. Contour lines correspond to 0.5, 1, 1.5, 2 kHz above the bottom of the trap. (b) Trap frequencies in each direction. (c) Separation of two trap centers and barrier height between two wells.

Surprisingly, a phase singularity was observed in the interference patterns with high visibility. The fork shape of interference fringes represents a phase winding around a vortex core [154]. This vortex interference pattern appeared more frequently with faster splitting and further separation and the observed phase singularity definitely shows the breakdown of adiabaticity of splitting process. Splitting might be considered as slicing condensates in two parts. Furthermore, the abrupt change of the moving trajectory from vertical to horizontal at the merge point could cause some 'rotation'. The fact that the observed "forks" (Figure 3-14) always open towards the top implies that the the slicing always occurred in the same

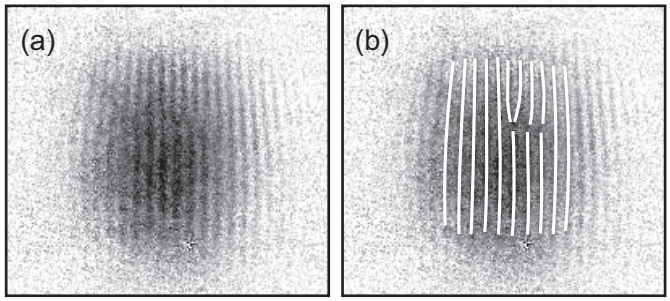

Figure 3-14: Vortex interference. (a) An absorption image showing the vortex interference pattern of a vortex state. The probability of vortex generation was ∼8 % with the experimental parameters in Fig. 3-12, where data points with vortices were not included. Vortex interference patterns appeared more frequently with faster splitting and further separation. (b) Same as (a), but with lines indicating regions with constant phase.

direction and created either vortices with positive charge on the left side or with negative charge on the right side. Experimental study on the probability of vortex generation with the slicing method was reported in Ref. [154].[6]

As a method to reduce the motional perturbation, one could consider starting with two weakly-linked condensates in a double-well potential where the barrier height is lower than the chemical potential of condensates and controlling the coupling between two condensates with a small change of the barrier height. However, because the sensitivity of the trapping potential to the magnetic field is extremely high, when the trap centers locate near the merge point, it was technically difficult to have a stable double-well potential with a small barrier height. Small fluctuations of currents or external magnetic field will shake and heat up condensates. The lifetime of condensates measured around the merge point was > 5 s away from the merge point ($\Delta B_x < -50$ mG or $\Delta B_x > 150$ mG) and < 100 ms near the merge point ($0 < \Delta B_x < 100$ mG).[7] The high field-sensitivity was also indicated in the measurements of remaining fraction of a condensate during splitting. In the splitting process changing ΔB_x from -140 mG to 250 mG for 500 ms, 60 % of a condensate disappeared. The remaining fractions of the condensates were inversely proportional to the time spent in the low lifetime region ($0 < \Delta B_x < 100$ mG) near the merge point.

With a barrier height of 0.5 kHz in our experiment, the sensitivity of the barrier height and the condensate separation to B_x is 0.04 kHz/mG and 0.3 μm/mG, respectively. $\delta B_x = 1$ mG corresponds to $\delta I_C = 7.5 \times 10^{-5}$ A. Therefore, extreme current stabilization and

[6] Another possible vortex formation mechanism is topological imprinting when the zero point of the magnetic field crosses though condensates resulting in a doubly quantized vortex in spin-1 condensates [8, 3]. However, since we have never observed the interference pattern of a doubly quantized vortex and turning off magnetic traps was done too fast for atom spins to adiabatically follow the magnetic field direction, we think that this scenario is unlikely.

[7] For "after-splitting" positions, condensates were moved only to the left well by detouring the merge point.

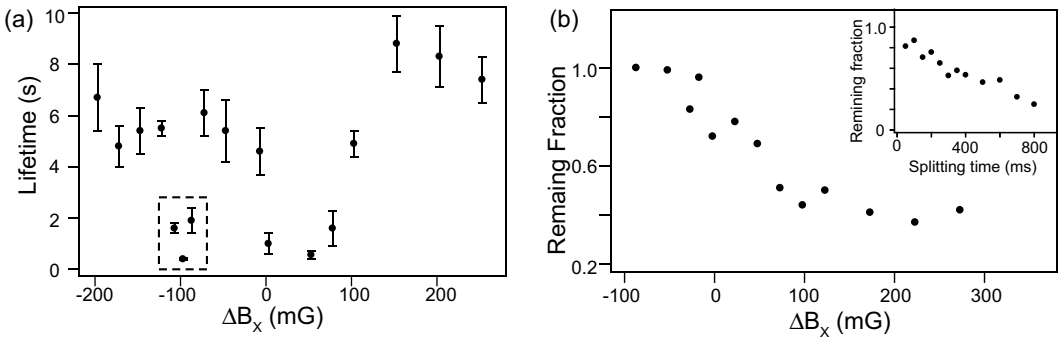

Figure 3-15: (a) Lifetime of a condensate near the merge point. Including gravity, the merged well was formed at $\Delta B_x \approx 50$ mG. For $\Delta B_x > 50$ mG, condensates were moved only to the left well by detouring the merge point. The data points in the dashed box showed bad lifetimes for unidentified technical reasons. (b) Remaining fraction of a condensate during splitting. The splitting process was changing ΔB_x from -140 mG to 250 mG over 500 ms. The number of condensed atoms were measured in the middle of splitting by suddenly releasing the condensate when ΔB_x reached a target value. The inset shows final remaining fraction versus splitting time.

shielding of ambient magnetic field fluctuations may be necessary for controlling a phase-coherent splitting process. Estève et al. [155] discussed the stability of a magnetic double-well potential on an atom chip and suggested that the separation of two wires be smaller than 10 μm in order to maintain the fluctuation of tunneling rate at less than 10% with $\delta B < 1$ mG.

3.3.5 Discussion: Alternative Splitting Schemes

We have demonstrated splitting of a Bose-Einstein condensate in a magnetic double-well potential on an atom chip and observed the interference of the two condensates released from an atom chip. High field sensitivity of the magnetic potential geometry around the merge point prevented coherent splitting with a predictable phase. Since coherent splitting of trapped condensates were demonstrated with our optical double-well system [1], there is, in principle, no fundamental limitation on realizing the same experiment with an atom chip, once the magnetic potential has a same level of stability. We emphasize that the current problem with the atom chip is a technical one. Recently, coherent splitting of a condensate on an atom chip was reported [103] using a field-induced adiabatic potential [156].

Actually, interesting double-well phenomena such as quantum tunneling and nonlinear self-trapping were directly observed in an optical double-well system which was created by combining a single optical dipole trap with a well-controlled periodic optical lattice potential [157]. Then, we can not help asking what are the advantages of magnetic micropotentials on an atom chip over these optical systems? As we mentioned before, in the viewpoint of

atom interferometry, the magnetic system looks more promising to extend to wave guiding potentials with a rotation-sensitive geometry. In the following, we suggest several alternative splitting schemes for preparing a coherent state of two condensates, which we plan on investigating with Atom chip-VI.

One-To-Two Scheme

In the splitting process of the two-wire scheme, a condensates trapped in the bottom well moves upward and abruptly split in the horizontal direction when it reaches the merge point. It is like having the condensate hit the top ceiling and splash violently. This rapid change of moving direction, which might induce some vortices in the condensate, could not be avoided due to the short lifetime around the merge point in our previous experiment.

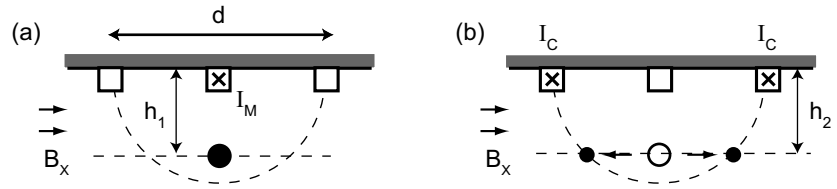

Figure 3-16: One-to-two scheme. Three chip wires are equally spaced on a chip surface. (a) A condensate is prepared in a single-wire trap using the middle chip wire. The external magnetic field $B_x > B_{x0}$. (b) The splitting process is done by decreasing the current in the middle wire, I_M, and simultaneously increasing the currents in the outer wires, I_C. When the final currents in the outer wires are same as the initial current in the middle wire, the distance of the trap centers from the chip surface is maintained at a same value, i.e., $h_1 = h_2$.

With the motivation to make the splitting process happen along one horizontal line, which is the case in the optical double-well system, we consider a 'one-to-two' scheme illustrated in Figure 3-16. Instead of increasing the external magnetic field with fixed currents in chip wires, the current distribution on the chip wires is controlled to deform a single well potential into a double-well potential at the same height. Three chip wires are equally spaced on a chip surface. The key idea is that the distance, h_1, from the chip surface in the single-wire case (Figure 3-16(a)) is the same as h_2 in the two-wire case (Figure 3-16(b)).

$$h_1 = \frac{\mu_0 I_M}{2\pi B_x}, \tag{3.5}$$

$$h_2 = \frac{d}{2}\cos\theta = \frac{\mu_0 I_C}{2\pi B_x}. \tag{3.6}$$

where I_M is the current in the middle chip wire and we used Eq. 3.3. When $I_M = I_C$, $h_1 = h_2$. Therefore, we can imagine a splitting process at a same height where $I_M(t) +$

$I_C(t)$ =constant. The numeric simulation including gravitation showed that this scheme is promising in terms of vertical motional perturbation.

Three-Wire Scheme

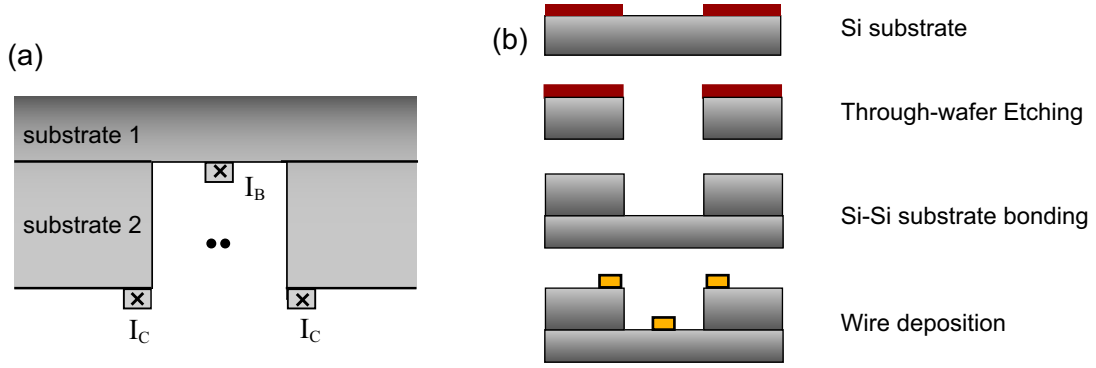

Figure 3-17: (a) Three-wire scheme. A double-well potential is generated by three built-in wires on an atom chip with no external control field. The control field is provided by the current of the inner wire, I_B, in the trench. (b) Three-dimensional structuring can be done by using through-wafer etching and Si-Si substrate bonding.

A double-well potential is generated by three chip wires as in Figure 3-17. The role of the external magnetic field in the two-wire scheme is substituted by the current of the inner wire I_B. This design allows for overall screening of external magnetic field noise and a more precise control of the splitting process with small currents. Furthermore, the field gradient from I_B enhances the tightness of the confinement. When the wires are connected in series, the final separation of the two wells will be intrinsically stable even with possible current fluctuations because the separation is determined by the ratio of I_B and I_C.

Axial Splitting

Another alternative for preparing a coherent state of two spatially separate condensates is first having two condensates in ground states in each well and establishing a well-defined relative phase later with an optical method [11], which is described in Chapter 4. Even though the optical phase imprinting method is almost non-destructive, it is desired to start with a large atom number for signal-to-noise ratio. Two separate condensates can be prepared without passing through the merge point where rapid heating was observed. The splitting procedure is illustrated in Figure 3-18. A condensate is first split in the axial direction and the two split condensates are then moved into the left well and the right well, respectively. The asymmetric effect due to the field gradient $\partial B_z/\partial y$ from a Z-shape wire in the middle is used for this purpose. At the end, I_Z is slowly turned off to place the two

condensates in the same axial position.

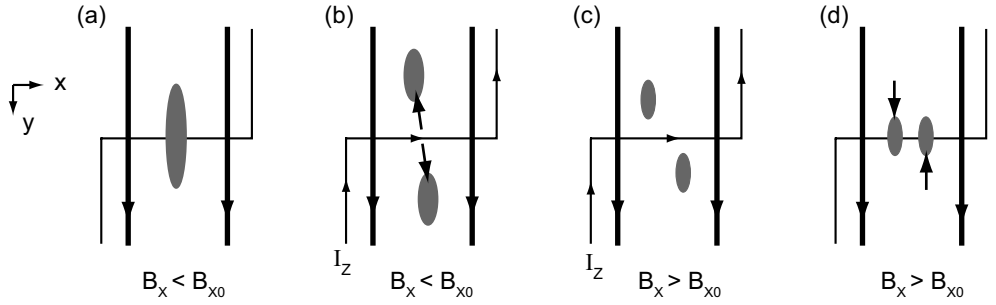

Figure 3-18: Axial splitting. (a) A condensate is prepared in the bottom well ($B_x < B_{x0}$). (b) The condensate is split in the axial direction by increasing the current in the Z-shaped wire, I_Z. (c) When B_x is increased over B_{x0}, the upper condensate moves to the left well and the lower condensate moves to the right well due to the field gradient $\partial B_z/\partial y$ generated from I_Z. (d) Two condensates are placed at the same axial position after turning I_Z off.

Chapter 4

Dynamics of Optically Coupled Condensates

This chapter deals with the situation where two spatially separate condensates are optically coupled by Bragg scattering. The experiments were reported in two publications:

- M. Saba, T. A. Pasquini, C. Sanner, Y. Shin, W. Ketterle, and D. E. Pritchard, *Light Scattering to Determine the Relative Phase of Two Bose-Einstein Condensates*, Science **307**, 1945 (2005). Included in Appendix D.
- Y. Shin, G.-B. Jo, M. Saba, T. A. Pasquini, W. Ketterle, and D. E. Pritchard, *Optical Weak Link between Two Spatially Separate Bose-Einstein Condensates*, Physical Review Letters **95**, 170402 (2005). Included in Appendix E.

The phase coherence of Bose-Einstein condensates was dramatically demonstrated by observation of matter wave interference of two condensates [16] and the phase dynamics of condensates was central for a variety of experiments, including solitons and vortices in a single condensate, and Josephson oscillation in two coupled condensates. However, most of phase measuring methods have been based on atom number counting via light absorption where the measurement processes involve whole condensates. For this reason, a well-defined initial phase is required in order to trace the temporal evolution of the phase dynamics, which is actually the same reason why we need a coherent beam splitter for atom interferometry. Therefore having a monitoring tool for condensate phases without destroying the whole condensates will definitely relax some technical limitation on the study of phase dynamics. This is the motivation of the experiments described in this chapter.

One of the simplest scheme for measuring the relative phase of two condensates without destroying all of them is using small portions of the condensates: *phase sampling* is illustrated in Figure 4-1. Some atoms are sampled out from the two big mother condensates, forming two little condensates. Let's call them son and daughter. The relative phase of

the son and the daughter condensate was measured by a conventional method using interference fringes or a phase-sensitive transition. Then, the relative phase of the two mother condensates can be deduced from that of the son and the daughter if they are *coherently* sampled out to have a well-defined phase relation to their own mother condensates. This idea can be extended by using continuous sampling: extracting continuous atom lasers from the condensates [158, 159, 160]. Each atom in the atom lasers carries the phase information of the source at the moment when it was coupled off. Two major challenges in the experimental implementation of this scheme are coherent sampling and phase measurement without perturbing the mother condensates.

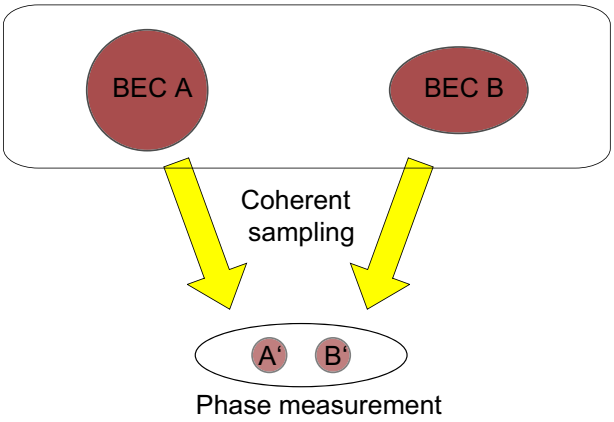

Figure 4-1: Phase sampling. The relative phase of two condensates, BEC A and BEC B, is determined by measuring the relative phase of small portions of two condensates, A′ and B′, which are coherently sampled out of mother condensates, BEC A and BEC B, respectively. The process of coherent sampling establishes well-defined phase relation between mother condensates and sampled son and daughter condensates.

In this chapter, I describe a series of experiments motivated by this phase sampling scheme. Two spatially separate Bose-Einstein condensates were prepared in an optical double-well potential as introduced in Chapter 3. Coherent continuous sampling, i.e., atom lasers from the two condensates were generated by Bragg scattering process and the relative phase of the two spatially separate condensates was determined by interference of the two atom lasers. Furthermore, the same phase information could be obtained from the stimulated light scattering accompanied with Bragg outcoupling. The optical signal would allow real-time phase measurement and novel quantum phase engineering such as phase feedback and phase creation. I develop a theoretical model for the situation, elaborating on the optical coupling which establishes phase-sensitive atomic currents between two spatially separate condensates. A concept is introduced, namely, Josephson coupling of two spatially non-overlapped quantum systems via intermediate systems. We experimentally

demonstrated that the atomic current can be controlled by an additional coupling phase due to the presence of the intermediate systems.

4.1 Continuous Measurement of the Relative Phase of Two Condensates

4.1.1 Beating between Two Atom Lasers

Our experiment situation is schematically illustrated in Figure 4-2(a). Two Bose-Einstein condensates containing $1 - 2 \times 10^6$ sodium atoms in the $|F = 1, m_F = -1\rangle$ state were prepared in an optical double-well potential where the potential barrier between the wells was so high and thick that the two condensates were expected to be independent (no tunneling). Phase measurement fundamentally requires the spatial overlap of two condensates under investigation. In other words, the son and the daughter condensate should meet each other to reveal their phase relation. We applied two counter-propagating laser beams for Bragg scattering to the two condensates in the separation direction so that the direction of imparted momentum from the scattering process was parallel to the displacement of the two condensates. Since the trap depth ($\simeq$ 5 kHz) was much smaller than the recoil energy ($\simeq$ 100 kHz), the Bragg scattered atoms flew away from the trap, establishing an outcouped atom beam from the condensate. Consequently, two atomic beams from each trapped condensates would overlap during propagation.

In our experiment, the Bragg laser beams were 1.1 GHz red detuned with repect to the $|F = 1\rangle \rightarrow |F' = 2\rangle$ transition and the frequency difference between the two Bragg beams, ν, was 102 kHz, resonant for Bragg scattering with counter propagating beams ($4\hbar^2k^2/2m = 4 \times h \times 25$ kHz, the additional 2 kHz accounted for the mean field energy). The Bragg scattering rate was of the order of 200 Hz and the spontaneous Rayleigh scattering rates of the Bragg beams were in the $10 - 100$Hz range.

Two atomic beams from the two condensates overlapped during propagation and a density oscillation was observed as the interference of the two atomic beams (Figure 4-2(b)-(d)). The spatial distribution of the outcoupled atomic beam density represents the temporal distribution of the relative phase of the two mother condensates. In order to confirm that the observed density oscillation was the manifestation of the relative phase evolution, we controlled the phase evolution rate by applying magnetic field gradients, B', in the separation direction. Since atoms were in the magnetic sensitive state, the field gradient induced the potential difference according to the spatial separation. The shift of the density oscillation frequency was linearly proportional to the applied magnetic field gradient (Figure 4-4(a)).[1]

[1]When atoms propagated out from the condensates, they were still affected by the field gradient. They

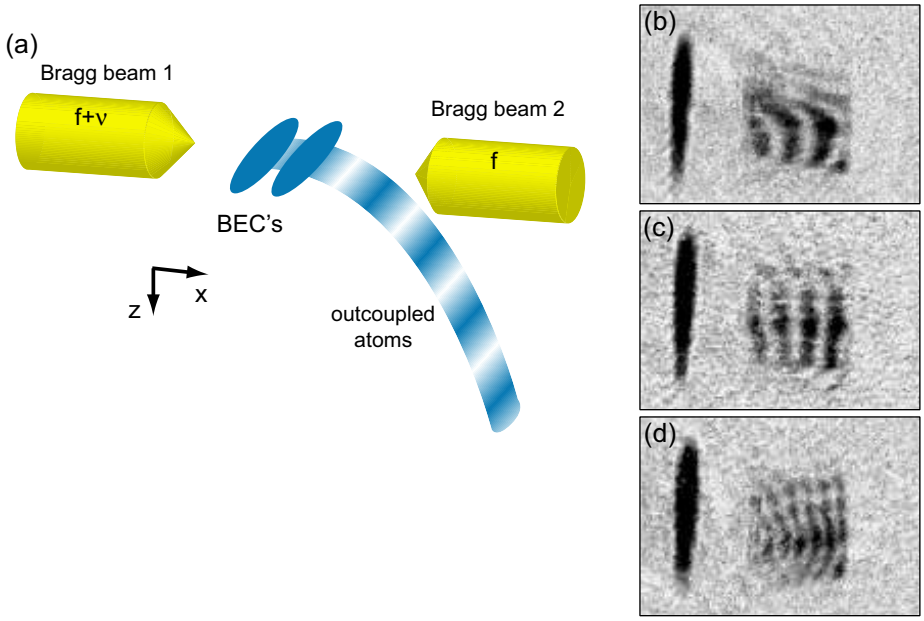

Figure 4-2: Continuous outcoupling from two separate condensates. (a) Schematic description of experimental situation. Two Bragg laser beams are applied to two separate, trapped condensates and outcouple an atomic beam from the condensates. In the typical condition, the separation between the two wells was ≈ 14 μm, the trap frequencies were $\simeq 325$ Hz radially and $\simeq 10$ Hz axially, and the overall trap depth $U_0 \simeq h \times 5$ kHz. The gravity is in $+z$-direction. (b)-(d) Absorption images (z-direction) were taken after 8 ms outcoupling and 5 ms additional time-of-fligh. High-contrast oscillation in the stream of outcoupled atoms are clearly visible. An additional magnetic field gradients of (b) 1.15 G/cm and (d) -0.77 G/cm were applied in $+x$-direction. The field of view in each image is 1.35 mm $\times$ 0.90 mm.

The concept of beating atom lasers was previously exploited in a couple of experiments. Spatial coherence in a single condensate was measured by generating two atom lasers from different positions of the condensate [161]. Gravity was measured by a beating frequency of atoms outcoupled from a vertical array of regularly spaced condensates in an optical lattice [37, 162], where the interference signal was actually established by Landau-Zehner tunneling between different band states but it can be regarded as interference of atom lasers originated from many sites in a generalized sense.

There is one question which helps understand what is really happening in our situation. What if the two source condensate are out of phase? Should the two atomic beams *already outcoupled* from the condensate suddenly disappear when they meet each other? This event would definitely violate the atom number conservation. What really happens in the situation is that the atoms outcoupled from the left condensates are pumped into the right condensates by the Bragg coupling when the atoms spatially pass though the right condensate. In the other case when the two condensate are in phase, more atoms will be coupled out from the right condensate due to constructive interference. Therefore, the observed interference pattern resulted from the fact that the outcoupling efficiency from the right condensates was enhanced or suppressed by the presence of the atoms outcoupled from the left condensate according to the phase relation. This picture based on the local dynamics in matter waves provides clear understanding of the underlying mechanism of our situation. This discussion will be elaborated in section 4.2.

4.1.2 Optical Measurement of Relative Phase Evolution

Even though in the previous experiment we were able to measure the temporal evolution of the relative phase of two condensates over 8 ms, we had to interrupt the experiment to illuminate atoms with a resonant laser beam to take an absorption image. In principle, we might be able to spatially mask the condensates from the probe beam and measure only outcoupled atoms to monitor the relative phase without destroying the whole condensates. However, this selective measurement requires a time delay for the outcoupled atoms to move away from the condensates. Bragg outcoupling method for generating atom lasers provide us with a great chance for optical detection. Bragg scattering is a two-photon stimulated scattering process and for each scattered (outcoupled) atom, a photon is transferred from one beam to the counter propagating one. Therefore, all information contained in the stream of outcoupled atoms is also present in the scattered light and can be collected by monitoring the intensity of one or both of the Bragg laser beams.

This optical detection was successfully demonstrated. The two Bragg beams were set

would eventually slow down or speed up, showing the chirping of the oscillation frequency. Because this effect was very small for our experimental conditions, we assumed that the density oscillation was uniform over the whole atomic beam.

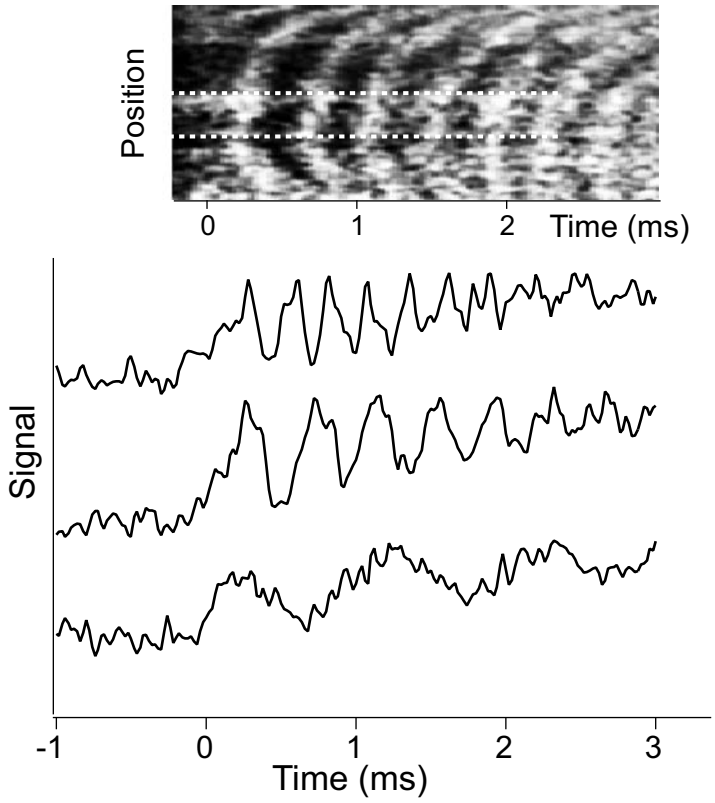

Figure 4-3: Continuous optical readout of the relative phase of two condensates. In the upper panel is the optical signal image detected by streaking the CCD camera. The traces, offset vertically for clarity, are cross sections of the images. The central trace corresponds to the upper image integrated between the dashed lines. Bragg scattering starts at $t = 0$ when the strong Bragg beam is turned on. The relative depth of the two wells was different for the three traces, generating a difference in the oscillation frequency. The overall slope of the traces was due to spontaneous Rayleigh scattering of the light from the atoms in the condensates. As the time went on, the condensates were depleted, the light transmission increased more due to the reduction of Rayleigh scattering. Excitations in the condensates appeared as tilted or curved fringes in the streak images; in such cases, we took cross sections from portions of the images where fringes were vertical and therefore the phase evolution was less perturbed.

to be minimally angled against each other in the horizontal plane so that one of the beams could be picked up after passing through the condensates. The signal was faint and care was taken to improve the signal-to-noise ratio. In order to reduce the intensity fluctuation of the background light without compromising the intensity of the Bragg scattered photons, the intensities of the two Bragg beams were strongly stabilized and set to be very asymmetric. The background intensity of the detected light was leveled down by decreasing the intensity of the picked Bragg beam, I_1, and the Bragg scattering rate was compensated by increasing the intensity of the other Bragg beam, I_2. Since the stimulated two-photon Bragg scattering rate is proportional to the product of the intensities of the two beams, $I_1 \times I_2$, and the spontaneous one-photon Rayleigh scattering rate is proportional to the sum of the intensities $I_1 + I_2$, the asymmetric intensities would result in fast depletion of condensates due to Rayleigh scattering. In our experiment, the intensity ratio was $I_1/I_2 \simeq 0.1$. Even though the Rayleigh scattering rate was increased by factor of 2, the effective gain in the signal-to-noise ratio was positive.

The dynamics of the optical signal was measured with a CCD camera in streaking mode. The light crossing the condensates was selected with a slit-shaped aperture and imaged on a few-pixel wide vertical stripe of the CCD camera. Streaking the CCD pixel rows horizontally at a 50 kHz rate produced images with time on one axis and spatial position along the condensates on the other axis (Figure 4-3). We first tried to use a low noise photo-multiplier tube (PMT) as a light detector, but failed to observe an oscillating signal. The advantage of using a CCD camera is the inherent spatial resolution of the CCD camera as well as a high quantum efficiency. When the condensates do not have a uniform relative phase along the axial direction, the integrated optical signal would have a reduced or completely diminished oscillation amplitude. Indeed, most of experimental data showed curved patterns.

In order to prevent the transient intensity fluctuation from deteriorating the light signal, we applied the weak, detecting Bragg beam 1 ms earlier than the strong Bragg beam. The intensity of the detecting Bragg beam oscillated in time at a frequency controlled by the relative energy between the two wells. The oscillating signal was observed to build up during the first $\simeq 250$ μs after the strong Bragg beam was applied. This delay is the time required for the outcoupled atoms to travel from one condensate to the other one and start interference. This observation supports the dynamic picture discussed before. Another noticeable observation is that the initial phase of the oscillation was random, indicating that the two condensates were independent.

A merit of the optical detection is that it directly measures the beat frequency with accuracy not depending on calibration of image magnification or other disturbances affecting atoms during time-of-flight. Furthermore, this technique can be developed into a *real-*

time measurement, opening interesting future perspectives. Active phase control could be achieved by feeding the real-time light signal back to a device providing external phase shifts and preparing the desired phase at the desired time. In principle, the uncertainty in the relative phase could even be squeezed by the feedback [163].

4.1.3 Interferometry without a Beam Splitter

Atom interferometry with two trapped Bose-Einstein condensates was realized by continuous monitoring of the time evolution of the relative phase. Figure 4-4 demonstrates the sensitivity of the interferometer to an applied external force (magnetic field gradient) and to the application of a potential difference between the two wells (ac Stark shift). The sensitivity of the present measurements was limited by mechanical excitations that cause chirping of the frequency during the observation time and shot-to-shot variations.

The atom interferometer demonstrated here has a remarkable feature. Since the interferometric information is contained in the beat frequency of two condensates and the continuous measurement allows for determining external phase shifts in a single experimental realization, the interferometer is independent of the initial relative phase between the condensates. This means that there is no need for a coherent beam splitter which was, in Chapter 3, described as indispensable to atom interferometry. This provoking statement becomes comprehensible if the purpose of an interferometer is clarified. In atom interferometers, we want to measure phase shifts associated with a given interaction so that at least two pieces of information should be obtained: phase before the interaction and phase after the interaction. In the conventional single-particle picture, these quantities can not be determined in a single experimental realization and thus a coherent beam splitter is required to ensure the initial phase. However, in our interferometer, the coherence of Bose-Einstein condensates allows for measuring the two quantities in a single experimental realization. The situation may be analogous to interference of two lasers. Coherent sampling may be regarded as a beam splitter that picks up a small portion of the laser; one can monitor the beating frequency of two lasers by mixing a small fraction of their intensities.

Furthermore, the atom interferometer works with two condensates even in a Fock state where the relative phase is completely undetermined. Phase measurement process drives the system into a state with an arbitrary but well-defined relative phase as a back action of the measurement [68, 164]. This effect physically originates from the fact that we do not know from which condensate outcoupled atoms come. No phase diffusion is expected during the measurement. This is a general manifestation of the influence of measurement on a quantum system [165], similar to the quantum Zeno effect where the time evolution is suppressed by repeated or continuous measurements.

On the other hand, our atom interferometer has a couple of fundamental limitations.

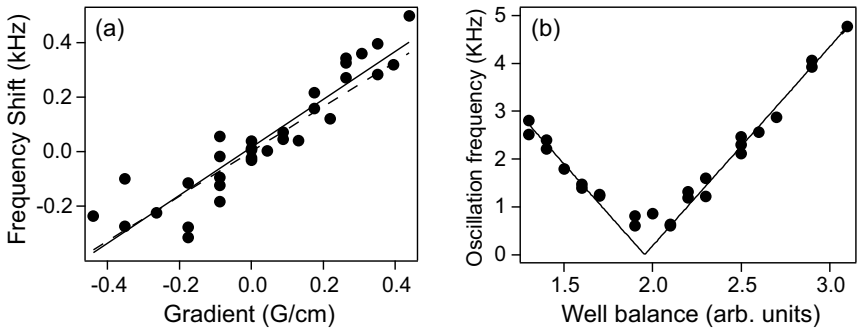

Figure 4-4: Interferometry with two trapped condensates. (a) The two well depths were prepared offset by $\simeq 0.53$ kHz in the absence of magnetic field gradients, and the shift of the beat frequency with respect to this initial value is plotted versus the applied magnetic field gradient. The beat frequency is determined from absorption images of the outcoupled atom stream (Figure 4-2). The solid line is a linear fit to the data; the dashed line represents the theoretical value $\mu_B B' d/2h$ expected for the evolution of the relative phase of the two condensates due to the difference in energy induced by the gradient (B' is the independently measured magnetic gradient, μ_B is Bohr magneton, and d is the separation of the two condensates). (b) Beat frequency measured in the optical signal is shown as a function of the relative depth of the two potential wells. The well balance parameter is proportional to the differnece in optical power used to create each of those wells.

While the phase measurement method introduced here is almost non-destructive, the finite number of atoms in the condensates limits the total interrogation time and consequently the signal-to-noise ratio. Instead of applying the Bragg beams continuously, using two Bragg pulses with a time delay may extend the effective interrogation time. The first phase measurement sets an initial relative phase between the two condensates at each experimental run and the second phase measurement determines a phase shift during the time delay.[2] This two-pulse scheme was experimentally demonstrated [11] (Appendix D) and the correlation between the first measured phase and the second measured phase was observed.

The second fundamental limitation is a nonlinear effect of the outcoupling process on the time evolution of a relative phase. As mentioned before, if the relative phase stays at a constant value, there is a possibility that the population of the right condensate is dramatically changed by constructive or destructive interference resulting in large asymmetric depletion. The induced chemical potential difference would affect the phase evolution in return and thus the measured beat frequency would reflect not only the environment but also the coupling mechanism. In our experiments, the outcoupling efficiency was set very low to ensure the linear regime. However, interestingly, we did not observe oscillation frequencies below 500 Hz (Figure 4-4). Short observation time and excitations could contribute to

[2]This scheme is different from the Ramsey separated-oscillatory-field technique which has a enhanced sensitivity based on the interference of the two separate fields.

this, but the ultimate limit is set by this nonlinear effect because the asymmetric depletion would be enhanced at low beat frequencies. The chemical potential difference induced by the asymmetric depletion would be as large as a few $h\times 100$ Hz in a few ms for our experimental parameters, which set a lower bound to the measurable beat frequency. This is analogous to the inhibition of slow large amplitude Josephson oscillations in a nonlinear junction [147]. One positive note is that if the relative phase is actively controlled, atoms can be coherently transferred from one well to the other one, replenishing one of the two condensates without scrambling its phase, a method that could lead to a continuous atom laser [7].

4.2 Theoretical Models for Phase Measurment

4.2.1 Momentum Interferometry

Several physical interpretations of the experiment are possible besides the interference of atom lasers from the condensates. Pitaevskii and Stringari [166] introduced the interference of two spatially separate condensates in *momentum* space and showed that in the presence of coherence, interference fringes appear in the dynamical structure factor, measurable through Bragg scattering. Also, they pointed out the possibility of creation of coherence as a back action of the measurement process.

Scattering experiments provide information on the excitation spectrum of a given physical system: by scattering a probe particle from the system and measuring the change in momentum and energy of the probe particle, we are allowed to watch the response properties of the system to the perturbation.[3] Bragg scattering directly probes density fluctuations and equally measures the dynamic structure factor $S(\vec{q},\omega)$, which is crucial in the theoretical description of many-body systems [91].

In the atomic viewpoint, Bragg scattering is an optical transition between two different momentum states as described in Section 2.1.3. Absorbing one photon and emitting another one in different direction, the atom receives a momentum kick without changing the internal state. This Bragg scattering is Doppler-sensitive; due to energy and momentum conservation, there is a resonant initial momentum state of the atom with given directions and frequencies of the photons. Therefore, we can simply conclude that the probability of the two-photon scattering is proportional to the probability for atoms to be in the specific momentum state.

The momentum distribution of two condensates is dependent of the relative phase of the two condensates. For example, we have two condensates described by wavefunctions, $\Psi_L(x)$ and $\Psi_R(x)$, respectively. The two condensates are separated by d and do not have a spatial

[3] It is not wrong to say that scattering is the only way to perturb and investigate a physical system.

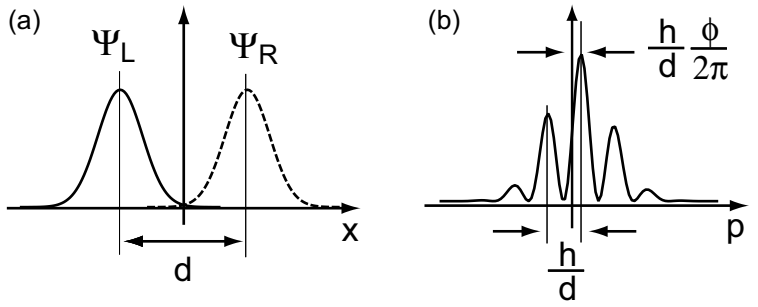

Figure 4-5: (a) Two condensates are described by wavefunctions, Ψ_L (solid) and Ψ_R (dashed), respectively, and the displacement of the two condensates is d in coordinate space. (b) Momentum representation of the two condensates when they have the relative phase of ϕ. The fringe pattern has a periodicity of $\frac{h}{d}$.

overlap, i.e., $\Psi_L(x)\Psi_R(x) = 0, \forall x$. For simplicity, we assume $\Psi_L(x + d/2) = \Psi_R(x - d/2)$. In the presence of coherence, the wavefunction for the whole condensates may be defined as,

$$\Psi(x) = \frac{1}{2}(\Psi_L(x) + e^{i\phi}\Psi_R(x)), \tag{4.1}$$

representing a coherent state with the relative phase of ϕ. Taking the Fourier transform of this coordinate representation of the wavefunction, we have the momentum representation of the wavefuntion, $\Phi(p)$. The momentum distribution $n(p)$ is given as

$$n(p) = |\Phi(p)|^2 = 2n_0(p)[1 + \cos(\frac{d}{\hbar}p + \phi)], \tag{4.2}$$

where $n_0(p)$ is the momentum distribution of one condensate, $\Psi_{L,R}(x)$. The momentum distribution shows a periodicity of h/d and an offset from zero determined by the relative phase as illustrated in Figure 4-5.

Bragg scattering from condensates becomes more complicated due to atom-atom interactions, but the underlying physical mechanism is the same as that in the single-particle case. By measuring the Bragg scattering rate, we probe the population in a specific momentum state, which is a phase-sensitive quantity. Moreover, time-resolved Bragg scattering becomes a probe for the temporal evolution of the relative phase as we demonstrated in the previous experiments [11].

This interpretation based on the momentum interference of the two condensates provides a complementary understanding to the atom-laser interpretation.

4.2.2 What is Really Interfering?

Optical readout of the relative phase of two condensates has been theoretically investigated and photon scattering from two separate wave packets provided a model system for this study. Cohen-Tannoudji [168] argued that photon scattering may be considered as position measurement of the scattered atom to localize the atom and reduce the length of spatial coherence. Localizing the atoms is incompatible with obtaining information about the relative phase. On the other hand, Rzążewski et al [169], and Dubetsky et al [170] showed that the spontaneous emission carries the information of the relative phase of the two wave packets in form of the spectral line shape of the emitted photon due to the Doppler shifts. They claimed that no information of the relative phase can be extracted from angular distribution of the emitted beam intensity because interference signal would be washed out after integrating over emitted photon frequency. In our experiments, we selected the frequency of emitted photons via Bragg two-photon stimulated scattering. There is one aspect we have to emphasize in this optical read-out discussion: the interference signal does not result only from the interference of photons emitted from the two wave packets, but also from the interference of final states of atoms.

In order to clarify what really determines the interference signal, we consider the situation where a glass wall is placed between the two atomic wave packets. The glass wall is perfectly transparent for photons, but is perfectly opaque for atoms. By calculating the dynamic structure factor $S(q,\omega)$, we sketch out the effect of the presence of the glass wall on the interference signal.

$$S(q,\omega) \equiv \sum_n |\langle n|e^{iqx}|0\rangle|^2 \delta(\omega - (\omega_n - \omega_0)), \tag{4.3}$$

where $|n\rangle$ is an eigenstate of the given system with energy of $\hbar\omega_n$ and $|0\rangle$ is the initial state of two wave packets. We assume that atoms are initially trapped in a double-well potential and the system has a well defined energy of $\hbar\omega_0$. Due to the presence of the glass wall, $|n\rangle$ is divided into two groups, the left eigenstates, $|n_L\rangle$ and the right eigenstates, $|n_R\rangle$. The glass wall is located at $x = 0$.

$$|n_{L,R}\rangle \sim \begin{cases} e^{iqx} - e^{-iqx} & (\mathrm{x} < 0,\ \mathrm{x} > 0) \\ 0 & (\mathrm{x} > 0,\ \mathrm{x} < 0) \end{cases} \tag{4.4}$$

With $|0\rangle = |\psi_L\rangle + e^{i\phi}|\psi_R\rangle$, where $|\psi_L\rangle$ ($|\psi_R\rangle$) represents the left (right) wave packet vanishing at $x > 0$ ($x < 0$),

$$S(q,\omega) \propto |\langle n_L|e^{iqx}|0\rangle|^2 + |\langle n_R|e^{iqx}|0\rangle|^2 \tag{4.5}$$

$$= |\langle n_L|e^{iqx}|\psi_L\rangle|^2 + |e^{i\phi}\langle n_R|e^{iqx}|\psi_R\rangle|^2 \tag{4.6}$$

$$= |\langle n_L|e^{iqx}|\psi_L\rangle|^2 + |\langle n_R|e^{iqx}|\psi_R\rangle|^2. \quad (4.7)$$

$S(q,\omega)$ does not depend on the relative phase any more, which means that the interference signal will disappear due to the presence of the glass wall. Physically, the glass wall modifies the Hamiltonian for atoms so that the left wave packet and the right wave packet are coupled to two distinctive groups of excited states via scattering process. Therefore, the phase-sensitivity of $S(q,\omega)$ results from the interference of the transition amplitudes of the two wave packets to the same excited states, which emphasizes the importance of the spatial overlap of scattered atoms in our experiments

This conclusion provides a interesting interpretation of the spectroscopic resolution necessary to measure the relative phase. If two wave packets are separated by d, then the oscillation in momentum space would have a periodicity of $\hbar/d$ and the energy difference between two peaks would be $\Delta E = v_{rec}(\hbar/d)$, where v_{rec} is the recoil velocity after Bragg scattering. Due to time-energy uncertainty, we need to have $\Delta t = \hbar/\Delta E = d/v_{rec}$ to resolve this energy difference. This is the travel time for scattered atoms from one wave packet to the other with the recoil velocity.

As a summary of this section, we conclude that in optical scattering process, the interference signal having the information of the relative phase is essentially from the interference of scattered atoms, not only from scattered photons. The relative phase of two condensates can not be measured without any type of spatial recombination of the two condensates.

4.2.3 Theoretical Model

In the previous discussion, we presented a dynamic structure factor interpretation as a complementary description to the atom-laser description. However, when two condensates have a different chemical potential and the relative phase evolves, this interpretation does not give a clear picture. Of course, we can divide the dynamic evolution into small pieces with a fixed relative phase, but this approach might not be able to provide unified understanding on the real situation.

In this section, we provide a theoretical model elaborating on the underlying mechanism of the optical outcoupling. We use the conventional wavefunction description for condensates in order to account for the temporal evolution of the relative phase. The simplified situation is illustrated in Figure 4-6. Two condensates 1 and 2 are trapped in a double-well potential and optically coupled into unconfined states by a single pair of Bragg beams. Ignoring the accumulated phase shifts due to the interaction with the condensates, we approximate the unconfined coupling states as truncated free propagating states, i.e., the excited coupling states from the two trapped condensates as $\psi_i(x,t) \propto \Theta(x-x_i)\sqrt{\gamma N_i}e^{i\chi_i(x,t)}$ $(i=1,2)$, respectively, where $\Theta(x)$ is the Heaviside step function, γ is the Bragg outcou-

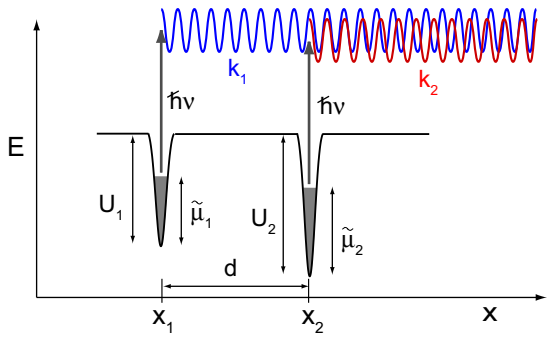

Figure 4-6: Optical out-coupling from two separate condensates. Two condensates are trapped at $x = x_1$ and x_2 ($d = x_2 - x_1$). A pair of Bragg beams in x direction with frequency difference ν are applied to two condensates and make transitions to higher momentum states to generate a continuous atomic beam from each condensate. The two atomic beams are overlapped in $x > x_2$, forming a matter wave interference pattern. U_1 (U_2) denotes the trap depth of the left (right) well, $\tilde{\mu_1}$ ($\tilde{\mu_2}$) the mean-field interaction energy of the left (right) condensate, and k_1 (k_2) the wave number of the atomic beam from the left (right) condensate outside the trap.

pling efficiency, N_i is the total atom number of condensate i. Because the excited states are free propagating states, $\chi_i(x,t) = k_i x - \omega_i t + \chi_{i0}$ is the phase of the coupling state with $\hbar\omega_i = \frac{\hbar^2 k_i^2}{2m}$, where m is atomic mass. The phase continuity at the coupling position $x = x_i$ requires

$$\chi_i(x_i,t) = \phi_i(t) + \phi_B(x_i,t) - \pi/2, \tag{4.8}$$

where $\phi_i(t)$ is the phase of the condensate, $\phi_B(x,t) = 2k_r x - \nu t + \phi_{B0}$ is the phase of the Bragg beams with wave number k_r and frequency difference ν, and the last phase term of $-\pi/2$ is the phase shift attributed to the scattering process [171].

In a linear regime with $\gamma \ll 1$, ϕ_i is not perturbed by the coupling, i.e., $\phi_i(t) = -\frac{\mu_i}{\hbar}t + \phi_{i0}$. $\mu_i = -U_i + \tilde{\mu_i}$ is the chemical potential of the condensate, where U_i denotes the trap depth and $\tilde{\mu_i}$ is the mean-field interaction energy of condensate i. Satisfying the phase relation Eq. (4.8) at all t requires

$$\hbar\omega_i = \hbar\nu + \mu_i, \tag{4.9}$$

$$\chi_{i0} = -\delta k_i x_i + \phi_{B0} + \phi_{i0} - \pi/2, \tag{4.10}$$

where $\delta k_i = k_i - 2k_r$. Eq. (4.9), the temporal part in Eq. (4.8), corresponds to energy conservation.

In the overlapping region, $x > x_2$, the two atomic beams from each condensate form a matter wave interference pattern, and the outcoupled atom density $n(x,t) = |\psi_1(x,t) + \psi_2(x,t)|^2$. For a better interpretation, we define the right outcoupled atom density $n_R(s,t) \equiv$

$n(s + x_2, t)$, where s indicates the distance from the right condensate,

$$n_R(s,t) = \frac{\gamma}{2v_r}(N_t + 2\sqrt{N_1 N_2}\cos(\Delta k\ s + \phi_r(t) - \delta k_1 d)), \tag{4.11}$$

where $N_t = N_1 + N_2$, $\Delta k = k_2 - k_1$, $d = x_2 - x_1$, and $\phi_r(t) = \phi_2(t) - \phi_1(t)$. We approximate the propagating velocity $v_i = \frac{\hbar k_i}{2m} \simeq 2v_r$ with $\delta k_i \ll 2k_r$, where $v_r = \frac{\hbar k_r}{m}$ is the recoil velocity. The spatial and temporal modulation of the outcoupled atom flux n_R represents the evolution of the relative phase ϕ_r, which was directly demonstrated in our previous experiments [11].

Using the wavefunction description is somewhat similar to the atom-laser description. Here, we want to remind ourselves of the matter wave interference interpretation, again. When atoms are outcoupled from condensate 1, they carry the phase information of the condensate. At the moment when they spatially overlap with condensate 2, the outcoupled atoms from condensate 1 are coupled into or amplified by condensate 2, depending on the relative phase ϕ_r. This aspect will be investigated in the experiment described in Section 4.3.

The finite size of the condensates affects the contrast of the interference signal. In the model described above, we assume the two condensates as point sources, and therefore the phase condition for matter wave interference is required at the condensate position. However, when the condensate have a finite size, the phase matching condition should be fulfilled over the whole condensate; a more stringent requirement. With a chemical potential difference $\Delta\mu$, the difference of the wave numbers of two atom laser is $\Delta k = m\Delta\mu/\hbar^2 k_r$, where we assume that the trap depth is smaller than the kinetic energy of outcoupled atoms. In order to obtain an interference signal with a reasonable contrast, the phase modulation over the condensate has to be $\Delta k l < 1$, where l is the size of the condensate. Naively speaking, constructive and destructive interference happen alternatively over the condensate when $\Delta k l > 1$, resulting in a decrease of the signal amplitude. This condition gives an upper bound for the measurable beat frequency,

$$\Delta\mu/\hbar < \hbar k_r/ml. \tag{4.12}$$

The same condition can be obtained by considering the momentum uncertainty δk of out-coupled atoms. δk might be the same as the initial momentum uncertainty of a single condensate, i.e., $\delta k \sim 1/l$, which can also be inferred from the energy uncertainty due to the finite coupling time between the mother condensate and out-coupled atoms. The coupling time is $\delta t = lm/\hbar k_r$ and the corresponding energy uncertainty is $\delta\varepsilon \sim 1/\delta t = \frac{\hbar^2 k_r}{m}\frac{1}{l} = \frac{\hbar^2 k_r \delta k}{m}$. When $\Delta\mu > \delta\varepsilon$, the energy state of atoms outcoupled from the left condensate is very different from that of atoms outcoupled from the right condensate. The two condensates are not coupled to the same excited state; no phase information and no

fringes are obtained. This condition is exactly equivalent to Eq. 4.12. With the upper bound condition, the maximum separation of two condensates in the gravitational direction would be $d_{max} \approx 40$ μm with condensates that extend over $l \approx 5$ μm.

In the above analysis, we simply considered the one-dimensional situation and neglected the effect of the Rayleigh scattering of Bragg photons. The divergence of the atom laser due to the mean-field interaction with the condensates [172] would be another factor reducing the signal amplitude.

4.3 Optical Weak Coupling of Two Spatially Separate Condensates

Josephson effects [144] are quantum phenomena in which the current between two weakly coupled, macroscopic quantum systems depends on the relative phase of the two systems. These effects have been considered as direct evidence for the existence of the phase of a macroscopic quantum system [67] and have been observed in quantum systems such as superconductors [173], superfluid ^{3}He [174], and Bose condensed gases [175, 157]. Josephson coupling between two systems is typically established via tunneling through a separating potential barrier or via an external driving field as in the internal Josephson effect [176, 177]. Both couplings require spatial overlap of the two systems due to the intrinsic locality of the coupling interactions.

The concept of Josephson coupling can be extended to include two *spatially separate* quantum systems by using intermediate coupling systems. If the phase relations among these systems are preserved and thus the net particle exchange is phase-sensitive, the two spatially separate systems might be regarded as being effectively Josephson-coupled via the intermediate systems. Furthermore, the phase of the coupling may be actively controlled by adjusting the coupling states of the intermediate systems. This idea has been theoretically introduced in the context of relative phase measurement [178].

In the previous section, we observed that there is an effective atomic current from the left condensate to the right condensate depending on the relative phase of the two condensates. According to the generalized Josephson coupling discussed above, these unconfined propagating atoms constitute the intermediate coupling system in our case. In this section, we investigate a situation where two condensates are irradiated by two pairs of Bragg beams, allowing bidirectional atom exchange between two separate condensates. The two pairs of Bragg beams couple out beams of atoms propagating to the left or the right, respectively. Depending on the relative phases of the two condensates and the coupling states, we observe only one outcoupled beam propagating to one or the other side, or two identical beams propagating in opposite directions (Figure 4-7). This demonstrates the control of coupling

phase and establishes a new scheme to realize Josephson effects with two non-overlapping condensates.

4.3.1 Bi-directional Bragg Outcoupling

In Section 4.2.3, we presented a theoretical model for the case with a single pair of Bragg beams, and derived the right outcoupled atom density $n_R(s,t)$. Now, we consider another pair of Bragg beams to out-couple atoms in $-x$ direction. Modifying the previous calculation by $k_{i,r} \rightarrow -k_{i,r}$, the left out-coupled atom density $n_L(s,t) \equiv n(x_1 - s)$ is obtained in a similar way.

$$n_L(s,t) = \frac{\gamma}{2v_r}(N_t + 2\sqrt{N_1 N_2}\cos(\Delta k s + \phi_r(t) + \delta k_2 d)), \tag{4.13}$$

$$n_R(s,t) = \frac{\gamma}{2v_r}(N_t + 2\sqrt{N_1 N_2}\cos(\Delta k s + \phi_r(t) - \delta k_1 d)). \tag{4.14}$$

Considering all atom flux for each condensate, we obtain the rate equations for N_1 and N_2. For example, the left condensate has influx of γN_2 from the right condensate and outflux of γN_1 and $n_L(0,t)$ in $+x$ and $-x$ direction, respectively. The final rate equations read

$$\dot{N}_1 = -2\gamma(N_1 + \sqrt{N_1 N_2}\cos(\phi_r(t) - \delta k_1 d)), \tag{4.15}$$

$$\dot{N}_2 = -2\gamma(N_2 + \sqrt{N_1 N_2}\cos(\phi_r(t) + \delta k_2 d)). \tag{4.16}$$

Except for the global depletion effect of Bragg scattering, the rate equations definitely show the Josephson-character of the optical coupling using bi-directional Bragg scattering, i.e., that the atom currents into the condensates depend on the relative phase of the two condensates.

One interesting observation is that there are additional phase terms, $-\delta k_1 d$ and $\delta k_2 d$. These phase terms can be interpreted as the phase shift which outcoupled atoms would accumulate during the flight from one condensate to the other with respect to the Bragg beam phase ϕ_B which is acting as the phase reference. This phase shift is the key element for an actively-controlled optical coupling and its physical importance will be manifest in the following experiment.

4.3.2 Phase-Controlled Optical Coupling

The optical Josephson coupling has a unique feature in the control of the phase accumulated by atoms in the coupling state [178]. Since the intermediate system "delivers" the phase information from one condensate to the other, the phase can be manipulated in transit and consequently, the phase of the effective coupling can be controlled without affecting the two condensates. In the bidirectional coupling scheme, the control of the coupling phase

is embodied by the phase shift terms, $-\delta k_1 d$ and $\delta k_2 d$. We define the coupling phase as $\theta \equiv (\delta k_1 + \delta k_2)d$, and with $\delta k_i \ll 2k_r$, approximate θ as

$$\theta = \frac{d}{v_r}(\nu - \frac{4E_r}{\hbar} + \frac{\mu_1 + \mu_2}{2\hbar}), \tag{4.17}$$

where $E_r = \frac{\hbar^2 k_r^2}{2m}$ is the recoil energy. θ is equivalent to the relative phase of n_L and n_R. When $\theta = 0$ $(\theta = \pi)$ $\pmod{2\pi}$, n_L and n_R will show (anti)symmetric correlation.

The control of the coupling phase θ was experimentally demonstrated. In this experiment, the $1/e^2$-intensity radius of a focused laser beam for a single well was 7.6 μm and the typical trap depth was $U_{1,2} \sim h \times 18$ kHz. The separation of the two wells was $d = 11.4$ μm and each well started with a condensate of $\sim 5 \times 10^5$ atoms. Two pairs of Bragg beams parallel to the separation direction were applied to the condensates by retroreflecting two copropagating laser beams with frequency difference ν. The lifetime of condensates was over 18 s and the $1/e$ depletion time due to Bragg scattering into both directions was 4.5 ms.

The coupling phase θ was controlled with Bragg frequency difference ν Eq. 4.17. When ν was varied, the outcoupling pattern cycled through symmetric and antisymmetric correlations (Figure 4-7). The coupling phase θ was fit to the observed patterns for each Bragg frequency (Figure 4-7(e)). The linear dependence was measured as $\partial\theta/\partial\nu = (2.4 \pm 0.2 \text{ kHz})^{-1}$, which is consistent with the predicted value $d/v_r = (2.6 \text{ kHz})^{-1}$. This clearly demonstrates the presence and control of the coupling phase in our optical coupling scheme. With the antisymmetric condition, $\theta = \pi$, as a function of the propagating relative phase, the output oscillated between predominantly to the left and predominantly to the right (Figure 4-7(c) and (d)). The experimental situation has perfect mirror symmetry. Unidirectional output in a symmetric situation is a macroscopic consequence of the condensates' phase.

We might expect that large depletion would give a chance to observe some of nonlinear effects such as the transition between symmetric correlation to antisymmetric correlation because the correlation phase is a function of the chemical potentials. However the weak signal after large depletion prevented from observing the transition in our experimental condition.[4]

The long condensates used here introduce a new degree of freedom into the usual point-like Josephson junctions: the condensates can have a spatially varying phase along the axial direction. Furthermore, spatial control with barrier heights or well separations could create spatially varying coupling along the condensate axis, and realize, e.g., ring currents. Josephson vortex [179] and modulational instabilities [180] in elongated coupled condensates were theoretically suggested.

[4] In a harmonic potential, the chemical potential decay as $\mu(t) = \mu_0 e^{-\frac{2}{5}\gamma t}$, much slower than the atom number $N(t) = N_0 e^{-\gamma t}$.

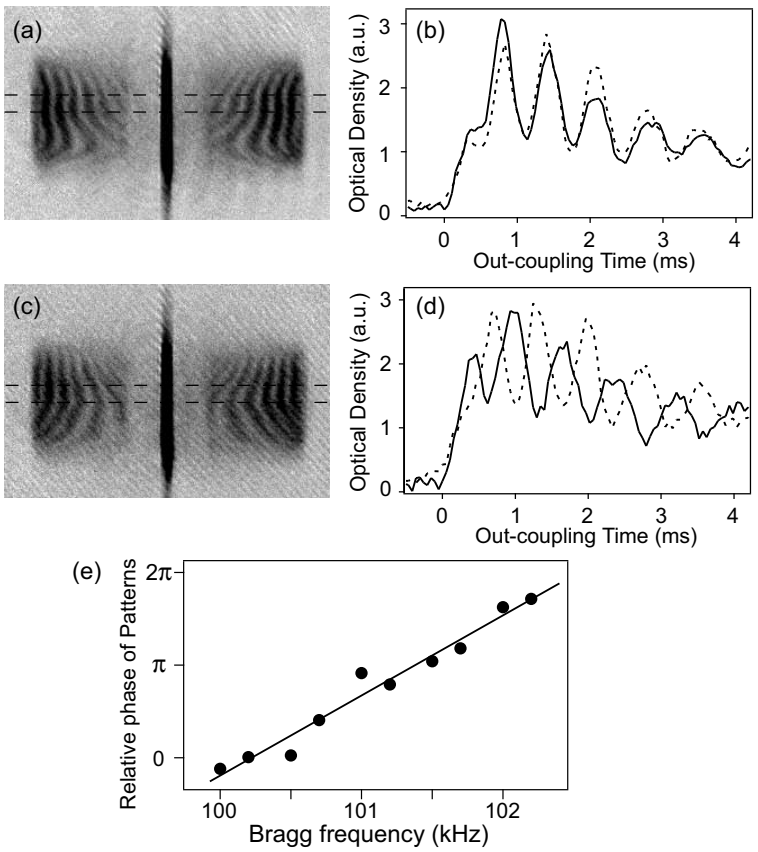

Figure 4-7: Symmetric and antisymmetric correlation between out-coupled atom patterns. Two pairs of Bragg beams with same frequency difference ν were applied to two condensates in order to out-couple atoms in either $+x$ or $-x$ direction. Absorption images were taken at 2 ms after 5 ms out-coupling and the left out-coupled atom patterns were compared with the corresponding right patterns. Symmetric correlation between two patterns was observed at (a) $\nu = 2\pi \times 100.5$ kHz and (c) antisymmetric at $\nu = 2\pi \times 101.5$ kHz. The field of view is 900 μm $\times$ 590 μm. (b,d) Out-coupled atom flux densities were obtained by integrating optical densities between the dashed lines and converting the spatial coordinate to the time coordinate. The solid (dashed) lines correspond to left (right) out-coupled atoms. (e) The correlation phase θ of the two out-coupled patterns showed a linear dependency on ν with $\partial\theta/\partial\nu = (2.4 \text{ kHz})^{-1}$.

4.3.3 Optical Josephson Coupling on a Ring Geometry

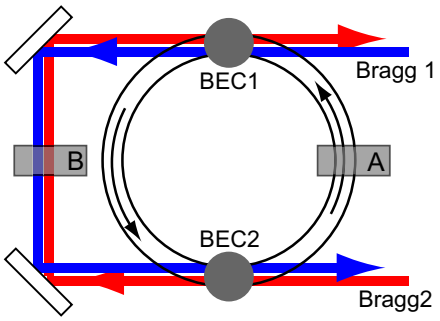

Figure 4-8: Optical coupling of two condensates on a ring. Two condensates are confined at opposite sides on a ring-shaped waveguide and a pair of Bragg beams out-couple atoms in the clockwise direction. The shaded boxes A and B are phase modulators for atoms and photons, respectively.

One limitation of the bidirectional coupling scheme is that atoms are depleted out of the system due to the linear geometry. Even though the pattern of outcoupled atoms is a crucial signal for monitoring the coupling dynamics, the coupling time is fundamentally limited due to the finite size of condensates. To overcome this shortcoming, we envisage a system preserving the total atom number like in Figure 4-8, where atoms circulate between two condensates in a ring waveguide. With assumptions that the traveling time δt for atoms from one condensate to the other is short enough to satisfy $\dot{\phi_r}\delta t \ll 1$ and that the density profiles are constant over the trajectories between the two condensates, the governing equation, in a linear regime, of the population difference of the two condensates is

$$\dot{N_2} - \dot{N_1} = 2\gamma\sqrt{N_1 N_2}\cos(\phi_r - \phi_m), \tag{4.18}$$

where ϕ_m is the effective coupling phase which is determined by the accumulated phase shift over the round trajectories and the phase of the Bragg beams. The derivation of the equation is straightforward and similar to the calculation in Section 4.2.3.

Particularly, the ring geometry has an enclosed area so that this scheme may be developed into a rotation-sensitive device using the Sagnac effect; a neutral atom analogue of a superconducting quantum interference device (SQUID). Confining potentials with ring geometry have already been realized [181, 182, 183]. Different from the typical atom interferometry, the two condensates in the above scheme are used as quantum phase references.

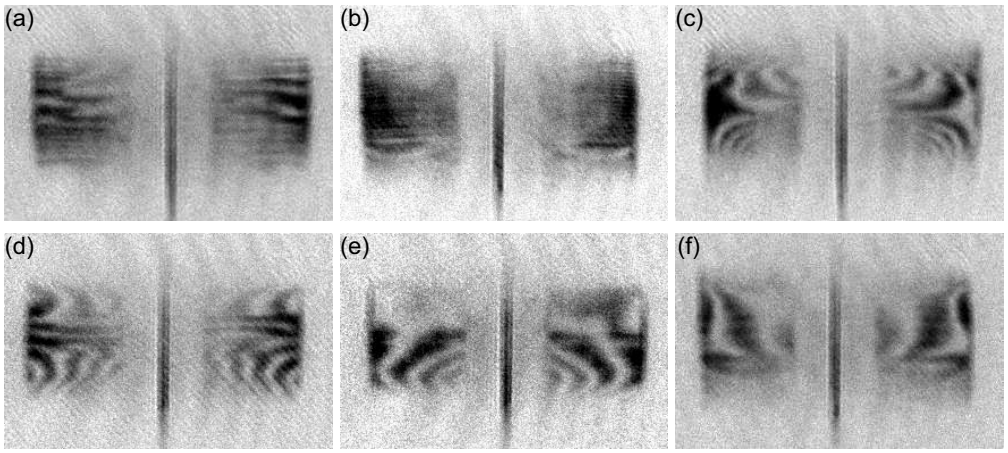

Figure 4-9: Monitoring of slow relative axial motions. Two chemical potentials were equalized within 400 Hz and the temporal evolution of the relative phase of two condensates along the axial (z) direction was recorded in the out-coupled atom patterns. (a) represent relative dipole oscillation, corresponding to relative velocity ≈ 0.3 mm/s, (b) relative quadruple oscillation.

4.4 Diagnostic Applications of Continuous Bragg Scattering

Continuous Bragg outcoupling can diagnose the relative axial motion of two condensates. Since the optical coupling is established selectively at the same axial position, axial gradients of the relative phase are directly observed through tilted fringes in the pattern of outcoupled atoms. In principle, we can rebuild the relative axial motion of the two condensates over the interrogation time from an out-coupled atom pattern. In Figure 4-9, we present several examples showing the effects of relative dipole and quadruple axial motions of two condensates. Furthermore, because the out-coupling efficiency is directly sensitive of the relative phase, there is no limit for detectable slow motions. Figure 4-9(a) represents a relative velocity ≈ 300 μm/s corresponding to ≈ 0.13 nK.[5]

Continuous Bragg scattering was used to characterize the trap depth and the trap frequency of a single optical trap (Figure 4-10). Since momentum and energy imparted in the scattering process are precisely defined, we can determine the depth of a trap by measuring the kinetic energy of atoms coupled out of the trap. We measured the traveling distance D of outcoupled atoms with fixed traveling time t, and determined the trap depth U from the relation, $D/t = \sqrt{4v_r^2 - 2U/m}$, ignoring the mean-field interaction with the condensate and the finite size of the trap. Additionally, the exact knowledge of the recoil velocity v_r calibrates the optical magnification of images.

The trap frequency was measured using velocity sensitivity of Bragg scattering. When a condensate oscillates in a trap, atoms are coupled out only when the condensate is at the

[5]We could not rule out the possibility that the observed motion is induced by the coupling process.

resonant velocity. Since the dipole oscillation of a condensate in a harmonic trap is the same as the trap frequency f, the outcoupling frequency is the same as f when Bragg beams are tuned at the maximum velocity (Figure 4-10(b)), $2f$ at zero velocity (Figure 4-10(c)). Even though the frequency resolution is limited by the finite coupling time, this method provides a lot of information in a single measurement. For example, the pattern of outcoupled atoms in Figure 4-10(b) is curved because the trap frequency changes along the axial direction.

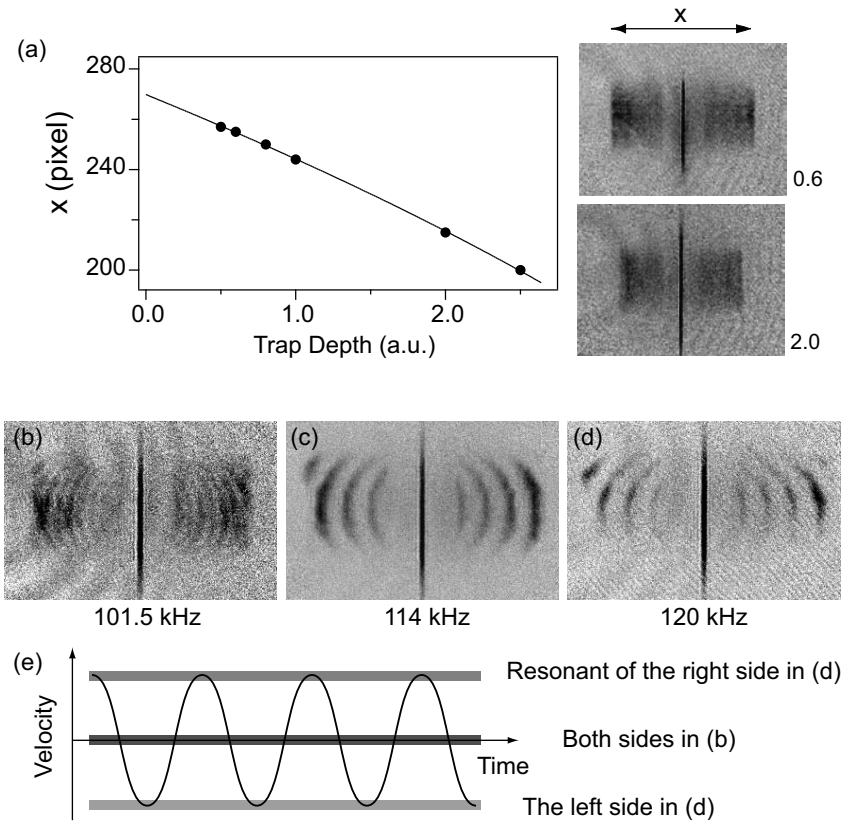

Figure 4-10: Trap characterization with a continuous outcoupling. (a) Trap depth measurement. Atoms were out-coupled from a single well and escape velocity v_f was measured by traveling distance D with fixed traveling time $t = 7$ ms, changing the trap depth U which was monitored in an arbitrary unit with the total power of the laser beam forming the single well. The solid line is a fitting curve (see the text for details.) with 1 a.u.= 18.0 kHz and 1 pixel= 3.11 μm. Dipole oscillation in x-direction was induced by suddenly shifting the trap center. Trap frequency measurement. The out-coupling pattern with Bragg frequency difference (b) $\nu = 2\pi \times 101.5$ kHz, (c) $\nu = 2\pi \times 114$ kHz, and (d) $\nu = 2\pi \times 120$ kHz, which correspond to the resonant velocity ≈ 0 mm/s, ≈ 4 mm/s, and ≈ 6 mm/s, respectively. In (c) and (d), the left and the right pattern have antisymmetric correlation because the resonant velocities for the left-side outcoupling and the right-side outcoupling have opposite signs.

Chapter 5

Distillation of Condensates

This chapter describes the experimental investigation on thermal relaxation in a double-well potential, which was reported in the publication:

- Y. Shin, M. Saba, A. Schirotzek, T. A. Pasquini, A. E. Leanhardt, D.E. Pritchard, and W. Ketterle, *Distillation of Bose-Einstein Condensates in a Double-Well Potential*, Physical Review Letters **92**, 150401 (2004). Included in Appendix F.

Bose-Einstein condensation is the accumulation of a macroscopic number of bosonic particles in the lowest quantum state and the formation process of a Bose-Einstein condensate and related thermodynamics have attracted great interest. People look for the answers for the following questions: how fast a condensate grows out of non-condensed atoms and how a condensate builds up the phase coherence in itself. Experimental studies of condensation dynamics have been carried out with dilute atomic gases, including the observations of the bosonic stimulation effect on the growth of condensates [184], the growth and collapse of condensates with attractive interactions [185], and local formation of condensates in hydrodynamic regime [186]. However, there are still discrepancies between theoretical predictions and experimental results [187, 188]. The description of the formation of the condensate is a current theoretical frontier and requires finite-temperature quantum kinetic theories.

Dynamics of a system can be investigated by perturbing the system quicker than any equilibration process and monitoring how the system in a nonequilibrium state evolves into thermal equilibrium. Experimental challenges are preparing the system in a well-defined nonequilibrium state and measuring the meaningful thermodynamic quantities of the evolving system without ambiguity. The aforementioned experiments [184, 188, 186] exploited a shock cooling method to prepare a well-defined initial state of thermal clouds, where a tail of the thermal distribution is quickly truncated. However, this quick forced evaporation may lead to a complicated initial state due to the one-dimensional nature of the truncation and nonergodic effects [189].

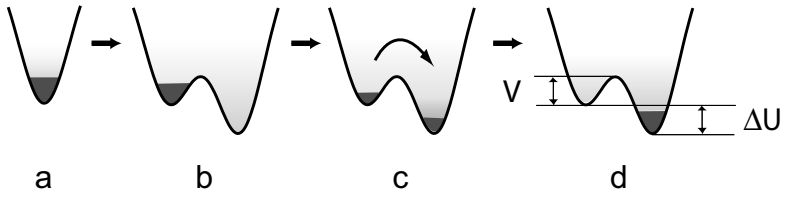

Figure 5-1: Scheme for distillation of condensates in a double-well potential. (a) Condensates are loaded into the left well. (b) A new ground state is created by linearly ramping the trap depth of the right well from zero to the final value. (c) Atoms transfer into the right well via high-energy thermal atoms, and a new condensate starts to form in the right well. (d) The whole system has equilibrated. V denotes the height of the potential barrier between the two wells, which is measured with respect to the bottom of the left well, and ΔU denotes the trap depth difference between the two wells.

Metastable states can help understand thermodynamic processes due to their intrinsically long relaxation time. Metastable situations for a condensate can be created by modifying a system to have one or more even lower quantum state. The original condensate realizes that it is in the wrong state and eventually migrates to the true ground state of the system. This is the situation which we experimentally explore using a double-well potential and we measure the time scale for this equilibration process.

The experimental scheme is described in Figure 5-1. Equilibrium Bose-Einstein condensates in an optical dipole trap are prepared and a metastable situation is set by creating a second trap horizontally adjacent to the first. When the new trap is deeper than the original trap, condensates happen to be not in the ground state any more and try to migrate into the empty well. The resulting double-well potential is characterized by the trap depth difference between the two wells, ΔU, and the height of the potential barrier between the two wells, V. Since the probability of quantum tunneling through the barrier is extremely small [62], the coupling between the two wells occurs only by the incoherent transfer of high-energy thermal atoms over the potential barrier between the two wells. Since ΔU and V are adjustable, we can control the flux of the incoherent coupling between the two potential wells. By monitoring the time evolution of the double-well system we characterize how these variables, ΔU and V, determine the dynamics.

This double-well system can be a good model system for studying thermodynamic processes, having the advantage of being an almost closed system (little evaporation) with well defined initial conditions and widely adjustable time scales (through the height of the barrier). A similar situation was investigated with spinor condensates. Spinor Bose-Einstein condensates are multi-component quantum systems where the components are coupled and can exchange particles, showing rich ground states and collective excitations [34]. Several groups have observed long-lived metastable configurations [190, 191, 192, 193] and specu-

lated about transport of atoms from one domain to another via the thermal cloud [190, 192]. While spinor condensates provide unique opportunities for studying Bose-Einstein thermodynamics with tunable heat and particle bath,[1] the systems involve additional complexities such as spin dynamics and collisional losses [194, 192, 193, 195]. The double-well system allows us to characterize thermal relaxation processes in their simplest realization.

The relaxation process we study is relevant for other questions. The incoherent transport observed here in a double well-potential imposes stringent limitations on future experiments aiming at the observation of coherent transport in Josephson junctions at finite temperature [147, 196, 197]. To observe quantum tunneling, the thermal relaxation time $\tau_{th}(\propto exp[V/k_BT])$ should be longer than the tunneling time $\tau_{tu}(\propto exp[\sqrt{V/m\hbar^2}w])$ where w is the thickness of the barrier. Our observation of condensate growth in one potential well due to the addition of thermal atoms realizes the key ideas of proposals on how to achieve a continuous atom laser [198] which is different from the experiment where condensates were replenished with transported condensates [7].

5.1 Thermal Relaxation in a Double-Well Potential

The following experiment was carried out with Bose-Einstein condensates in the $|F = 1, m_F = -1\rangle$ state using the optical double-well potential as in Chapter 3 and 4. The $1/e^2$ intensity radius of the focused beam corresponding to a single well was 11.3 μm. The details of the initial preparation and the experimental procedures are described in Ref. [2] (Appendix F). The potential was transformed into a double-well potential by linearly ramping the right well potential from zero to the final value of U_R over 500 ms while keeping U_L constant. The effective ramping time during which the trap depth difference is less than the temperature, T_i, was 500 ms$\times(T_i/U_R) \approx 40$ ms which is much faster than the typical relaxation time of ≈ 500 ms. The barrier height was set higher than the peak atomic mean field energy of condensates so that condensed atoms remained confined to the left well during the transformation.

Figure 5-2 shows the dynamical evolution for a situation where the right well was much deeper than the left well. In that case, the right well was filled first by thermal atoms, which then formed a new condensate. Condensates that initially existed only in the left well were almost completely distilled within 3 s to form condensates of comparable size in the right well.

The whole system may be partitioned into five parts: 1) condensed atoms in the left well, 2) condensed atoms in the right well, 3) thermal atoms in the left well with kinetic energy lower than the potential barrier, 4) thermal atoms in the right well with kinetic

[1] In spinor condensate system, magnetic fields act as a barrier height, using the magnetic properties of atoms.

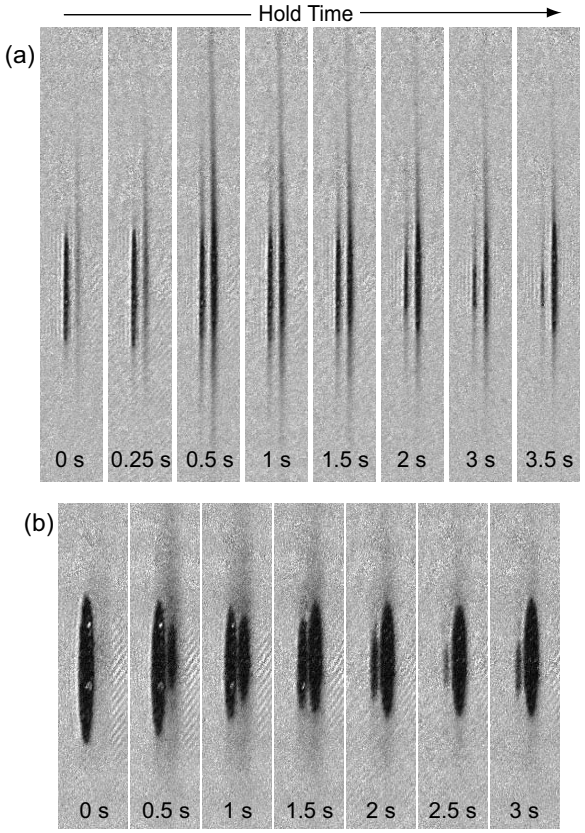

Figure 5-2: Time evolution of atom clouds in a double-well potential. (a) The absorption images were taken for various hold times after creating the right well. The field of view of each absorption image is 130 μm $\times$ 1160 μm. Before ramping up the right well, the temperature of the initial clouds in the left well was $T_i = (180 \pm 90)$ nK and the number of condensed atoms was $N_i = (1.1 \pm 0.1) \times 10^6$ with a peak mean field energy of $\tilde{\mu}_0 \approx k_B \times$ 300 nK. The trap depths were $U_L = k_B \times$ 2.4 μK (left well) and $U_R = k_B \times$ 2.9 μK (right well) with a potential barrier of $V = k_B \times$ 510 nK between them. During the hold time, the radial separation between the potential wells was 15.9 μm. For clarity, the separation was increased to $d = 31.2$ μm just before taking absorption images. (b) A series of absorption images after 1 ms ballistic expansion. The initial condensate was distilled from the left to the right well.

energy lower than the potential barrier, and 5) thermal atoms accessible to the both wells with high kinetic energy. The particle exchanges among the subparts might be modeled with simple rate equations to describe the full evolution of the system. However, due to possible ambiguity, we did not try this approach.

The time evolution of the double-well system was characterized by monitoring the number of condensed atoms and the temperature of clouds in each well. Actually, the system under investigation was not in equilibrium and thus the temperature might not hold its definition in our situation. Especially at the beginning of the thermal relaxation, the hottest thermal atoms in the left well spilled over the potential barrier to fill and share the trapping volume of the right well. We, however, assumed local equilibrium in each well and determined the temperature with the density distribution of thermal atoms, which was necessary to extract physically relevant information from our observation. This assumption might be justified by a short collision time, $\tau_{\rm col} \approx 1$ ms, but its validity should be carefully examined.

The fitted value of the temperature of clouds and the number of condensed atoms in each well were obtained by fitting radially-integrated one-dimensional atomic density cross sections to a bimodal distribution. For the condensate, we used a Thomas-Fermi distribution, and determined the number of condensed atoms by measuring the axial length of the condensate. This measurement was supplemented by taking absorption images with 1 ms ballistic expansion to distinguish the condensate from the thermal atoms around it (Figure 5-2(b)). For thermal clouds, the fits to a Bose-Einstein distribution were restricted only to the wings to avoid the distortions due to the mean field repulsion of the condensate [199].

The temperature turned out to be very sensitive to the value of the chemical potential of the thermal clouds. Assuming local equilibrium, we set the chemical potential of the thermal clouds in each well equal to that of the condensates in the same well. This constraint means that thermal clouds in contact with condensates always have the phase-space density at its saturated value of 2.61. In the dynamical situation, the presence of a condensate coexisting with a thermal cloud with a phase-space density less than 2.61 can not be excluded [194, 195], but a precise measurement of a value of the phase-space density is generally difficult in a non-equilibrium situation. In the absence of a condensate, the chemical potential of the thermal cloud was determined by the fit to a Bose-Einstein distribution.

Density Distribution of a Bose Gas

We consider the density distribution of Bose condensed atomic gases trapped in a three-dimensional harmonic potential:

$$U(\vec{r}) = \frac{1}{2}m(\omega_x^2 x^2 + \omega_y^2 y^2 + \omega_z^2 z^2). \tag{5.1}$$

In the Thomas-Fermi limit, the density of the condensate part is

$$n_c(\vec{r}) = \max(\frac{\mu_c - U(\vec{r})}{g}, 0), \tag{5.2}$$

where μ_c is the chemical potential of the condensate and $g = 4\pi\hbar^2 a/m$. In the harmonic trap, the condensate has a parabolic density profile

$$n_c(\vec{r}) = \frac{15}{8\pi}\frac{N}{x_m y_m z_m}\max(1 - \frac{x^2}{x_m^2} - \frac{y^2}{y_m^2} - \frac{z^2}{z_m^2}, 0), \tag{5.3}$$

where N is the total number of condensed atoms, $i_m = \sqrt{2\mu_c/m\omega_i^2}$ $(i = x, y, z)$. The column density $\tilde{n}_c$ and the radially (xy)-integrated one-dimensional density $\bar{n}_c$ are given by

$$\tilde{n}_c(x,z) \equiv \int dy\ n_c = \frac{5}{2\pi}\frac{N}{x_m z_m}\max((1 - \frac{x^2}{x_m^2} - \frac{z^2}{z_m^2})^{3/2}, 0) \tag{5.4}$$

$$\bar{n}_c(z) \equiv \int dydx\ n_c = \frac{15}{16}\frac{N}{z_m}\max((1 - \frac{z^2}{z_m^2})^2, 0) \tag{5.5}$$

With the assumption $k_B T \gg \hbar\omega_{x,y,z}$, we can obtain the density distribution of the thermal atoms,

$$n_{th}(\vec{r}) = \frac{1}{\lambda_{dB}^3} g_{\frac{3}{2}}(\zeta(\vec{r})), \tag{5.6}$$

where $\lambda_{dB} = \sqrt{2\pi\hbar^2/mk_B T}$, $\zeta(\vec{r}) = \exp((\mu_{th} - V(\vec{r}))/k_B T)$, μ_{th} is the chemical potential of the thermal cloud, and $V(\vec{r})$ is the potential thermal atoms feel at $\vec{r}$. The Bose functions are given by $g_\alpha(z) = \sum_{l=0}^{\infty} z^l/l^\alpha$.

In the absence of a condensate, $V(\vec{r}) = U(\vec{r})$. The column density $\tilde{n}_{th}$ and the radially$(x-y)$-integrated one-dimensional density $\bar{n}_{th}$ are given by

$$\tilde{n}_{th}(x,z) \equiv \int dy\ n_{th} = \frac{\sqrt{\pi}}{\lambda_{dB}^3} y_{th} g_2(e^{(\mu_{th} - \frac{m}{2}(\omega_x^2 x^2 + \omega_z^2 z^2))/k_B T}) \tag{5.7}$$

$$\bar{n}_{th}(z) \equiv \int dydx\ n_{th} = \frac{\pi}{\lambda_{dB}^3} x_{th} y_{th} g_{\frac{5}{2}}(e^{(\mu_{th} - \frac{1}{2}m\omega_z^2 z^2)/k_B T}), \tag{5.8}$$

where $i_{th} = \sqrt{2k_B T/m\omega_i^2}$ $(i = x, y)$.

In the presence of a condensate, the mean-field repulsion from the condensate results in $V(\vec{r}) = U(\vec{r}) + 2gn_c(\vec{r})$. There are no simple analytic expressions for $\tilde{n}_{th}$ and $\bar{n}_{th}$, but in the region $|z| > z_m$ outside the condensate, Eq. (5.7) and (5.8) can be used with $\mu_{th} = \mu_c$.

Fitting Results

Figure 5-3 displays the evolution of the condensed atom number and temperature for the situation in Figure 5-2. The initial, abrupt increase in the temperature of the thermal clouds

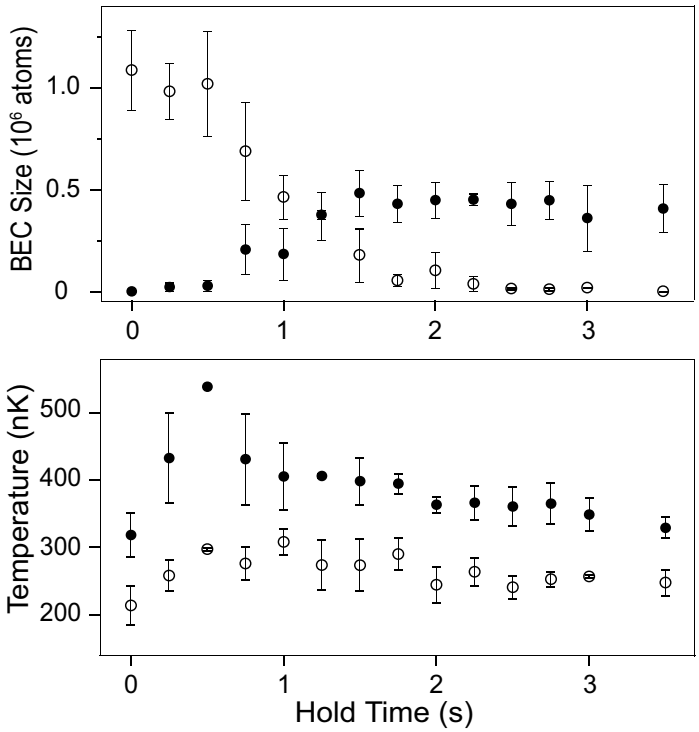

Figure 5-3: Approach to thermal equilibrium in a double-well potential. The temperature and the number of condensed atoms in each well are shown as a function of hold time after creating the right well. Open and solid circles represent atoms in the left and the right well, respectively. Every data point is averaged over three measurements, and the error bar shows ± one standard deviation. The experimental parameters are the same as for the results shown in Fig. 5-2.

in the right well indicates that high energy thermal atoms rapidly transferred into the right well.[2] Condensates started to form in the right well after (400 ± 150) ms and saturated within 2 s, resulting in $\sim 50\%$ of the condensate being transferred. The final temperature in the right well was $T_f \sim 350$ nK, which is ~ 150 nK higher than the initial temperature T_i. This increase of temperature reflects the energy gained by the atoms when they "fall" into the right potential well which is deeper by $\Delta U = 480$ nK. After 3.5 s, the total number of atoms in the whole system was $N_f = (0.6 \pm 0.1) \times 10^6$, which is 15% less than expected for the measured lifetime of $\tau = 12.1$ s. Evaporative cooling due to finite trap depth may explain both the atom loss and the fact that the temperature increase was much less than ΔU.

Even after 3.5 s hold time, full global equilibrium was not reached. This can be seen in both the temperature and the condensed atom numbers. As the chemical potential of condensates in the right well was lower than the trap bottom of the left well, there should

[2]The fit values for the temperature of the right well at hold times less than 1 s parametrize a cloud our of equilibrium due to the violent evolution.

not have been any condensate remaining in the left well in global equilibrium. However, Figure 5-2 shows a small condensate of $\sim 10^3$ atoms in the left well even after 3.5 s holding. Furthermore, the temperature in the left well was measured ~ 100 nK lower than in the right well. Note that in our trap geometry, the exchange of thermal atoms might be geometrically suppressed due to the small "contact area" between the two elongated cigar shaped clouds. Moreover, if the transferred thermal atoms have high angular momentum, they have poor collisional coupling to the cold trapped atoms like the Oort cloud in magnetic traps [200]. Indeed, the density of thermal atoms with higher energy than the potential barrier in the left well after 3.5 s holding is $\sim 3 \times 10^{11}/\mathrm{cm}^3$, and their collision time with the atoms confined in this well is $(n\sigma v_{rel})^{-1} \approx 0.5$ s. More quantitative study of the slow relaxation process with this metastable state might lead to useful insights.

5.1.1 Relaxation Rate

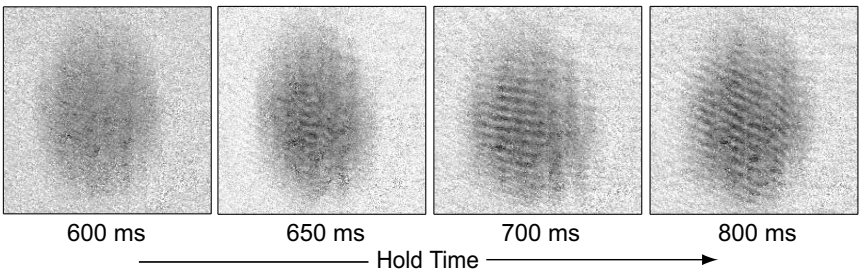

Figure 5-4: Measurement of the onset of condensation with interference fringes. The onset time in the right well was measured by observing the appearance of a matter wave interference pattern when the condensates were released from the double-well potential. The separation of the two wells was $d = 15.9$ μm and the trap depth difference was $\Delta U \approx 420$ nK. Absorption images with variable hold times are provided and resolvable fringe patterns appear after 650 ms hold time.

Another quantity of interest in the condensate formation process is the onset time of condensation, i.e., the hold time until a condensate first appears in the newly created adjacent well [184, 187, 188]. The formation of a new condensate is a clearly distinctive event in the thermal relaxation. To avoid ambiguities in fitting small condensates, we determined the onset time in the right well by observing the appearance of interference fringes when two condensates were released from the double-well potential (Figure 5-4). For two pure condensates, the visibility of the interference fringes is larger than 55% as long as the number ratio of the two condensates is larger than η =0.05. Using the methods described in Ref. [1], we have observed discernible interference fringes down to $\eta = 0.08$, corresponding to $\sim 8 \times 10^4$ condensed atoms in the right well.

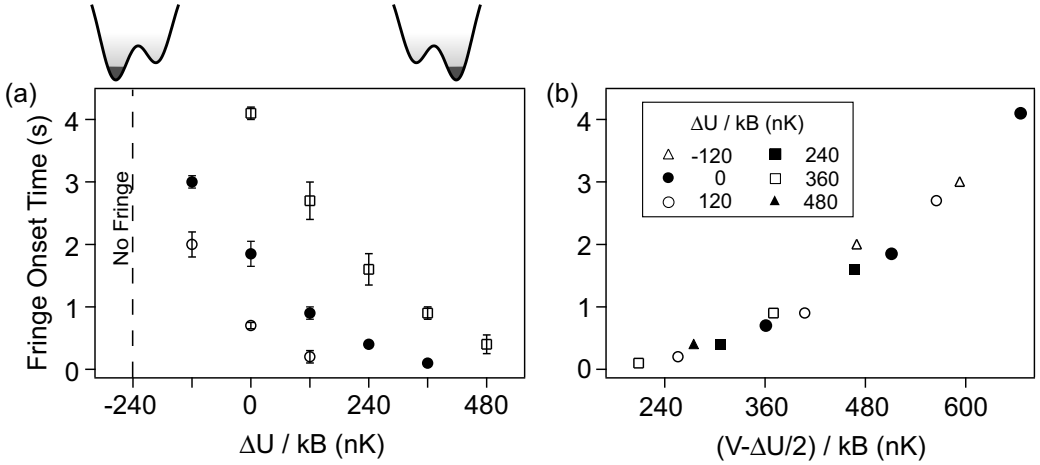

Figure 5-5: Onset time of condensation. U_L was kept at $k_B \times 2.4$ μK for all experiments. (a) The separations of the two wells, d, were 14.3 μm (open circle), 15.1 μm (solid circle), and 15.9 μm (open square). Interference fringes were not observed at $\Delta U = -k_B \times 240$ nK even after 20 s hold time. The energy diagrams for the double-well potential are provided. (b) The same data are plotted vs. $V - \Delta U/2$ where V is the height of the potential barrier.

Onset times were measured as a function of d and ΔU (Figure 5-5). The qualitative understanding of the dependence of the thermal relaxation rate on V and ΔU can be easily obtained. The barrier of height V provides the 'resistance' against equilibration, since thermal atoms must have a kinetic energy larger than V to transfer from the left well to the right well. On the other hand, the potential well difference ΔU can expedite the process. When thermal atoms transfer to the right well, they would be rethermalized by themselves. Some of them would be captured in the right well and some of them would come back in the original left well with higher kinetic energy, accelerating the process by heating the condensate in the left well. Therefore, the equilibrium process will be faster with larger ΔU and smaller V.

The experimental result definitely shows this behavior. Phenomenologically, we found that the condensate onset time depends only on the combination $(V - \Delta U/2)$ with an almost exponential dependence (Figure 5-5(b)). $(V - \Delta U/2)$ can be considered as $(V_{eff} - \Delta U)$, where $V_{eff} = [V + (V + \Delta U)]/2$ is the average height of the barrier measured from each well. The exponential behavior of the Maxwell-Boltzmann distribution may explain the observed dependence.

In two limiting cases, no interference patterns were observed. When the trap depth difference is larger than the peak atomic mean field energy of condensates, i.e. $|\Delta U| > \tilde{\mu}_0$, it is energetically favorable for condensates to remain in the lower well. We observed no interference pattern when $\Delta U = -k_B \times 240$ nK even after 20 s hold time. On the other hand, when $\Delta U \geq k_B \times 360$ nK, the 'appearance and then disappearance' of interference

fringes was observed because the condensates were completely distilled into the right well. In the limit where the barrier height is smaller than the peak atomic mean field energy of condensates, i.e. $V < \tilde{\mu}_0$, condensate atoms can directly 'spill' over the potential barrier. Indeed, we observed that condensates appeared in the right well immediately for V less than $\sim k_B \times 290$ nK, consistent with $\tilde{\mu}_0 \sim k_B \times 300$ nK.

5.2 Discussion

In conclusion, we have created Bose-Einstein condensates in a metastable state in a double-well potential and studied their dynamical evolution. The observed distillation was driven by thermal atoms spilling over the potential barrier separating the two wells and then forming a new condensate. The onset time of a new condensate was measured over a very broad range from a few ten millisecond to a few seconds with various trap parameters.

Kinetics of Bose-Einstein condensation is generally believed to have several qualitatively different stages [201, 202, 203, 204]. In a rapidly cooled atomic gas near the critical temperature, particles first relax into low energy states according to classical Boltzmann kinetics, and once the particles are concentrated enough in the low energy states where interparticle interaction energy is dominant over kinetic energy, the coherent evolution of the low lying levels should be taken into account and from this point the occupation number in each level can not represent the state of the system. It is theoretically anticipated that a quasi-condensate with suppressed density fluctuation would appear having a spatially fluctuating phase. A genuine condensate with a uniform phase would emerge after a system-dependent phase relaxation time [203, 205]. A numerical simulation based on full quantum kinetic theory [206, 187, 207] showed a quantitative agreement with this phase ordering scenario, emphasizing the role of highly occupied low-lying excitation levels. Furthermore, the local formation of condensates reported in Ref. [186] shows the experimental feasibility of the study of this phenomenon.

We speculate that the interference method used for detecting new condensates might allow to study how the phase coherence emerges with condensation. Taking advantage of having another condensate as phase reference might be a more direct method to study the phase coherence build-up mechanism in condensation than Bragg scattering [42] and condensate focusing [186]. Indeed, this was the original motivation of this distillation experiment. We could verify the nonuniformity of the phase of a newly formed condensate by observing a fragmented fringe pattern (see the 650 ms-holdtime image in Figure 5-4), but unfortunately the experiment apparatus was not stable enough to allow systematic studies.

Chapter 6

Dynamical Instability of a Doubly Quantized Vortex State

This chapter describes vortex experiments on atom chips. Experimental results were reported in the following publications.

- A. E. Leanhardt, A. Görlitz, A. P. Chikkatur, D. Kielpinski, Y. Shin, D. E. Pritchard, and W. Ketterle, *Imprinting Vortices in a Bose-Einstein Condensate using Topological Phases*, Physical Review Letters **89**, 190403 (2002).
- A. E. Leanhardt, Y. Shin, D. Kielpinski, D. E. Pritchard, and W. Ketterle, *Coreless Vortex Formation in a Spinor Bose-Einstein Condensate*, Physical Review Letters **90**, 140403 (2003). Included in Appendix G.
- Y. Shin, M. Saba, M. Vengalattore, T.A. Pasquini, C. Sanner, A.E. Leanhardt, M. Prentiss, D.E. Prichard, and W. Ketterle, *Dynamical Instability of a Doubly Quantized Vortex in a Bose-Einstein condensate*, Physical Review Letters **93**, 160406 (2004). Included in Appendix H.

A Bose-Einstein condensate is described by a macroscopic wave function and the velocity is represented by the spatial gradient of the quantum phase, meaning that a condensate can sustain a rotational flow only around a density singularity. Since the condensate wave function should be single-valued, the change of the phase value over any closed path must be a multiple of 2π. This is the Onsager-Feynman quantization condition [208, 209]. Consequently, atoms in a Bose-Einstein condensate circulate with angular momentum only equal to an integer multiple of $\hbar$, in the form of a quantized vortex [210].

Superfluidity is closely related to a Bose-Einstein condensates and it is generally believed that Bose-Einstein condensation is an underlying physical mechanism for superfluidity. However, Huang [211] clearly stated that superfluidity and Bose-Einstein condensation are independent concepts, showing that superfluidity emerges in lower dimension without Bose-Einstein condensation and a Bose-Einstein condensate in a disordered system does

not have superfluidity. Simply, the ideal Bose gas at zero temperature is not a superfluid because of the absence of atom-atom interaction. Superfluidity is a collective property not relying on the existence of Bose-Einstein condensates.

One aspect of superfluidity of a Bose-Einstein condensate can be investigated with the stability of a quantized vortex state. Vortices are excited states of motion and therefore energetically unstable towards relaxation into the stationary ground state. However, quantization constrains the decay: a vortex in Bose-Einstein condensates cannot simply fade away or disappear, it is only allowed to move out of the condensate or annihilate with another vortex of opposite circulation. Vortex decay and metastability have been a central issue in the study of superfluidity [212, 213, 214, 215, 216, 217]. Since stable quantized vortices indicate the existence of a condensate wave function and phonon-like quasiparticles in the excitation spectrum, the observation of stable quantized vortices is taken as conclusive evidence for superfluidity. In almost pure condensates, vortices with lifetimes up to tens of seconds have been observed in atomic condensates [17, 18, 19].

Generally, the study of topological excitation and their stability is an active frontier in the field of quantum degenerate gases. One of interesting subjects is the stability of multiply-quantized vortex states. Giving a Bose-Einstein condensate angular momentum per particle larger than $\hbar$ can result in one multiply-quantized vortex with large circulation or, alternatively, in many singly-quantized vortices each with angular momentum $\hbar$. The kinetic energy of atoms circulating around the vortex is proportional to the square of the angular momentum; therefore the kinetic energy associated with the presence of a multiply-quantized vortex is larger than the kinetic energy of a collection of singly-quantized vortices carrying the same angular momentum. In an energetic sense, a multiply-quantized vortex may decay into many singly-quantized vortices. Observations of arrays of singly-quantized vortices in rapidly rotating condensates [18, 19] indirectly suggests that the instability leads to fast decay of multiply-quantized vortices.

A multiply-quantized vortex is believed to decay coherently by splitting into singly-quantized vortices and transferring the kinetic energy to coherent excitation modes. This phenomenon is called dynamical instability and it is driven not by dissipation in an external bath, but by atomic interactions [214, 218, 219, 220]. On the other hand, the existence of stable multiply-quantized vortices in trapped Bose-Einstein condensates has been predicted with a localized pinning potential [218] or in a quartic trapping potential [221]. Stable doubly-quantized vortices were observed in superconductors in presence of pinning forces [222] and in superfluid ^{3}He-A which has a multicomponent order parameter [223]. Recently, surprisingly long lifetime of a "giant" vortex core has been reported [224]. In this chapter, I describe our experimental study of a doubly quantized vortex state.

6.1 Topological Imprinting of a Vortex State

Preparing condensates in vortex states is an experimentally challenging task. One of the simplest methods for injecting angular momentum into condensates is mechanically rotating the condensates, analogous to the rotating bucket experiments with ^{4}He. Vortices have been generated by rotating condensates with an optical stirer (a repulsive optical potential) [18, 19] and an anisotropic trapping potential [225, 226], and slicing condensates above the critical velocity [154].

Another type of methods for creating vortex states is directly imprinting the phase pattern of the vortex states on condensates. With two-component condensates, a dynamical phase imprinting technique was demonstrated [227, 17]. The phase imprinting technique is versatile because the spatial phase pattern can be directly tailored according to the final target state. Furthermore, this technique provides a unique opportunity for studying dynamically unstable states due to the fast preparation. Dynamics of solitons in condensates were investigated with the phase imprinting technique, and actually vortices were also observed through the decay of solitons [228, 66, 229].

In the experiments described in this chapter, a doubly quantized vortex state was prepared using a topological phase imprinting method [230, 8]. In the following subsections, the working principle of the method is presented.

6.1.1 Berry's Phase in Spin Rotation

Berry introduced additional quantum phase factors for a quantum system experiencing adiabatic changes, and formulated the geometric feature of the quantum phase factors in his seminal paper [231]. This subsection shows the basic definition of Berry's phase and illustrate its consequences in spin rotation.

When a quantum system is governed by time-independent Hamilitonian H and the system is in the nth eigenstate $|n_H\rangle$ from the ground state $|0\rangle$ of the system, the state of the system $|\psi\rangle$, in Schrödinger picture, evolves as

$$|\psi(t)\rangle = e^{-iE_n t/\hbar}|n_H\rangle, \tag{6.1}$$

where E_n is the corresponding eigenenergy and $|\psi(0)\rangle = |n_H\rangle$. The phase factor $e^{-iE_n t/\hbar}$ is called a dynamic phase factor due to the energy of the system. Let's imagine that the external environment for the system is time-dependent. For simplicity, assume that the Hamilitonian H is parameterized with χ, i.e., $H = H(\chi)$ and $\chi = \chi(t)$. If R is changing very slowly, slower than any transition frequency, we can expect the state of the system to adiabatically follow the change and keep staying in the nth eigenstate $|n_{H(\chi)}\rangle$ which is also time-dependent. Naively we might think the phase factor would be $e^{-\frac{i}{\hbar}\int_0^t dt' E_n(\chi(t'))}$.

However, Berry verified that the final state should be

$$|\psi(t)\rangle = e^{-\frac{i}{\hbar}\int_0^t dt' E_n(\chi(t'))} e^{i\gamma(C)} |n_{H(\chi)}\rangle, \tag{6.2}$$

reflecting the adiabatic change, where γ in the second phase factor is called Berry's phase. At first sight, it might be claimed that we can simplify the situation by redefining the nth eigenstate as $e^{i\gamma}|n_H(\chi)\rangle$. However, Berry's phase $\gamma(C)$ depends on not only the final value of R but also the trajectory of R to the final value.

The path-dependence of Berry's phase is clearly illustrated in spin rotation. Imagine a spin-1 particle pointing in $+z$ direction and rotate the spin direction to $-z$ direction. In the conventional notation taking $+z$ direction as a quantization axis, angular momentum operator $\overrightarrow{F}$ is presented as

$$\frac{F_x}{\hbar} = \frac{1}{\sqrt{2}} \begin{pmatrix} 0 & 1 & 0 \\ 1 & 0 & 1 \\ 0 & 1 & 0 \end{pmatrix}, \; \frac{F_y}{\hbar} = \frac{i}{\sqrt{2}} \begin{pmatrix} 0 & -1 & 0 \\ 1 & 0 & -1 \\ 0 & 1 & 0 \end{pmatrix}, \; \frac{F_z}{\hbar} = \begin{pmatrix} 1 & 0 & 0 \\ 0 & 0 & 0 \\ 0 & 0 & -1 \end{pmatrix}. \tag{6.3}$$

The rotation operator $\mathrm{R}(\hat{n}, \theta) = e^{-\frac{i}{\hbar}\hat{n}\cdot\overrightarrow{F}\theta}$, which rotates the spin by θ in $\hat{n}$ direction ($|\hat{n}| = 1$). Consider rotation with $\hat{n} = \hat{x}\cos\phi + \hat{y}\sin\phi$, and then

$$\mathrm{R}(\phi, \theta) = e^{-\frac{i}{\hbar}\theta(F_x\cos\phi + F_y\sin\phi)} = \begin{pmatrix} \cos^2\frac{\theta}{2} & -\frac{i}{\sqrt{2}}\sin\theta e^{-i\phi} & -\sin^2\frac{\theta}{2}e^{-i2\phi} \\ -\frac{i}{\sqrt{2}}\sin\theta e^{i\phi} & \cos\theta & -\frac{i}{\sqrt{2}}\sin\theta e^{-i\phi} \\ -\sin^2\frac{\theta}{2}e^{i2\phi} & -\frac{i}{\sqrt{2}}\sin\theta e^{i\phi} & \cos^2\frac{\theta}{2} \end{pmatrix}. \tag{6.4}$$

Applying $\mathrm{R}(\phi, \pi)$ on the initial state $|+1\rangle_z$ makes the spin point in $-z$ direction at the end of the rotation.

$$\mathrm{R}(\phi, \pi)|+1\rangle_z = \begin{pmatrix} \cos^2\frac{\pi}{2} \\ -\frac{i}{\sqrt{2}}\sin\pi e^{i\phi} \\ -\sin^2\frac{\pi}{2}e^{i2\phi} \end{pmatrix} = -e^{i2\phi}|-z\rangle_z. \tag{6.5}$$

Notice that the phase factor $e^{i2\phi}$ depends on the rotation axis. For example, a final state with π-rotation in $+x$ and one with with π-rotation in $+y$ are completely out of phase.

The above consideration can be straightforwardly extended to the case with a particle with spin-F. Especially, when the spin travels back to its initial position, Berry's phase accompanying the spin trajectory can be unambiguously defined without bothering the definition of the final state. For a spin F particle in a eigenstate $|m_F\rangle$, Berry's phase, $\gamma(C)$, accompanying an adiabatic change represented by a closed loop, C, on the surface of the spin sphere in Figure 6-1 is given by $\gamma(C) = -m_F\Omega(C)$, where Ω is the solid angle subtended by a surface bounded by the spin trajectory, C [231]. The relation to a solid

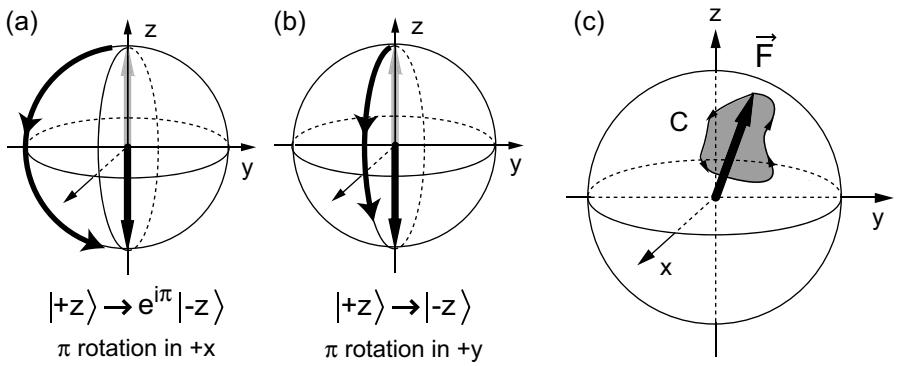

Figure 6-1: Berry's phase in spin rotation. When a spin initially prepared in the $|+z\rangle$ state is transformed into the $|-z\rangle$ by rotation, the final phase factor of the spin state depends on the direction of the rotation axis. The final state with (a) π-rotation in $+x$ direction is out of phase to that with (b) π-rotation in $+y$ direction. Generally, Berry's phase, $\gamma(C)$, accompanying an adiabatic change represented by a closed loop, C, on the surface of the spin sphere is proportional to the solid angle subtended by a surface bounded by the spin trajectory, C.

angle in Hamiltonian's parameter space is a universal property of Berry's phase, and that is why it is called a geometrical phase in contrast to a dynamical phase.[1]

6.1.2 Phase Imprinting of Multiply Quantized Vortex States

Gaseous condensates trapped in a magnetic trap are generally spin polarized so that the spin direction of each atom in the condensate can be manipulated by adiabatically changing a magnetic field direction at the position of the atom. Therefore, a specific phase pattern in a condensate can be prepared by rotating each atom in a proper direction because the final phase of a spin state depends on the direction of a rotation axis as we discussed in the previous subsection.

A vortex formation method using a magnetic field rotation was suggested in Refs. [232, 230, 233, 234]. Let's assume that a spinor condensate polarized in $|F, m_F\rangle$ is prepared in a Ioffe-Pritchard trap. The quantization axis is in the $+z$ direction. The transverse field configuration of the magnetic trap is given in Figure 6-2(a). The initial axial magnetic field is in $+z$ direction and is ramped down to a negative value. This field inversion process is carried on slowly enough that spins can adiabatically follow the field direction. Due to the nonzero transverse field, spins effectively rotate and the rotation direction is determined by the transverse field direction. As we can see in Figure 6-2, the rotation axis $\hat{n}$ changes along

[1] In mathematics, the difference between 'geometrical' and 'topological' is whether length(measure) is important or not in description. We named the vortex generation method as a 'topological' phase imprinting, instead of 'geometrical', because the spatial dependence, i.e., the topological shape of rotation axes is essential to generate a vortex state.

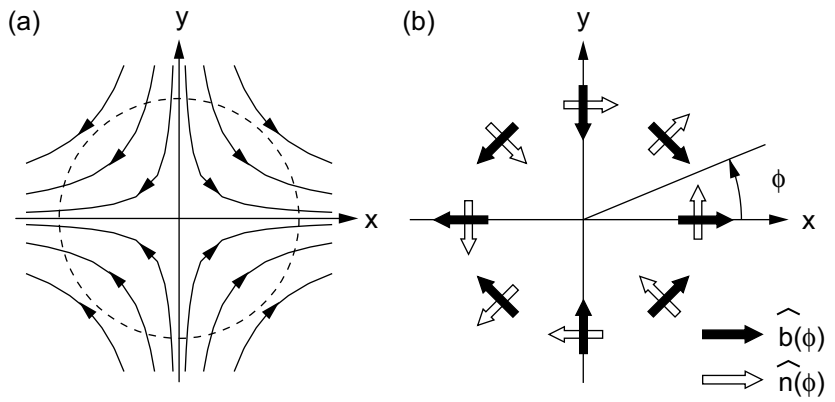

Figure 6-2: (a) The transverse magnetic field in a Ioffe-Pritchard magnetic trap has a quadrupole field configuration. When the axial (z-direction) magnetic field changes from a positive value to a negative value, the rotation axis, $\hat{n}$, of the magnetic field depends on the azimuthal angle, ϕ. (b) The rotation axis, $\hat{n}(\phi)$, and the transverse field direction, $\hat{b}$ along the dashed circumference.

the circumference indicated by a dashed line.

$$\hat{n}(\phi) = \hat{x}\sin\phi + \hat{y}\cos\phi, \tag{6.6}$$

where ϕ is the azimuthal angle at the atomic position. Assuming that the field inversion makes π-rotation from $+z$ direction to $-z$ direction, the final spin state after the rotation is given by

$$\begin{aligned} |\psi\rangle &= e^{-\frac{i\pi}{\hbar}\hat{n}(\phi)\cdot\overrightarrow{F}}|F, m_F\rangle & (6.7)\\ &= (-1)^{F+m_F}e^{-i2m_F\phi}|F, -m_F\rangle. & (6.8)\end{aligned}$$

Reflecting the azimuthal dependence of the rotation axis $\hat{n}(\phi)$, the condensate after the field inversion ends up with a $4m_F\pi$ phase winding; a multiply quantized vortex state for $F \geq 1$.

Rotating spins in a twisted way results in a spatial phase modulation in a condensate, injecting angular momentum and kinetic energy into the condensate. It is generally believed that state-to-state transfer by an adiabatic change always leaves the entropy of a system unchanged so that the ground states of two Hamiltonians can be connected by an adiabatic transfromation from one Hamiltonian to the other. However, the above situation shows that this general belief is not universally true because of the presence of singularities.[2]

[2]The situation may be considered as a two-dimensional space embedded in a three-dimensional space because the spin rotation is not applicable at the trap center.

6.1.3 Vortex Experiments on an Atom Chip

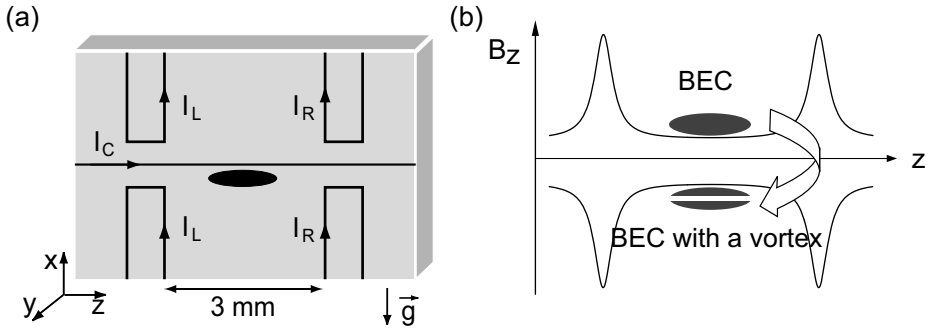

Figure 6-3: Vortex experiment on an atom chip. (a) Wire pattern on the atom chip. A magnetic trap is formed by a current I_C flowing through the center wire in conjunction with a external uniform magnetic field B_x. The axial confinement along z direction is generated by currents I_L and I_R in the end-cap wires. Each current is controlled independently. (b) Imprinting of a vortex in a Bose-Einstein condensate. By inverting the z direction magnetic field B_z, a doubly quantized vortex was imprinted in $|F = 1\rangle$ condensates. The direction of I_L and I_R were also reversed to maintain the axial confinement.

Our vortex experiments were carried out with atom chips. Bose-Einstein condensates of ^{23}Na atoms in the $|F = 1, m_F = -1\rangle$ state were loaded into a Ioffe-Pritchard magnetic trap generated by a microfabricated atom chip, and vortices were topologically imprinted in the condensates by inverting the axial magnetic field. The wire pattern on the atom chip is shown in Figure 6-3(a). We designed an atom chip with separate end-cap wires, allowing independent control of the axial magnetic field. Also, the axial trap position and the axial trap frequency of the inverted trap were matched to those of the original wire trap by adjusting the final values for I_L and I_R after field inversion. With the simple Z-shaped wire trap, it is technically impossible to change the sign of the axial magnetic field curvature. Typical radial trap frequency $f_r \sim 250$ Hz, and axial trap frequency $f_z \sim 3$ Hz. B_z was ramped linearly from ~ 0.5 G to ~ -0.5 G in ≈ 10 ms. More detailed information on experiment parameters such as size of condensates, life times of condensates, and loss rate due to spin flips, were described in Ref. [8, 10, 3].

Atom chips demonstrated their superb capability for precise manipulation of atoms throughout the vortex experiments. The experimental implementation of the vortex formation method might look simple; just inverting the axial magnetic field. However, to maintain the confinement after inverting, the axial field curvature should be also inverted. Furthermore, matching the trap parameters before and after imprinting is crucial for preparing clean vortex states. In real experiments, since the radial trap frequency f_r is proportional to the square root of axial magnetic field B_z ($f_r \propto |B_z|^{-1/2}$), the vortex imprinting process is accompanied by sudden mechanical perturbations: 1) squeezing in the radial direction

as B_z passes through zero can lead quadruple excitations, 2) the change in the vertical trap position due to a gravitational sag ($\propto f_r^{-2}$) can induce vertical dipole excitation, 3) mismatching in the axial trap position and the axial trap frequency after the field inversion will bring axial excitations. Small operating currents and adequate spatial design of atom chips made the vortex experiments possible.[3]

6.2 Observation of Splitting of a Doubly Quantized Vortex Core

The topological phase imprinting method was experimentally demonstrated in our first vortex experiment [8], generating multiply quantized vortex states with $F = 1$ and $F = 2$ atoms. The axial angular momentum per particle of the vortex states were measured using surface wave spectroscopy [236, 237, 238], showing the consistence with the predicted values, $2\hbar$ for $F = 1$ atoms and $4\hbar$ for $F = 2$ atoms. This experiment was carried out with a Z-wire trap on Atom chip-I. As mentioned before, it was technically impossible to keep condensates confined after imprinting.

With a newly designed atom chip (Figure 6-3), we investigated the stability of a doubly quantized vortex state, focusing on how a doubly-quantized vortex core decays into two singly-quantized core. Absorption images was taken along the imprinted vortex line after releasing the condensate and letting it expand during time-of-flight. The size of a doubly-quantized vortex core was typically ~ 40 μm with 15 ms time-of-flight.

However, the visibility of a vortex core in an integrated absorption image completely vanished within 30 ms (Figure 6-4(a)) so that further evolution of the vortex core could not be monitored with integrated absorption images. To reduce blurring due to possible bending of the vortex line [239], we employed a tomographic imaging technique [16]. As illustrated in Figure 6-4(b), a 30 μm thick central slice of the condensate was selectively pumped into the $F = 2$ hyperfine level with a sheet of laser light perpendicular to the condensate long axis, and then the radial profile of the condensate in the selected region was imaged with a light pulse resonant with the $F = 2 \rightarrow F' = 3$ cycling transition. This tomographic imaging technique was crucial for observing the time evolution of vortex cores beyond 30 ms.

A series of absorption images of the splitting process of a doubly-quantized vortex core is provided in Figure 6-5. Images taken just after imprinting show a doubly-quantized vortex core of high visibility. The visibility of the core decreased with evolution time, which we attribute to bending of the vortex line [239] and other excitations created during the

[3]The same vortex imprinting method was implemented with ^{87}Rb atoms in a macroscopic trap and deleterious effects due to a gravitational sag were reported [235].

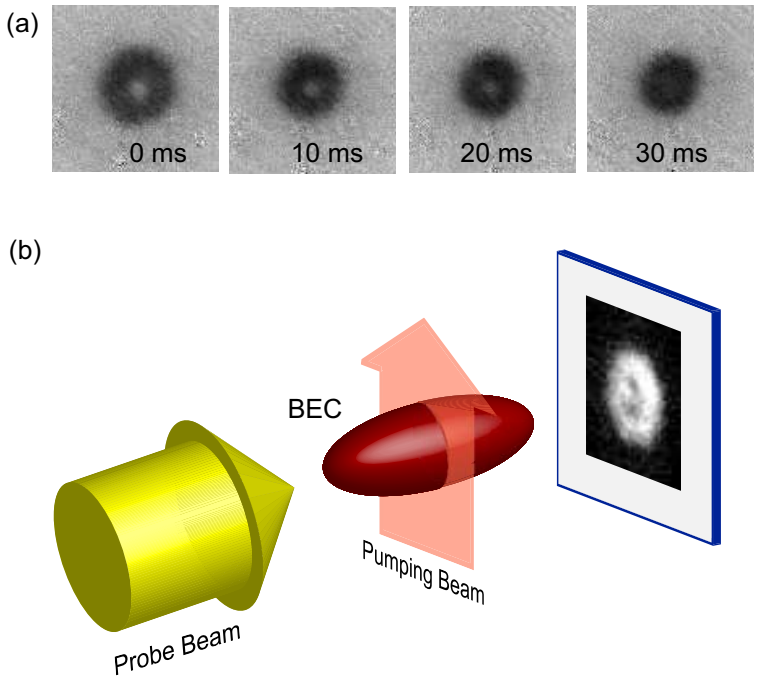

Figure 6-4: Tomographic imaging technique. (a) The visibility of a vortex core in an integrated $F = 1$ absorption image completely vanished within 30 ms. (b) A central slice of a condensate in the $F = 1$ hyperfine state is selectively pumped into the $F = 2$ hyperfine state with a sheet of a pumping beam, and then the radial profile of the condensate in the selected region is imaged with a probe pulse resonant with the $F = 2 \rightarrow F' = 3$ cycling transition.

imprinting process which we discussed in the previous section. Later in the evolution, the central core deformed into an elliptical shape and split into two closely-spaced cores. Once the two cores were separated by their diameter, they appeared well resolved in our images. The angular position of the two cores was random for each experimental realization with the same evolution time, so the precession frequency and the precession direction of two cores could not be determined with our destructive image technique.

6.2.1 Density dependence of Decay Rate

To investigate the dependence of the instability of a doubly-quantized vortex state on the mean field atomic interaction, we measured the characteristic time scale of the splitting of a doubly-quantized vortex core as a function of the atom density. Atom density was controlled by removing a variable number of atoms with rf evaporation before imprinting a vortex. Images were classified as follows: images where the two cores were separated by more than one core diameter were labelled as "two visible cores"; images with a clearly-defined circular central core were labelled as "one core"; images in the intermediate range,

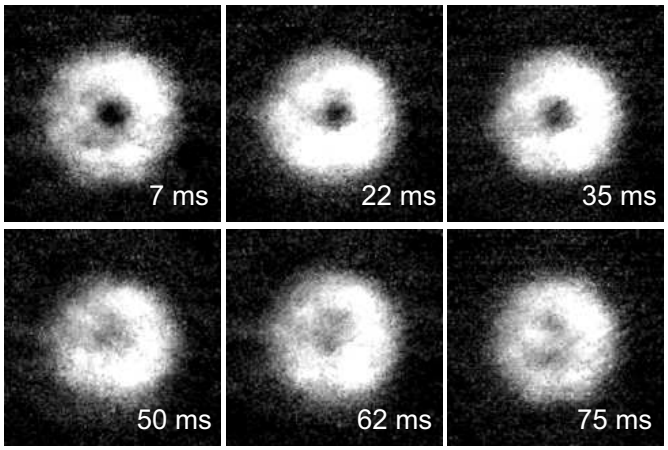

Figure 6-5: Splitting of a doubly-quantized vortex core. Axial absorption images of condensates was taken after 15 ms of ballistic expansion with a variable hold time after imprinting a doubly quantized vortex. A tomographic imaging technique was used. A doubly quantized vortex decayed into two singly quantized vortices. For this data, the interaction strength was $an_z \approx 7.5$ (see text for definition). The field of view in each image is 320 μm $\times$ 320 μm.

where the central core was elliptical but the two cores were not resolved, or with a bad visibility were labelled as "undetermined". For example, the images at 62 ms and 75 ms in Figure 6-5 and Figure 6-6A were classified as "two visible cores", and 50 ms in Figure 6-5, and Figure 6-7(a) and (c) as "undetermined".

Experimental results are provided in Figure 6-6 as a function of the linear atom density n_z (along the condensate long axis) multiplied by the s-wave scattering length a. The rescaled quantity, $an_z = a\int |\psi(r)|^2 dxdy$ corresponds to the strength of the mean field interaction, with $\psi(r)$ being the condensate wavefunction. The total atom number in the absorption image is linearly proportional to n_z because only a central slice of the condensate contributes to the image. Results in Figure 6-6 clearly demonstrate that a doubly-quantized vortex core splits more slowly as the density becomes higher.

6.2.2 Dynamical Instability

Multiply-quantized vortices in a harmonic potential are predicted to be dynamically unstable [214], i.e., the vortices spontaneously decay into other states even in the absence of dissipation and external perturbations. Static stability is concerned with that the energy of the given system has a local extreme in the parameterized Hamilitonian space and dynamical stability considers the temporal evolution of the given system with arbitrary infinitesimal perturbation. Typically, the analysis on dynamical stability uses approximate linearized equations of motions. In the Bogoliubov framework, which is believed to well describe quantized vortices in one component condensates, this dynamical instability manifests as

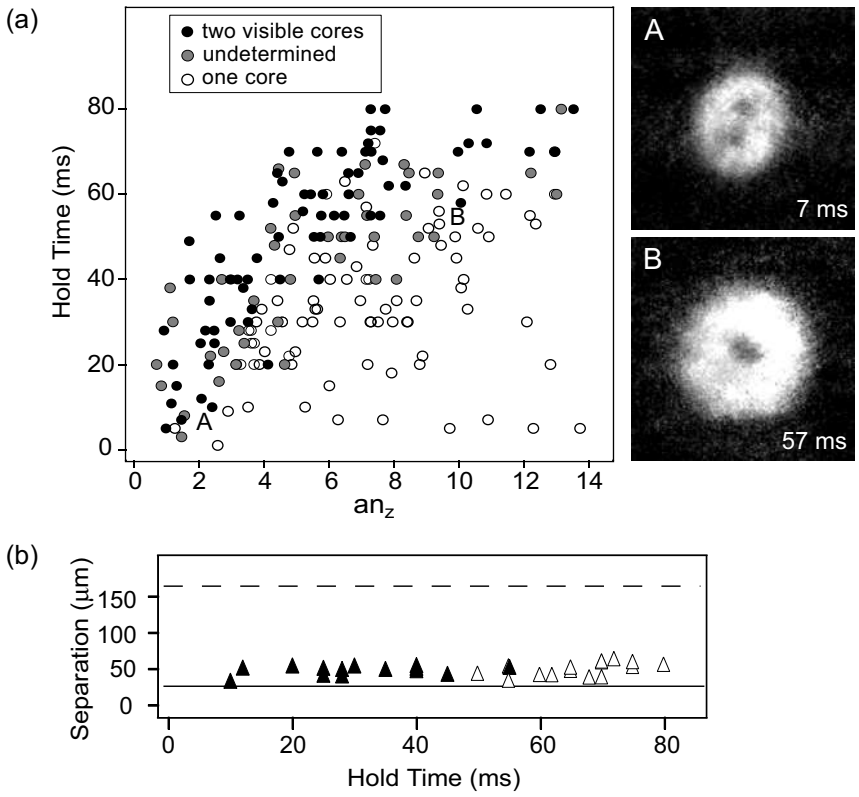

Figure 6-6: Density dependence of the decay process. (a) The time scale for the decay process of doubly quantized vortex states was measured by observing the vortex cores and classifying them as one vortex (open circles) or two vortices (solid circles). Data were collected with three axial trap frequencies $f_z = 2.7$, 3.7, 12.1 Hz and the interaction strength an_z was controlled by changing the atom number by rf induced evaporation before imprinting. Typical absorption images for (A) fast decay at low density ($an_z = 1.5$) and (B) slow decay at high density ($an_z = 10.1$). The field of view in the absorption images is 300 μm $\times$ 300 μm. (b) The separation of two visible cores vs. the hold time for $2 < an_z < 3$ (solid triangles) and $6 < an_z < 8$ (open triangles). The solid and dashed lines indicate the diameter of one vortex core and of the condensate, respectively.

the existence of excitation modes with a complex eigenfrequency. The nonvanishing imaginary part of the eigenfrequency implies an exponential growth in time of the corresponding excitation mode, leading to decay of the multiply-quantized vortex state. This spectral instability is a general parametric phenomenon occurring when several modes compete during coherent evolution and has been studied in many other nonlinear physical systems.

For a doubly-quantized vortex state in a cylindrically symmetric condensate, it was theoretically found that there are two excitation modes with a complex eigenfrequency [214, 219]. One of them is confined inside the doubly-quantized vortex core; the growth of this so-called "core" mode induces splitting of the original doubly-quantized vortex core into two separate singly-quantized vortex cores. The other mode, having the conjugate eigenfrequency, grows with the core mode in order to conserve energy. In the low density limit, this mode corresponds to the co-rotating quadrupole mode, leading to oscillations in the surface shape of condensates. We always observed that the surface of condensates changed into a quadrupole shape as the two cores appeared, as shown in Figure 6-6A, and the ellipticity was larger at lower density.

Once the doubly-quantized vortex core splits into two cores, the distance between the two cores was almost constant (~ 50 μm) during the further evolution, as shown in Figure 6-6(b). This is evidence that the separation process was driven mainly by the dynamical instability, and not by dissipation, which would gradually increase the separation of the two cores. Dissipative processes were minimized by performing the experiments at the lowest possible temperature. Condensates did not have any discernible thermal components even after extended hold time. Furthermore, the energy released by the dissociation of the doubly-quantized vortex was ~ 5 nK negligible to the critical temperature ~ 240 nK. For the upper bound to the temperature of < 100 nK, Ref. [240] predicts that dissipative decay time to be ≈ 1.5 s for a single vortex, a time scale much longer than what we observed.

What is the further evolution of the two cores? Some of the images at low density showed a regular surface modulation, as in Figure 6-7(a), which was not seen in clouds with a single core. This indicates that higher-order surface modes are excited during the coherent evolution [241]. Several images, especially those labelled as "undetermined", suggest that vortex lines crossed [219, 242], as in Figure 6-7(c). In our system, it was difficult to trace the positions of the two cores beyond 80 ms hold time.

6.2.3 Discussion

According to the above observations such as the ellipticity of the cloud, the surface modulation, and the rapid saturation of the core separation, the decay of the doubly-quantized vortex state seems to be due to dynamical instability. However, there is a qualitative discrepancy between theoretical calculation and our observation. The dynamical instability

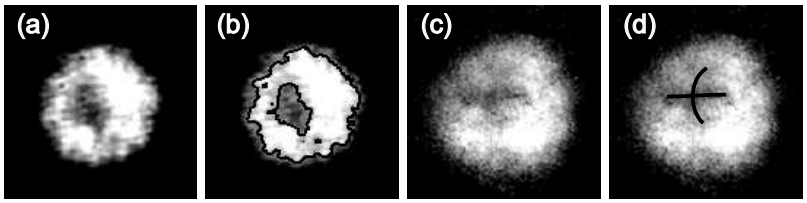

Figure 6-7: Examples for the dynamic evolution after imprinting a doubly quantized vortex: (a) Surface Exicitation. Regular density modulation of the surface was observed after 51 ms hold time for $an_z = 1.8$ (b) same as (a) with a contour line. (c) Crossing of vortex lines. 55 ms hold time and $an_z = 8.4$. (d) same as (c) with guide lines for vortex lines. The field of view is 270 μm $\times$ 270 μm.

of the doubly-quantized vortex state is related to the magnitude of the imaginary part of the complex eigenfrequency, and, according to the numeric calculation in Ref. [219], non-vanishing imaginary part of the eigenfrequency appears at $an_z < 3$ and $an_z \sim 12$, showing a quasi-periodic behavior as a function of the interaction strength, an_z. In contrast to this prediction, the experiment showed a monotonic increase of the lifetime with no hint of periodic behavior.

However, we should remind that the calculated instability is not directly comparable to the observed lifetime. In the theoretical calculation, the imaginary part represents only the initial instability, whereas our criterion for decay was the observation of two *separated* vortex cores. Therefore, there is no information on how the exponential growth of excitation modes would affect the following evolution and it is possible that the dynamical instability changes after the doubly-quantized vortex state is significantly perturbed [215, 220]. Furthermore, the theoretical investigation was based on two-dimensional calculation. The real situation is more complicated: 1) The density, i.e., the interaction strength is changed along the axial direction. One might imagine the twisting of two vortex lines in three dimension [219]. 2) The trap has $\sim 2\%$ asymmetry in the radial trap frequency due to the gravitational sag. 3) A certain amount of excitations must be induced by the imprinting process, as described in Section 6.1.3.

Recently, Jackson et al. [243] emphasized the role of static instability of the doubly-quantized vortex state. Even though we excluded the possibility of thermal dissipation, the slow decay with a higher atom density reminds of the zero-point energy argument: Since the size of the vortex core decreases with a higher peak density, the zero-point energy of the core mode increases and consequently slows down the thermal dissipation of the vortex state [212]. Interestingly, Gawryluk et al. [244] presented a three-dimensional numerical simulation consistent with our observation.

One possible extension of this experiment is combining this setup with an one-dimensional optical lattice along the axial direction, which would realize a two-dimensional trap array.

Reducing the axial dimension, one may have a simpler situation. Dynamics of a vortex line in a stack of weakly coupled two-dimensional condensates were theoretically investigated [245, 246].

6.3 Observation of Coreless Vortices: Spin Textures

In spinless or spin-polarized condensates, vortices need to have cores where the density of condensed particles is zero because the condensate wave function is single-valued. However, in spinor condensates represented by a complex vector wave function with an internal, spin degree of freedom, coreless vortices exist as spin textures [247, 248]. With the spin-rotation topological imprinting technique, we created coreless vortices where each spin component has a different phase winding [10]. Coreless vortices in spinor condensates are different from the vortex states with two component condensates [17] where one component fill up the core of the vortex cores of the other condensate. Fundamentally, condensate mixtures are different from spinor condensates because of the presence of coherent coupling among components [210].

Let's have a closer look at what is happening inside condensates during the field inversion. The axial magnetic field B_z is ramped from $+B_{z0}(>0)$ to $-B_{z0}$, and the rotation angle θ is given by $\theta(B_z) = \cot^{-1}(B_z/B_r)$ with the assumption that the initial spin is parallel to z-direction ($B_{z0} \gg B_r$), where B_r is the transverse field at atom position. According to Eq. (6.3), a spinor condensate initially prepared in the $|1,-1\rangle_z$ state is transformed into

$$\mathrm{R}(\phi,\theta(B_z))|1,-1\rangle_z = \begin{pmatrix} \sin^2\frac{\theta}{2}e^{i2\phi} \\ -\frac{1}{\sqrt{2}}\sin\theta e^{i\phi} \\ \cos^2\frac{\theta}{2} \end{pmatrix}, \tag{6.9}$$

where $\phi \to \frac{\pi}{2} - \phi$ to account for the field direction in Figure 6-2. During the field inversion $\theta : 0 \to \pi$, the population transfers from the $|1,-1\rangle$ state with no vortex into the $|1,0\rangle$ state with a singly quantized vortex and the $|1,+1\rangle$ state with a doubly quantized vortex. Because $B_r \propto r$, the rotation angle θ also has radial dependence and outer atoms will rotate further when $B_z > 0$. We can imagine a coreless vortex state where a vortexless $|1,-1\rangle$ component in the center is surrounded by other circulating components.

When $\theta \approx \frac{\pi}{2}(B_z \approx 0)$, a physically interesting situation happens; all three spin states are almost equally populated, but each state has a different phase winding from each other so that the corresponding centrifugal force would separate them in the radial direction. However, the atomic Zeeman energy would compete this segregation effect because the misalignment of spins from the magnetic field direction costs energy. The competition between kinetic energy and Zeeman energy would cause interesting dynamics of the spin

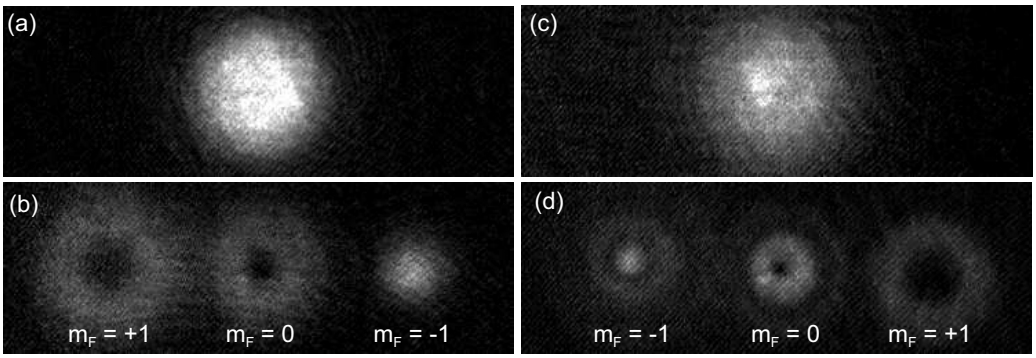

Figure 6-8: Coreless vortices in $F = 1$ spinor condensates. Coreless vortices were imprinted by ramping the axial magnetic filed B_z to zero in a Ioffe-Pritchard magnetic trap. The spin texture was diagnosed by a projection method, suddenly switching (a,b) $B_z \ll 0$ and (c,d) $B_z \gg 0$. Axial absorption images were taken after 20 ms time-of-flight. In (b) and (d), the three spin states were spatially separated by a magnetic field gradient. The magnetic sublevel number m_F is defined with respect to $+z$ quantization axis.

texture.

The nature of the spin texture with $B_z \approx 0$ was experimentally studied by a projection method. The experimental conditions for producing the spin texture were similar to those for the previous vortex experiments. After ramping down $B_z \to 0$, the strong axial magnetic field was suddenly switched on to project the condensate wave function onto a basis quantized in the axial, z direction. This experimental technique corresponds to the theoretical decomposition of the wave function in the z quantization axis. Following the field projection, condensates were released and each spin component was spatially separated during time-of-flight by an additional field gradient, an implementation of the Stern-Gerlach effect. Coreless vortices having three spin states with different vorticities were observed and a typical absorption image is provided in Figure 6-8.

When the projection field was applied in $+z$ direction (positive projection), additional ring structures were observed in $|1, -1\rangle$ and $|1, 0\rangle$ states. They may be a signature of spin wave excitations [34, 35], but we attribute these effects mainly to technical imperfections in our field control. Detailed analysis of the projection method and possible technical issues are described in Ref. [10]. Changing the final value of B_z in the vortex imprinting process, the spin textures were measured (Figure 6-9), which clearly demonstrates that the population transfers from the $|1, -1\rangle$ state to the $|1, +1\rangle$ state.

Studying the dynamic evolution and the stability of the spin texture was limited by the short lifetime of condensates which was $\sim$ 1 ms with $B_z \approx 0$ due to non-adiabatic (Majorana) spin flips at the trap center. The spin flip effect was directly confirmed by observing atom leakage out of the magnetic trap. Using an optical dipole trap might be an

alternative method to study the dynamics. However, it was technically difficult to overlap an optical trap with a magnetic trap and hold atoms stably.

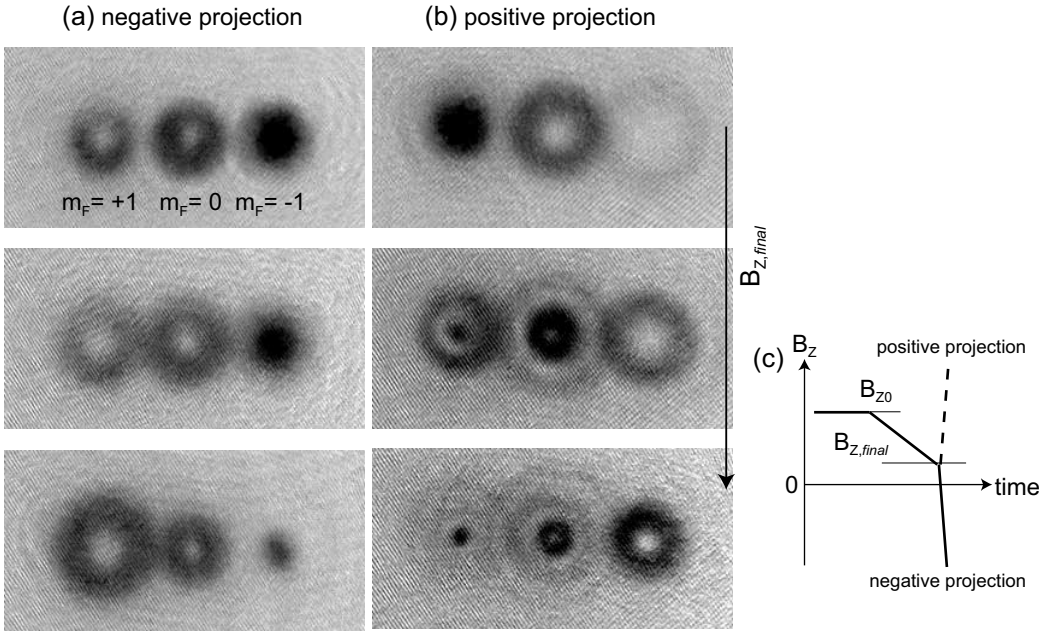

Figure 6-9: Spin textures vs. final axial magnetic field. Vortex states were imprinted by ramping down B_z from B_{z0} to $B_{z,final} \approx 0$. Changing the final field value $B_{z,final}$ around zero, spin textures were measured by suddenly switching (a) $B_z \ll 0$ (negative projection) and (b) $B_z \gg 0$ (positive projection). The field control is sketched in (c).

Chapter 7

Conclusion

Experimental breakthroughs that access previously unexplored regions and interactions, which may be ultrafast phenomena, ultra small objects, ultra low temperatures, or extremely large cosmic objects, have always uncovered new and unexpected physical scenarios. This indisputable fact always drives and challenges experimentalists to expand the experimentally accessible realm with new techniques and systems. Experimental realization of Bose-Einstein condensation with a weakly interacting neutral atoms is one clear example of these efforts. Since 1995, the quantum degenerate atomic gas system has provided a magnificent playground where experimentalists can play at will with quantum coherent matter waves and a simplified bridge to many-body physics through which one can investigate sophisticated concepts in condensed matter physics.

As a small effort along this line, I and my colleagues have tried to expose condensates to new environments to see something unobservable before. The main theme in this thesis research was phase dynamics of Bose-Einstein condensates, and for this we have developed an optical double-well system and magnetic microtraps on an atom chip. Dynamic coherent splitting of a trapped condensate was demonstrated by deforming a single well potential into a double-well potential and this coherent beam splitter allowed performing a 'proof-of-principle' experiment of confined atom interferometry with Bose-Einstein condensates. Coherent optical coupling and incoherent thermal coupling of two spatially separate condensates were investigated in a double-well potential system. An optical read-out of the relative phase of the two condensates was developed using phase-sensitive atomic currents between the two condensates. A doubly-quantized vortex state was topologically imprinted by adiabatic spin rotation and the reliability of the creation method made it possible to study the stability of a doubly-quantized vortex state.

The idea of the atom chip was suggested at first for the technical advantages of using the proximity of the potential source such as tighter confinement with small power consumption and precise spatial control due to microfabrication. This idea has been successfully

demonstrated in the last decade and now people desire and investigate to integrate every experimental manipulation tool on a microchip, such as optical fibers, optical cavities, and electric field sources. Experiments meticulously designed on a micron scale would open many prospects. For examples, an atom chip combined with an optical cavity would allow a strong coupling between atoms and photons because of its precise positioning ability and one with a single-atom detector would open up the field of quantum atom optics. The atom chip technology is envisioned to be a platform with a quantum tool box for future atomic physics experiments.

Fundamentally, miniaturization brings us deeper into quantum regime. Quantum phenomena such as quantum tunneling become important at a microscopic scale and thus, I believe that the future development of the atom chip technology will be directed toward more miniaturization down to a sub-micron scale beyond simple integration of conventional components. Well-controlled sub-micron potentials would give us a chance to study quantum transport, effects of disorder potentials, and low-dimensional physics. Currently, an optical lattice may be a unique system with a sub-micron scale and implementing sub-micron potentials on a microchip is hampered by the deleterious proximity effects. This surface effects might be regarded as being a fundamentally unavoidable limit, but given the previous achievements in many other research groups, I expect that this limit will be pushed back at the end.

Appendix A

Designs for the Apparatus

This appendix contains the diagrams for the laser system and the science chamber pumping body.

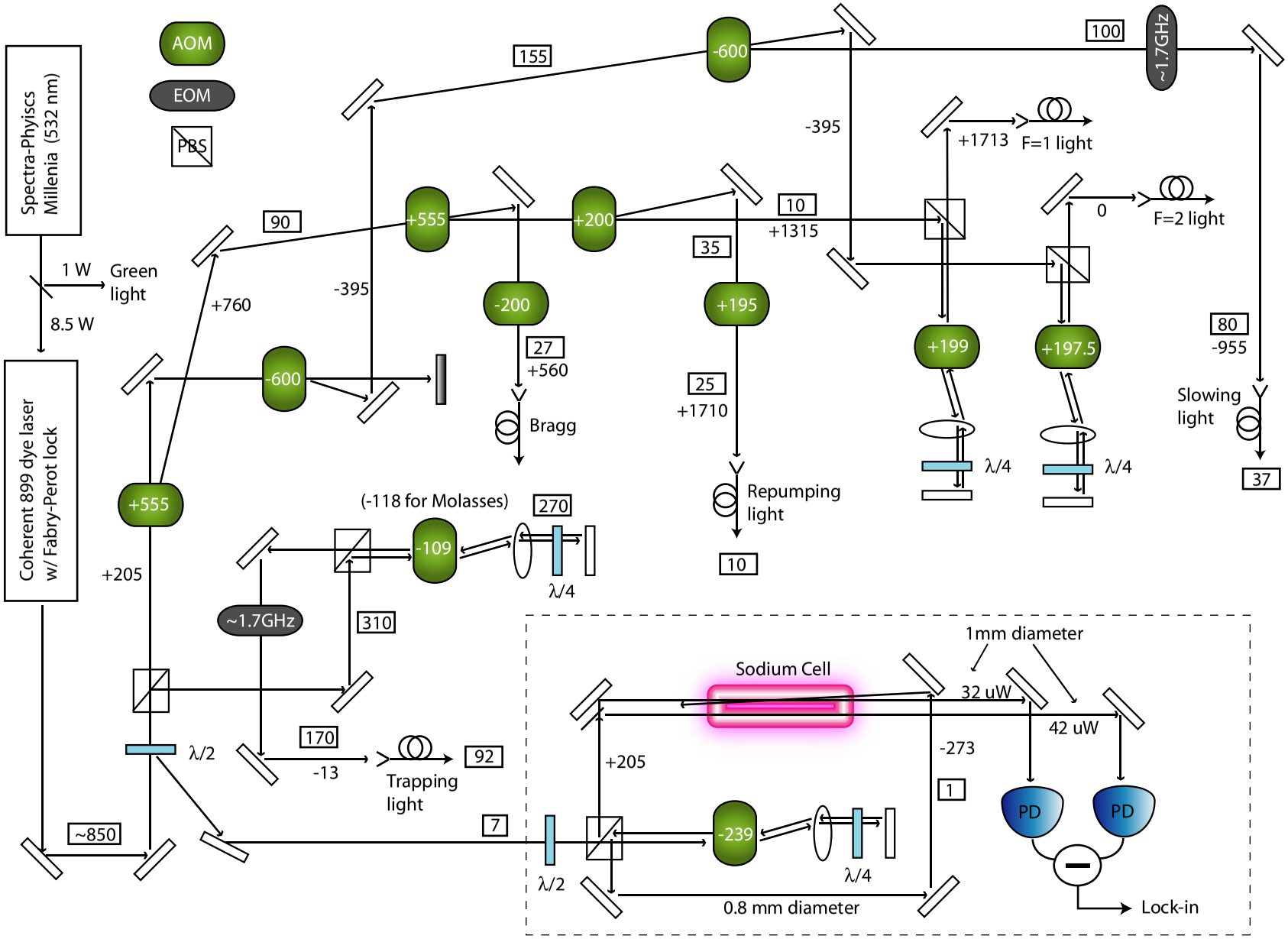

Laser system diagram. A 518 nm yellow laser light is generated from a dye laser system pumped by a 532 nm green light. The laser frequency is locked to a Fabry-Perot cavity, and the reference for the cavity is an external saturation-absorption spectroscopy (SAS) lock-in scheme enclosed by a dashed line. Modulation frequencies of acousto-optic modulators (AOMs) and electro-optic modulators (EOMs) are indicated inside the corresponding modulators. The numbers along the laser line represent laser frequency in MHz with respect to the F=2 -> F'=3 transition. The numbers inside boxes represent laser power in mW.

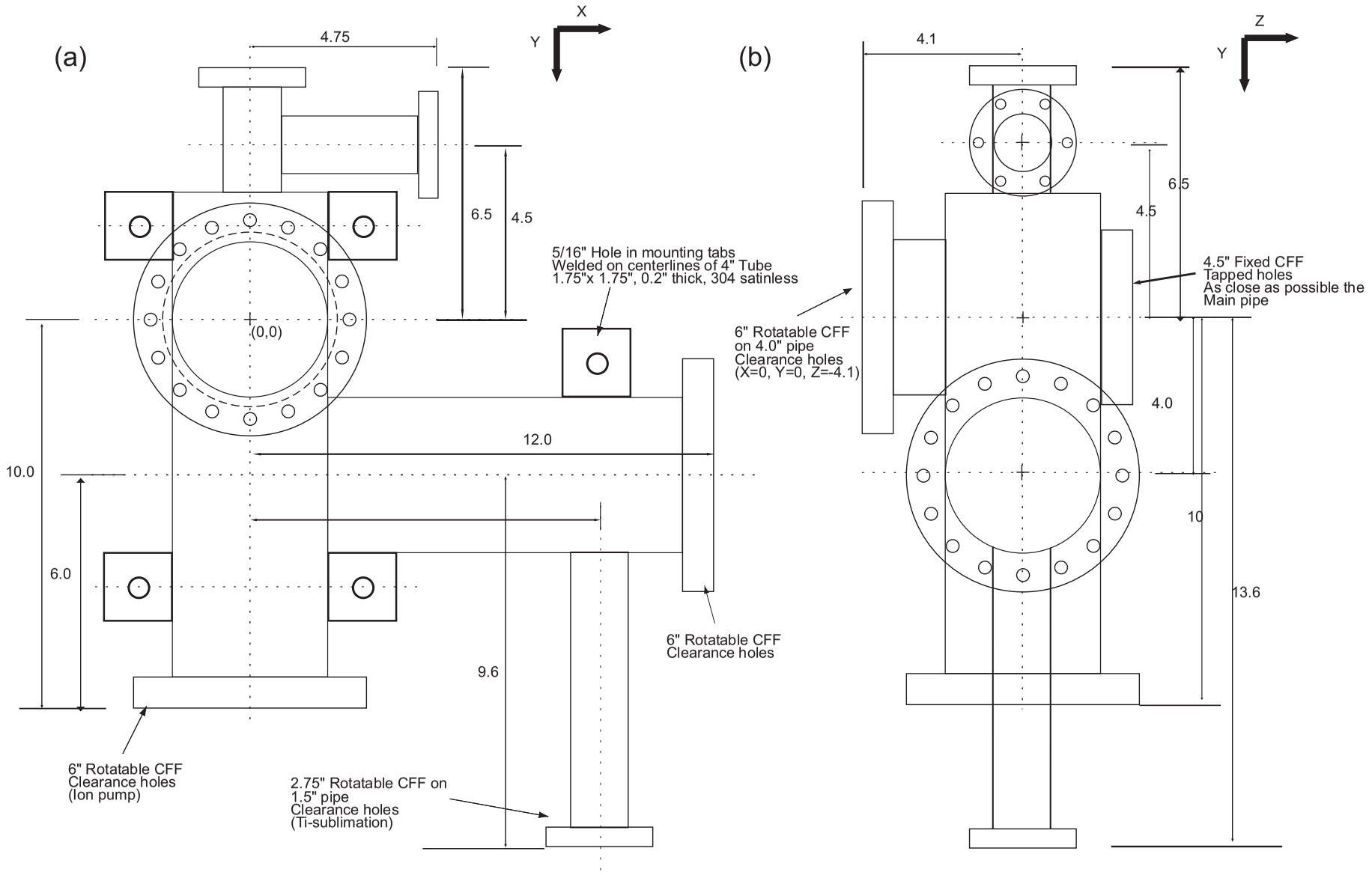

Science chamber pumping body. (a) Top view. (b) Side view.
The axis direction follows the BEC-III convention: +x to the hallway, +y to BEC-I, and +z in gravity.

Appendix B

Atom Interferometry with Bose-Einstein Condensates in a Double-Well Potential

This appendix contains a reprint of Ref. [1]: Y. Shin, M. Saba, T.A. Pasquini, W. Ketterle, D.E. Pritchard, and A.E. Leanhardt, *Atom Interferometry with Bose-Einstein Condensates in a Double-Well Potential*, Physical Review Letters **92**, 050405 (2004).

Atom Interferometry with Bose-Einstein Condensates in a Double-Well Potential

Y. Shin, M. Saba, T. A. Pasquini, W. Ketterle, D. E. Pritchard, and A. E. Leanhardt*

Department of Physics, MIT-Harvard Center for Ultracold Atoms, and Research Laboratory of Electronics, Massachusetts Institute of Technology, Cambridge, Massachusetts 02139, USA

(Received 17 July 2003; published 6 February 2004)

A trapped-atom interferometer was demonstrated using gaseous Bose-Einstein condensates coherently split by deforming an optical single-well potential into a double-well potential. The relative phase between the two condensates was determined from the spatial phase of the matter wave interference pattern formed upon releasing the condensates from the separated potential wells. Coherent phase evolution was observed for condensates held separated by 13 μm for up to 5 ms and was controlled by applying ac Stark shift potentials to either of the two separated condensates.

DOI: 10.1103/PhysRevLett.92.050405 PACS numbers: 03.75.Dg, 03.75.Lm, 39.20.+q

Atom interferometers have been used to sense accelerations [1,2] and rotations [3,4], monitor quantum decoherence [5], characterize atomic and molecular properties [6], and measure fundamental constants [1,7]. Demonstrating atom interferometry with particles confined by magnetic [8–11] and optical [12] microtraps and waveguides would realize the matter wave analog of optical interferometry using fiber-optic devices. Current proposals for confined-atom interferometers rely on the separation and merger of two potential wells to split and recombine atomic wave packets [13–15]. Atom-atom interactions tend to localize particles in either potential well and reduce the coherence of the splitting and recombination processes [16,17], whereas tunneling serves to delocalize the atomic wave packets and maintain a well-defined relative phase between the potential wells [16].

Bose-Einstein condensates are to matter wave interferometry what lasers are to optical interferometry, i.e., a coherent, single-mode, and highly brilliant source. Condensates have been coherently delocalized over multiple sites in optical lattices where the tunneling energy dominates the on-site atom-atom interaction energy due to the submicron barrier between neighboring potential wells [2,18–21]. Here, the thin barrier helps to maintain phase coherence across the lattice, but also prevents addressing individual lattice sites. To construct a versatile atom interferometer capable of sensing forces with arbitrary spatial variation two individually addressable interfering paths are needed. This apparently simple requirement represents a considerable challenge when it comes to splitting a Bose-Einstein condensate with a thick barrier that prevents tunneling and separates the resulting condensate pair by large distances (that allow for individual addressability) without affecting their quantum mechanical phase in an uncontrolled way. In addition to the technical challenges, it is not even clear theoretically if the two condensates generated after splitting will share the same phase (a phase-coherent state) or if each will have a well-defined number of particles without relative phase coherence (a number-squeezed state) [16,22–24].

In this Letter, we demonstrate that a condensate can be split coherently along two separated paths by deforming an initially single-well potential into two wells. The relative phase between the two condensates was determined from the spatial phase of the matter wave interference pattern formed upon releasing the atoms from the separated potential wells [25,26]. This scheme realizes a trapped-atom interferometer. The large well separation (13 μm) (i) allowed ac Stark phase shifts to be applied to either condensate by temporarily turning off the laser beam generating its potential well and (ii) suppressed tunneling such that the phase of each condensate evolved independently. Without the aid of tunneling to preserve phase coherence, the measured coherence time of the separated condensates was 5 ms.

Bose-Einstein condensates containing over 10^7 ^{23}Na atoms were created in the $|F = 1, m_F = -1\rangle$ state in a magnetic trap, captured in the focus of a 1064 nm optical tweezers laser beam, and transferred into an auxiliary "science" chamber as described in Ref. [27]. In the science chamber, the condensate was loaded from the optical tweezers into a secondary optical trap formed by a counterpropagating, orthogonally polarized 1064 nm laser beam. The secondary optical trap was formed by a collimated laser beam that passed through an acousto-optic modulator (AOM) and was focused onto the condensate with a lens [Fig. 1(a)]. The AOM was driven simultaneously by two radio frequency (rf) signals to tailor the shape of the potential from single well [Fig. 1(b)] to double well [Fig. 1(c)]. The separation between the potential wells was controlled by the frequency difference between the rf drives. The waist of each focused beam was 5 μm. A single, isolated potential well was characterized by a trap depth $U_0 = h \times 5$ kHz, where h is Planck's constant, and a radial (axial) trap frequency $f_r = 615$ Hz ($f_z = 30$ Hz).

Condensates were initially loaded from the tweezers into a single-well trap [Fig. 1(b)]. After holding the cloud for 15 s to damp excitations, the condensate contained $\sim 10^5$ atoms with a peak atomic mean field energy

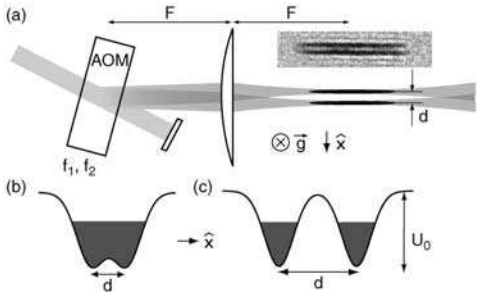

FIG. 1. Optical double-well potential. (a) Schematic diagram of the optical setup for the double-well potential. An acousto-optic modulator (AOM) was driven by two frequencies, f_1 and f_2, and diffracted a collimated beam into two beams. The AOM was placed in the focal plane of a lens of focal length F so that the two beams propagated parallel to each other. The radial separation of the potential wells, d, was controlled by the frequency difference, $\Delta f = |f_1 - f_2|$. The acceleration due to gravity, $\vec{g}$, points into the page. The absorption image shows two well-separated condensates confined in the double-well potential diagrammed in (c). The field of view is 70×300 μm. Energy diagrams for (b) initial single-well trap with $d = 6$ μm and (c) final double-well trap with $d = 13$ μm. In both (b) and (c), $U_0 = h \times 5$ kHz and the peak atomic mean field energy was $\sim h \times 3$ kHz. The potential "dimple" in (b) was $< h \times 500$ Hz which was much less than the peak atomic mean field energy allowing the trap to be characterized as a single well. The potential "barrier" in (c) was $h \times 4.7$ kHz which was larger than the peak atomic mean field energy allowing the resulting split condensates to be characterized as independent.

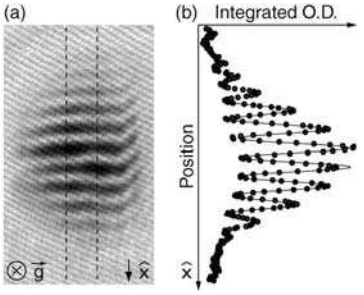

FIG. 2. Matter wave interference. (a) Absorption image of condensates released from the double-well potential in Fig. 1(c) immediately after splitting and allowed to overlap during 30 ms of ballistic expansion. The imaging axis was parallel to the direction of gravitational acceleration, $\vec{g}$. The field of view is 600×350 μm. (b) Radial density profiles were obtained by integrating the absorption signal between the dashed lines, and typical images gave $> 60\%$ contrast. The solid line is a fit to a sinusoidally modulated Gaussian curve from which the phase of the interference pattern was extracted (see text). This figure presents data acquired in a single realization of the experiment.

$\mu \approx h \times 3$ kHz. The single-well trap was deformed into a double-well potential [Fig. 1(c)] by linearly increasing the frequency difference between the rf signals driving the AOM over 5 ms. The amplitudes of the rf signals were tailored during the splitting process to yield nearly equal atom number and trap depths for each potential well.

Condensates realized from the double-well potential ballistically expanded, overlapped, and interfered (Fig. 2). Each realization of the experiment produced a matter wave interference pattern with the same spatial phase. This reproducibility demonstrated that deforming the optical potential from a single well into a double well coherently split the condensate into two clouds with deterministic relative phase, i.e., the relative phase between the two condensates was the same from shot to shot.

This experiment derived its double-well potential from a single laser beam passing through an AOM. Vibrations and fluctuations of the laser beam were common mode to both wells, and a clean and rapid trap turn-off was achieved by switching off the rf power driving the AOM. In contrast, past experiments created a double-well potential by splitting a magnetically trapped condensate with a blue-detuned laser beam [25]. Such work was unable to observe a reproducible relative phase between the split condensates, due to fluctuations in the blue-detuned laser beam and irreproducible turn-off of the high current magnetic trap that initiated ballistic expansion.

The relative phase between the two separated condensates was determined by the spatial phase of their matter wave interference pattern. For a ballistic expansion time $t \gg 1/f_r$, each condensate had a quadratic phase profile [28], $\psi_\pm(\vec{r}, t) = \sqrt{n_\pm(\vec{r}, t)} \exp[i(m/2\hbar t)|\vec{r} \pm \vec{d}/2|^2 + \phi_\pm]$, where $\pm$ denotes either well, $n_\pm$ is the condensate density, m is the atomic mass, $\vec{d}$ is a vector connecting the two wells, $\phi_\pm$ is the condensate phase, and $\hbar = h/2\pi$. Interactions between the two condensates during ballistic expansion have been neglected. The total density profile for the matter wave interference pattern takes the form

$$n(\vec{r}, t) = \left[n_+ + n_- + 2\sqrt{n_+ n_-} \cos\left(\frac{md}{\hbar t} x + \phi_r\right)\right], \quad (1)$$

where $\phi_r = \phi_+ - \phi_-$ is the relative phase between the two condensates and $\vec{d} = d\hat{x}$. To extract ϕ_r, an integrated cross section of the matter wave interference pattern [Fig. 2(b)] was fitted with a sinusoidally modulated Gaussian curve, $G(x) = A \exp[-(x - x_c)^2/\sigma^2]\{1 + B \cos[(2\pi/\lambda)(x - x_0) + \phi_f]\}$, where ϕ_f is the phase of the interference pattern with respect to a chosen fixed x_0. Ideally, if x_0 was set at the center of the two wells, then $\phi_r = \phi_f$. However, misalignment of the imaging axis with the direction of gravitational acceleration created a constant offset, $\phi_f = \phi_r + \delta\phi$. With $t = 30$ ms the measured fringe period, $\lambda = 41.5$ μm, was within 4% of the point source formula prediction [Eq. (1)], $ht/md = 39.8$ μm.

The relative phase between the separated condensates was observed to evolve linearly in time [Fig. 3(a)]. This evolution was primarily due to a small difference in the well depths and could be tailored by adjusting the relative intensity of the two laser beams generating the wells.

The standard deviation of eight measurements of ϕ_r was $<90°$ for condensates split then held separated for ≤ 5 ms [Fig. 3(b)]. For hold times ≤ 1 ms, the standard deviation was substantially smaller, $<40°$. Since a random distribution of phases between $-180°$ and $+180°$ would have a standard deviation of $\sim 104°$, the measured results quantitatively confirm the reproducible nature of the splitting process and the coherent evolution of the separated condensates.

The number-phase uncertainty principle provides a fundamental limit to the phase coherence between isolated condensates due to phase diffusion [16,22–24,29,30]. For Poissonian number fluctuations about a mean condensate atom number N, we expect a phase diffusion time $\sim 1/(2\mu/5h\sqrt{N}) \sim 250$ ms. Atom-atom interactions may localize particles in either potential well during splitting and reduce the relative number fluctuations. This would reduce the measured coherence of the split condensates, but extend the phase diffusion time. The uncertainty in determining ϕ_r at hold times >5 ms is attributed to axial and breathing-mode excitations created during the splitting process. These excitations led to interference fringes that were angled and had substantial curvature, rendering a determination of ϕ_r impossible. Splitting the condensate more slowly did not improve the measured stability of ϕ_r since we were unable to split the condensate much slower than the axial trap period and much faster than the expected phase diffusion time.

The phase sensitivity of the trapped-atom interferometer was demonstrated by applying ac Stark phase shifts to either (or both) of the two separated condensates. Phase shifts were applied to individual condensates by pulsing off the optical power generating the corresponding potential well for a duration $\tau_p \ll 1/f_r$. The spatial phase of the matter wave interference pattern shifted linearly with the pulse duration, as expected [Fig. 4(a)]. Because of the inhomogeneous optical potential, $U(r)$, the applied ac Stark phase shifts varied across the condensate as $\Delta\phi(r) = -U(r)\tau_p/\hbar$. Inhomogeneous phase shifts should lead to an excitation of the condensate that was

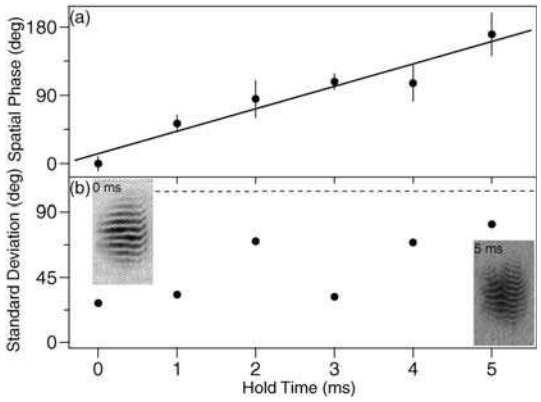

FIG. 3. Phase coherence of the separated condensates. (a) The spatial phase of the matter wave interference pattern is plotted versus hold time after splitting the condensate. Each point represents the average of eight measurements. The phase evolution was due to unequal trap depths for the two wells, which was determined from the linear fit to be $h \times 70$ Hz or $\sim 1\%$ of the trap depth. (b) Standard deviation of eight measurements of the relative phase. A standard deviation $\sim 104°$ (dashed line) is expected for random relative phases. Matter wave interference patterns after 0 and 5 ms holding are displayed. The curvature of the interference fringes increased with hold time limiting the coherence time of the separated condensates to 5 ms.

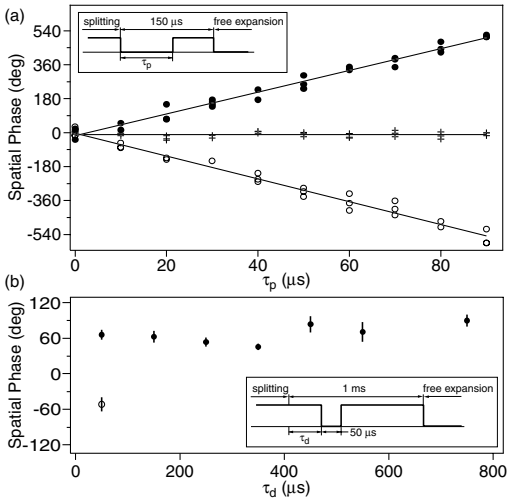

FIG. 4. Trapped-atom interferometry. (a) ac Stark phase shifts were applied to either well exclusively (solid circles and open circles) or both wells simultaneously (crosses) by turning off the corresponding rf signal(s) driving the AOM for a duration τ_p. The resulting spatial phase of the matter wave interference pattern scaled linearly with τ_p and hence the applied phase shift. Applying the ac Stark shift to the opposite well (solid versus open circles) resulted in an interference pattern phase shift with opposite sign. Applying ac Stark shifts to both wells (crosses) resulted in no phase shift for the interference pattern. These data were taken with a slightly modified experimental setup such that the trap depth of the individual potential wells was $U_0 = h \times 17$ kHz, corresponding to a 270° phase shift for a 50 μs pulse. (b) A 50 μs pulse induced a 70° shift independent of the pulse delay, τ_d. The experimental setup was as described in Fig. 1 ($U_0 = h \times 5$ kHz). Solid and open circles have the same meaning as in (a). The insets show the time sequence of the optical intensity for the well(s) temporarily turned off.

probably too small to be observed. We assume that the measured phase shift can be found by averaging the applied inhomogeneous phase shift over the inhomogeneous condensate density: $\Delta\bar{\phi} = \frac{1}{N}\int d^3\vec{r} n(\vec{r})\Delta\phi(\vec{r}) = (U_0 - \frac{2}{7}\mu)\Delta t/\hbar$, where $N = \int d^3\vec{r} n(\vec{r})$ is the number of atoms. The measured phase shifts yielded $U_0 = h \times 5$ kHz [Fig. 4(b)], which was consistent with calculations based on the measured trap frequencies.

The measured phase shifts in the interferometer depended only on the time integral of the applied ac Stark phase shifts [Fig. 4(b)]. For uncoupled condensates, the final relative phase, ϕ_r, should be the same on any phase trajectory because the history of phase accumulation does not affect the total amount of accumulated phase. For coupled condensates, Josephson oscillations between the wells would cause the relative phase to vary nonlinearly with time and produce a time dependent signal in Fig. 4(b). The single-particle tunneling rate and Josephson oscillation frequency in our system were calculated to be $\sim 5 \times 10^{-4}$ Hz [28] and ~ 1 Hz [31], respectively.

In conclusion, we have performed atom interferometry with Bose-Einstein condensates confined by optical potentials. A coherent condensate beam splitter was demonstrated by deforming a single-well potential into a double-well potential. The large spatial separation between the potential wells allowed each condensate to evolve independently and for addressing each condensate individually. Recombination was performed by releasing the atoms from the double-well potential and allowing them to overlap while expanding ballistically. Implementing a similar readout scheme with magnetic potentials generated by microfabricated current carrying wires should be possible. Propagating the separated condensates along a microfabricated waveguide prior to phase readout would create an atom interferometer with an enclosed area, and hence with rotation sensitivity.

We thank W. Jhe, C. V. Nielsen, and A. Schirotzek for experimental assistance and S. Gupta, Z. Hadzibabic, and M. W. Zwierlein for critical comments on the manuscript. This work was funded by ARO, NSF, ONR, and NASA. M. S. acknowledges additional support from the Swiss National Science Foundation.

*URL: http://cua.mit.edu/ketterle_group/

[1] A. Peters, K. Y. Chung, B. Young, J. Hensley, and S. Chu, Philos. Trans. R. Soc. London, Ser. A **355**, 2223 (1997).
[2] B. P. Anderson and M. A. Kasevich, Science **282**, 1686 (1998).
[3] A. Lenef, T. D. Hammond, E. T. Smith, M. S. Chapman, R. A. Rubenstein, and D. E. Pritchard, Phys. Rev. Lett. **78**, 760 (1997).
[4] T. L. Gustavson, P. Bouyer, and M. A. Kasevich, Phys. Rev. Lett. **78**, 2046 (1997).
[5] M. S. Chapman, T. D. Hammond, A. Lenef, J. Schmiedmayer, R. A. Rubenstein, E. Smith, and D. E. Pritchard, Phys. Rev. Lett. **75**, 3783 (1995).
[6] C. R. Ekstrom, J. Schmiedmayer, M. S. Chapman, T. D. Hammond, and D. E. Pritchard, Phys. Rev. A **51**, 3883 (1995).
[7] S. Gupta, K. Dieckmann, Z. Hadzibabic, and D. E. Pritchard, Phys. Rev. Lett. **89**, 140401 (2002).
[8] H. Ott, J. Fortagh, G. Schlotterbeck, A. Grossmann, and C. Zimmermann, Phys. Rev. Lett. **87**, 230401 (2001).
[9] W. Hänsel, P. Hommelhoff, T. W. Hänsch, and J. Reichel, Nature (London) **413**, 498 (2001).
[10] A. E. Leanhardt, A. P. Chikkatur, D. Kielpinski, Y. Shin, T. L. Gustavson, W. Ketterle, and D. E. Pritchard, Phys. Rev. Lett. **89**, 040401 (2002).
[11] S. Schneider, A. Kasper, C. vom Hagen, M. Bartenstein, B. Engeser, T. Schumm, I. Bar-Joseph, R. Folman, L. Feenstra, and J. Schmiedmayer, Phys. Rev. A **67**, 023612 (2003).
[12] R. Dumke, T. Müther, M. Volk, W. Ertmer, and G. Birkl, Phys. Rev. Lett. **89**, 220402 (2002).
[13] E. A. Hinds, C. J. Vale, and M. G. Boshier, Phys. Rev. Lett. **86**, 1462 (2001).
[14] W. Hänsel, J. Reichel, P. Hommelhoff, and T. W. Hänsch, Phys. Rev. A **64**, 063607 (2001).
[15] E. Andersson, T. Calarco, R. Folman, M. Andersson, B. Hessmo, and J. Schmiedmayer, Phys. Rev. Lett. **88**, 100401 (2002).
[16] C. Menotti, J. R. Anglin, J. I. Cirac, and P. Zoller, Phys. Rev. A **63**, 023601 (2001).
[17] J. A. Stickney and A. A. Zozulya, Phys. Rev. A **66**, 053601 (2002).
[18] C. Orzel, A. K. Tuchman, M. L. Fenselau, M. Yasuda, and M. A. Kasevich, Science **291**, 2386 (2001).
[19] F. S. Cataliotti, S. Burger, C. Fort, P. Maddaloni, F. Minardi, A. Trombettoni, A. Smerzi, and M. Inguscio, Science **293**, 843 (2001).
[20] M. Greiner, I. Bloch, O. Mandel, T. W. Hänsch, and T. Esslinger, Phys. Rev. Lett. **87**, 160405 (2001).
[21] M. Greiner, O. Mandel, T. Esslinger, T. W. Hänsch, and I. Bloch, Nature (London) **415**, 39 (2002).
[22] J. Javanainen and M. Wilkens, Phys. Rev. Lett. **78**, 4675 (1997).
[23] A. J. Leggett and F. Sols, Phys. Rev. Lett. **81**, 1344 (1998).
[24] J. Javanainen and M. Wilkens, Phys. Rev. Lett. **81**, 1345 (1998).
[25] M. R. Andrews, C. G. Townsend, H.-J. Miesner, D. S. Durfee, D. M. Kurn, and W. Ketterle, Science **275**, 637 (1997).
[26] O. Mandel, M. Greiner, A. Widera, T. Rom, T. W. Hänsch, and I. Bloch, Phys. Rev. Lett. **91**, 010407 (2003).
[27] T. L. Gustavson, A. P. Chikkatur, A. E. Leanhardt, A. Görlitz, S. Gupta, D. E. Pritchard, and W. Ketterle, Phys. Rev. Lett. **88**, 020401 (2002).
[28] F. Dalfovo, S. Giorgini, L. P. Pitaevskii, and S. Stringari, Rev. Mod. Phys. **71**, 463 (1999).
[29] M. Lewenstein and L. You, Phys. Rev. Lett. **77**, 3489 (1996).
[30] J. A. Dunningham, M. J. Collett, and D. F. Walls, Phys. Lett. A **245**, 49 (1998).
[31] A. Smerzi, S. Fantoni, S. Giovanazzi, and S. R. Shenoy, Phys. Rev. Lett. **79**, 4950 (1997).

Appendix C

Interference of Bose-Einstein Condensates split with an Atom Chip

This appendix contains a reprint of Ref. [4]: Y. Shin, C. Sanner, G.-B. Jo, T. A. Pasquini, M. Saba, W. Ketterle, D. E. Pritchard, M. Vengalattore and M. Prentiss, *Interference of Bose-Einstein Condensates split with an Atom Chip*, Physical Review A **72**, 021604(R) (2005).

PHYSICAL REVIEW A **72**, 021604(R) (2005)

Interference of Bose-Einstein condensates split with an atom chip

Y. Shin, C. Sanner, G.-B. Jo, T. A. Pasquini, M. Saba, W. Ketterle, and D. E. Pritchard*
MIT-Harvard Center for Ultracold Atoms, Research Laboratory of Electronics, Department of Physics, Massachusetts Institute of Technology, Cambridge, Massachusetts 02139, USA

M. Vengalattore and M. Prentiss
MIT-Harvard Center for Ultracold Atoms, Jefferson Laboratory, Physics Department, Harvard University, Cambridge, Massachusetts 02138, USA
(Received 10 June 2005; published 11 August 2005)

We have used a microfabricated atom chip to split a single Bose-Einstein condensate of sodium atoms into two spatially separated condensates. Dynamical splitting was achieved by deforming the trap along the tightly confining direction into a purely magnetic double-well potential. We observed the matter wave interference pattern formed upon releasing the condensates from the microtraps. The intrinsic features of the quartic potential at the merge point, such as zero trap frequency and extremely high field-sensitivity, caused random variations of the relative phase between the two split condensates. Moreover, the perturbation from the abrupt change of the trapping potential during the splitting was observed to induce vortices.

DOI: 10.1103/PhysRevA.72.021604 PACS number(s): 03.75.Dg, 03.75.Kk, 39.20.+q

Coherent manipulation of matter waves is the ultimate goal of atom optics, and diverse atom optical elements have been developed such as mirrors, beamsplitters, gratings, and waveguides. An atom chip integrates these elements on a microfabricated device allowing precise and stable alignment [1–3]. Recently, this atom chip technology has been combined with Bose-Einstein condensed atoms [4,5], and opened the prospect for chip-based atom interferometers with Bose-Einstein condensates. Despite various technical problems [6–10], there have been advances toward that goal, such as excitationless propagation in a waveguide [6] and demonstration of a Michelson interferometer involving splitting along the axis of a single waveguide [11].

Coherent splitting of matter waves into spatially separate atomic wave packets with a well-defined relative phase is a prerequisite for further applications such as atom interferometry and quantum information processing, and it has been a major experimental challenge. The methods envisioned for coherent splitting on atom chips can be divided in two classes. One is splitting in momentum space and subsequently generating a spatial separation, using scattering of atoms from a periodic optical potential [11,12]. The other is dynamical splitting by directly deforming a single wave packet into two spatially separated wave packets, which can be considered as cutting off the link between two wave packets, i.e., stopping tunneling through the barrier separating two wave packets. Splitting in momentum space has led to remarkably clean interferometric measurements when the atoms were allowed to propagate freely after splitting, but it has been pointed out that momentum splitting of confined atoms (e.g., inside a waveguide) is problematic due to spatially dependent phase shifts induced by atom-atom interactions during separation [11,13]. Dynamical splitting in real space instead is perfectly compatible with keeping atoms confined, a feature beneficial to the versatility of interferometers. There has been a theoretical debate concerning the adiabatic condition for coherent dynamical splitting [14–17]. In our recent experiment with an optical double-well potential, we demonstrated that it is possible to dynamically split a condensate into two parts in a coherent way [18].

In this work, we studied the dynamical splitting of condensates in a purely magnetic double-well potential on an atom chip. We developed an atom chip to generate a symmetric double-well potential and succeeded in observing the matter wave interference of two split condensates, from which the coherence of the splitting process was investigated. We found that the mechanical perturbations during splitting are violent enough to generate vortices in condensates. We discuss the adiabatic condition of the splitting process.

A magnetic double-well potential was realized with an atom chip using a two-wire scheme [19]. The experimental setup of the atom chip is shown in Fig. 1. When two chip wires have currents, I_C, in the $-y$ direction and the external magnetic field, B_x, is applied in the $+x$ direction, two lines of local minima in the magnetic field are generated above the chip surface. Each local minimum has a quadruple field configuration in the xz plane, and with an additional nonzero magnetic field in the axial direction (y-direction), two Ioffe-Pritchard magnetic traps can be formed. The relative magnitude of B_x to the field from I_C determines the direction of separation and the distance of the two traps. The atom chip was set to face downward and the two traps are vertically (horizontally) separated when $B_x < B_{x0} (B_x > B_{x0})$. $B_{x0} = \mu_0 I_C / \pi d$ is the critical field magnitude for merging two magnetic harmonic potentials to form a single quartic potential, where d is the distance between the two chip wires and μ_0 is the permeability of the vacuum. The merge point is located at the middle of the two wires and $d/2$ away from the chip surface. In our experiment, $d = 300\ \mu$m; thus, the splitting happened

*URL: http://cua.mit.edu/ketterle_group/

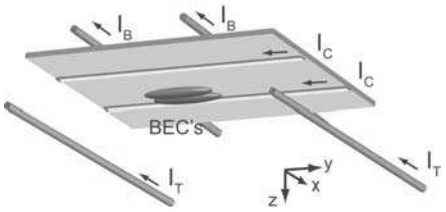

FIG. 1. (Color online) Schematic diagram of the atom chip. A magnetic double-well potential was created by two chip wires with a current I_C in conjunction with an external magnetic field. The distance between the two chip wires was 300 μm. A pair of external wires with I_B provided the axial confinement along the y direction, and another pair of external wires with I_T were used for reducing the antisymmetry effect. (For details, see text.) Gravity was in the $+z$ direction.

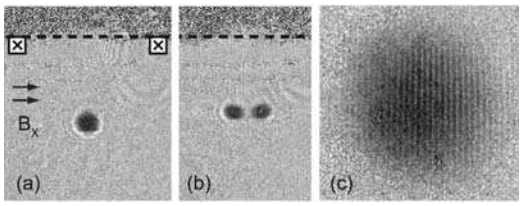

FIG. 2. Splitting of condensates. (a) Condensates were initially loaded and prepared in the bottom well and (b) split into two parts by increasing the external magnetic field, B_x. For clarity, two condensates were split by 80 μm. The dash line indicates the chip surface position. The currents in the chip wires flow into the page and B_x is parallel to the wire separation. Two condensates were released from the magnetic double-well potential and the matter wave interference pattern of two condensates formed after time-of-flight. (c) Typical absorption image of interference fringes taken after 22 ms time-of-flight. The fringe spacing was 14.8 μm, corresponding to a condensate separation of 25.8 μm.

more than 200 μm away from the chip wires to avoid deleterious surface effects [6–10]. The chip wires of 12 μm height and 50 μm width were electroplated with Au on a thermally oxidized Si substrate with a 2-μm-thick Au evaporated film. The chip was glued on an Al block for heat dissipation [20] and the current capacity was 5 A in a continuous mode.

The axial trapping potential was carefully designed to ensure that condensates split perpendicular to the axial direction and stay in the same axial position. The two wells have opposite responses to B_z: positive B_z makes the left (right) well move upward (downward). If B_z changes along the axial direction, the two wells are no longer parallel and the gravitational force would cause an axial displacement of the two split condensates. When endcap wires are placed only on the chip surface as in our previous work [21], a nonzero field gradient $\partial B_z/\partial y$ inevitably accompanies a field curvature $\partial^2 B_y/\partial y^2$ for the axial confinement, i.e., B_z changes from positive to negative along the axial direction. In order to provide the axial confinement and at the same time minimize $\partial B_z/\partial y$, we placed two pairs of external wires 1.5 mm above and 4 mm below the chip surface. This three-dimensional design of axial confinement was necessary for obtaining the interference signal of two split condensates. Moreover, maintaining the geometric symmetry of two wells will be crucial for longer coherence time after splitting [18].

The splitting process was demonstrated with the experimental procedures described in Fig. 2. Bose-Einstein condensates of $|F=1, m_F=-1\rangle$ ^{23}Na atoms were transferred and loaded in a magnetic trap generated by the atom chip [6,21,22]. Experimental parameters were $I_C=1.8$ A, $B_{x0}=24$ G, $B_y=1$ G, and the axial trap frequency $f_y=13$ Hz. Condensates were first loaded in the bottom well, 500 μm away from the chip surface, brought up to 30 μm below the merge point in 1 s, and held there for 2 s to damp out excitations. The long-living axial dipole excitation induced in the transfer phase was damped by applying a repulsive potential wall at the one end of the condensates with a blue-detuned laser beam (532 nm)[1]. The whole procedure was carried out with a radio-frequency (rf) shield and, just before splitting, condensates contained over 8.0×10^5 atoms without a discernible thermal population. Splitting was done by ramping $\Delta B_x = B_x - B_{x0}$ linearly from -140 mG to 100 ± 20 mG in 200 ms. The separation between two condensates was controlled by the final value of B_x. The magnetic trap was then quickly turned off within 20 μs, a duration much shorter than the inverse of any trap frequency, preventing random perturbations. High-contrast matter wave interference fringes were observed after releasing the condensates and letting them expand in time-of-flight (Fig. 2), indicating that the splitting procedure was smooth enough to produce two condensates having uniform phases along their long axial axis perpendicular to the splitting direction. In order to study the coherence of the splitting, the relative phase of the two split condensates was determined from the spatial phase of the matter wave interference pattern.

The relative phase of two split condensates turned out to be unpredictable when they were fully separated (Fig. 3). The separation of two condensates was determined from the spacing, λ_s, of the interference fringes, using the formula $d = ht/m\lambda_s$ where h is Planck's constant, m is atomic mass, and t is time-of-flight. The typical fringe spacing was $\lambda \approx 15$ μm with $t=22$ ms, corresponding to $d\approx26$ μm. Given the precise knowledge of the fabricated wires, the full trap parameters can be calculated. Assuming that the condensates followed trap centers in the motional ground state, it was found that when the barrier height was over 1.5 kHz, the

[1]In a perfectly symmetric double-well potential, two condensates would oscillate in phase after splitting. Furthermore, this could be used for developing a rotation-sensitive atom interferometer with a guiding potential. However, the axial trap frequencies for the two wells were found to be different by 12% due to the imperfect fabrication of wires.

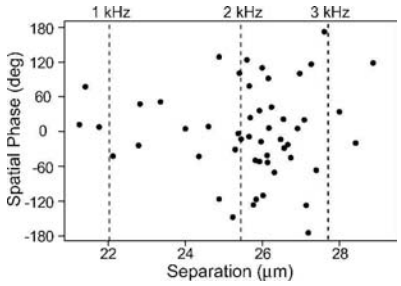

FIG. 3. Spatial phase of interference fringes. The separation of two condensates was determined from the spacing of interference fringes. Fifty repetitions of the same experiment are plotted, where the experimental control value for the external magnetic field, B_x, was fixed when the atoms were released. Three dash lines indicate the separations of two wells with the barrier height of 1 kHz, 2 kHz, and 3 kHz, respectively.

relative phase started to be random.[2] Since the chemical potential of the condensates, $\mu = 1.4 \pm 0.2$ kHz, was very close to this barrier height, the condensates just started to lose their coupling at this point.

Surprisingly, a phase singularity was observed in the interference patterns with high visibility. The fork shape of interference fringes represents a phase winding around a vortex core [23]. This vortex interference pattern appeared more frequently with faster splitting and further separation. An external perturbation can lead to internal excitations in condensates. Splitting might be considered as slicing condensates in two parts. The fact that the observed "forks" (Fig. 4) always open towards the top implies that the slicing always occurred in the same direction and created either vortices with positive charge on the left side or with negative charge on the right side. A possible vortex formation mechanism is topological imprinting when the zero point of the magnetic field crosses though condensates resulting in a doubly quantized vortex in spin-1 condensates [21,22]. However, since we have never observed the interference pattern of a doubly quantized vortex, we think that this scenario is unlikely.

We now discuss how the trapping potential changes during the splitting process (Fig. 5). When condensates split into two wells, the trap frequency, f_x, in the splitting direction vanishes and the separation of two wells abruptly increases to 15 μm with a small magnetic field change of $\delta B_x \approx 10$ mG. For a single particle in a harmonic potential, the quantity $\alpha \equiv (1/f_x^2)(\partial f_x/\partial B_x)(dB_x/dt)$ accounts for the transition probability from the ground state to the first excited state and parametrizes the external adiabaticity of the process, neglecting the collective excitations of a condensate. $\alpha \ll 1$ should be maintained to keep condensates staying in the motional ground state. With $dB_x/dt = 1.2$ G/s, $\alpha < 1$ at $f_x > 150$ Hz, but obviously, α diverges to infinity near the merge point and its definition no longer holds. Since the

[2]When the separation was less than 20 μm and two condensates were linked, the uncertainty of the spatial phase of fringes was less than 60°.

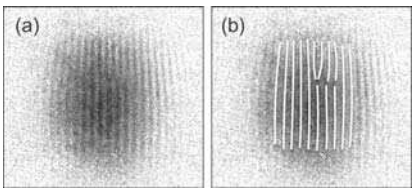

FIG. 4. Vortex interference. (a) An absorption image showing the vortex interference pattern of a vortex state. The probability of vortex generation was ~8% for the experimental parameters of Fig. 3, where data points with vortices were not included. Vortex interference patterns appeared more frequently with faster splitting and further separation. (b) Same as (a), but with lines indicating regions with constant phase.

energy level spacing diminishes, the adiabatic condition in the quartic potential around the merge point becomes more stringent. The abrupt change of trapping potential will induce mechanical perturbations of condensates. Subsequent dissipation or coupling into internal excitation modes [24] would make the relative phase of two split condensates unpredictable. The observed phase singularity definitely shows the breakdown of adiabaticity.

One possible alternative to avoid passing through the merge point is starting with two weakly linked condensates in a double-well potential where the barrier height is lower than the chemical potential of condensates and controlling the coupling between two condensates with a small change of the barrier height. This method was used to reduce the motional perturbation in our previous work [18]. However,

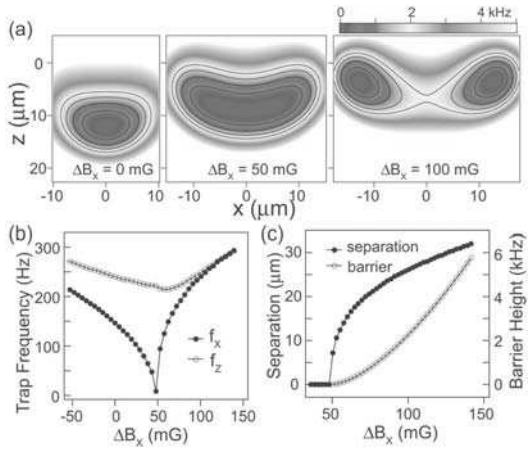

FIG. 5. (Color online) Trapping potential during splitting. (a) Radial cross sections of trapping potential including gravity for $\Delta B_x = 0$, 50, and 100 mG, where ΔB_x is the field deviation from the critical field magnitude B_{x0} which is the field magnitude for forming a single quartic trap. The origin of coordinates is the merge point without gravity. Contour lines correspond to 0.5, 1, 1.5, and 2 kHz above the bottom of the trap. (b) Trap frequencies in each direction. (c) Separation of two trap centers and barrier height between two wells.

since the sensitivity of the trapping potential to the magnetic field is extremely high when the trap centers are close to the merge point, it was technically difficult to have a stable double-well potential with a small barrier height. The lifetime of condensates measured around the merge point was >5 s away from the merge point ($\Delta B_x < -50$ mG or $\Delta B_x > 150$ mG) and <100 ms near the merge point ($0 < \Delta B_x < 100$ mG).[3] With a barrier height of 0.5 kHz in our experiment, the sensitivity of the barrier height and the condensate separation to B_x is 0.04 kHz/mG and 0.3 μm/mG, respectively. $\delta B_x = 1$ mG corresponds to $\delta I_C = 7.5 \times 10^{-5}$ A. Extreme current stabilization and shielding of ambient magnetic field fluctuations may be necessary for controlling a phase-coherent splitting process. Another alternative for preparing a coherent state of two spatially separated condensates is first preparing two condensates in the ground states in each well and then establishing a well-defined relative phase with an optical method [25]. This scheme is currently under investigation.

In conclusion, we have demonstrated the interference of two Bose-Einstein condensates released from an atom chip. The condensates were created by dynamical splitting of a single condensate and could be kept confined in a magnetic double-well potential, separated by an arbitrary distance. We studied the coherence of the dynamical splitting process by measuring the relative phase of two split condensates and identified technical limitations, intrinsic to the magnetic field geometry, that prevented coherent splitting with a predictable phase. This study is a promising step in the route towards atom chip interferometers and might serve as a guide for the design of future microfabricated atom optics devices.

This work was funded by ARO, NSF, ONR, DARPA, and NASA. C.S. acknowledges additional support from the Studienstiftung des deutschen Volkes, G.-B.J. from the Samsung Lee Kun Hee Scholarship Foundation, and M.S. from the Swiss National Science Foundation.

[3] For positions with $\Delta B_x > 0$ ("after" splitting), the condensates were moved to the left well without passing through the merge point.

[1] D. Müller, D. Z. Anderson, R. J. Grow, P. D. D. Schwindt, and E. A. Cornell, Phys. Rev. Lett. **83**, 5194 (1999).
[2] N. H. Dekker, C. S. Lee, V. Lorent, J. H. Thywissen, S. P. Smith, M. Drndić, R. M. Westervelt, and M. Prentiss, Phys. Rev. Lett. **84**, 1124 (2000).
[3] R. Folman, P. Krüger, D. Cassettari, B. Hessmo, T. Maier, and J. Schmiedmayer, Phys. Rev. Lett. **84**, 4749 (2000).
[4] H. Ott, J. Fortagh, G. Schlotterbeck, A. Grossmann, and C. Zimmermann, Phys. Rev. Lett. **87**, 230401 (2001).
[5] W. Hänsel, P. Hommelhoff, T. W. Hänsch, and J. Reichel, Nature (London) **413**, 498 (2001).
[6] A. E. Leanhardt, A. P. Chikkatur, D. Kielpinski, Y. Shin, T. L. Gustavson, W. Ketterle, and D. E. Pritchard, Phys. Rev. Lett. **89**, 040401 (2002).
[7] J. Fortágh, H. Ott, S. Kraft, A. Günther, and C. Zimmermann, Phys. Rev. A **66**, 041604(R) (2002).
[8] A. E. Leanhardt, Y. Shin, A. P. Chikkatur, D. Kielpinski, W. Ketterle, and D. E. Pritchard, Phys. Rev. Lett. **90**, 100404 (2003).
[9] M. P. A. Jones, C. J. Vale, D. Sahagun, B. V. Hall, and E. A. Hinds, Phys. Rev. Lett. **91**, 080401 (2003).
[10] J. Estève, C. Aussibal, T. Schumm, C. Figl, D. Mailly, I. Bouchoule, C. I. Westbrook, and A. Aspect, Phys. Rev. A **70**, 043629 (2004).
[11] Y.-J. Wang, D. Z. Anderson, V. M. Bright, E. A. Cornell, Q. Diot, T. Kishimoto, M. Prentiss, R. A. Saravanan, S. R. Segal, and S. Wu, Phys. Rev. Lett. **94**, 090405 (2005).
[12] P. J. Martin, B. G. Oldaker, A. H. Miklich, and D. E. Pritchard, Phys. Rev. Lett. **60**, 515 (1988).
[13] M. Olshanii and V. Dunjko, e-print cond-mat/0505358.
[14] J. Javanainen and M. Wilkens, Phys. Rev. Lett. **78**, 4675 (1997).
[15] A. J. Leggett and F. Sols, Phys. Rev. Lett. **81**, 1344 (1998).
[16] C. Menotti, J. R. Anglin, J. I. Cirac, and P. Zoller, Phys. Rev. A **63**, 023601 (2001).
[17] L. Pezzé, A. Smerzi, G. P. Berman, A. R. Bishop, and L. A. Collins, e-print cond-mat/0411567.
[18] Y. Shin, M. Saba, T. A. Pasquini, W. Ketterle, D. E. Pritchard, and A. E. Leanhardt, Phys. Rev. Lett. **92**, 050405 (2004).
[19] E. A. Hinds, C. J. Vale, and M. G. Boshier, Phys. Rev. Lett. **86**, 1462 (2001).
[20] S. Groth, P. Krüger, S. Wildermuth, R. Folman, T. Fernholz, J. Schmiedmayer, M. Mahalu, and I. Bar-Joseph, Appl. Phys. Lett. **85**, 2980 (2004).
[21] Y. Shin, M. Saba, M. Vengalattore, T. A. Pasquini, C. Sanner, A. E. Leanhardt, M. Prentiss, D. E. Pritchard, and W. Ketterle, Phys. Rev. Lett. **93**, 160406 (2004).
[22] A. E. Leanhardt, A. Görlitz, A. P. Chikkatur, D. Kielpinski, Y. Shin, D. E. Pritchard, and W. Ketterle, Phys. Rev. Lett. **89**, 190403 (2002).
[23] S. Inouye, S. Gupta, T. Rosenband, A. P. Chikkatur, A. Görlitz, T. L. Gustavson, A. E. Leanhardt, D. E. Pritchard, and W. Ketterle, Phys. Rev. Lett. **87**, 080402 (2001).
[24] H. Ott, J. Fortágh, S. Kraft, A. Günther, D. Komma, and C. Zimmermann, Phys. Rev. Lett. **91**, 040402 (2003).
[25] M. Saba, T. A. Pasquini, C. Sanner, Y. Shin, W. Ketterle, and D. E. Pritchard, Science **307**, 1945 (2005).

Appendix D

Light Scattering to Determine the Relative Phase of Two Bose-Einstein Condensates

This appendix contains a reprint of Ref. [11]: M. Saba, T.A. Pasquini, C. Sanner, Y. Shin, W. Ketterle, D.E. Pritchard, *Light Scattering to Determine the Relative Phase of Two Bose-Einstein Condensates*, Science **307**, 1945 (2005).

Light Scattering to Determine the Relative Phase of Two Bose-Einstein Condensates

M. Saba,* T. A. Pasquini, C. Sanner, Y. Shin, W. Ketterle, D. E. Pritchard

We demonstrated an experimental technique based on stimulated light scattering to continuously sample the relative phase of two spatially separated Bose-Einstein condensates of atoms. The phase measurement process created a relative phase between two condensates with no initial phase relation, read out the phase, and monitored the phase evolution. This technique was used to realize interferometry between two trapped Bose-Einstein condensates without need for splitting or recombining the atom cloud.

The outstanding property of atoms in a Bose-Einstein condensate (BEC) is their coherence: They all have the same phase. This property became apparent when high-contrast interference between condensates was observed (*1*–*3*). Phase coherence between spatially separated condensates has led to the observation of a host of phenomena, including Josephson oscillations (*3*, *4*), number squeezing (*5*), and the transition from superfluid to Mott insulator (*6*).

The evolution of the phase is affected by external potentials acting on the atoms and has

been exploited for interferometric measures of gravity and other interactions (*3*, *7*–*9*). Ideally, one could reach extreme interferometric sensitivity by coherently extracting atoms from two distant condensates and letting them interfere (*10*). So far, however, the relative phase of condensates has been measured only destructively, by taking an absorption image of interfering atomic waves.

Several methods have been considered to determine the relative phase of two separated atomic wavepackets spectroscopically by the scattering of light. In the simple case of a single atom delocalized in two separate wells, spontaneous photon scattering leaves the atom localized in one well, destroying the spatial coherence without giving any interferometric information (*11*, *12*). On the other hand, selecting the frequency of the scattered photons makes it possible to retrieve interference from specially prepared wavepackets, like two spatially separated components moving on parallel trajectories (*13*). BECs offer the possibility of scattering many photons out of the same coherent ensemble, affecting only a small fraction of the atoms in the condensates and providing an almost nondestructive measurement of the relative phase between the two condensates (*14*–*16*). Thus, light scattering could be used to compare the phase of two separate condensates at multiple subsequent times, realizing an interferometer with neither coherent splitting nor recombination of the wavepacket.

Even if the condensates are in states with poorly defined relative phase (such as the so-called Fock states, in which the atom number is well defined), they still interfere with each other. In this case, the relative phase is "created" in the measurement process by projecting the system on a coherent state with a well-defined phase (*17*–*21*).

We show that stimulated light scattering can be used to continuously sample the relative phase between two spatially separate BECs. The basis of our measurement is that the structure factor of two neighboring BECs shows interference fringes in momentum space (*21*). This interference can be pictured in a very direct way: Let us continuously impart some momentum $\vec{q}$ to a fraction of the atoms in each condensate, so that they move parallel to the displacement of the two condensates. When the atoms from the first condensate reach the second one, the two streams of atoms moving with momentum $\vec{q}$ will overlap and interfere. The process can be rephrased as beating of two atom lasers originating from the two condensates. If the relative phase of the condensates is fixed, the total number of moving atoms depends on the value of the momentum q and oscillates sinusoidally with periodicity h/d as q is scanned (h is Planck's constant and d is the displacement of the condensates). If instead the phase evolves in time and the momentum $\vec{q}$ is fixed, the number of atoms in the moving stream will vary in time at the same rate as the relative phase.

The experimental tool used to impart a precise momentum to atoms in a BEC is Bragg scattering (*22*, *23*). Two counterpropagating laser beams with wavevectors $\vec{k}_{1,2}$ hit the atoms so that, by absorbing a photon from one beam and reemitting it into the other one, the atoms acquire recoil momentum $\hbar(\vec{k}_2 - \vec{k}_1)$, provided that the energy difference between photons matches the atom recoil energy.

In our experiment (Fig. 1, A and B), two independent cigar-shaped BECs containing $\approx 10^6$ sodium atoms were prepared in a double-well optical dipole trap (*8*) and were

Department of Physics, MIT-Harvard Center for Ultracold Atoms, and Research Laboratory of Electronics, Massachusetts Institute of Technology, Cambridge, MA 02139, USA.

*To whom correspondence should be addressed. E-mail: msaba@mit.edu

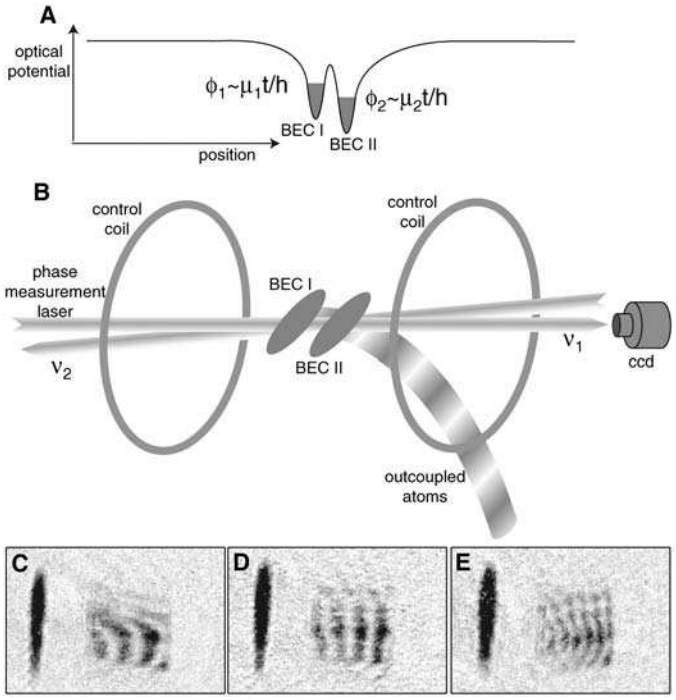

Fig. 1. Interference of two atom lasers coupled out from two independent condensates. (**A**) Energy diagram of the two BECs (BEC I and BEC II) confined in an optical double-well trap. (**B**) Experimental scheme for continuous phase measurement. Two laser beams were applied to the condensates to outcouple a few atoms from the trap. Detecting the rate of outcoupled atoms or the number of scattered photons gives a measurement of the relative phase between the condensates. The control coils generate magnetic field gradients that affect the frequency of interference oscillations. Gravity points down in this picture. (**C** to **E**) Absorption images showing the optical density of the atom clouds were taken from top after applying the Bragg beams (gravity points into the page). The thick shadows on the far left in each panel are the unresolved two condensates; to the right are the atoms that were continuously outcoupled and flew from left to right. High-contrast oscillations in the stream of outcoupled atoms are clearly visible. In the central picture (D), oscillations originated from the imbalance in the depth of the two wells. In (C), an additional magnetic field gradient of 1.15 G/cm was applied with the control coils; in (E), the gradient was −0.77 G/cm (with the positive direction pointing to the right). Images were taken after an additional 5 ms of time of flight, and the field of view in each picture is 1.35 mm × 0.90 mm.

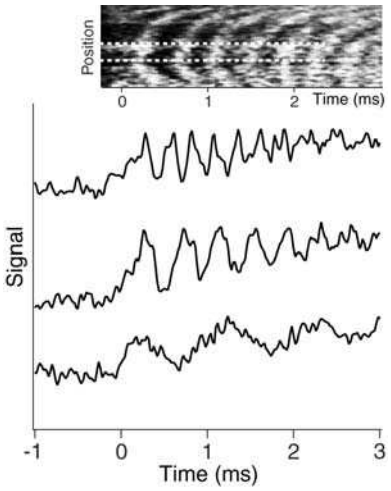

Fig. 2. Continuous optical readout of the relative phase of two condensates. In the upper panel is the optical signal image detected by streaking the CCD camera (*24*). The traces, offset vertically for clarity, are cross sections of the images (the central trace corresponds to the upper image integrated between the dashed lines). Bragg scattering starts at $t = 0$ when the second beam is turned on. The relative depth of the two wells was different for the three traces, generating a difference in the oscillation frequency. The overall slope on the traces was due to spontaneous Rayleigh scattering of the light from the atoms in the condensates. As the time went on, the condensates were depleted and the Rayleigh scattering was reduced. Excitations in the condensates appeared as tilted or curved fringes in the streak image; in such cases, we took cross sections from portions of the images where fringes were vertical and therefore the phase evolution was less perturbed.

illuminated with two counterpropagating Bragg beams to impart recoil momentum to a few atoms (*24*). The Bragg-scattered atoms flew away from the trap because the trap was shallower than the recoil energy. In the stream of outcoupled atoms (Fig. 1, C to E), the spatial modulations in the absorption images reflect temporal oscillations in the number of atoms outcoupled from the two condensates, implying a continuous evolution of the relative phase ϕ with time t at a rate $d\phi/dt = \Delta E/h$, caused by the energy offset ΔE between the condensates. The three images were taken with different magnetic field gradients applied with the control coils. The difference in magnetic field between the two wells modifed the energy offset ΔE and therefore affected the beat frequency $d\phi/dt$ of the two condensates. The fact that the fringes are not straight everywhere can be related to motional excitations in the condensates and the perturbing effect of the optical dipole potential on the time-of-flight trajectory of the atoms.

For each atom outcoupled from the condensate, a photon was transferred from one beam to the counterpropagating one. Therefore, all information contained in the stream of outcoupled atoms was also present in the scattered light and could be gathered in real time by monitoring the intensity of one of the Bragg laser beams, instead of interrupting the experiment to illuminate atoms with a resonant laser for absorption imaging. The dynamics of the optical signal was measured with a charge-coupled device (CCD) camera in streaking mode, generating images with time on one axis and spatial information on the other (Fig. 2) (*24*). The intensity of the Bragg beam oscillated in time at a frequency controlled by the relative energy between the two wells. The oscillating signal built up during the first $\approx$ 250 μs, this being the time required for the outcoupled atoms to travel from one condensate to the other one and start interference.

Interferometry between two trapped BECs was realized by continuous monitoring of their beat frequency. Figure 3 demonstrates the sensitivity of the interferometer to an applied external force (magnetic field gradient) and to the application of a potential difference between the two wells (dynamical Stark shift induced by increasing the laser power in one of the two wells).

We did not observe oscillation frequencies below 500 Hz. Short observation times and excitations could contribute to this, but there is a fundamental limitation to the minimum measurable frequency due to interactions between atoms. If the phase stays (almost) constant for a long time, one of the two condensates can end up continuously amplifying or deamplifying the atoms outcoupled from the other one, causing asymmetric depletion of the condensates and therefore a difference in chemical potential, as large as a few $h \times 100$ Hz in a few milliseconds under our experimental parameters. This is analogous to the inhibition of slow, large-amplitude Josephson oscillations in a nonlinear junction (*25*). If the relative phase is actively controlled, atoms can be coherently transferred from one well to the other, replenishing one of the two condensates without scrambling its phase; a method that could lead to a continuous atom laser (*26*).

The interferometric information contained in the beat frequency of two condensates is independent of the initial phase between the condensates and eliminates the need for coherent beam splitting (*10*). The present measurements already show a sensitivity below 100 Hz, limited by mechanical excitations that cause chirping of the frequency during the observation time and shot-to-shot variations. More fundamentally, the finite number of atoms in the condensates limits the number of Bragg-scattered photons and therefore the signal-to-noise ratio. No phase diffusion is expected during the measurement, the oscillations being continuously driven by the laser beams (*27*, *28*). This is a general manifestation of the influence of measurement on a quantum system (*29*), similar to the quantum Zeno effect, where the time evolution is suppressed by repeated or continuous measurements.

A more versatile interferometric scheme can be obtained by applying two successive Bragg pulses to the pair of condensates and exploiting the fact that the optical phase readout allows comparison of subsequent measurements on the same pair of condensates. A first Bragg pulse lasting 1 ms determined a randomly varying relative phase between the two condensates at each realization of the experiment (Fig. 4B). A second Bragg pulse followed after allowing the two condensates to evolve for some delay (0.5 ms) and measured a relative phase again random at each shot

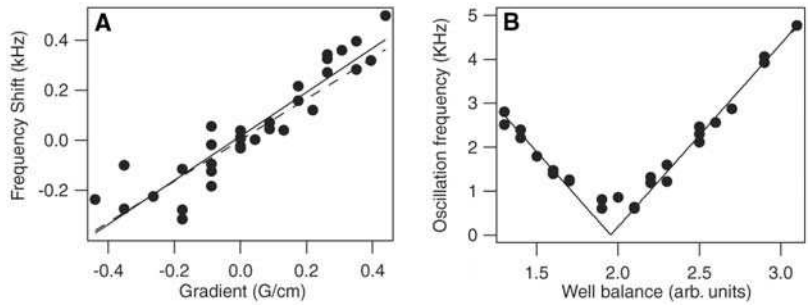

Fig. 3. Interferometry with two trapped BECs. (**A**) The two well depths were prepared offset by $\approx$ 0.53 kHz in the absence of magnetic field gradients, and the shift of the beat frequency with respect to this initial value is plotted versus the applied magnetic field gradient. The beat frequency is determined from pictures similar to those in Fig. 2. The solid line is a linear fit to the data; the dashed line represents the frequency $\mu_B B' d/2h$ expected for the evolution of the relative phase of the two condensates due to the difference in energy induced by the gradient (B' is the independently measured magnetic gradient, μ_B is half Bohr magneton corresponding to the magnetic moment of the atoms, and d is the displacement of the two condensates). (**B**) Beat frequency measured in the optical signal is shown as a function of the relative depth of the two potential wells. The well balance parameter is proportional to the difference in optical power used to create each of those wells and was controlled by the power in each of the two radio frequencies fed into the acousto-optical modulator. arb., arbitrary.

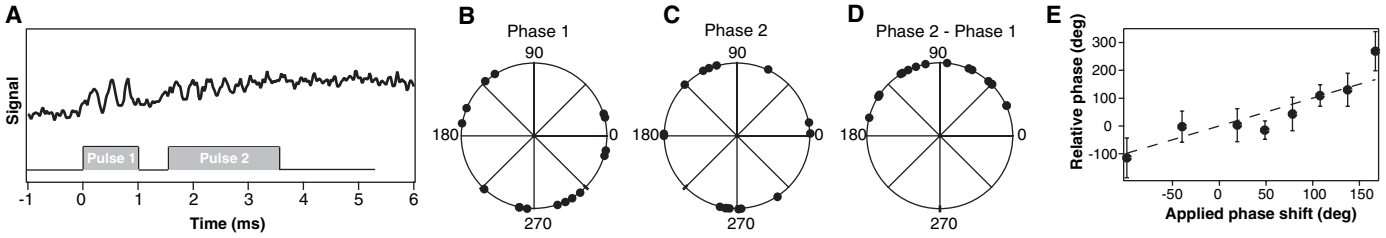

Fig. 4. Preparing a relative phase between two independent BECs with no initial phase relation. (**A**) The temporal trace of the Bragg beam intensity shown with the pulse sequence. (**B**) Phase of the oscillations recorded during the first pulse. (**C**) Phase during the second pulse. (**D**) Phase difference between (B) and (C). (**E**) Phase difference between the oscillations in two pulses as a function of the phase shift applied during the evolution time between pulses. Each point is the average of several shots (between 3 and 10).

(Fig. 4C). Comparison with the phase measured in the first pulse shows that the two measurements were correlated (Fig. 4D). In other words, the first measurement established a definite relative phase between the two condensates that may not have had a defined phase before, and the second measurement verified that the condensates evolved with that particular phase during the interval between pulses.

Interferometry was demonstrated by putting an interaction time between the two pulses and changing the outcome of the second measurement. We briefly modified the energy offset between the two wells during the interval between the pulses, when the phase was not being observed. Figure 4E compares the measured phase shift with the value $\Delta E \Delta t/h$ expected from an energy offset ΔE applied for a time Δt. The agreement between the prediction and the measurement demonstrates that the relative phase can be engineered by applying external forces to the atoms.

Active control of the phase opens interesting future perspectives: One could measure the light signal in real time and feed back the phase measurement into the control coils (or into the acousto-optical modulator that controls the two laser powers, creating the double-well potential), preparing the desired phase at the desired time. In principle, the uncertainty in the relative phase could even be squeezed by the feedback, allowing sub–shot noise interferometry (*5*, *10*, *30*).

Several physical interpretations of the experiment are possible besides the interference of two atom lasers. One is interference in momentum space (*21*): The zero-momentum component of the momentum distribution of the double condensate depends sinusoidally on the relative phase of the condensates and is probed with Doppler-sensitive spectroscopy (realized by Bragg scattering). Yet another point of view is that light scattering probes the excitation spectrum through the dynamical structure factor. The structure factor is phase-sensitive and shows interference fringes without requiring spatial overlap between the two condensates, as long as the excited states (after light scattering) have spatial overlap. This picture emphasizes that overlap between scattered atoms, as well as scattered photons, is crucial to our method: No phase information can be retrieved from two atomic wavepackets that scatter the same light but whose excited states are disconnected, like two condensates separated by a transparent glass wall.

The concept of beating atom lasers was previously exploited to measure spatial coherence in a single condensate (*31*) and for experiments done in optical lattices, where atoms outcoupled from a large vertical array of regularly spaced condensates interfered and their beating frequency measured gravity (*3*, *10*). In this case, condensates were split coherently by raising the optical lattice potential. Coupling was established by tunneling of atoms between adjacent lattice sites and depended exponentially on the barrier shape, whereas the laser beams in our scheme established a coupling through a state delocalized over the barrier. In principle, larger barriers could be overcome by imparting larger momenta in the Bragg process. From the standpoint of precision interferometry, optical lattices have the advantage of a very well-known and controlled displacement between condensates, whereas the optical detection that we introduce here measures the beat frequency continuously and in real time, with accuracy not depending on the calibration of image magnification (*3*) or other disturbances affecting atoms during time of flight.

Our scheme to nondestructively measure the beat frequency of two previously independent condensates, thus establishing phase coherence, could permit us to couple condensates displaced by tens of microns on atom chips or in other microtraps, to explore Josephson oscillations, phase diffusion, and self-trapping. We have already demonstrated its potential in exploiting the phase coherence of BECs to create a novel type of atom interferometer.

References and Notes

1. M. R. Andrews *et al.*, *Science* **275**, 637 (1997).
2. D. S. Hall, M. R. Matthews, C. E. Wieman, E. A. Cornell, *Phys. Rev. Lett.* **81**, 1543 (1998).
3. B. P. Anderson, M. A. Kasevich, *Science* **282**, 1686 (1998).
4. F. S. Cataliotti *et al.*, *Science* **293**, 843 (2001).
5. C. Orzel, A. K. Tuchman, M. L. Fenselau, M. Yasuda, M. A. Kasevich, *Science* **291**, 2386 (2001).
6. M. Greiner, O. Mandel, T. Esslinger, T. W. Hänsch, I. Bloch, *Nature* **415**, 39 (2002).
7. S. Gupta, K. Dieckmann, Z. Hadzibabic, D. E. Pritchard, *Phys. Rev. Lett.* **89**, 140401 (2002).
8. Y. Shin *et al.*, *Phys. Rev. Lett.* **92**, 050405 (2004).
9. Y. J. Wang *et al.*, preprint available at http://www.arxiv.org/abs/cond-mat/0407689 (2004).
10. M. A. Kasevich, *CR Acad. Sci. IV* **2**, 497 (2001).
11. C. CohenTannoudji, F. Bardou, A. Aspect, in *Laser Spectroscopy X*, M. Ducloy, E. Giacobino, Eds. (World Scientific, Singapore, 1992), p. 3.
12. K. Rzążewski, W. Żakovicz, *J. Phys. B* **25**, L319 (1992).
13. B. Dubetsky, P. R. Berman, *J. Mod. Opt.* **49**, 55 (2002).
14. J. Javanainen, *Phys. Rev. A* **54**, 4629(*R*) (1996).
15. A. Imamoglu, T. A. B. Kennedy, *Phys. Rev. A* **55**, 849(*R*) (1997).
16. J. Ruostekoski, D. F. Walls, *Phys. Rev. A* **56**, 2996 (1997).
17. J. Javanainen, S. M. Yoo, *Phys. Rev. Lett.* **76**, 161 (1996).
18. M. Naraschewski, H. Wallis, A. Schenzle, J. I. Cirac, P. Zoller, *Phys. Rev. A* **54**, 2185 (1996).
19. J. I. Cirac, C. W. Gardiner, M. Naraschewski, P. Zoller, *Phys. Rev. A* **54**, 3714(*R*) (1996).
20. Y. Castin, J. Dalibard, *Phys. Rev. A* **55**, 4330 (1997).
21. L. Pitaevskii, S. Stringari, *Phys. Rev. Lett.* **83**, 4237 (1999).
22. M. Kozuma *et al.*, *Phys. Rev. Lett.* **82**, 871 (1999).
23. J. Stenger *et al.*, *Phys. Rev. Lett.* **82**, 4569 (1999).
24. Information on materials and methods is available on *Science* Online.
25. A. Smerzi, S. Fantoni, S. Giovanazzi, S. R. Shenoy, *Phys. Rev. Lett.* **79**, 4950 (1997).
26. A. P. Chikkatur *et al.*, *Science* **296**, 2193 (2002).
27. M. Lewenstein, L. You, *Phys. Rev. Lett.* **77**, 3489 (1996).
28. J. Javanainen, M. Wilkens, *Phys. Rev. Lett.* **78**, 4675 (1997).
29. J. A. Wheeler, W. H. Zurek, *Quantum Theory and Measurement* (Princeton Univ. Press, Princeton, NJ, 1983).
30. J. M. Geremia, J. K. Stockton, H. Mabuchi, *Science* **304**, 270 (2004).
31. I. Bloch, T. W. Hansch, T. Esslinger, *Nature* **403**, 166 (2000).

32. This work was funded by the Army Research Office, the Defense Advanced Research Projects Agency, NSF, the Office of Naval Research, and NASA. M.S. acknowledges additional support from the Swiss National Science Foundation and C.S. from the Studienstiftung des deutschen Volkes. We thank G. Jo for experimental assistance, A. Schirotzek for contributions in the early stage of the work, and M. Zwierlein for a critical reading of the manuscript. We are indebted to A. Leanhardt for stimulating suggestions that initiated this research and insightful comments on the experiment and the manuscript.

Supporting Online Material

www.sciencemag.org/cgi/content/full/307/5717/1945/DC1

Materials and Methods

16 December 2004; accepted 3 February 2005

10.1126/science.1108801

Appendix E

Optical Weak Link between Two Spatially Separated Bose-Einstein Condensates

This appendix contains a reprint of Ref. [5]: Y. Shin, G.-B. Jo, M. Saba, T.A. Pasquini, W. Ketterle, D.E. Pritchard, *Optical Weak Link between Two Spatially Separated Bose-Einstein Condensates*, Physical Review Letters **95**, 170402 (2005).

Optical Weak Link between Two Spatially Separated Bose-Einstein Condensates

Y. Shin, G.-B. Jo, M. Saba, T. A. Pasquini, W. Ketterle, and D. E. Pritchard*

Department of Physics, MIT-Harvard Center for Ultracold Atoms, and Research Laboratory of Electronics, Massachusetts Institute of Technology, Cambridge, Massachusetts, 02139, USA

(Received 6 July 2005; published 17 October 2005)

Two spatially separate Bose-Einstein condensates were prepared in an optical double-well potential. A bidirectional coupling between the two condensates was established by two pairs of Bragg beams which continuously outcoupled atoms in opposite directions. The atomic currents induced by the optical coupling depend on the relative phase of the two condensates and on an additional controllable coupling phase. This was observed through symmetric and antisymmetric correlations between the two outcoupled atom fluxes. A Josephson optical coupling of two condensates in a ring geometry is proposed. The continuous outcoupling method was used to monitor slow relative motions of two elongated condensates and characterize the trapping potential.

DOI: 10.1103/PhysRevLett.95.170402 PACS numbers: 03.75.Lm, 03.75.Pp, 74.50.+r

Josephson effects [1] are quantum phenomena in which the current between two weakly coupled, macroscopic quantum systems depends on the relative phase of the two systems. These effects are direct evidence for the existence of the phase of a macroscopic quantum system [2] and observed in quantum systems such as superconductors [3], superfluid ^{3}He [4], and Bose condensed gases [5,6]. Josephson coupling between two systems is typically established via tunneling through a separating potential barrier or via an external driving field as in the internal Josephson effect [7,8]. Both couplings require spatial overlap of the two systems due to the intrinsic locality of the coupling interactions.

The concept of Josephson coupling can be extended to include two *spatially separate* quantum systems by using intermediate coupling systems. If the phase relations among these systems are preserved and thus the net particle exchange is phase sensitive, the two spatially separate systems might be regarded as being effectively Josephson coupled via the intermediate systems. Furthermore, the phase of the coupling may be actively controlled by adjusting the coupling states of the intermediate systems. This idea has been theoretically introduced in the context of relative phase measurement [9].

In this Letter, we experimentally demonstrate phase-sensitive optical coupling of two spatially separate Bose-Einstein condensates using Bragg scattering. The situation we are investigating is two condensates, irradiated by two pairs of Bragg beams [Fig. 1(a)]. The two pairs of Bragg beams couple out beams of atoms propagating to the left or the right, respectively, and these unconfined propagating atoms constitute the intermediate coupling system in our scheme. Depending on the relative phases of the two condensates and the coupling states, we observe only one outcoupled beam propagating to one or the other side, or two identical beams propagating in opposite directions (Fig. 2). This demonstrates phase control of currents and establishes a new scheme to realize Josephson effects with two nonoverlapping condensates. In the following, we present a model for the phase-sensitive outcoupling process and an experimental test of the prediction that the phase of the atomic currents into each condensate can be controlled. Finally, we suggest a Josephson optical coupling of two condensates in a ring geometry.

First, we elaborate on the situation with a unidirectional optical coupling [Fig. 1(b)]. We use the conventional wave function description for condensates. Two condensates 1 and 2 are trapped in a double-well potential and optically coupled into unconfined states by a single pair of Bragg beams. Ignoring the accumulated phase shifts due to the interaction with the condensates, we approximate the unconfined coupling states as truncated free propagating states, i.e., $\psi_i(x,t) \propto \Theta(x - x_i)\sqrt{\gamma N_i}e^{i\chi_i(x,t)}$ $(i = 1, 2)$, where $\Theta(x)$ is the Heaviside step function, γ is the outcoupling efficiency of the Bragg beams, N_i is the total atom

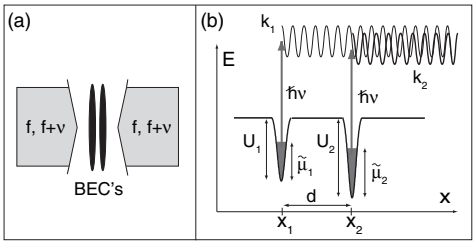

FIG. 1. Optical coupling between two separate condensates. (a) Bidirectional coupling. Two pairs of Bragg beams with frequencies f and $f + \nu$ are applied to two separate condensates. (b) Outcoupling process. Two condensates are trapped at $x = x_1$ and x_2 $(d = x_2 - x_1)$. A pair of Bragg beams with frequency difference ν generate a continuous atomic beam from each condensate. The two atomic beams overlap in $x > x_2$, forming a matter wave interference pattern. U_1 (U_2) denotes the trap depth of the left (right) well, $\tilde{\mu_1}$ $(\tilde{\mu_2})$ the mean-field interaction energy of the left (right) condensate, and k_1 (k_2) the wave number of the atomic beam from the left (right) condensate outside the trap.

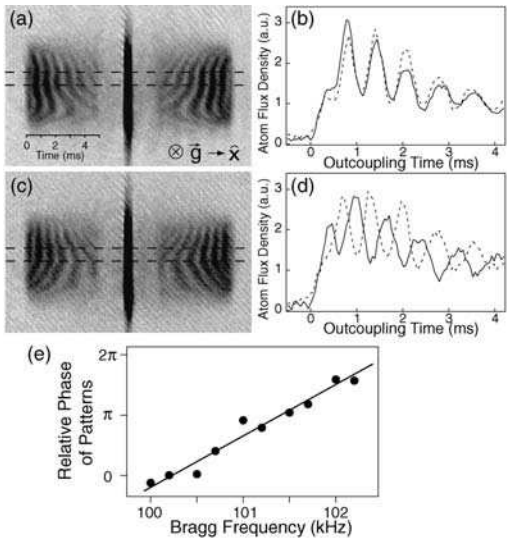

FIG. 2. Symmetric and antisymmetric correlation between outcoupled atom patterns. Two pairs of Bragg beams [Fig. 1(a)] outcoupled atoms in either $+x$ or $-x$ direction. Absorption images were taken after 5 ms outcoupling and 2 ms additional ballistic expansion. The left outcoupled atom patterns were compared with the corresponding right patterns. Symmetric correlation between two patterns was observed at (a) $\nu = 2\pi \times$ 100.5 kHz and (c) antisymmetric at $\nu = 2\pi \times 101.5$ kHz. The field of view is 900 μm $\times$ 590 μm. (b), (d) Outcoupled atom flux densities were obtained by integrating optical densities between the dashed lines and converting the spatial coordinate to the time coordinate. The solid (dashed) lines correspond to left (right) outcoupled atoms. (e) The coupling phase θ of the two outcoupled patterns showed a linear dependence on ν with $\partial\theta/\partial\nu = (2.4\ \text{kHz})^{-1}$.

number of condensate i, and $\chi_i(x, t) = k_i x - \omega_i t + \chi_{i0}$ is the phase of the coupling state with $\hbar\omega_i = \frac{\hbar^2 k_i^2}{2m}$, where m is atomic mass. The phase continuity at the coupling position $x = x_i$ requires

$$\chi_i(x_i, t) = \phi_i(t) + \phi_B(x_i, t) - \pi/2, \tag{1}$$

where $\phi_i(t)$ is the phase of the condensate, $\phi_B(x, t) = 2k_r x - \nu t + \phi_{B0}$ is the phase of the Bragg beams with wave number k_r and frequency difference ν, and $-\pi/2$ is the phase shift attributed to the scattering process [10]. In a linear regime with $\gamma \ll 1$, ϕ_i is not perturbed by the coupling, i.e., $\phi_i(t) = -\frac{\mu_i}{\hbar} t + \phi_{i0}$, where $\hbar$ is Planck's constant divided by 2π and $\mu_i = -U_i + \tilde{\mu}_i$ [Fig. 1(b)] is the chemical potential of the condensate. Satisfying the phase relation Eq. (1) at all t requires

$$\hbar\omega_i = \hbar\nu + \mu_i, \tag{2}$$

$$\chi_{i0} = -\delta k_i x_i + \phi_{B0} + \phi_{i0} - \pi/2, \tag{3}$$

where $\delta k_i = k_i - 2k_r$. Equation (2), the temporal part in Eq. (1), corresponds to energy conservation.

In the overlapping region, $x > x_2$, the two atomic beams from each condensate form a matter wave interference pattern, and the outcoupled atom density $n(x, t) = |\psi_1(x, t) + \psi_2(x, t)|^2$. For a better interpretation, we define the right outcoupled atom density $n_R(s, t) \equiv n(s + x_2, t)$, where s indicates the distance from the right condensate,

$$n_R(s, t) = \frac{\gamma}{2v_r}\left(N_t + 2\sqrt{N_1 N_2}\cos[\Delta k s + \phi_r(t) - \delta k_1 d]\right), \tag{4}$$

where $N_t = N_1 + N_2$, $\Delta k = k_2 - k_1$, $d = x_2 - x_1$, and $\phi_r(t) = \phi_2(t) - \phi_1(t)$. We approximate the propagating velocity $v_i = \frac{\hbar k_i}{2m} \simeq 2v_r$ with $\delta k_i \ll 2k_r$, where $v_r = \frac{\hbar k_r}{m}$ is the recoil velocity. According to the relative phase ϕ_r, outcoupled atoms from the left condensate are coupled into or amplified by the right condensate. The spatial and temporal modulation of the outcoupled atom flux n_R represents the evolution of the relative phase ϕ_r, which was directly demonstrated in our previous experiments [11].

The phase term $-\delta k_1 d$ can be interpreted as the phase shift which outcoupled atoms would accumulate during the flight from the left condensate to the right with respect to the Bragg beam phase ϕ_B which is acting as the phase reference. A similar relation between n_R and ϕ_r can be obtained in terms of the dynamic structure factor of 2 separate condensates [12], but the phase modulation of coupling states in the middle of two condensates is likely to be ignored in the conventional impulse approximation [13]. This phase shift is the key element for an actively controlled optical coupling and its physical importance will be manifest in the following bidirectional coupling scheme.

We now add another pair of Bragg beams to outcouple atoms in the $-x$ direction. Modifying the above calculation by $k_{i,r} \rightarrow -k_{i,r}$, the left outcoupled atom density $n_L(s, t) \equiv n(x_1 - s)$ is given as

$$n_L(s, t) = \frac{\gamma}{2v_r}\left(N_t + 2\sqrt{N_1 N_2}\cos[\Delta k s + \phi_r(t) + \delta k_2 d]\right). \tag{5}$$

Considering the atom flux for each condensate, we find rate equations for N_1 and N_2. For example, the left condensate has influx of γN_2 from the right condensate and outflux of γN_1 and $n_L(0, t)$ in $+x$ and $-x$ direction, respectively. The final rate equations read

$$\dot{N}_{1,2} = -2\gamma\left(N_{1,2} + \sqrt{N_1 N_2}\cos[\phi_r(t) \mp \delta k_{1,2} d]\right). \tag{6}$$

Except for the global depletion effect of Bragg scattering, the rate equations describe Josephson oscillations due to the bidirectional optical coupling, i.e., that the atomic currents into the condensates depend on the relative phase.

The optical Josephson coupling has a unique feature in the control of the phase accumulated by atoms in the

coupling state [9]. Since the intermediate system "delivers" the phase information from one condensate to the other, the phase can be manipulated in transit and consequently, the phase of the effective coupling can be controlled without affecting the two condensates. In the bidirectional coupling scheme, the control of the coupling phase is embodied in the phase shift terms, $-\delta k_1 d$ and $\delta k_2 d$. We define the coupling phase as $\theta \equiv (\delta k_1 + \delta k_2)d$, and with $\delta k_i \ll 2k_r$, approximate θ as

$$\theta = \frac{d}{v_r}\left(\nu - \frac{4E_r}{\hbar} + \frac{\mu_1 + \mu_2}{2\hbar}\right), \tag{7}$$

where $E_r = \frac{\hbar^2 k_r^2}{2m}$ is the recoil energy. θ is equivalent to the relative phase of n_L and n_R. When $\theta = 0\,(\theta = \pi)\ (\mathrm{mod}\, 2\pi)$, n_L and n_R will show (anti)symmetric correlation.

The control of the coupling phase θ was experimentally demonstrated. Condensates of ^{23}Na atoms in the $|F = 1, m_F = -1\rangle$ state were prepared in an optical double-well potential as described in Ref. [14]. The $1/e^2$-intensity radius of a focused laser beam for a single well was 7.6 μm and the typical trap depth was $U_{1,2} \sim h \times 18$ kHz. The separation of the two wells was $d = 11.4$ μm and each well started with a condensate of $\sim 5 \times 10^5$ atoms. Two pairs of Bragg beams parallel to the separation direction were applied to the condensates by retroreflecting two copropagating laser beams with frequency difference ν. The lifetime of condensates was over 18 s. The $1/e$ depletion time due to Bragg scattering into both directions was 4.5 ms, resulting in the magnitude of initial atom currents $\sim 1.1 \times 10^8$ atoms/s. Outcoupling patterns were measured by taking absorption images of outcoupled atoms.

When the Bragg frequency difference ν was varied, the outcoupling pattern cycled through symmetric and antisymmetric correlations (Fig. 2). The coupling phase θ was fit to the observed patterns for each Bragg frequency [Fig. 2(e)]. The linear dependence was measured as $\partial\theta/\partial\nu = (2.4 \pm 0.2\ \mathrm{kHz})^{-1}$, which is consistent with the predicted value $d/v_r = (2.6\ \mathrm{kHz})^{-1}$. This clearly demonstrates the presence and control of the coupling phase in our optical coupling scheme. With the antisymmetric condition, $\theta = \pi$, as a function of the propagating relative phase, the output oscillated between predominantly to the left and predominantly to the right [Figs. 2(c) and 2(d)]. The experimental situation has perfect mirror symmetry. Unidirectional output in a symmetric situation is a macroscopic consequence of the condensates' phase.

Control of the coupling phase can be used to introduce temporal and spatial variations of Josephson-type coupling. Temporal control with real-time feedback could ensure the coherent and continuous replenishment of a condensate [see Ref. [15]]. For elongated condensates, as used here, spatial control with barrier heights or well separations could create spatially varying coupling along the condensate axis, and realize, e.g., ring currents.

One limitation of the bidirectional coupling scheme is that atoms are depleted out of the system due to the linear geometry. Even though the pattern of outcoupled atoms is a crucial signal for monitoring the coupling dynamics, the coupling time is fundamentally limited. To overcome this shortcoming, we envisage a system preserving total atom number like in Fig. 3, where atoms circulate between two condensates in a ring waveguide. With assumptions that the traveling time δt for atoms from one condensate to the other is short enough to satisfy $\dot{\phi}_r \delta t \ll 1$ and that the density profiles are constant over the trajectories between the two condensates, the governing equation, in a linear regime, is

$$\dot{N}_2 - \dot{N}_1 = 2\gamma\sqrt{N_1 N_2}\cos(\phi_r - \phi_m), \tag{8}$$

where ϕ_m is the effective coupling phase which is determined by the accumulated phase shift over the round trajectories and the phase of the Bragg beams.

The long condensates used here introduce a new degree of freedom into the usual pointlike Josephson junctions: the condensates can have a spatially varying phase along the axial direction. Since the optical coupling is selectively established between condensates at the same axial position, axial gradients of the relative phase are directly observed through tilted fringes in the pattern of outcoupled atoms. In Fig. 4, we present two examples showing the effects of relative dipole and quadruple axial motions of two condensates. Josephson vortex [16] and modulational instabilities [17] in elongated coupled condensates were theoretically suggested.

Continuous Bragg scattering was used to characterize the trap depth and the trap frequency of a single optical trap (Fig. 5). Since momentum and energy imparted in the scattering process are precisely defined, the kinetic energy of atoms coupled out of a trap determines the depth of the trap. We measured the traveling distance D of outcoupled atoms with fixed traveling time t, and determined the trap depth U from the relation, $D/t = \sqrt{4v_r^2 - 2U/m}$, ignoring the mean-field interaction with the condensate and the finite size of the trap. Additionally, the exact knowledge

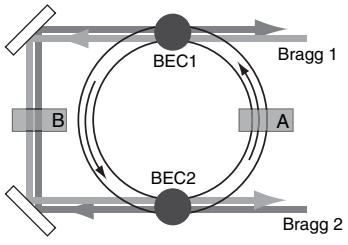

FIG. 3. Optical coupling of two condensates on a ring. Two condensates are confined at opposite sides on a ring-shaped waveguide and a pair of Bragg beams (Bragg 1 and 2) outcouple atoms in the clockwise direction. The shaded boxes A and B are phase modulators for atoms and photons, respectively.

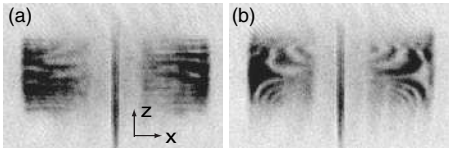

FIG. 4. Monitoring of slow relative axial motions. Two chemical potentials were equalized within 400 Hz and the temporal evolution of the relative phase of two condensates along the axial (z) direction was recorded in the outcoupled atom patterns. (a) represents relative dipole oscillation, corresponding to relative velocity ≈ 300 μm/s or kinetic energy of ≈ 130 pK $\times k_B$, and (b) relative quadruple oscillation. k_B is the Boltzmann constant.

of the recoil velocity v_r calibrates the optical magnification of images.

On the other hand, the trap frequency was measured using velocity sensitivity of Bragg scattering. When a condensate oscillates in a trap, atoms are coupled out only when the condensate is at the resonant velocity. Since the dipole oscillation of a condensate in a harmonic trap is the same as the trap frequency f, the outcoupling frequency is the same as f when Bragg beams are tuned at the maximum velocity [Fig. 5(b)], $2f$ at zero velocity [Fig. 5(c)]. Even though the frequency resolution is limited by the finite coupling time, this method provides a lot of information in a single measurement. For example, the pattern of outcoupled atoms in Fig. 5(b) is curved because the trap frequency changes along the axial direction.

The system studied here is perfectly symmetric. Nevertheless, in any realization of the experiment, the relative phase of the two condensates assumes a specific value and spontaneously breaks the symmetry. The unidirectional output is equivalent to the magnetization in a ferromagnet, which, by spontaneous symmetry breaking, points into a specific direction. Spontaneous symmetry breaking can be observed in the interference pattern of two overlapping condensates which has a definite phase [18]. Unidirectional output in a symmetric situation more dramatically shows the existence of the condensates' phase.

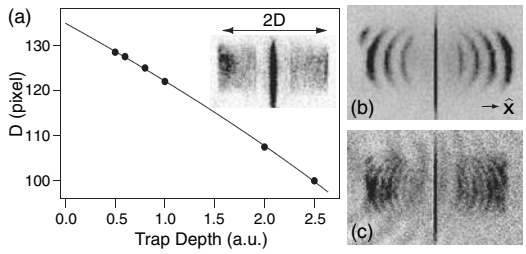

FIG. 5. Trap characterization by continuous outcoupling. (a) Atoms were outcoupled from a single well and the traveling distance D with fixed traveling time $t = 7$ ms was measured, changing the trap depth U by varying the total power of the laser beam forming the single well. The solid line is a fitting curve (see the text for details) with 1 a.u. $= 18.0$ kHz and 1 pixel $= 3.11$ μm. Dipole oscillation in the x direction was induced by suddenly shifting the trap center. (b) Outcoupling pattern with Bragg frequency difference $\nu = 2\pi \times 114$ kHz and (c) $\nu = 2\pi \times 101.5$ kHz, which correspond to resonant velocities of ≈ 4 mm/s and ≈ 0 mm/s, respectively. In (b), the left and the right pattern have antisymmetric correlation.

In conclusion, we experimentally studied the optical coupling between two spatially separate condensates using bidirectional Bragg scattering and demonstrated that the phase of the coupling currents can be controlled. This scheme is a new approach for observing Josephson phenomena, but also for monitoring condensate motion and characterizing trapping potentials.

This work was funded by NSF, ONR, DARPA, ARO, and NASA. G.-B. J. acknowledges additional support from the Samsung Lee Kun Hee Foundation, and M. S. from the Swiss National Science Foundation.

*URL: http://cua.mit.edu/ketterle_group/

[1] B. D. Josephson, Phys. Lett. **1**, 251 (1962).
[2] P. W. Anderson, in *Lectures on The Many-Body Problem*, edited by E. R. Caianiello (Academic, New York, 1964), Vol. 2, pp. 113–135.
[3] P. W. Anderson and J. W. Rowell, Phys. Rev. Lett. **10**, 230 (1963).
[4] S. V. Pereverzev, A. Loshak, S. Backhaus, J. C. Davis, and R. E. Packard, Nature (London) **388**, 449 (1997).
[5] F. S. Cataliotti, S. Burger, C. Fort, P. Maddaloni, F. Minardi, A. Trombettoni, A. Smerzi, and M. Inguscio, Science **293**, 843 (2001).
[6] M. Albiez, R. Gati, J. Fölling, S. Hunsmann, M. Cristiani, and M. K. Oberthaler, Phys. Rev. Lett. **95**, 010402 (2005).
[7] J. Williams, R. Walser, J. Cooper, E. Cornell, and M. Holland, Phys. Rev. A **59**, R31 (1999).
[8] P. Öhberg and S. Stenholm, Phys. Rev. A **59**, 3890 (1999).
[9] A. Imamoglu and T. A. B. Kennedy, Phys. Rev. A **55**, R849 (1997).
[10] J. M. Vogels, J. K. Chin, and W. Ketterle, Phys. Rev. Lett. **90**, 030403 (2003).
[11] M. Saba, T. A. Pasquini, C. Sanner, Y. Shin, W. Ketterle, and D. E. Pritchard, Science **307**, 1945 (2005).
[12] L. Pitaevskii and S. Stringari, Phys. Rev. Lett. **83**, 4237 (1999).
[13] F. Zambelli, L. Pitaevskii, D. M. Stamper-Kurn, and S. Stringari, Phys. Rev. A **61**, 063608 (2000).
[14] Y. Shin, M. Saba, T. A. Pasquini, W. Ketterle, D. E. Pritchard, and A. E. Leanhardt, Phys. Rev. Lett. **92**, 050405 (2004).
[15] A. P. Chikkatur, Y. Shin, A. E. Leanhardt, D. Kielpinski, E. Tsikata, T. L. Gustavson, D. E. Pritchard, and W. Ketterle, Science **296**, 2193 (2002).
[16] V. M. Kaurov and A. B. Kuklov, Phys. Rev. A **71**, 011601(R) (2005).
[17] I. Bouchoule, physics/0502050.
[18] M. R. Andrews, C. G. Townsend, H.-J. Miesner, D. S. Durfee, D. M. Kurn, and W. Ketterle, Science **275**, 637 (1997).

Appendix F

Distillation of Bose-Einstein Condensates in a Double-Well Potential

This appendix contains a reprint of Ref. [2]: Y. Shin, M. Saba, A. Schirotzek, T.A. Pasquini, A.E. Leanhardt, D.E. Pritchard, W. Ketterle, *Distillation of Bose-Einstein Condensates in a Double-Well Potential*, Physical Review Letters **92**, 150401 (2004).

Distillation of Bose-Einstein Condensates in a Double-Well Potential

Y. Shin, M. Saba, A. Schirotzek, T. A. Pasquini, A. E. Leanhardt, D. E. Pritchard, and W. Ketterle*
Department of Physics, MIT-Harvard Center for Ultracold Atoms,
and Research Laboratory of Electronics, Massachusetts Institute of Technology, Cambridge, Massachusetts 02139, USA
(Received 21 November 2003; published 13 April 2004)

Bose-Einstein condensates of sodium atoms, prepared in an optical dipole trap, were distilled into a second empty dipole trap adjacent to the first one. The distillation was driven by thermal atoms spilling over the potential barrier separating the two wells and then forming a new condensate. This process serves as a model system for metastability in condensates, provides a test for quantum kinetic theories of condensate formation, and also represents a novel technique for creating or replenishing condensates in new locations.

DOI: 10.1103/PhysRevLett.92.150401 PACS numbers: 03.75.Lm, 64.60.My

The characteristic feature of Bose-Einstein condensation is the accumulation of a macroscopic number of particles in the lowest quantum state. Condensate fragmentation, the macroscopic occupation of two or more quantum states, is usually prevented by interactions [1], but may happen in spinor condensates [2,3]. However, multiple condensates may exist in metastable situations. Let us assume that an equilibrium condensate has formed in one quantum state, but now we modify the system allowing for one even lower state. How does the original condensate realize that it is in the wrong state and eventually migrate to the true ground state of the system? What determines the time scale for this equilibration process? This is the situation which we experimentally explore in this Letter using a double-well potential.

The process we study is relevant for at least four different questions. (1) The description of the formation of the condensate is a current theoretical frontier and requires finite-temperature quantum kinetic theories. There are still discrepancies between theoretical predictions and experimental results [4,5]. Our double-well system has the advantage of being an almost closed system (little evaporation) with well-defined initial conditions and widely adjustable time scales (through the height of the barrier). (2) Spinor condensates show rich ground states and collective excitations due to the multicomponent order parameter [2]. Several groups have observed long-lived metastable configurations [6–9] and speculated about transport of atoms from one domain to another via the thermal cloud [6,8]. The double-well potential allows us to characterize such distillation processes in their simplest realization. (3) The incoherent transport observed here in a double-well potential imposes stringent limitations on future experiments aiming at the observation of coherent transport in Josephson junctions [10–12]. (4) Our observation of condensate growth in one potential well due to the addition of thermal atoms realizes the key ideas of proposals on how to achieve a continuous atom laser [13] which is different from the experiment where condensates were replenished with transported condensates [14].

The scheme of the experiment is shown in Fig. 1. Bose-Einstein condensates in an optical dipole trap were prepared in a metastable state by creating a second trap horizontally adjacent to the first. Since the probability of quantum tunneling through the barrier was extremely small [15], the coupling between the two wells occurred only by the incoherent transfer of high-energy thermal atoms over the potential barrier between the two wells. The second trap was filled first by thermal atoms, which then formed a new condensate. By monitoring the time evolution of the double-well system, we characterized how differences in chemical potential and the height of the barrier determined the dynamics.

Bose-Einstein condensates containing over 10^7 ^{23}Na atoms were created in the $|F = 1, m_F = -1\rangle$ state in a magnetic trap, captured in the focus of a 1064 nm optical tweezers laser beam, and transferred into an separate "science" chamber as described in Ref. [16]. In the science chamber the condensate was transferred from the optical tweezers into another optical trap formed by a

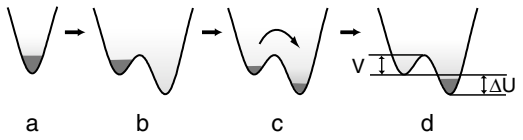

FIG. 1. Scheme for distillation of condensates in a double-well potential. (a) Condensates are loaded into the left well. (b) A new ground state is created by linearly ramping the trap depth of the right well from zero to the final value. (c) Atoms transfer into the right well via high-energy thermal atoms, and a new condensate starts to form in the right well. (d) The whole system has equilibrated. V denotes the height of the potential barrier between the two wells, which is measured with respect to the bottom of the left well, and ΔU the trap depth difference between the two wells.

counterpropagating, orthogonally polarized 1064 nm laser beam. As in Ref. [17], the double-well potential was created by passing a collimated laser beam through an acousto-optic modulator that was driven by two radio-frequency (rf) signals. The separation between the potential wells, d, was proportional to the frequency difference, and the individual trap depth was tailored by controlling the rf power at the two frequencies. Typical parameters were an $1/e^2$ radius of each focused beam of 11.3 μm, a single-well potential depth of $U = k_B \times 2.4$ μK, where k_B is the Boltzmann constant, and a radial (axial) trap frequency, $f_r = 830$ Hz ($f_z = 12.4$ Hz). As shown in Fig. 1, condensates were initially loaded into the left well with depth U_L while the trap depth of the right well, U_R, was maintained at zero. After holding the condensates for 2 s to damp excitations which might have been caused by the loading process, the temperature was $T_i = (180 \pm 90)$ nK, the number of condensed atoms $N_i = (1.1 \pm 0.1) \times 10^6$ with a peak mean field energy of $\tilde{\mu}_0 \approx k_B \times 300$ nK, and the lifetime $\tau = (12.1 \pm 1.5)$ s.

The potential was transformed into a double-well potential by linearly ramping the right well potential from zero to the final value of U_R over 500 ms while keeping U_L constant. This time scale was chosen to be much longer than the radial trap period of $\sim$1 ms to avoid excitations. The resulting double-well potential is characterized by the trap depth difference between the two wells, $\Delta U = U_R - U_L$, and the height of the potential barrier between the two wells, V, which is measured with respect to the bottom of the left well, i.e., the well initially full of atoms. The barrier height was set higher than the peak atomic mean field energy of condensates so that condensed atoms remained confined to the left well during the transformation.

The thermal relaxation process was observed by taking absorption images of clouds confined in the double-well potential for various hold times after turning on the right well. In order to fully resolve the clouds in the two wells, their distance was increased to $d = 31.2$ μm just before taking absorption images. We assume that this did not change either the number of atoms in each well or the axial density distributions, since this additional separation was done in 10 ms, which is much shorter than the axial trap period of $\sim$100 ms, and the height of the potential barrier exponentially increases when the two wells move apart.

Figure 2 shows the dynamical evolution for a situation where the right well was much deeper than the left well. In that case, condensates that initially existed only in the left well were almost completely distilled within 3 s to form condensates of comparable size in the right well.

The time evolution of the double-well system was characterized by monitoring the number of condensed atoms and the temperature of clouds in each well. These numbers were obtained by fitting radially integrated one-dimensional atomic density cross sections to a bimodal

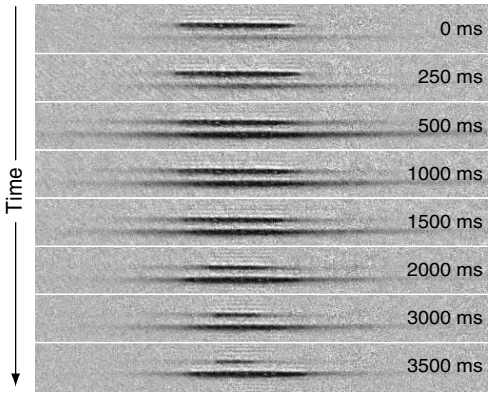

FIG. 2. Time evolution of atom clouds in a double-well potential. The left (right) well appears as the top (bottom) atom cloud in the images. A condensate was distilled from the left to the right well. The absorption images were taken for various hold times after creating the right well. The field of view of each absorption image is 130 μm $\times$ 1160 μm. The trap depths were $U_L = k_B \times 2.4$ μK (left well) and $U_R = k_B \times 2.9$ μK (right well) with a potential barrier of $V = k_B \times 510$ nK between them. During the hold time, the radial separation between the potential wells was $d = 15.9$ μm.

distribution. The assumption of local equilibrium in each well is justified by a short collision time $\tau_{\text{col}} \approx 1$ ms. For the condensate, we used a Thomas-Fermi distribution, and for the thermal clouds the fits to a Bose-Einstein distribution were restricted only to the wings to avoid the distortions due to the mean field repulsion of the condensate [18]. The temperature turned out to be very sensitive to the value of the chemical potential of the thermal clouds. Assuming local equilibrium, we set the chemical potential of the thermal clouds in each well equal to that of the condensates in the same well. In the absence of a condensate, the chemical potential of the thermal cloud was determined by the fit to a Bose-Einstein distribution.

Figure 3 displays the condensed atom number and temperature for the images of Fig. 2. Condensates started to form in the right well after (400 $\pm$ 150) ms and saturated within 2 s, resulting in $\sim$50% of the condensate being transferred. The final temperature in the right well was $T_f \sim 350$ nK, which is $\sim$150 nK higher than the initial temperature T_i. This increase of temperature reflects the energy gained by the atoms when they "fall" into the right potential well which is deeper by $\Delta U =$ 480 nK. After 3.5 s, the total number of atoms of the whole system was $N_f = (0.6 \pm 0.1) \times 10^6$, which is 15% less than expected for the measured lifetime of $\tau =$ 12.1 s. Evaporative cooling due to finite trap depth may explain both the atom loss and the fact that the temperature increase was much less than ΔU.

Even after 3.5 s hold time, full global equilibrium was not reached. This can be seen in both the temperature and

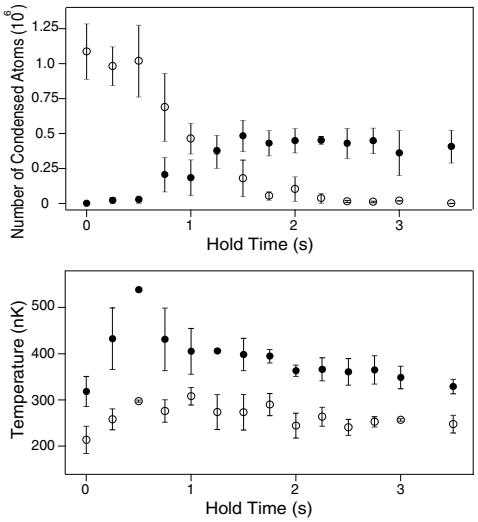

FIG. 3. Approach to thermal equilibrium in a double-well potential. The temperature and the number of condensed atoms in each well are shown as a function of hold time after creating the right well. Open and solid circles represent atoms in the left and the right well, respectively. Every data point is averaged over three measurements, and the error bar shows ± one standard deviation. The experimental parameters are the same as for the results shown in Fig. 2.

the condensed atom numbers. As the chemical potential of condensates in the right well was lower than the trap bottom of the left well, there should not have been any condensate remaining in the left well in global equilibrium. However, Fig. 2 shows a small condensate of $\sim 10^3$ atoms in the left well even after 3.5 s holding. Furthermore, the temperature in the left well was measured ~ 100 nK lower than in the right well.

On first sight, this slow approach towards equilibrium is surprising. In evaporative cooling, one has very fast cooling for a ratio of the height of the potential barrier to the temperature of less than 3 [19], as in our experiment. Note, however, that in our trap geometry the exchange of thermal atoms is geometrically suppressed due to the small "contact area" between the two elongated cigar-shaped clouds. Moreover, if the transferred thermal atoms have high angular momentum, they have poor collisional coupling to the cold trapped atoms such as the Oort cloud in magnetic traps [20]. Indeed, the density of thermal atoms with higher energy than the potential barrier in the left well after 3.5 s holding is $\sim 3 \times 10^{11}/\mathrm{cm}^3$, and their collision time with the atoms confined in this well is $(n\sigma v_{\mathrm{rel}})^{-1} \approx 0.5$ s.

Another quantity of interest in the condensate formation process is the onset time of condensation, the hold time until a condensate first appears [4,5,21]. To avoid ambiguities in fitting small condensates, we determined the onset time in the right well by observing the appearance of interference fringes when two condensates were released from the double-well potential. For two pure condensates, the visibility of the interference fringes is larger than 55% as long as the number ratio of the two condensates is larger than $\eta = 0.05$. Using the methods described in Ref. [17], we have observed discernible interference fringes down to $\eta = 0.08$, corresponding to $\sim 8 \times 10^4$ condensed atoms in the right well.

Onset times were measured as a function of d and ΔU (Fig. 4). The condensate formation is driven by the potential well difference ΔU, whereas the barrier of height V provides the "resistance" against equilibration, since thermal atoms must have a kinetic energy larger than V to transfer from the left well to the right well. Phenomenologically (see inset of Fig. 4), the condensate onset time depends only on the combination $(V - \Delta U/2)$ with an almost exponential dependence. $(V - \Delta U/2)$ can be considered as $(V_{\mathrm{eff}} - \Delta U)$, where $V_{\mathrm{eff}} = [V + (V + \Delta U)]/2$ is the average height of the barrier measured from each well.

In two limiting cases, no interference patterns were observed. When the trap depth difference is larger than the peak atomic mean field energy of condensates, i.e., $|\Delta U| > \tilde{\mu}_0$, it is energetically favorable for condensates to remain in the lowest well. We observed no interference pattern when $\Delta U = -k_B \times 240$ nK even after 20 s hold time. The disappearance of interference fringes was observed when $\Delta U \geq k_B \times 360$ nK due to complete distillation of the condensates into the right well. In the limit

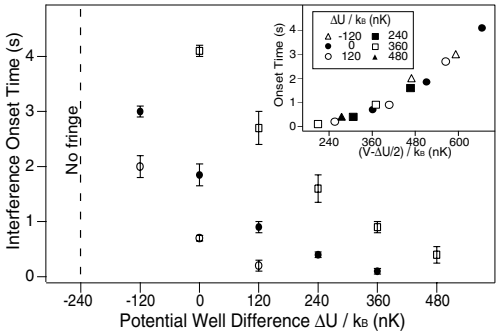

FIG. 4. Onset time of condensation. The onset time in the right well was measured by observing the appearance of a matter wave interference pattern when the condensates were released from the double-well potential. The trap depth difference is defined as $\Delta U = U_R - U_L$. U_L was kept at $k_B \times 2.4$ μK for all experiments. The separations of the two wells, d, were 14.3 μm (open circle), 15.1 μm (solid circle), and 15.9 μm (open square). Interference fringes were not observed at $\Delta U = -k_B \times 240$ nK even after 20 s hold time. The inset shows the same data plotted vs $V - \Delta U/2$, where V is the height of the potential barrier.

where the barrier height is smaller than the peak atomic mean field energy of condensates, i.e., $V < \tilde{\mu}_0$, condensate atoms can "spill" over the potential barrier. Indeed, we observed that condensates appeared in the right well immediately for V less than $\sim k_B \times 290$ nK, consistent with $\tilde{\mu}_0 \sim k_B \times 300$ nK.

To observe quantum tunneling, the thermal relaxation time $\tau_{th} (\propto \exp[V/k_B T])$ should be longer than the tunneling time $\tau_{tu} (\propto \exp[\sqrt{V/m\hbar^2} w])$, where w is the thickness of the barrier. For a thick barrier such as ours ($> 5\ \mu$m), the tunneling time is extremely long ($> 10^5$ s) and thermal relaxation is likely to dominate. A high and thin barrier is necessary to observe tunneling and the related Josephson effects.

In conclusion, we have created Bose-Einstein condensates in a metastable state in a double-well potential and studied the dynamical evolution. The observed distillation process is important for equilibration in spinor condensates and for replenishing condensates in continuous atom lasers.

This work was funded by ARO, NSF, ONR, and NASA. We thank K. Xu for a critical reading of the manuscript. M. S. acknowledges additional support from the Swiss National Science Foundation.

*URL: http://cua.mit.edu/ketterle_group/

[1] P. Nozières, in *Bose-Einstein Condensation*, edited by A. Griffin, D.W. Snoke, and S. Stringari (Cambridge University Press, Cambridge, 1995).
[2] T.-L. Ho, Phys. Rev. Lett. **81**, 742 (1998).
[3] T. Ohmi and K. Machida, J. Phys. Soc. Jpn. **67**, 1822 (1998).
[4] C.W. Gardiner, M. D. Lee, R. J. Ballagh, M. J. Davis, and P. Zoller, Phys. Rev. Lett. **81**, 5266 (1998).
[5] M. Köhl, M. J. Davis, C.W. Gardiner, T.W. Hänsch, and T. Esslinger, Phys. Rev. Lett. **88**, 080402 (2002).
[6] H.-J. Miesner, D. M. Stamper-Kurn, J. Stenger, S. Inouye, A. P. Chikkatur, and W. Ketterle, Phys. Rev. Lett. **82**, 2228 (1999).
[7] D. M. Stamper-Kurn, H.-J. Miesner, A. P. Chikkatur, S. Inouye, J. Stenger, and W. Ketterle, Phys. Rev. Lett. **83**, 661 (1999).
[8] H. Schmaljohann, M. Erhard, J. Kronjäger, M. Kottke, S. van Staa, K. Arlt, J. Bongs, and K. Sengstock, Phys. Rev. Lett. **92**, 040402 (2004).
[9] M.-S. Chang, C. D. Hamley, M. D. Barrett, J. A. Sauer, K. M. Fortier, W. Zhang, L. You, and M. S. Chapman, Phys. Rev. Lett. **92**, 140403 (2004).
[10] A. Smerzi, S. Fantoni, S. Giovanazzi, and S. R. Shenoy, Phys. Rev. Lett. **79**, 4950 (1997).
[11] S. Giovanazzi, A. Smerzi, and S. Fantoni, Phys. Rev. Lett. **84**, 4521 (2000).
[12] L. Pitaevskii and S. Stringari, Phys. Rev. Lett. **87**, 180402 (2001).
[13] M. Holland, K. Burnett, C. Gardiner, J. I. Cirac, and P. Zoller, Phys. Rev. A **54**, R1757 (1996).
[14] A. P. Chikkatur, Y. Shin, A. E. Leanhardt, D. Kielpinski, E. Tsikata, T. L. Gustavson, D. E. Pritchard, and W. Ketterle, Science **296**, 2193 (2002).
[15] F. Dalfovo, S. Giorgini, L. P. Pitaevskii, and S. Stringari, Rev. Mod. Phys. **71**, 463 (1999).
[16] T. L. Gustavson, A. P. Chikkatur, A. E. Leanhardt, A. Görlitz, S. Gupta, D. E. Pritchard, and W. Ketterle, Phys. Rev. Lett. **88**, 020401 (2002).
[17] Y. Shin, M. Saba, T. A. Pasquini, W. Ketterle, D. E. Pritchard, and A. E. Leanhardt, Phys. Rev. Lett. **92**, 050405 (2004).
[18] M. Naraschewski and D. M. Stamper-Kurn, Phys. Rev. A **58**, 2423 (1998).
[19] W. Ketterle and N. J. van Druten, Adv. At. Mol. Opt. Phys. **37**, 181 (1996).
[20] E. A. Cornell, J. R. Ensher, and C. E. Wieman, in *Proceedings of the International School of Physics-Enrico Fermi*, edited by M. Inguscio, S. Stringari, and C. E. Wieman (IOS, Amterdam, 1999).
[21] H.-J. Miesner, D. M. Stamper-Kurn, M. R. Andrews, D. S. Durfee, S. Inouye, and W. Ketterle, Science **279**, 1005 (1998).

Appendix G

Coreless Vortex Formation in a Spinor Bose-Einstein Condensate

This appendix contains a reprint of Ref. [10]: A.E. Leanhardt, Y. Shin, D. Kielpinski, D.E. Pritchard, W. Ketterle, *Coreless Vortex Formation in a Spinor Bose-Einstein Condensate*, Physical Review Letters **90**, 140403 (2003).

Coreless Vortex Formation in a Spinor Bose-Einstein Condensate

A. E. Leanhardt, Y. Shin, D. Kielpinski, D. E. Pritchard, and W. Ketterle*

Department of Physics, MIT-Harvard Center for Ultracold Atoms, and Research Laboratory of Electronics, Massachusetts Institute of Technology, Cambridge, Massachusetts 02139

(Received 20 December 2002; published 9 April 2003)

Coreless vortices were phase imprinted in a spinor Bose-Einstein condensate. The three-component order parameter of $F = 1$ sodium condensates held in a Ioffe-Pritchard magnetic trap was manipulated by adiabatically reducing the magnetic bias field along the trap axis to zero. This distributed the condensate population across its three spin states and created a spin texture. Each spin state acquired a different phase winding which caused the spin components to separate radially.

DOI: 10.1103/PhysRevLett.90.140403 PACS numbers: 03.75.Lm, 03.65.Vf, 03.75.Mn, 67.57.Fg

Spin textures play a central role in describing the physics of elementary particles [1], liquid ^{3}He-A [2–4], the quantum Hall effect [5], and gaseous Bose-Einstein condensates [6–10]. Topological defects vary between superfluid systems described by scalar and vector order parameters. In spinless or spin-polarized condensates, line defects such as vortices have cores where the density of condensed particles is necessarily zero to keep the order parameter single valued [11–13]. However, in condensates with an internal, spin degree of freedom, coreless vortices exist as spin textures [4,14]. Such structures are referred to as skyrmions (Anderson-Toulouse vortices [3]) or merons (half-skyrmions, Mermin-Ho vortices [2]) depending on the boundary conditions of the system.

In this Letter, we study spin textures in a Bose-Einstein condensate. Coreless vortices were created in $F = 1$ spinor condensates held in a Ioffe-Pritchard magnetic trap by adiabatically reducing the magnetic bias field along the trap axis to zero. This continuously transformed the initially spin-polarized condensate into a coherent superposition of three spin states, each with a different phase winding. The resulting angular momentum per particle varied between spin states and the condensate evolved such that states with more angular momentum per particle circulated around states with less angular momentum per particle. Thus, the condensate had a net axial magnetization that varied with radial position. Previous work on vortices in a two-component system used laser, microwave, and radio frequency fields to spatially and temporally control the interconversion between components [14]. However, without these applied fields the two components evolved independently as distinguishable fluids. In our work, the spin states can freely interconvert at all points in space and time such that the spin texture would continually heal itself even in the presence of state-dependent losses.

In cylindrical coordinates, the spin-F condensate wave function can be written as $|\Psi(r, \phi, z)\rangle = \sqrt{n(r, \phi, z)}|\zeta(r, \phi, z)\rangle$, where n is the atomic number density and the $2F + 1$ component spinor $|\zeta\rangle = \sum_{m_z=-F}^{F} \zeta_{m_z}|F, m_z\rangle$, $|\langle\zeta|\zeta\rangle|^2 = 1$ describes a spin texture. A Ioffe-Pritchard magnetic trap consists of an axial bias field (with curvature) and a two-dimensional quadrupole field in the orthogonal plane [15,16]:

$$\vec{B}(r, \phi, z) = B_z\hat{z} + B'r(\cos(2\phi)\hat{r} - \sin(2\phi)\hat{\phi}), \quad (1)$$

where B' is the radial magnetic field gradient and quadratic terms have been neglected. For a condensate of radial extent R confined in a Ioffe-Pritchard magnetic trap with $B_z \gg B'R > 0$, $|\zeta\rangle = |F, m_z = m_F\rangle$, where m_z and m_F are the projection of the atomic spin along the z axis and local magnetic field direction, respectively. Adiabatically ramping B_z from $B_z \gg B'R > 0$ to zero rotates the atomic spin about the position-dependent axis $\hat{n}(\phi) = \sin\phi\hat{x} + \cos\phi\hat{y}$, and drives the transition $|F, m_z = m_F\rangle \rightarrow \sum_{m_z=-|m_F|}^{|m_F|} \zeta_{m_z} \exp[i(m_z - m_F)\phi]|F, m_z\rangle$ [17,18]. Thus, the condensate population is distributed across $2|m_F| + 1$ spin states with each acquiring a different topological phase factor and angular momentum per particle due to the variation of Berry's phase with magnetic quantum number [19].

The condensate remains in the state $|F, m_F\rangle$ with respect to the local magnetic field provided the local Zeeman energy, $\sim g_F\mu_B[B_z^2 + (B'r)^2]^{1/2}$, dominates the local kinetic energy associated with the spin texture, $\sim\hbar^2/mr^2$, where g_F is the Landé g factor, μ_B is the Bohr magneton, and m is the atomic mass. For $B_z = 0$, atomic spins aligned with the quadrupole magnetic field produce the planar spin texture in Fig. 1(a). However, the infinite kinetic energy associated with the wave function singularity at $r = 0$ creates a nonplanar spin texture over a disk of radius $\sim(\hbar^2/mg_F\mu_B B')^{1/3}$, with higher angular momentum spin states residing outside those with lower angular momentum.

Bose-Einstein condensates containing over 10^7 ^{23}Na atoms were created in the $|1, -1\rangle$ state in a magnetic trap, captured in the focus of an optical tweezers laser beam, and transferred into an auxiliary "science" chamber as described in Ref. [21]. In the science chamber, the condensate was loaded into a microfabricated Ioffe-Pritchard magnetic trap formed by a Z-shaped

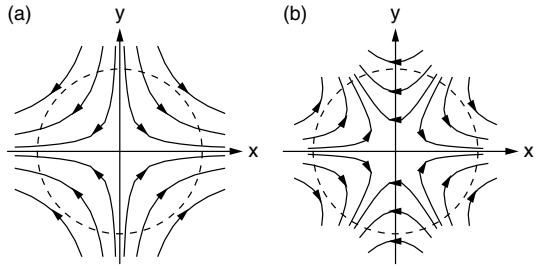

FIG. 1. Planar spin textures. Spins aligned with two-dimensional (a) quadrupole and (b) hexapole magnetic fields produce textures with winding numbers -1 and -2, respectively. Counterclockwise traversal of the dashed contours in (a) and (b) leads to clockwise (negative) spin rotation, with the winding number defined as the integer number of revolutions made by the spin vector while circumnavigating the singularity at the origin [20].

50 μm $\times$ 10 μm electroplated copper wire carrying current I and an external magnetic bias field, $B_\perp$, as described in Ref. [22]. Typical wiretrap parameters were $I = 720$ mA, $B_\perp = 5.3$ G, and $B_z = 1.3$ G, resulting in a radial magnetic field gradient $B' = 180$ G/cm. This produced axial and radial trap frequencies $\omega_z = 2\pi \times 4$ Hz and $\omega_\perp = 2\pi \times 250$ Hz, respectively. Condensates in the wiretrap had $\geq 2 \times 10^6$ atoms, a Thomas-Fermi radius of ≈ 5 μm, and a lifetime ≥ 25 s.

Coreless vortices imprinted onto the condensate wave function by adiabatically ramping $B_z \rightarrow 0$ are shown in Fig. 2. To observe the nature of the spin texture, an axial bias field was switched on nonadiabatically along either the negative [Figs. 2(b)–2(d)] or positive [Figs. 2(e)–2(h)] z axis. Switching the axial bias field on suddenly "froze" the atomic spins and effectively "projected" the condensate wave function onto a basis quantized with respect to the local (axial) magnetic field. This allowed the spin states to be separated by a magnetic field gradient applied during ballistic expansion. Switching the direction of the axial projection field exchanged the roles of the $|1, -1\rangle$ and $|1, +1\rangle$ states. Figures 2(a) and 2(e) show the coreless nature of the vortices, while Figs. 2(b) and 2(f) show the concentric cylinder structure resulting from the competition between the atomic Zeeman energy and the kinetic energy of the rotating spin states. We assume that the two-dimensional ($\omega_z \ll \omega_\perp$) ballistic expansion process simply magnifies the condensate wave function, as it does in the expansion of a single-component condensate with vortices [23,24].

Along the wiretrap axis, the magnetic field was

$$\vec{B}(r = 0, \phi, z) = (B_z + \tfrac{1}{2}B'' z^2)\hat{z}, \tag{2}$$

where quadratic terms neglected in Eq. (1) are included. Nonzero axial magnetic field curvature, $B'' \approx 5$ G/cm^2, implies that the spin texture had a slight axial dependence. The axial bias field was ramped linearly from $B_z = 1.3$ G to $B_z \approx 0$ in 10 ms to imprint the coreless vortices. This compressed the condensate radially and increased the condensate chemical potential from $\mu \approx (\mu_B/2) \times 3$ mG to $\mu \approx (\mu_B/2) \times 27$ mG. Ramping $B_z \rightarrow 0$ fast compared to the axial trap period (250 ms), but slow compared to the initial radial trap period (4 ms), guaranteed that the axial magnetic field variation remained constant throughout the experiment at $\Delta B_z \approx 3$ mG, while at $B_z \approx 0$ the radial magnetic field variation was $\Delta B_r \approx 27$ mG. The images shown in Fig. 2 integrated the atomic number density along the z axis and therefore averaged over the minor ($\Delta B_z \ll \Delta B_r$) axial variation to the spin texture.

To project the condensate wave function onto a basis quantized with respect to the local magnetic field, an ≈ 10 G axial bias field was switched on at a rate of $\dot{B}_z = 2 \times 10^5$ G/s along either the negative or the positive z axis. 100 μs later the magnetic trap was switched off allowing the atoms to expand ballistically. For $0 \leq B_r \leq \Delta B_r$, the Landau-Zener nonadiabatic transition probability, $\exp(-\pi\mu_B B_r^2/\hbar\dot{B}_z) \geq 0.9$, was sufficiently close to unity that the atomic spins remained "frozen" during the sudden application of the axial bias field and the spin texture could be accurately diagnosed. While the total condensate density monotonically decreased as a function of radial position [Figs. 2(a) and 2(e)], the density of each spin component peaked at a different radius signifying a variation in the angular momentum per particle between spin states [Figs. 2(b) and 2(f)].

Applying the projection field along the positive z axis generated additional rings of atoms in the $|1, -1\rangle$ and $|1, 0\rangle$ states [Fig. 2(f)]. Ramping $B_z \rightarrow 0$ in 10 ms caused nonadiabatic spin flips for atoms near $r = 0$ resulting in an atom loss of $\approx 50\%$ [18]. If these atoms had not left the condensate before the projection field was applied, they may have contributed to the images displayed in Fig. 2(f). The additional rings of atoms may also correspond to a low energy, radial spin-wave excitation [6,7]. However, we could not identify any asymmetry between applying the projection field along the positive versus negative z axis that would account for the presence of the extra rings in Fig. 2(f), but not in Fig. 2(b).

Engineering topological states in a Bose-Einstein condensate has received much theoretical attention [17,25–30]. The evolution of a condensate confined in a Ioffe-Pritchard magnetic trap while ramping $B_z \rightarrow 0$ is described by a position-dependent spin rotation about the $\hat{n}(\phi)$ axis through an angle $\beta(r)$ [18]

$$|\zeta(r, \phi, z)\rangle = e^{-i(\vec{\mathcal{F}}/\hbar)\cdot\hat{n}(\phi)\beta(r)}|\zeta_0\rangle, \tag{3}$$

where $\vec{\mathcal{F}}$ is the spin operator and $|\zeta_0\rangle = |F, m_z = m_F\rangle$ is a polarized spinor. For $|\zeta_0\rangle = |1, -1\rangle$, Eq. (3) gives the condensate spinor in the laboratory frame as

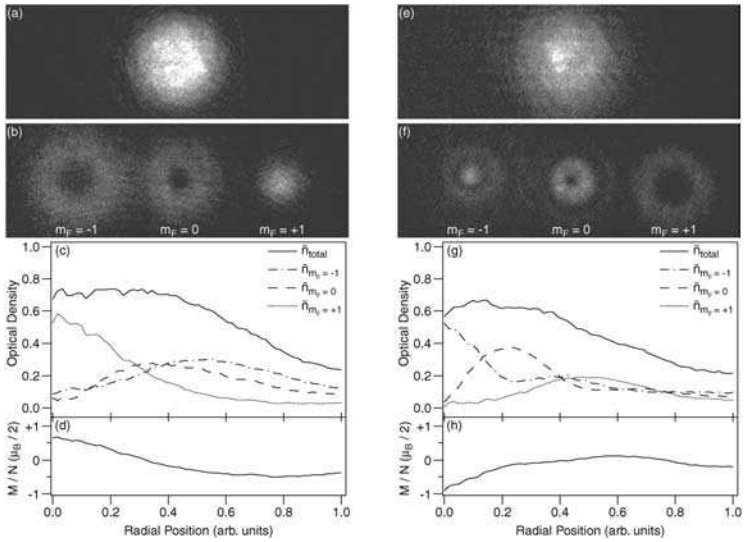

FIG. 2. Coreless vortex formation in a spinor Bose-Einstein condensate. Coreless vortices were imprinted by ramping $B_z \to 0$ and diagnosed by suddenly switching (a)–(d) $B_z \ll 0$ and (e)–(h) $B_z \gg 0$. Axial absorption images display the optical density of condensates after 20 ms of ballistic expansion (a),(e) without and (b),(f) with a magnetic field gradient applied to separate the different spin states. (c),(g) Azimuthally averaged optical density vs radial position for spin components shown in (b) and (f), respectively. The radial separation of the spin states resulted from their relative phase windings and is a clear signature of the skyrmion/meron wave function [Eq. (4)]. (d),(h) Axial magnetization per particle, $M/N = (\mu_B/2) \times (\tilde{n}_{m_F=+1} - \tilde{n}_{m_F=-1})/\tilde{n}_{\text{total}}$, vs radial position. The absorption imaging light was resonant with the $F = 2 \to F' = 3$ transition. The atoms were optically pumped into the $F = 2$ hyperfine level with a pulse resonant with the $F = 1 \to F' = 2$ transition. This provided equal imaging sensitivity to each spin state. The field of view in (a), (b), (e), and (f) is 1.0 mm × 3.0 mm.

$$|\zeta(r, \phi, z)\rangle = \cos^2[\beta(r)/2]|1, -1\rangle + \frac{-1}{\sqrt{2}} \sin[\beta(r)] e^{i\phi} |1, 0\rangle + \sin^2[\beta(r)/2] e^{i2\phi} |1, +1\rangle. \quad (4)$$

$\beta(0) = 0$ and skyrmions (merons) are described by the boundary condition $\beta(\infty) = \pi$ [$\beta(\infty) = \pi/2$].

The radial dependence of $\beta(r)$ is determined by requiring the Gross-Pitaevskii energy functional,

$$E = \int d^3\vec{r}\, n\left(\frac{\hbar^2}{2m}\langle\nabla\zeta|\nabla\zeta\rangle + V + \left(\frac{c_0}{2} + \frac{c_2}{2}\frac{|\vec{F}|^2}{\hbar^2}\right)n\right), \quad (5)$$

be stationary with respect to variations in β. Equation (5) uses the Thomas-Fermi approximation, and $\langle\nabla\zeta|\nabla\zeta\rangle = \sum_{m_z=-F}^{F} \nabla\zeta_{m_z}^{\dagger} \cdot \nabla\zeta_{m_z}$, $V = -g_F\mu_B\vec{F}\cdot\vec{B}/\hbar$, $\vec{F} = \langle\zeta|\vec{\mathcal{F}}|\zeta\rangle$, $c_0 = 4\pi\hbar^2\bar{a}/m$, and $c_2 = 4\pi\hbar^2\Delta a/m$. Here $\bar{a} = (2a_0 + a_2)/3$ and $\Delta a = (a_2 - a_0)/3$ characterize two-body interactions, where a_0 and a_2 are scattering lengths for collisions with total angular momentum $F = 0$ and $F = 2$, respectively [6]. For $c_2 > 0$, the atomic interactions are antiferromagnetic (polar), as in ^{23}Na [31], while for $c_2 < 0$ they are ferromagnetic, as in ^{87}Rb [32].

Using Eq. (4) as a trial spinor, we find that $\beta(r)$ satisfies the meron boundary conditions and varies from $\beta(0) = 0$, due to the kinetic energy of the spin texture, to $\beta(\infty) = \pi/2$, due to the atomic Zeeman energy, over a characteristic length scale given by the larger of $(\hbar^2/mg_F\mu_B B')^{1/3}$ and $|B_z|/B'$. We observed that the boundary condition $\beta(0) = 0$ was maintained regardless of the sign of B_z, i.e., atomic spins along the trap axis always remained in the initial state. If the atomic spins had simply followed the local magnetic field, $\beta(r)$ would satisfy $\tan\beta(r) = B'r/B_z$. Thus, scanning B_z from slightly positive to slightly negative would instantaneously change the boundary condition at the origin from $\beta(0) = 0$ to $\beta(0) = \pi$ and flip the atomic spins along the trap axis.

The trial spinor in Eq. (4) does not have the most general form since it was derived by rotating a polarized spinor [Eq. (3)] and is inherently ferromagnetic, $|\vec{F}| = \hbar$. Accordingly, the spin-dependent interaction term in Eq. (5) does not vary with β and therefore does not contribute to the determination of $\beta(r)$. This restriction is not severe since the Zeeman energy dominates the spin-dependent interaction energy in our experiment.

In future experiments, it should be possible to overlap the condensate with an optical dipole trap so that, after ramping $B_z \to 0$, relaxing the radial magnetic field

gradient would allow for the spin-dependent interactions to determine the evolution of the condensate. It is predicted that skyrmions/merons in condensates with antiferromagnetic (ferromagnetic) interactions are unstable (stable) [9,10,33–39]. Presently, excitations created during the field ramping process have prevented a study of the stability of coreless vortices in an antiferromagnetic ^{23}Na condensate. However, we were able to imprint the spin texture in the presence of an optical dipole trap, as well as produce vortices with a 4π phase winding in an optical dipole trap by fully inverting the axial bias field [18]. At zero magnetic field, it may be possible to observe multiply charged vortices in a spinor condensate "unwind" themselves as predicted in Ref. [6]. The unwinding process is precisely the position-dependent spin rotation demonstrated in previous work [18], with the spin texture investigated here as an intermediate state [37].

In conclusion, we have demonstrated a robust technique for creating coreless vortices in a Bose-Einstein condensate. Our technique can be extended to generate spin textures with arbitrary winding number and variable angular momentum per particle by using higher-order, axisymmetric multipole magnetic fields and condensates with different spin. This work opens up the opportunity to study the stability of topological defects in spinor Bose-Einstein condensates.

We are grateful to K. Machida for bringing the spin texture studied here to our attention. We thank T. Pasquini for experimental assistance and J. R. Anglin and M. Crescimanno for valuable discussions. This work was funded by ONR, NSF, ARO, NASA, and the David and Lucile Packard Foundation.

*Electronic address: http://cua.mit.edu/ketterle_group/

[1] T. H. R. Skyrme, Proc. R. Soc. London A **260**, 127 (1961).
[2] N. D. Mermin and T.-L. Ho, Phys. Rev. Lett. **36**, 594 (1976).
[3] P.W. Anderson and G. Toulouse, Phys. Rev. Lett. **38**, 508 (1977).
[4] R. Blaauwgeers, V. B. Eltsov, M. Krusius, J. J. Ruohio, R. Schanen, and G. E. Volovik, Nature (London) **404**, 471 (2000).
[5] D.-H. Lee and C. L. Kane, Phys. Rev. Lett. **64**, 1313 (1990).
[6] T.-L. Ho, Phys. Rev. Lett. **81**, 742 (1998).
[7] T. Ohmi and K. Machida, J. Phys. Soc. Jpn. **67**, 1822 (1998).
[8] S.-K. Yip, Phys. Rev. Lett. **83**, 4677 (1999).
[9] U. A. Khawaja and H. Stoof, Nature (London) **411**, 918 (2001).
[10] U. A. Khawaja and H.T. C. Stoof, Phys. Rev. A **64**, 043612 (2001).
[11] E. J. Yarmchuk, M. J.V. Gordon, and R. E. Packard, Phys. Rev. Lett. **43**, 214 (1979).
[12] K.W. Madison, F. Chevy, W. Wohlleben, and J. Dalibard, Phys. Rev. Lett. **84**, 806 (2000).
[13] J. R. Abo-Shaeer, C. Raman, J. M. Vogels, and W. Ketterle, Science **292**, 476 (2001).
[14] M. R. Matthews, B. P. Anderson, P. C. Haljan, D. S. Hall, C. E. Wieman, and E. A. Cornell, Phys. Rev. Lett. **83**, 2498 (1999).
[15] Y.V. Gott, M. S. Ioffe, and V. G. Tel'kovskii, Nucl. Fusion (Suppl.) **3**, 1045 (1962).
[16] D. E. Pritchard, Phys. Rev. Lett. **51**, 1336 (1983).
[17] T. Isoshima, M. Nakahara, T. Ohmi, and K. Machida, Phys. Rev. A **61**, 063610 (2000).
[18] A. E. Leanhardt, A. Görlitz, A. P. Chikkatur, D. Kielpinski, Y. Shin, D. E. Pritchard, and W. Ketterle, Phys. Rev. Lett. **89**, 190403 (2002).
[19] M.V. Berry, Proc. R. Soc. London A **392**, 45 (1984).
[20] N. D. Mermin, Rev. Mod. Phys. **51**, 591 (1979).
[21] T. L. Gustavson, A. P. Chikkatur, A. E. Leanhardt, A. Görlitz, S. Gupta, D. E. Pritchard, and W. Ketterle, Phys. Rev. Lett. **88**, 020401 (2002).
[22] A. E. Leanhardt, A. P. Chikkatur, D. Kielpinski, Y. Shin, T. L. Gustavson, W. Ketterle, and D. E. Pritchard, Phys. Rev. Lett. **89**, 040401 (2002).
[23] E. Lundh, C. J. Pethick, and H. Smith, Phys. Rev. A **58**, 4816 (1998).
[24] F. Dalfovo and M. Modugno, Phys. Rev. A **61**, 023605 (2000).
[25] J. Williams and M. J. Holland, Nature (London) **401**, 568 (1999).
[26] J. Ruostekoski, Phys. Rev. A **61**, 041603(R) (2000).
[27] K.-P. Marzlin, W. Zhang, and B. C. Sanders, Phys. Rev. A **62**, 013602 (2000).
[28] U. Leonhardt and G. E. Volovik, JETP Lett. **72**, 46 (2000).
[29] J. Ruostekoski and J. R. Anglin, Phys. Rev. Lett. **86**, 3934 (2001).
[30] H. Pu, S. Raghavan, and N. P. Bigelow, Phys. Rev. A **63**, 063603 (2001).
[31] J. Stenger, S. Inouye, D. M. Stamper-Kurn, H.-J. Miesner, A. P. Chikkatur, and W. Ketterle, Nature (London) **396**, 345 (1998).
[32] N. N. Klausen, J. L. Bohn, and C. H. Greene, Phys. Rev. A **64**, 053602 (2001).
[33] R. A. Battye, N. R. Cooper, and P. M. Sutcliffe, Phys. Rev. Lett. **88**, 080401 (2002).
[34] T. Mizushima, K. Machida, and T. Kita, Phys. Rev. Lett. **89**, 030401 (2002).
[35] T. Isoshima and K. Machida, Phys. Rev. A **66**, 023602 (2002).
[36] Y. Zhang, W.-D. Li, L. Li, and H. J.W. Müller-Kirsten, Phys. Rev. A **66**, 043622 (2002).
[37] J.-P. Martikainen, A. Collin, and K.-A. Suominen, Phys. Rev. A **66**, 053604 (2002).
[38] T. Mizushima, K. Machida, and T. Kita, Phys. Rev. A **66**, 053610 (2002).
[39] H. Zhai, W. Chen, Z. Xu, and L. Chang, cond-mat/0210397.

Appendix H

Dynamical Instability of a Doubly Quantized Vortex in a Bose-Einstein Condensate

This appendix contains a reprint of Ref. [3]: Y. Shin, M. Saba, M. Vengalattore, T.A. Pasquini, C. Sanner, A.E. Leanhardt, M. Prentiss, D.E. Pritchard, W. Ketterle, *Dynamical Instability of a Doubly Quantized Vortex in a Bose-Einstein Condensate*, Physical Review Letters **93**, 160406 (2004).

Dynamical Instability of a Doubly Quantized Vortex in a Bose-Einstein Condensate

Y. Shin,[1] M. Saba,[1] M. Vengalattore,[2] T. A. Pasquini,[1] C. Sanner,[1] A. E. Leanhardt,[1] M. Prentiss,[2] D. E. Pritchard,[1] and W. Ketterle[1,*]

[1]*MIT-Harvard Center for Ultracold Atoms, Research Laboratory of Electronics, Department of Physics, Massachusetts Institute of Technology, Cambridge, Massachusetts, 02139, USA*

[2]*MIT-Harvard Center for Ultracold Atoms, Jefferson Laboratory, Physics Department, Harvard University, Cambridge, Massachusetts, 02138, USA*

(Received 1 July 2004; published 14 October 2004)

Doubly quantized vortices were topologically imprinted in $|F = 1\rangle$ ^{23}Na condensates, and their time evolution was observed using a tomographic imaging technique. The decay into two singly quantized vortices was characterized and attributed to dynamical instability. The time scale of the splitting process was found to be longer at higher atom density.

DOI: 10.1103/PhysRevLett.93.160406 PACS numbers: 03.75.Kk, 03.75.Lm, 67.90.+z

Quantum fluids, like superfluid He, electrons in a superconductor, or a Bose-Einstein condensate of atoms, are described by a macroscopic wave function. This requires the flow field to be irrotational, and gives rise to superfluidity and quantized circulation [1]. Atoms in a Bose-Einstein condensate, for example, can only circulate with an angular momentum equal to an integer multiple of $\hbar$, in the form of a quantized vortex [2].

Vortices are excited states of motion and therefore energetically unstable towards relaxation into the ground state, where the condensate is at rest. However, quantization constrains the decay: a vortex in Bose-Einstein condensates cannot simply fade away or disappear, it is only allowed to move out of the condensate or annihilate with another vortex of an opposite circulation. Vortex decay and metastability, due to inhibition of decay, has been a central issue in the study of superfluidity [3–8]. In almost pure condensates, vortices with lifetimes up to tens of seconds have been observed [9–11].

Giving a Bose-Einstein condensate an angular momentum per particle larger than $\hbar$ can result in one multiply quantized vortex with large circulation or, alternatively, in many singly quantized vortices each with an angular momentum $\hbar$. The kinetic energy of atoms circulating around the vortex is proportional to the square of the angular momentum; therefore the kinetic energy associated with the presence of a multiply quantized vortex is larger than the kinetic energy of a collection of singly quantized vortices carrying the same angular momentum. A multiply quantized vortex can decay coherently by splitting into singly quantized vortices and transferring the kinetic energy to coherent excitation modes, a phenomenon called dynamical instability, which is driven by atomic interactions [5,12–14] and not caused by dissipation in an external bath. Observations of arrays of singly quantized vortices in rapidly rotating condensates [10,11] indirectly suggest that the dynamical instability leads to fast decay of multiply quantized vortices. However, the existence of stable multiply quantized vortices in trapped Bose-Einstein condensates has been predicted with a localized pinning potential [12] or in a quartic potential [15]. Stable doubly quantized vortices were observed in superconductors in the presence of pinning forces [16] and in superfluid ^{3}He-A, which has a multicomponent order parameter [17]. Recently, formation of a multiply quantized vortex in a Bose-Einstein condensate has been demonstrated using topological phases [18,19], and surprisingly, a long lifetime of a "giant" vortex core has been reported [20]. The study of topological excitation and its stability is an active frontier in the field of quantum degenerate gases [21,22].

In this Letter, we study the time evolution of a doubly quantized vortex state in a Bose-Einstein condensate, and directly confirm its dynamical instability by observing that a doubly quantized vortex core splits into two singly quantized vortex cores. The characteristic time scale of the splitting process was determined as a function of atom density and was longer at higher atomic density.

Bose-Einstein condensates of ^{23}Na atoms were transferred into an auxiliary chamber [23] and loaded into a Ioffe-Pritchard magnetic trap generated by a microfabricated atom chip [24–26]. The wire pattern on the atom chip is shown in Fig. 1(a). In our previous work [19], we used a Z-shaped wire trap where changing the sign of the axial magnetic field curvature was technically impossible so that we could not trap condensates after imprinting a vortex. To overcome this technical difficulty, we designed our new chip with separate end cap wires, allowing independent control of the axial magnetic field. Typical wire currents were $I_C = 1.53$ A in the center wire and $I_L = I_R = 0.1$ A in the end cap wires, and the external magnetic field was $B_z = 450$ mG and $B_x = 5.3$ G, resulting in a radial (axial) trap frequency $f_r = 220$ Hz ($f_z = 3$ Hz) and a distance of the trap from the chip surface of $d = 600$ μm. After holding condensates for 2 s to damp excitations, which might have been caused by the loading process, condensates contained over 1.5×10^6 atoms, and

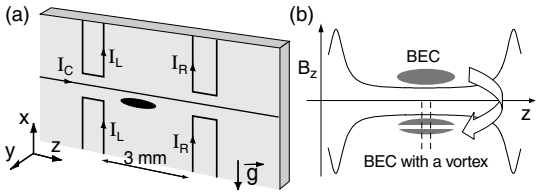

FIG. 1. (a) Wire pattern on the atom chip. A magnetic trap is formed by a current I_C flowing through the center wire in conjunction with an external uniform magnetic field B_x. The axial confinement along the z direction is generated by currents I_L and I_R in the end cap wires. Each current is controlled independently. A 2 μm thick Au film was deposited by evaporation on a thermally oxidized Si substrate and wires were patterned by photolithography and wet etching. The width of the center wire and the end cap wires were 50 μm and 100 μm, respectively. (b) Imprinting of a vortex in a Bose-Einstein condensate. By inverting the z direction magnetic field B_z, a doubly quantized vortex was imprinted in $|F = 1\rangle$ condensates, using topological phases as in Ref. [19]. The direction of I_L and I_R were also reversed to maintain the axial confinement. The dashed lines indicate the selective probing region for tomographic imaging as described in the text.

the lifetime of condensates was ≈ 8 s with a radio-frequency (rf) shield [27].

Doubly quantized vortices were topologically imprinted in condensates by inverting the axial magnetic field, B_z, as in Ref. [19]. B_z was ramped linearly from 450 mG to -460 mG in 12 ms. As B_z passed zero, the sign of the axial field curvature was changed by reversing the directions of I_L and I_R in 1 ms. The trap position and the axial trap frequency of the inverted trap were matched to those of the original wire trap by adjusting the final values for I_L and I_R. Losses due to nonadiabatic spin flips as B_z passed through zero reduced the number of atoms in the condensate after imprinting to about $\sim 1 \times 10^6$, giving a typical healing length of $\xi = 0.4$ μm. The lifetime of condensates after imprinting was less than 2 s.

The vortex imprinting process was accompanied by a sudden mechanical squeeze in the radial direction and a kick in the vertical direction. The radial trap frequency is inversely proportional to the square root of the bias magnetic field ($f_r \propto |B_z|^{-1/2}$) and became temporarily higher during field inversion. Additionally, the vertical position of the trap center changed as the gravitational sag ($\propto f_r^{-2}$) changed from 5.1 μm to zero. The Thomas-Fermi radius of condensates in the loading phase was ~ 5 μm. After imprinting a vortex, the amplitude of quadruple oscillation in the axial direction was $\sim 20\%$ of the axial length of condensates (≈ 600 μm), but there was no detectable dipole oscillation in the vertical direction.

The decay of a doubly quantized vortex state was studied by taking absorption images along the imprinted vortex line after releasing the condensate and letting it expand for 15 ms. The visibility of a vortex core in an integrated absorption image completely vanished within 30 ms. To reduce blurring due to possible bending of the vortex line [28], we employed a tomographic imaging technique [29]. A 30 μm thick central slice of the condensate [see Fig. 1(b)] was selectively pumped into the $F = 2$ hyperfine level with a sheet of laser light perpendicular to the condensate long axis; the radial profile of the condensate in the selected region was then imaged with a light pulse resonant with the $F = 2 \rightarrow F' = 3$ cycling transition. In our absorption images, the size of a doubly quantized vortex core was typically ~ 40 μm. This tomographic imaging technique was crucial for observing the time evolution of vortex cores beyond 30 ms.

A series of absorption images of the splitting process is provided in Fig. 2. Images taken just after imprinting show a doubly quantized vortex core of high visibility; the visibility of the core decreased with time, an effect we attribute to bending of the vortex line [28] and other excitations created during the imprinting process. Later in the evolution, the central core deformed into an elliptical shape and split into two closely-spaced cores. Once the two cores were separated by their diameter, they appeared well resolved in our images. The angular position of the two cores was random for each experimental realization with the same evolution time, so the precession frequency of the two cores could not be determined with our destructive image technique.

To investigate the dependence of the instability on the mean field atomic interaction, we measured the characteristic time scale of splitting of a doubly quantized vortex core as a function of the atom density. Atom density was controlled by removing a variable number of atoms with rf evaporation before imprinting a vortex. Images were classified as follows: images where the two cores were separated by more than one core diameter were labeled as "two visible cores"; images with a clearly-defined circu-

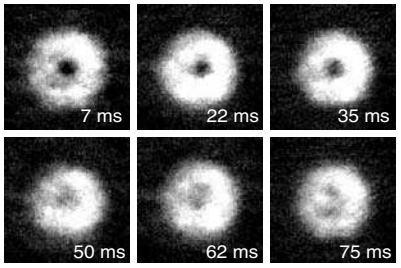

FIG. 2. Decay of a doubly quantized vortex. Axial absorption images of condensates after 15 ms of ballistic expansion with a variable hold time after imprinting a doubly quantized vortex. A doubly quantized vortex decayed into two singly quantized vortices. For this data, the interaction strength was $an_z \approx 7.5$ (see text for definition). The field of view in each image is 320 μm $\times$ 320 μm.

lar central core were labeled as "one core"; images in the intermediate range, where the central core was elliptical but the two cores were not resolved, and images with a bad visibility were labeled as "undetermined". For example, the images at 62 ms and 75 ms in Fig. 2 and Fig. 3(a) were classified as two visible cores, and at 50 ms in Fig. 2, and Fig. 4(a) and 4(c) as undetermined.

Experimental results are provided in Fig. 3 as a function of the linear atom density n_z (along the condensate long axis) multiplied by the s-wave scattering length a. The rescaled quantity, $an_z = a\int|\psi(r)|^2 dxdy$ corresponds for a cylindrical condensate to the strength of the mean field interaction, with $\psi(r)$ being the condensate wave function. Results in Fig. 3 clearly demonstrate that a doubly quantized vortex core splits more slowly as the density becomes higher.

Once the doubly quantized vortex core split into two cores, the distance between the two cores was almost constant ($\sim 50\ \mu$m) during the further evolution, as shown in Fig. 3(c). This is evidence that the separation process was driven mainly by the dynamical instability, and not by dissipation, which would gradually increase the separation of the two cores. Dissipative processes were minimized by performing the experiments at the lowest possible temperature. Condensates did not have any discernible thermal atoms even after an extended hold time. Furthermore, the energy released by the dissociation of the doubly quantized vortex was $\sim$5 nK, negligible to the critical temperature $\sim$240 nK. For the upper bound of temperatures $<$100 nK, Ref. [30] predicts that the dissipative decay time be $\approx$ 1.5 s for a single vortex, a time scale much longer than what we observed.

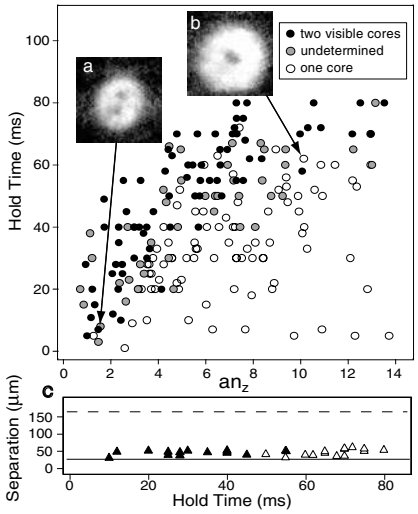

FIG. 3. Density dependence of the decay process. The time scale for the decay process of doubly quantized vortex states was measured by observing the vortex cores and classifying them as one vortex (open circles) or two vortices (solid circles). Data were collected with three axial trap frequencies $f_z = 2.7$, 3.7, and 12.1 Hz and the interaction strength an_z was controlled by changing the atom number by rf induced evaporation before imprinting. Typical absorption images for (a) fast decay at low density ($an_z = 1.5$) and (b) slow decay at high density ($an_z = 10.1$). The field of view in the absorption images is 300 μm $\times$ 300 μm. (c) The separation of two visible cores vs the hold time for $2 < an_z < 3$ (solid triangles) and $6 < an_z < 8$ (open triangles). The solid and dashed lines indicate the diameter of one vortex core and of the condensate, respectively.

Multiply quantized vortices in a harmonic potential are predicted to spontaneously decay into other states even in the absence of dissipation and external perturbations [5]. In the Bogoliubov framework, which is believed to describe well quantized vortices in one component condensates, the dynamical instability manifests as the existence of excitation modes with a complex eigenfrequency. The nonvanishing imaginary part of the eigenfrequency implies an exponential growth in time of the corresponding excitation mode, leading to decay of the multiply quantized vortex state. This spectral instability is a general parametric phenomenon occurring when several modes compete during coherent evolution, and has been studied in many other nonlinear physical systems (see, e.g., Ref. [31,32], and references therein).

For a doubly quantized vortex state in a cylindrically symmetric condensate, it was theoretically found that there are two excitation modes with a complex eigenfrequency [5,13]. One of them is confined inside the doubly quantized vortex core; the growth of this so-called "core" mode induces splitting of the original doubly quantized vortex core into two separate singly quantized vortex cores. The other mode, having the conjugate eigenfrequency, grows with the core mode in order to conserve energy. In the low density limit, this mode corresponds to the corotating quadrupole mode, leading to oscillations in the surface shape of condensates. We always observed that the surface of condensates changed into a quadrupole shape as the two cores appeared, as shown in Fig. 3(a), and the ellipticity was larger at lower density.

The dynamical instability of the doubly quantized vortex state is related to the magnitude of the imaginary

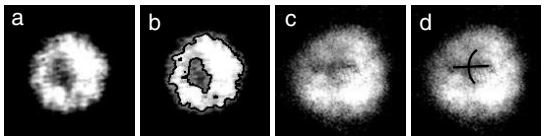

FIG. 4. Examples for the dynamic evolution after imprinting a doubly quantized vortex: (a) Surface excitation. Regular density modulation of the surface was observed after 51 ms hold time for $an_z = 1.8$. (b) Same as (a) with a contour line. (c) Crossing of vortex lines. 55 ms hold time and $an_z = 8.4$. (d) Same as (c) with guidelines for vortex lines. The field of view is 270 μm $\times$ 270 μm.

part of the complex eigenfrequency, and, according to the numeric calculation in Ref. [13], the nonvanishing imaginary part of the eigenfrequency appears at $an_z < 3$ and $an_z \sim 12$, showing a quasiperiodic behavior as a function of the interaction strength an_z. The experiment showed a monotonic increase of the lifetime with no hint of periodic behavior. However, the calculated instability is not directly comparable to the observed lifetime. The imaginary part represents only the initial instability. Our criterion for decay was the observation of two *separated* vortex cores. It is possible that the dynamical instability changes after the doubly quantized vortex state is significantly perturbed [7,14]. It would be helpful to have more inclusive calculations leading to a lifetime directly comparable with the experiments.

What is the further evolution of the two cores? Some of the images at low density showed a regular surface modulation, as in Fig. 4(a), which was not seen in clouds with a single core. This indicates that higher-order surface modes are excited during the coherent evolution [33]. Several images, especially those labeled as undetermined, suggest that vortex lines crossed [13,34], as in Fig. 4(c). In our system, it was difficult to trace the positions of the two cores beyond 80 ms hold time.

In conclusion, we observed how a doubly quantized vortex splits into a pair of singly quantized vortices, and found higher stability at higher atom density. The topological phase imprinting technique is unique in generating doubly quantized or quadruply quantized vortex states [19,35]; a key feature is the rapid preparation of well-determined vortex states, which gives access to their dynamical instabilities and coherent evolution.

This work was funded by ARO, NSF, ONR, and NASA. M. S. acknowledges additional support from the Swiss National Science Foundation and C. S. from the Studienstiftung des deutschen Volkes. We thank M. Möttönen and K. Machida for helpful discussions.

*Electronic address: http://cua.mit.edu/ketterle_group/

[1] P. Nozière and D. Pines, *The Theory of Quantum Liquids* (Addison-Wesley, Redwood City, 1990).
[2] C. J. Pethick and H. Smith, *Bose-Einstein Condensation in Dilute Gases* (Cambridge University Press, Cambridge, England 2002).
[3] D. S. Rokhsar, Phys. Rev. Lett. **79**, 2164 (1997).
[4] R. J. Dodd, K. Burnett, M. Edwards, and C.W. Clark, Phys. Rev. A **56**, 587 (1997).
[5] H. Pu, C. K. Law, J. H. Eberly, and N. P. Bigelow, Phys. Rev. A **59**, 1533 (1999).
[6] D. A. Butts and D. S. Rokhsar, Nature (London) **397**, 327 (1999).
[7] J. J. García-Ripoll and V. M. Pérez-García, Phys. Rev. A **60**, 4864 (1999).
[8] S. M. M. Virtanen, T. P. Simula, and M. M. Salomaa, Phys. Rev. Lett. **86**, 2704 (2001).
[9] M. R. Matthews, B. P. Anderson, P. C. Haljan, D. S. Hall, C. E. Wieman, and E. A. Cornell, Phys. Rev. Lett. **83**, 2498 (1999).
[10] K.W. Madison, F. Chevy, W. Wohlleben, and J. Dalibard, Phys. Rev. Lett. **84**, 806 (2000).
[11] J. R. Abo-Shaeer, C. Raman, J. M. Vogels, and W. Ketterle, Science **292**, 476 (2001).
[12] T. P. Simula, S. M. M. Virtanen, and M. M. Salomaa, Phys. Rev. A **65**, 033614 (2002).
[13] M. Möttönen, T. Mizushima, T. Isoshima, M. M. Salomaa, and K. Machida, Phys. Rev. A **68**, 023611 (2003).
[14] T. Isoshima, J. Huhtamäki, and M. M. Salomaa, Phys. Rev. A **68**, 033611 (2003).
[15] E. Lundh, Phys. Rev. A **65**, 043604 (2002).
[16] M. Baert, V.V. Metlushko, R. Jonckheere, V.V. Moshchalkov, and Y. Bruynseraede, Phys. Rev. Lett. **74**, 3269 (1995).
[17] R. Blaauwgeers, V. B. Eltsov, M. Krusius, J. J. Ruohio, R. Schanen, and G. E. Volovik, Nature (London) **404**, 471 (2000).
[18] T. Isoshima, M. Nakahara, T. Ohmi, and K. Machida, Phys. Rev. A **61**, 063610 (2002).
[19] A. E. Leanhardt, A. Görlitz, A. P. Chikkatur, D. Kielpinski, Y. Shin, D. E. Pritchard, and W. Ketterle, Phys. Rev. Lett. **89**, 190403 (2002).
[20] P. Engels, I. Coddington, P. C. Haljan, V. Schweikhard, and E. A. Cornell, Phys. Rev. Lett. **90**, 170405 (2003).
[21] U. A. Khawaja and H. Stoof, Nature (London) **411**, 918 (2001).
[22] J. Ruostekoski and J. R. Anglin, Phys. Rev. Lett. **91**, 190402 (2003).
[23] T. L. Gustavson, A. P. Chikkatur, A. E. Leanhardt, A. Görlitz, S. Gupta, D. E. Pritchard, and W. Ketterle, Phys. Rev. Lett. **88**, 020401 (2002).
[24] H. Ott, J. Fortagh, G. Schlotterbeck, A. Grossmann, and C. Zimmermann, Phys. Rev. Lett. **87**, 230401 (2001).
[25] W. Hänsel, P. Hommelhoff, T.W. Hänsch, and J. Reichel, Nature (London) **413**, 498 (2001).
[26] A. E. Leanhardt, A. P. Chikkatur, D. Kielpinski, Y. Shin, T. L. Gustavson, W. Ketterle, and D. E. Pritchard, Phys. Rev. Lett. **89**, 040401 (2002).
[27] W. Ketterle, D. S. Durfee, and D. M. Stamper-Kurn, in *Proceedings of the International School of Physics—Enrico Fermi*, edited by M. Inguscio, S. Stringari, and C. E. Wieman (IOS, Amsterdam, 1999).
[28] P. Rosenbusch, V. Bretin, and J. Dalibard, Phys. Rev. Lett. **89**, 200403 (2002).
[29] M. R. Andrews, C. G. Townsend, H.-J. Miesner, D. S. Durfee, D. M. Kurn, and W. Ketterle, Science **275**, 637 (1997).
[30] P. O. Fedichev and G. V. Shlyapnikov, Phys. Rev. A **60**, R1779 (1999).
[31] J. R. Anglin, Phys. Rev. A **67**, 051601 (2003).
[32] G. P. Agrawal, P. L. Baldeck, and R. R. Alfano, Phys. Rev. A **39**, 3406 (1989).
[33] K. Kasamatsu, M. Tsubota, and M. Ueda, Phys. Rev. A **67**, 033610 (2003).
[34] J. J. García-Ripoll and V. M. Pérez-García, Phys. Rev. A **64**, 053611 (2001).
[35] Y. Kawaguchi and T. Ohmi, cond-mat/0402553.

Bibliography

[1] Y. Shin, M. Saba, T. A. Pasquini, W. Ketterle, D. E. Pritchard, and A. E. Leanhart. Atom interferometry with Bose-Einstein condensates in a double-well potential. *Physical Review Letters*, 92:050405, February 2004.

[2] Y. Shin, M. Saba, A. Schirotzek, T.A. Pasquini, A. E. Leanhardt, D. E. Pritchard, and W. Ketterle. Distillation of Bose-Einstein condensates in a double-well potential. *Physical Review Letters*, 92:150401, April 2004.

[3] Y. Shin, M. Saba, M. Vengalattore, T. A. Pasquini, C. Sanner, A. E. Leanhardt, M. Prentiss, D. E. Pritchard, and W. Ketterle. Dynamical instability of a doubly quantized vortex in a Bose-Einstein condensate. *Physical Review Letters*, 93:160406, October 2004.

[4] Y. Shin, C. Sanner, G.-B. Jo, T. A. Pasquini, M. Saba, W. Ketterle, D. E. Pritchard, M. Vengalattore, and M. Prentiss. Interference of Bose-Einstein condensates split with an atom chip. *Pysical Review A*, 72:021604(R), August 2005.

[5] Y. Shin, G.-B. Jo, C. Sanner, M. Saba, T. A. Pasquini, K. Ketterle, and D. E. Pritchard. Optical weak link between two spatially separate Bose-Einstein condensates. *Physical Review Letters*, 95:170402, October 2005.

[6] A. E. Leanhardt, A. P. Chikkatur, D. Kielpinski, Y. Shin, T. L. Gustavson, W. Ketterle, and D. E. Pritchard. Propagation of Bose-Einstein condensates in a magnetic waveguide. *Physical Review Letters*, 89:040401, July 2002.

[7] A. P. Chikkatur, Y. Shin, A. E. Leanhardt, D. Kielpinski, E. Tsikata, T. L. Gustavson, D. E. Pritchard, and W. Ketterle. A continuous source of Bose-Einstein condensed atoms. *Science*, 296:2193, June 2002.

[8] A. E. Leanhardt, A. Görlitz, A. P. Chikkatur, D. Kielpinski, Y. Shin, D. E. Pritchard, and W. Ketterle. Imprinting vortices in a Bose-Einstein condensate using topological phases. *Physical Review Letters*, 89:190403, November 2002.

[9] A. E. Leanhardt, Y. Shin, A. P. Chikkatur, D. Kielpinski, W. Ketterle, and D. E. Pritchard. Bose-Einstein condensates near a microfabricated surface. *Physical Review Letters*, 90:100404, March 2003.

[10] A. E. Leanhardt, Y. Shin, D. Kielpinski, D. E. Pritchard, and W. Ketterle. Coreless vortex formation in a spinor Bose-Einstein condensate. *Physical Review Letters*, 90:140403, April 2003.

[11] M. Saba, T. A. Pasquini, C. Sanner, Y. Shin, W. Ketterle, and D. E. Pritchard. Light scattering to determine the relative phase of two Bose-Einstein condensates. *Science*, 307:1945, March 2005.

[12] S. N. Bose. Plancks gesetz und lichtquantenhypothese. *Zeitschrift fuer Physik*, 26:178, 1924.

[13] A. Einstein. Quantentheorie des einatomigen idealen gases - zweite abhandlung. *Sitzungsberichte der Preussischen Akademie der Wissenschaften*, Bericht 1:3, 1925.

[14] A. Griffin. A brief history of our understanding of BEC:From Bose to Beliaev. In M. Inguscio, S. Stringari, and C. E. Wieman, editors, *Bose-Einstein Condensation in Atomic Gases*, page 1, Amsterdam, 1999. IOS Press.

[15] M. H. Anderson, J. R. Ensher, M. R. Matthews, C. E. Wieman, and E. A. Cornell. Observation of Bose-Einstein condensation in a dilute atomic vapor. *Science*, 269:198, July 1995.

[16] M. R. Andrews, C. G. Townsend, H.-J. Miesner, D. S. Durfee, D. M. Kurn, and W. Ketterle. Observation of interference between two Bose condensates. *Science*, 275:637, January 1997.

[17] M. R. Matthews, B. P. Anderson, P. C. Haljan, D. S. Hall, C. E. Wieman, and E. A. Cornell. Vortices in a Bose-Einstein condensate. *Physical Review Letters*, 83:2498, August 1999.

[18] K. W. Madison, F. Chevy, W. Wohlleben, and J. Dalibard. Vortex formation in a stirred Bose-Einstein condensate. *Physical Review Letters*, 84:806, January 2000.

[19] J. R. Abo-Shaeer, C. Raman, J. M. Vogels, and W. Ketterle. Observation of vortex lattices in Bose-Einstein condensates. *Science*, 292:496, April 2001.

[20] E. A. Cornell and C. E. Wieman. Nobel lecture: Bose-Einstein condensation in a dilute gas, the first 70 years and some recent experiments. *Reviews of Modern Physics*, 74:875, July 2002.

[21] W. Ketterle. Nobel lecture: When atoms behave as waves: Bose-Einstein condensation and the atom laser. *Reviews of Modern Physics*, 74:1131, October 2002.

[22] M. Inguscio, S. Stringari, and C. E. Wieman, editors. *Bose-Einstein Condensation in Atomic Gases*. IOS Press, Amsterdam, 1999.

[23] J. R. Anglin and W. Ketterle. Bose-Einstein condensation of atomic gases. *Nature*, 416:211, March 2002.

[24] K. B. Davis, M.-O. Mewes, M. R. Andrews, N. J. van Druten, D. S. Durfee, D. M. Kurn, and W. Ketterle. Bose-Einstein condensation in a gas of sodium atoms. *Physical Review Letters*, 75:3969, November 1995.

[25] C. C. Bradley, C. A. Sackett, J. J. Tollett, and R. G. Hulet. Evidence of Bose-Einstein condensation in an atomic gas with attractive interactions. *Physical Review Letters*, 75:1687, August 1995.

[26] C. C. Bradley, C. A. Sackett, and R. G. Hulet. Bose-Einstein condensation of lithium: Observation of limited condensate number. *Physical Review Letters*, 78:985, Februrary 1997.

[27] D. G. Fried, T. C. Killian, L. Willmann, D. Landhuis, S. C. Moss, D. Kleppner, and T. J. Greytak. Bose-Einstein condensation of atomic hydrogen. *Physical Review Letters*, 81:3811, November 1998.

[28] S. L. Cornish, N. R. Claussen, J. L. Roberts, E. A. Cornell, and C. E. Wieman. Stable ^{85}Rb Bose-Einstein condensates with widely tunable interactions. *Physical Review Letters*, 85:1795, August 2000.

[29] A. Robert, O. Sirjean, A. Browaeys, J. Poupard, S. Nowak, D. Boiron, C. I. Westbrook, and A. Aspect. A Bose-Einstein condensate of metastable atoms. *Science*, 292:461, April 2001.

[30] F. Pereira Dos Santos, J. Léonard, J. Wang, C. J. Barrelet, F. Perales, E. Rasel, C. S. Unnikrishnin, M. Leduc, and C. Cohen-Tannoudji. Bose-Einstein condensation of metastable helium. *Physical Review Letters*, 86:3459, April 2001.

[31] G. Modugno, G. Ferrari, G. Roati, R. J. Brecha, A. Simoni, and M. Inguscio. Bose-Einstein condensation of potassium atoms by sympathetic cooling. *Science*, 294:1320, November 2001.

[32] T. Weber, J. Herbig, M. Mark, H.-C. Nägerl, and R. Grimm. Bose-Einstein condensation of cesium. *Science*, 299:232, January 2003.

[33] Axel Griesmaier, Jörg Werner, Sven Hensler, Jürger Stuhler, and Tilman Pfau. Bose-Einstein condensation of chromium. *Physical Review Letters*, 94:160401, April 2005.

[34] T.-L. Ho. Spinor Bose condensates in optical traps. *Physical Review Letters*, 81:742, July 1998.

[35] T. Ohmi and K. Machida. Bose-Einstein condensation with internal degrees of freedom in alkali atom gases. *Journal of the Physical Society of Japan*, 67:1822, June 1998.

[36] J. Stenger, S. Inouye, D. M. Stamper-Kurn, H.-J. Miesner, A. P. Chikkatur, and W. Ketterle. Spin domains in ground-state Bose-Einstein condensates. *Nature*, 396:345, November 1998.

[37] B. P. Anderson and M. A. Kasevich. Macroscopic quantum interference from atomic tunnel arrays. *Science*, 282:1686, November 1998.

[38] M. Greiner, O. Mandel, T. Esslinger, T. W. Hänsch, and I. Bloch. Quantum phase transition from a superfluid to a Mott insulator in a gas of ultracold atoms. *Nature*, 415:39, January 2002.

[39] S. Dettmer, D. Hellweg, P. Ryytty, J. J. Arlt, W. Ertmer, K. Sengstock, D. S. Petrov, G. V. Shlyapnikov, H. Kreutzmann, L. Santos, and M. Lewenstein. Observation of phase fluctuations in elongated Bose-Einstein condensates. *Physical Review Letters*, 87:160406, October 2001.

[40] A. Görlitz, J. M. Vogels, A. E. Leanhardt, C. Raman, T. L. Gustavson, J. R. Abo-Shaeer, A. P. Chikkatur, S. Gupta, S. Inouye, T. Rosenband, and W. Ketterle. Realization of Bose-Einstein condensates in lower dimensions. *Physical Review Letters*, 87:130402, September 2001.

[41] D. Hellweg, L. Cacciapuoti, M. Kottke, T. Schulte, K. Sengstock, W. Ertmer, and J. J. Arlt. Measurement of the spatial correlation function of phase fluctuating Bose-Einstein condensates. *Physical Review Letters*, 91:010406, July 2003.

[42] S. Richard, F. Gerbier, J. H. Thywissen, M. Hugbart, P. Bouyer, and A. Aspect. Momentum spectroscopy of 1D phase fluctuations in Bose-Einstein condensates. *Physical Review Letters*, 91:010405, July 2003.

[43] T. Kinoshita, T. Wenger, and D. S. Weiss. Observation of a one-dimensional Tonk-Girardeau gas. *Science*, 305:1125, July 2004.

[44] B. DeMarco and D. S. Jin. Onset of Fermi degeneracy in a trapped atomic gas. *Science*, 285:1703, September 1999.

[45] A. G. Truscott, K. E. Strecker, W. I. McAlexander, G. B. Partridge, and R. G. Hulet. Observation of Fermi pressure in a gas of trapped atoms. *Science*, 291:2570, March 2001.

[46] F. Reif. *Fundamentals of statistical and thermal physics*. McGraw-Hill, 1965.

[47] J. M. Leinaas and Myrheim J. On the theory of identical particles. *Nuovo Cimento So. Ital. fis.*, 37B:1–23, January 1977.

[48] F. E. Camino, W. Zhou, and V. J. Goldman. Direct observation of fractional statistics in two dimensions. *arXiv:con-mat/0502406*, 2005.

[49] M. E. Peskin and D. V. Schroeder. *An Introduction to Quantum Field Theory*. Perseus Books, Cambridge, Massachusetts, 1995.

[50] W. Pauli. The connection between spin and statistics. *Physical Review*, 58:716–722, August 1940.

[51] R. F. Streater and A. S. Wightman. *PCT, Spin and Statistics, and All That*. Benjamin, New York, 1964.

[52] O. Penrose and L. Onsager. Bose-Einstein condensation and liquid helium. *Physical Review*, 104:576, November 1956.

[53] C. N. Yang. Concept of off-diagonal long-range order and the quantum phases of liquid He and of superconductors. *Reviews of Modern Physics*, 34:694, October 1962.

[54] K. Huang. *Statistical Mechanics*. John Wiley & Sons, 1987.

[55] F. London. The λ-phenomenon of liquid helium and the Bose-Einstein degeneracy. *Nature*, 141:643, April 1938.

[56] P. Anderson. *Basic Notions of Condensed Matter Physics*. Perseus Books Group, second edition, 1997.

[57] L. D. Landau and E. M. Lifshitz. *Statistical Physics Part I.* Butterworth-Heinemann, Oxford, third edition, 1980.

[58] W. Ketterle, D. S. Durfee, and D. M. Stamper-Kurn. Making, probing and understanding Bose-Einstein condensates. In M. Inguscio, S. Stringari, and C. E. Wieman, editors, *Bose-Einstein Condensation in Atomic Gases*, page 67, Amsterdam, 1999. IOS Press.

[59] F. A. van Abeelen and B. J. Verhaar. Determination of collisional properties of cold Na atoms from analysis of bound-state photoassociation and Feshbach resonance field data. *Physical Review A*, 59:578, January 1999.

[60] A. J. Leggett. Bose-Einstein condensation in the alkali gases: Some fundamental concepts. *Reviews of Modern Physics*, 73:307, April 2001.

[61] A. S. Parkins and D. F. Walls. The physics of trapped dilute-gas Bose-Einstein condensates. *Physics Reports*, 303:1, 1997.

[62] F. Dalfovo, S. Giorgini, L. P. Pitaevskii, and S. Stringari. Theory of Bose-Einstein condensation in trapped gases. *Reviews of Modern Physics*, 71:463, April 1998.

[63] S. Inouye, T. Pfau, S. Gupta, A. P. Chikkatur, A. Görlitz, D. E. Pritchard, and W. Ketterle. Phase-coherent amplification of atomic matter waves. *Nature*, 402:641, December 1999.

[64] L. Deng, E. W. Hagley, J. Wen, M. Trippenbach, Y. Band, P. S. Julienne, J. E. Simsarian, K. Helmerson, S. L. Rolston, and W. D. Phillips. Four-wave mixing with matter waves. *Nature*, 398:218, March 1999.

[65] J. M. Vogels, K. Xu, and W. Ketterle. Generation of macroscopic pair-correlated atomic beams by four-wave mixing in Bose-Einstein condensates. *Physical Review Letters*, 89:020401, July 2002.

[66] B. P. Anderson, P. C. Haljan, C. A. Regal, D. L. Feder, L. A. Collins, C. W. Clark, and E. A. Cornell. Watching dark solitons decay into vortex rings in a Bose-Einstein condensate. *Physical Review Letters*, 86:2926, April 2001.

[67] P. W. Anderson. Special effects in superconductivity. In E. R. Caianiello, editor, *Lectures on The Many-Body Problem*, volume 2, page 113, New York, 1964. Academic Press.

[68] J. Javanainen and S. M. Yoo. Quantum phase of a Bose-Einstein condensate with an arbitrary number of atoms. *Physical Review Letters*, 76:161, January 1996.

[69] K. Mølmer. Optical coherence: a convenient fiction. *Physical Review A*, 55:3195, April 1997.

[70] C. W. Gardiner. Particle-number-conserving bogoliubov method which demonstrates the validity of the time-dependent gross-pitaevskii equation for a highly condensed Bose gas. *Physical Review A*, 56:1414, August 1997.

[71] Y. Castin and R. Dum. Low-temperature Bose-Einstein condensate in time-dependent traps: Beyond the $u(1)$ symmetry-breaking approach. *Physical Review A*, 57:3008, April 1998.

[72] S. Stenholm. The question of phase in a Bose-Einstein condensate. *Physica Scripta*, T102:89, 2002.

[73] J. A. Dunningham and K. Burnett. Phase standard for Bose-Einstein condensates. *Physical Review Letters*, 82:3729, May 1999.

[74] E. H. Lieb, R. Seiringer, and J. Yngvason. Justification of c-number substitutions in bosonic hamiltonian. *Physical Review Letters*, 94:080401, March 2005.

[75] A. Sütő. Equivalence of Bose-Einstein condensation and symmetry breaking. *Physical Review Letters*, 94:080402, March 2005.

[76] W. Ketterle, K. B. Davis, M. A. Joffe, A. Martin, and D. E. Pritchard. High densities of cold atoms in a *dark* spontaneous-force optical trap. *Physical Review Letters*, 70:2253, April 1991.

[77] W. Petrich, M. H. Anderson, J. R. Ensher, and E. A. Cornell. Stable, tightly confining magnetic trap for evaporative cooling of neutral atoms. *Physical Review Letters*, 74:3352, April 1995.

[78] M. D. Barrett, J. A. Sauer, and M. S. Chapman. All-optical formation of an atomic Bose-Einstein condensate. *Physical Review Letters*, 8:010404, June 2001.

[79] H. Ott, J. Fortagh, G. Schlotterbeck, A. Grossmann, and C. Zimmermann. Bose-Einstein condensation in a surface microtrap. *Physical Review Letters*, 87(23):230401, December 2001.

[80] W. Hänsel, P. Hommelhoff, T. W. Hänsch, and J. Reichel. Bose-Einstein condensation of a microelectric chip. *Nature*, 413:498–501, October 2001.

[81] A. P. Chikkatur. *Colliding and Moving Bose-Einstein Condensates: Studies of superfluidity and optical tweezers for condensate transport*. Ph.D. Thesis, Massachusetts Institute of Technology, October 2002.

[82] D. M. Stamper-Kurn. *Peeking and poking at a new quantum fluid: Studies of gaseous Bose-Einstein condensates in magnetic and optical traps*. Ph.D. Thesis, Massachusetts Institute of Technology, February 2000.

[83] E. L. Raab, M. Prentiss, A. Cable, S. Chu, and D. E. Pritchard. Trapping of neutral sodium atoms with radiation pressure. *Physical Review Letters*, 59:2631, December 1987.

[84] S. Chu. The manipulation of neutral particles. *Review of Modern Physics*, 70:685, July 1998.

[85] C. N. Cohen-Tannoudji. Manipulating atoms with photons. *Review of Modern Physics*, 70:707, July 1998.

[86] W. D. Phillips. Laser cooling and trapping of neutral atoms. *Review of Modern Physics*, 70:721, July 1998.

[87] H. J. Metcalf and P. van der Straten. *Laser Cooling and Trapping*. Springer-Verlag, New York, 1999.

[88] T. W. Hänsch, I. S. Shahin, and A. L. Schawlow. High-resolution saturation spectroscopy of the sodium D lines with a pulsed tunable dye laser. *Physical Review Letters*, 27:707, September 1971.

[89] R. Grimm, M. Weidemüller, and Y. B. Ovchinnikov. Optical dipole traps for neutral atoms. *Advances in Atomic, Molecular, and Optical Physics*, 42:95, 2000.

[90] O. Mandel, M. Greiner, A. Widera, T. Rom, T. W. Hänsch, and I. Bloch. Coherent transport of neutral atoms in spin-dependent optical lattice potentials. *Physical Review Letters*, 91:010407, July 2003.

[91] P. Nozières and D. Pines. *The Theory of Quantum Liquids*. Perseus Books Publishing, 1999.

[92] J. Stenger, S. Inouye, A. P. Chikkatur, D. M. Stamper-Kurn, D. E. Pritchard, and W. Ketterle. Bragg spectroscopy of a Bose-Einstein condensate. *Physical Review Letters*, 82:004569, June 1999.

[93] S. Inouye, M. R. Andrews, J. Stenger, H.-J. Miesner, D. M. Stamper-Kurn, and W. Ketterle. Observation of Feshbach resonances in a Bose-Einstein condensate. *Nature*, 392:151, March 1998.

[94] M. R. Andrews, M.-O. Mewes, N. J. van Druten, D. S. Durfee, D. M. Kurn, and W. Ketterle. Direct, nondestructive observation of a Bose condesate. *Science*, 273:84, 1996.

[95] R. Folman and J. Schmiedmayer. Matering the language of atoms. *Nature*, 413:466, October 2001.

[96] D. Müller, D. Z. Anderson, R. J. Grow, P. D. D. Schwindt, and E. A. Cornell. Guiding neutral atoms around curves with lithographically patterned current-carrying wires. *Physical Review Letters*, 83:5194, December 1999.

[97] N. H. Dekker, C. S. Lee, V. Lorent, J. H. Thywissen, S. P. Smith, M. Drndić, R. M. Westervelt, and M. Prentiss. Guiding neutral atoms on a chip. *Physical Review Letters*, 84:1124, February 2000.

[98] J. Reichel, W. Hänsel, and T. W. Hänsch. Atomic micromanipulation with magnetic surface traps. *Physical Reveiw Letters*, 83:3398, October 1999.

[99] R. Folman, P. Krüger, D. Cassettari, B. Hessmo, T. Maier, and J. Schmiedmayer. Controlloing cold atoms using nanofabricated surfaces: Atom chips. *Physical Review Letters*, 84:4749, May 2000.

[100] D. Cassettari, B. Hessmo, R. Folman, T. Maier, and J. Schmiedmayer. Beam splitter for guided atoms. *Physical Review Letters*, 85:5483, December 2000.

[101] H. Ott, J. Fortágh, S. Kraft, A. Günther, D. Komma, and C. Zimmermann. Nonlinear dynamics of a Bose-Einstein condesate in a magnetic waveguide. *Physical Review Letters*, 91:040402, July 2003.

[102] Y.-J. Wang, D. Z. Anderson, V. M. Bright, E. A. Cornell, Q. Diot, T. Kishimoto, M. Prentiss, R. A. Saravanan, S. R. Segal, and S. Wu. An atom michelson interferometer on a chip using a Bose-Einstein condensate. *Physical Review Letters*, 94:090405, March 2005.

[103] T. Schumm, S. Hofferberth, L. M. Andersson, S. Wildermuth, S. Groth, I. Bar-Joseph, J. Schmiedmayer, and P. Krüger. Matter wave interferometry in a double well on an atom chip. *Nature Physics*, 1:57, October 2005.

[104] E. A. Hinds and I. G. Hughes. Magnetic atom optics: mirrors, guides, traps, and chips for atoms. *Journal of Physics D: Appled Physics*, 32:R119, September 1999.

[105] R. Folman, P. Krüger, J. Schmiedmayer, J. Denschlag, and C. Henkel. Microscopic atom optics: From wire to an atom chip. *Advances in Atomic, Molecular, and Optical Physics*, 48:263, 2002.

[106] I. Brodie and J. J. Muray. *The Physics of Micro/Nano-Fabricatoin*. Plenum Press, New York, 1992.

[107] J. Fortágh, H. Ott, S. Kraft, A. Günther, and C. Zimmermann. Surface effects in magnetic microtraps. *Physical Review A*, 66:041604(R), October 2002.

[108] M. P. A. Jones, C. J. Vale, D. Sahagun, B. V. Hall, and E. A. Hinds. Spin coupling between cold atoms and the thermal fluctuations of a metal surface. *Physical Review Letters*, 91:080401, August 2003.

[109] S. Kraft, A. Günther, H. Ott, D. Wharam, C. Zimmermann, and J. Fortágh. Anomalous longitudinal magnetic field near the surface of copper conductors. *Journal of Physics B: Atomic, Molecular and Optical Physics*, 35:L469, November 2002.

[110] M. P. A. Jones, C. J. Vale, D. Sahagun, B. V. Hall, C. C. Eberlein, B. E. Sauer, K. Furusawa, D. Richardson, and E. A. Hinds. Cold atoms probe the magnetic field near a wire. *Journal of Physics B: Atomic, Molecular and Optical Physics*, 37:L15, January 2004.

[111] J. Estève, C. Aussibal, T. Schumm, C. Figl, D. Mailly, I. Bouchoule, I. Westbrook, and A. Aspect. Role of wire imperfections in micromagnetic traps for atoms. *Physical Review A*, 70:043629, October 2004.

[112] T. Schumm, J. Estève, C. Figl, J.-B. Trebbia, C. Aussibal, H. Nguyen, D. Mailly, I. Bouchoule, C. I. Westbrook, and A. Aspect. Atom chips in the real world: the effects of wire currugation. *European Physics Journal D*, 32:171, 2005 2005.

[113] J. R. Lloyd. Electromigration in integrated circuit conductors. *Journal of Physics D: Applied Physics*, 32:R109, 1999.

[114] B. D. Schrag and G. Xiao. Submicron electrical current density imaging of embedded microstructure. *Applied Physics Letters*, 82:3272, May 2003.

[115] P. Krüger, L. M. Andersson, S. Wildermuth, S. Hofferberth, E. Haller, S. Aigner, S. Groth, I. Bar-Joseph, and J. Schmiedmayer. Disorder potentials near lithographically fabricated atom chips. *arXiv:cond-mat/0504686*, April 2005.

[116] T. Varpula and T. Poutanen. Magnetic field fluctuations arising from thermal motion of electric charge in conductors. *Journal of Applied Physics*, 55:4015, June 1984.

[117] J. M. McGuirk, D. M. Harber, J. M. Obrecht, and E. A. Cornell. Alkali-metal adsorbate polarization on conducting and insulating surfaces probed with Bose-Einstein condensates. *Physical Review A*, 69:062905, June 2004.

[118] Y.-J. Lin, I. Teper, C. Chin, and V. Vuletić. Impact of Casimir-Polder potential on Johnson noise on Bose-Einstein condensate stability near surfaces. *Physical Reveiw Letters*, 92:050404, February 2004.

[119] C. Henkel and M. Wilkins. Heating of trapped atoms near thermal surfaces. *Europhysics Letters*, 47:414, August 1999.

[120] C. Henkel, S. Pötting, and M. Wilkens. Loss and heating of particles in small and noisy traps. *Applid Physics B*, 69:379, December 1999.

[121] C. Henkel and S. Pötting. Coherent transport of matter waves. *Applied Physics B*, 72:73–80, January 2001.

[122] C. Henkel, P. Krüger, R. Folman, and J. Schmiedmayer. Fundamental limits for coherent manipulation on atom chips. *Applied Physics B*, 76:173–182, February 2003.

[123] C. Henkel and S. A. Gardiner. Decoherence of Bose-Einstein condensates in microtraps. *Physical Review A*, 69:043602, April 2004.

[124] C. Schroll, W. Belzig, and C. Bruder. Decoherence of cold atomic gases in magnetic microtraps. *Physical Review A*, 68:043618, October 2003.

[125] P. Treutlein, P. Hommelhoff, T. Steinmetz, T. W. Hänsch, and J. Reichel. Coherence in microchip traps. *Physical Review Letters*, 92:203005, May 2004.

[126] V. Dicovsky, Y. Japha, C. Henkel, and R. Folman. Reduction of magnetic noise in atom chips by material optimization. *European Physics Journal D*, 35:87, July 2005.

[127] M. Drndić, K. S. Johnson, J. H. Thywissen, M. Prentiss, and R. M. Westervelt. Micro-electromagnets for atom manipulation. *Applied Physics Letters*, 72:2906, June 1998.

[128] S. Groth, P. Krüger, S. Wildermuth, R. Folman, T. Fernholz, J. Schmiedmayer, M. Mahalu, and I. Bar-Joseph. Atom chips: Fabrication and thermal properties. *Applied Physics Letters*, 85:2980, October 2004.

[129] E. A. Hinds, C. J. Vale, and M. G. Boshier. Two-wire waveguide and interferometer for cold atoms. *Physical Review Letters*, 86:1462, February 2001.

[130] A. Peters, K. Y. Chung, B. Young, J. Hensley, and S. Chu. Precision atom interferometry. *Philosophical Transactions of the Royal Society of London A*, 355:2223, 1997.

[131] A. Lenef, T. D. Hammond, E. T. Smith, M. S. Chapman, R. A. Rubenstein, and D. E. Pritchard. Rotation sensing with an atom interferometer. *Physical Review Letters*, 78:760, February 1997.

[132] T. L. Gustavson, P. Bouyer, and M. A. Kasevich. Precision rotation measurements with an atom interferometer gyroscope. *Physical Review Letters*, 78:2046, March 1997.

[133] M. S. Chapman, T. D. Hammond, A. Lenef, J. Schmiedmayer, R. A. Rubenstein, E. Smith, and D. E. Pritchard. Photon scattering from atoms in an atom interferometer: Coherence lost and regained. *Physical Review Letters*, 75:3783, November 1995.

[134] C. R. Ekstrom, J. Schmiedmayer, M. S. Chapman, T. D. Hammond, and D. E. Pritchard. Measurement of the electric polarizability of sodium with an atom interferometer. *Physical Review A*, 51:3883, May 1995.

[135] S. Gupta, K. Dieckmann, Z. Hadzibabic, and D. E. Pritchard. Contrast interferometry using Bose-Einstein condensates to measure h/m and α. *Physical Review Letters*, 89:140401, September 2002.

[136] W. Hänsel, J. Reichel, P. Hommelhoff, and T. W. Hänsch. Trapped-atom interferometer in a magnetic microtrap. *Physical Review A*, 64:063607, 2001.

[137] E. Andersson, T. Calarco, R. Folman, M. Andersson, B. Hessmo, and J. Schmiedmayer. Multimode interferometer for guided matter waves. *Physical Review Letters*, 88:100401, March 2002.

[138] J. Javanainen and M. Wilkens. Phase and phase diffusion of a split Bose-Ephysical review lettersinstein condensate. *Physical Review Letters*, 78:4675, June 1997.

[139] A. J. Leggett and F. Sols. Comment on "phase and phase diffusion of a split Bose-Einstein condensate". *Physical Review Letters*, 81:1344, August 1998.

[140] J. Javanainen and M. Wilkens. *Physical Review Letters*, 81:1345, August 1998.

[141] C. Menotti, J. R. Anglin, J. I. Cirac, and P. Zoller. Dynamic splitting of a Bose-Einstein condensate. *Physical Review A*, 63:023601, 2001.

[142] P. J. Martin, B. G. Oldaker, A. H. Miklich, and D. E. Pritchard. Bragg scattering of atoms from a standing light wave. *Physical Review Letters*, 60:515, February 1988.

[143] M. Olshanii and V. Dunjko. Interferometry in dense nonlinear media and interaction-induced loss of contrast in microfabricated atom interferometers. *arXiv:cond-mat/0505358*, 2005.

[144] B. D. Josephson. Possible new effects in superconductive tunneling. *Physics Letters*, 1:251, July 1962.

[145] R. W. Spekkens and J. E. Sipe. Spatial fragmentation of a Bose-Einstein condensate in a double-well potential. *Physical Review A*, 59:3868, May 1999.

[146] J. Javanainen and M. Y. Ivanov. Splitting a trap containing a Bose-Einstein condensate: Atom number fluctuations. *Physical Review A*, 60:2351, September 1999.

[147] A. Smerzi, S. Fantoni, S. Giovanazzi, and S. R. Shenoy. Quantum coherent atomic tunneling between two trapped Bose-Einstein condensates. *Physical Review Letters*, 79:4950, December 1997.

[148] S. Raghavan, A. Smerzi, S. Fantoni, and S. R. Shenoy. Coherent oscillations between two weakly coupled Bose-Einstein condensates: Josephson effects, π oscillations, and macroscopic quantum self-trapping. *Pysical Review A*, 59:620, January 1999.

[149] M. Lewenstein and L. You. Quantum phase diffusion of a Bose-Einstein condensate. *Physical Review Letters*, 77:3489, October 1996.

[150] J. A. Dunningham, M. J. Collett, and D. F. Walls. Quantum state of a trapped Bose-Einstein condensate. *Physics Letters A*, 245:49, August 1998.

[151] L. A. Collins, L. Pezzé, A. Smerzi, G. P. Berman, and A. R. Bishop. Double-slit interferometry with a bose-einstein condensate. *Physical Review A*, 71:033628, March 2005.

[152] James A. Stickney and Alex A. Zozulya. Wave-function recombination instability in cold-atom interferometers. *Phys. Rev. A*, 66:053601, 2002.

[153] D. M. Harber, J. M. Obrecht, J. M. McGuirk, and E. A. Cornell. Measurement of the casimir-polder force through center-of-mass oscillations of a Bose-Einstein condensate. *Physical Review A*, 72:033610, September 2005.

[154] S. Inouye, S. Gupta, T. Rosenbend, A. P. Chikkatur, A. Görlitz, T. L. Gustavson, A. E. Leanhardt, D. E. Pritchard, and W. Ketterle. Observation of vortex phase singularities in Bose-Einstein condensates. *Physical Review Letters*, 87:080402, August 2001.

[155] J. Estève, T. Schumm, J.-B. Trebbia, I. Bouchoule, A. Aspect, and C. I. Westbrook. Realizing a stable magnetic double-well potential on an atom chip. *European Physical Journal D*, 35:141, July 2005.

[156] O. Zobay and B. M. Garraway. Two-dimensional atom trapping in field-induced adiabatic potentials. *Physical Review Letters*, 86:1195, February 2001.

[157] M. Albiez, R. Gati, J. Fölling, S. Hunsmann, M. Cristiani, and M. K. Oberthaler. Direct observation of tunneling and nonlinear self-trapping in a single Bosonic Josephson junction. *Physical Review Letters*, 95:010402, July 2005.

[158] M.-O. Mewes, M. R. Andrews, D. M. Kurn, D. S. Durfee, C. G. Townsend, and W. Ketterle. Output coupler for Bose-Einstein condensed atoms. *Physical Review Letters*, 78:582, January 1997.

[159] E. W. Hagley, L. Deng, M. Kozuma, J. Wen, K. Helmerson, S. L. Rolston, and W. D. Phillips. Quasi-continuous atom laser. *Science*, 283:1706, March 1999.

[160] I. Bloch, W. Hänsch, and T. Esslinger. Atom laser with a cw output coupler. *Physical Review Letters*, 82:3008, april 1999.

[161] I. Bloch, T. W. Hänsch, and T. Esslinger. Measurement of the spatial coherence of a trapped Bose gas at the phase transition. *Nature*, 403:166, January 2000.

[162] M. Kasevich. Atom inteferometry with Bose-Einstein condensed atoms. *Comptes Rendus de l'Académie des Sciences Série IV*, 2:497, April 2001.

[163] J. M. Geremia, J. K. Stockton, and H. Mabuchi. Real-time quantum feedback control of atomic spin-squeezing. *Science*, 304:270, April 2004.

[164] Y. Castin and J. Dalibard. Relative phase of two Bose-Einstein condensates. *Physical Review A*, 55:4330, June 1997.

[165] J. A. Wheeler and W. H. Zurek. *Quantum Theory of Measurement*. Princeton University Press, Princeton, NJ, 1983.

[166] L. Pitaevskii and S. Stringari. Interference of Bose-Einstein condensates in momentum space. *Physical Review Letters*, 83:4237, November 1999.

[167] Miye Park. *How to Grow Our Nigella*. (private communication), Boston, MA, 2005.

[168] C. Cohen-Tannoudji. Review on fundamental processes in laser cooling. In M. Ducloy and E. Giacobino, editors, *Laser Spectroscopy X*, page 3, Singapore, 1992. World Scientific.

[169] K. Rzążewski and W. Żakowicz. Spontaneous emission from an extended wave packet. *Journal of Physics B*, 25:L319, 1992.

[170] B. Dubetsky and P. R. Berman. Spectrum of light scattering from an extended atomic wave packet. *Journal of Modern Optics*, 49:55, March 2002.

[171] J. M. Vogels, J. K. Chin, and W. Ketterle. Coherent collisions between Bose-Einstein condensates. *Physical Review Letters*, 90:030403, January 2003.

[172] Y. Le Coq, J. H. Thywissen, S. A. Rangwala, F. Gerbier, S. Richard, G. Delannoy, P. Bouyer, and A. Aspect. Atom laser divergence. *Physical Review Leters*, 87:170403, October 2001.

[173] P. W. Anderson and J. W. Rowell. Probable observation of the Josephson superconducting tunneling effect. *Physical Review Letters*, 10:230, March 1963.

[174] S. V. Pereverzev, A. Loshak, S. Backhaus, J. C. Davis, and R. E. Packard. Quantum oscillations between two weakly coupled resrvoirs of superfluid ^{3}He. *Nature*, 388:449, July 1997.

[175] F. S. Cataliotti, S. Burger, C. Fort, P. Maddaloni, F. Minardi, A. Trombettoni, A. Smerzi, and M. Inguscio. Josephson junction arrays with Bose-Einstein condensates. *Science*, 293:843, August 2001.

[176] J. Williams, R. Walser, J. Cooper, E. Cornell, and M. Holland. Nonlinear Josephson-type oscillations of a driven, two-component Bose-Einstein condensate. *Physical Review A*, 59:R31, January 1999.

[177] P. Öhber and S. Stenholm. Internal Josephson effect in trapped double codensates. *Physical Review A*, 59:3890, May 1999.

[178] A. Imamoglu and T. A. B. Kennedy. Optical measurements of the condensate phase. *Physical Review A*, 55:R849, February 1997.

[179] V. M. Kaurov and A. B. Kuklov. Josephson vortex between two atomic Bose-Einstein condesates. *Physical Review A*, 71:011601(R), January 2005.

[180] I. Bouchoule. Modulational instabilities in Josephson oscillations of elongated coupled condensates. *European Physical Journal D*, 35:147, June 2005.

[181] J. A. Sauer, M. D. Barrett, and M. S. Chapman. Storage ring for neutral atoms. *Physical Review Letters*, 87:270401, December 2001.

[182] S. Gupta, K. W. Murch, K. L. Moore, T. P. Purdy, and D. M. Stamper-Kurn. Bose-Einstein condensation in a circular waveguide. *Physical Review Letters*, 95:143201, September 2005.

[183] A. S. Arnold, C. S. Garvie, and E. Riis. A condensate storage ring. *arXiv:cond-mat/0506142*, June 2005.

[184] H.-J. Miesner, D. M. Stamper-Kurn, M. R. Andrews, D. S. Durfee, S. Inouye, and W. Ketterle. Bosonic stimulation in the formation of a Bose-Einstein condensate. *Science*, 279:1005, February 1998.

[185] J. M. Gerton, D. Strekalov, I. Prodan, and R. G. Hulet. Direct observation of growth and collapse of a Bose-Einstein condensate with attractive interactions. *Nature*, 408:692, December 2000.

[186] I. Shvarchuck, Ch. Buggle, D. S. Petrov, K. Dieckmann, M. Zielonkowski, M. Kemmann, T. G. Tiecke, W. von Klitzing, G. V. Shlyapnikov, and J. T. M. Walraven. Bose-Einstein condensation into nonequilibrium states studied by condensate focusing. *Physical Review Letters*, 89:270404, December 2002.

[187] C. W. Gardiner, M. D. Lee, R. J. Ballagh, M. J. Davis, and P. Zoller. Quantum kinetic theory of condensate growth: Comparison of experiment and theory. *Physical Review Letters*, 81:5266, December 1998.

[188] M. Köhl, M. J. Davis, C. W. Gardiner, T. W. Hänsch, and T. Esslinger. Growth of Bose-Einstein condensates from thermal vapor. *Physical Review Letters*, 88:080402, February 2002.

[189] W. Ketterle and N. J. van Druten. Evaporative cooling of trapped atoms. *Advances in Atomic, Molecular, and Optical Physics*, 37:181, 1996.

[190] H.-J. Miesner, D. M. Stamper-Kurn, J. Stenger, S. Inouye, A. P. Chikkatur, and W. Ketterle. Observation of metastable states in spinor Bose-Einstein condensates. *Physical Review Letters*, 82:2228, March 1999.

[191] D. M. Stamper-Kurn, H.-J. Miesner, A. P. Chikkatur, S. Inouye, J. Stenger, and W. Ketterle. Quantum tunneling across spin domains in a Bose-Einstein condensate. *Physical Review Letters*, 83:661, July 1999.

[192] H. Schmaljohann, M. Erhard, J. Kronjäger, M. Kottke, S. van Staa, K. Arlt, J. Bongs, and K. Sengstock. Dynamics of $F = 2$ spinor Bose-Einstein condensates. *Physical Review Letters*, 92:040402, January 2004.

[193] M.-S. Chang, C. D. Hamley, M. D. Barrett, J. A. Sauer, K. M. Fortier, W. Zhang, L. You, and M. S. Chapman. Observation of spinor dynamics in optically trapped 87rb Bose-Einstein condensates. *Physical Review Letters*, 92:140403, April 2004.

[194] H. J. Lewandowski, J. M. McGuirk, D. M. Harber, and E. A. Cornell. Decoherence-driven cooling of a degenerate spinor Bose gas. *Physical Review Letters*, 91:240404, December 2003.

[195] M. Erhard, H. Schmaljohann, J. Kronjäger, K. Bongs, and K. Sengstock. Bose-Einstein condensation at constant temperature. *Physical Review A*, 70:031602(R), September 2004.

[196] S. Giovanazzi, A. Smerzi, and S. Fantoni. Josephson effects in dilute Bose-Einstein condensates. *Physical Review Letters*, 84:4521, May 2000.

[197] L. Pitaevskii and S. Stringari. Thermal vs quantum decoherence in double well trapped Bose-Einstein condensates. *Physical Review Letters*, 87:180402, October 2001.

[198] M. Holland, K. Burnett, C. Gardiner, J. I. Cirac, and P. Zoller. Theory of an atom laser. *Physical Review A*, 54:R1757, September 1996.

[199] M. Naraschewski and D. M. Stamper-Kurn. Analytical description of a trapped semi-ideal Bose gas at finite temperature. *Physical Review A*, 58:2423, September 1998.

[200] M. Inguscio, S. Stringari, and C. Wieman, editors. *Bose-Einstein Condensation in Atomic Gases, Proceedings of the International School of Physics "Enrico Fermi," Course CXL*, Amsterdam, 1999. IOS.

[201] D. V. Semikoz and I. I. Tkachev. Kinetics of Bose condensation. *Physical Review Letters*, 74:3093, April 1995.

[202] Yu. M. Kagan, B. V. Svistunov, and G. V. Shlyapnikov. *Sov. Phys. JETP*, 75:387, 1992.

[203] Yu. Hagan. Kinetics of Bose-Einstein condensate formation in an interaction Bose gas. In A. Griffin, D. W. Snoke, and S. Stringari, editors, *Bose-Einstein Condensation*, page 202, New York, 1995. Camridge University Press.

[204] H. T. C. Stoof. Initial stages of Bose-Einstein condensation. *Physical Review Letters*, 78:768, February 1997.

[205] K. Damle, S. N. Majumdar, and S. Sachdev. Phase ordering kinetics of the Bose gas. *Physical Review A*, 54:5037, December 1996.

[206] C. W. Gardiner, P. Zoller, R. J. Ballagh, and M. J. Davis. Kinetics of Bose-Einstein condensation in a trap. *Physical Review Letters*, 79:1793, September 1997.

[207] M. D. Lee and C. W. Gardiner. Quantum kinetic theory. vi. the growth of a Bose-Einstein condensate. *Physical Review A*, 62:033606, August 2000.

[208] L. Onsager. *Suppl. N. Cim.*, 6:249, 1949.

[209] R. P. Feynman. In C. J. Gorter, editor, *Progress in Low Temperature Physics*, volume 1, page 17, Amsterdam, 1955. North-Holland.

[210] C. J. Pethick and H. Smith. *Bose-Einstein Condensation in Dilute Gases*. Cambridge University Press, New York, 2002.

[211] K. Huang. Bose-Einstein condensation and superfluidity. In A. Griffin, D. W. Snoke, and S. Stringari, editors, *Bose-Einstein Condensation*, page 31, New York, 1995. Camridge University Press.

[212] D. S. Rokhsar. Vortex stability and persistent currents in trapped Bose gases. *Physical Review Letters*, 79:2164, September 1997.

[213] R. J. Dodd, K. Burnett, M. Edwards, and C. W. Clark. Excitation spectroscopy of vortex states in dilute Bose-Einstein condensed gases. *Physical Review A*, 56:587, July 1997.

[214] H. Pu, C. W. Law, J. H. Eberly, and N. P. Bigelow. Coherent disintegration and stability of vortices in trapped Bose condensates. *Physical Review A*, 59:1533, February 1999.

[215] J. J. García-Ripoll and V. M. Pérez-García. Stability of vortices in inhomogenous Bose-Condensates subject to rotation: A 3D analysis. *Physical Review A*, 60:4864, December 1999.

[216] D. A. Butts and D. S. Rokhsar. Predicted signatur of rotating Bose-Einstein condensates. *Nature*, 397:327, January 1999.

[217] S. M. M. Virtanen, T. P. Simula, and M. M. Salomaa. Structure and stability of vortices in dilute Bose-Einstein condensates at ultralow temperatures. *Physical Review Letters*, 86:2704, March 2001.

[218] T. P. Simula, S. M. M. Virtanen, and M. M. Salomaa. Stability of multiquantum vortices in dilute Bose-Einstein condensates. *Physical Review A*, 65:033614, February 2002.

[219] M. Möttönen, T. Mizushima, T. Isoshima, M. M. Salomaa, and K. Machida. Splitting of a doubly quantized vortex through interwinding in Bose-Einstein condensates. *Physical Review A*, 68:023611, August 2003.

[220] T. Isoshima, J. Huhtamäki, and M. Salomaa. Instabilities of off-centered vortices in a Bose-Einstein condensate. *Physical Review A*, 68:033611, September 2003.

[221] E. Lundh. Multiply quantized vortices in Bose-Einstein condensates. *Physical Review A*, 65:043604, March 2002.

[222] M. Baert, V. V. Metlushko, R. Jonckheere, V. V. Moshchalkov, and Y. Bruynseraede. Composite flux-line lattices stabilized in superconducting films by a regular array of artificial defects. *Physical Review Letters*, 74:3269, April 1995.

[223] R. Blaauwgeers, V. B. Eltsov, M. Krusius, J. J. Ruohio, R. Schanen, and G. E. Volovik. Double-quantum vortex in superfluid 3He-A. *Nature*, 404:471, March 2000.

[224] P. Engels, I. Coddington, P. C. Haljan, V. Schweikhard, and E. A. Cornell. Observation of long-lived vortex aggregates in rapidly rotating Bose-Einstein condensates. *Physical Review Letters*, 90:170405, May 2003.

[225] P. C. Haljan, I. Coddington, P. Engels, and E. A. Cornell. Driving Bose-Einstein-Condensate vorticity with a rotating normal cloud. *Physical Review Letters*, 87:210403, November 2001.

[226] E. Hodby, G. Hechenblaikner, S. A. Hopkins, O. M. Maragò, and C. J. Foot. Vortex nucleation in Bose-Einstein condensates in an oblate, purely magnetic potential. *Physical Review Letters*, 88:010405, January 2002.

[227] J. E. Williams and M. J. Holland. Preparing topological states of a Bose-Einstein condensate. *Nature*, 401:568, October 1999.

[228] Z. Dutton, M. Budde, C. Slowe, and L. V. Hau. Observation of quantum shock waves created with ultra-compressed slow light pulses in a Bose-Einstein condensate. *Science*, 293:663, July 2001.

[229] N. S. Ginsberg, J. Brand, and L. V. Hau. Observation of hybrid soliton vortex-ring structures in Bose-Einstein condensates. *Physical Review Letters*, 94:040403, February 2005.

[230] T. Isoshima, M. Nakahara, T. Ohmi, and K. Machida. Creation of a persistent current and vortex in a Bose-Einstein condensate of alkali-metal atoms. *Physical Review A*, 61:063610, June 2000.

[231] M. V. Berry. Quantal phase factors accompanying adiabatic changes. *Procedings of the Royal Society of London A*, 392:45, March 1984.

[232] M. Nakahara, T. Isoshima, K. Machida, S.-I. Ogawa, and T. Ohmi. A simple method to create a vortex in a Bose-Einstein condensate of alkali atoms. *Physica B*, 284-288:17, July 2000.

[233] S.-I. Ogawa, M. Möttönen, M. Nakahara, T. Ohmi, and H. Shimada. Method to create a vortex in a Bose-Einstein condensate. *Physical Review A*, 66:013617, July 2002.

[234] M. Möttönen, N. Matsumoto, M. Nakahara, and T. Ohmi. Continuous creation of a vortex in a Bose-Einstein condensate with hyperfine spin $F = 2$. *Journal of Physics: Condensed Matter*, 14:13481, December 2002.

[235] Y. Kawaguchi, M. Nakahara, and T. Ohmi. Topological vortex formation in a Bose-Einstein condensate under gravitational field. *Physical Review A*, 70:043605, October 2004.

[236] F. Zambelli and S. Stringari. Quantized vortices and collective oscillations of a trapped Bose-Einstein condensate. *Physical Review Letters*, 81:1754, August 1998.

[237] F. Chevy, K. W. Madison, and J. Dalibard. Measurement of the angular momentum of a rotating Bose-Einstein condensate. *Physical Review Letters*, 85:2223, September 2000.

[238] P. C. Haljan, B. P. Anderson, I. Coddington, and E. A. Cornell. Use of surface-wave spectroscopy to characterize tilt modes of a vortex in a Bose-Einstein condensate. *Physical Review Letters*, 86:2922, April 2001.

[239] P Rosenbusch, V. Bretin, and J. Dalibard. Dynamics of a single vortex line in a Bose-Einstein condensate. *Physical Review Letters*, 89:200403, November 2002.

[240] P. O. Fedichev and G. V. Shlyapnikov. Dissipative dynamics of a vortex state in a trapped Bose-condensed gas. *Physical Review A*, 60:R1779, September 1999.

[241] K. Kasamatsu, M. Tsubota, and M. Ueda. Nonlinear dynamics of vortex lattice formation in a rotating Bose-Einstein condensate. *Physical Review A*, 67:033610, March 2003.

[242] J. J. García-Ripoll and V. M. Pérez-García. Vortex bending and tightly packed vortex lattices in Bose-Einstein condensates. *Phyical Review A.*, 64:053611, October 2001.

[243] A. D. Jackson, G. M. Kavoulakis, and E. Lundh. Stability of the solutions of the Gross-Pitaevskii equation. *arXiv:cond-mat/0507455*, July 2005.

[244] K. Gawryluk, M. Brewczyk, and K. Rzążewski. Thermal instability of a doubly quantized vortex in a Bose-Einstein condensate. *arXiv:cond-mat/0505725*, May 2005.

[245] J.-P. Martikainen and H. T. C. Stoof. Quantum theory of a vortex line in an optical lattice. *Physical Review A*, 69:053617, May 2004.

[246] J.-P. Martikainen and H. T. C. Stoof. Vortex-line solitons in a peroidically modulated Bose-Einstein condensate. *Physical Review Letters*, 93:070402, August 2004.

[247] U. A. Khawaja and H. Stoof. Skyrmions in a ferromagnetic Bose-Einstein condensate. *Nature*, 411:918–920, June 2001.

[248] U. A. Khawaja and H. T. C. Stoof. Skyrmion physics in Bose-Einstein ferromagnets. *Physical Review A*, 64:043612, October 2001.